



University
of Glasgow

Czosnyka, Katarzyna (2011) *Studies towards the synthesis of fibronectin-based peptidomimetics*. PhD thesis.

<http://theses.gla.ac.uk/2806/>

Copyright and moral rights for this thesis are retained by the author

A copy can be downloaded for personal non-commercial research or study, without prior permission or charge

This thesis cannot be reproduced or quoted extensively from without first obtaining permission in writing from the Author

The content must not be changed in any way or sold commercially in any format or medium without the formal permission of the Author

When referring to this work, full bibliographic details including the author, title, awarding institution and date of the thesis must be given

*Studies Towards the Synthesis of
Fibronectin-Based Peptidomimetics*

Katarzyna Czosnyka

**Thesis submitted to the University of Glasgow
for the degree of Doctor of Philosophy**



Department of Chemistry

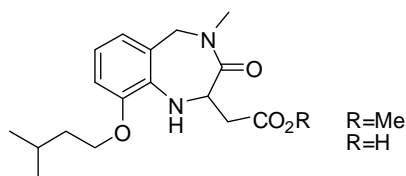
September 2010

© *Katarzyna Czosnyka 2010*

Abstract

Fibronectin (FN) protein was discovered in the early 1970s by Richard Hynes.¹ Since then this large, multidomain glycoprotein present in the extracellular matrix and in body fluids has been intensively research, and has been found to play a fundamental role in cell adhesion, cell migration, cell survival, angiogenesis, and other important biological processes. In recent years the interest in FN has risen; the novel FN isoform, termed Migration Stimulating Factor (MSF) has been cloned and characterized, and new results documenting the involvement of FN and MSF in wound healing, cancer progression and bacterial metastasis have been presented.²

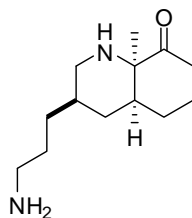
The recent findings have shown that MSF's bioactivities (e.g. stimulation of cell motility, hyaluronan synthesis and angiogenesis) are mediated by the highly conserved amino acid motif *Ile-Gly-Asp* (IGD), and are mimicked by small synthetic peptides containing this sequence. The aim of this project was to design and synthesize first generation non-peptidic compounds which could mimic the biological activity of MSF (i.e. IGD peptidomimetics).



The first generation IGD peptidomimetics

The second part of this thesis describes the role of FN in bacterial pathogenesis. *Staphylococcus aureus* is commonly present in the nose and on the skin of one third of all people, and is normally harmless at these sites. However, the microorganism possesses the ability to enter the body, invade cells and cause infection. The mechanism for *S. aureus* adhesion to, and invasion of, human cells has been extensively studied. It is now postulated that bacterial invasion is mediated by FN, that acts as a bridge between bacterial proteins adhesins and integrin receptors

present on the cell surfaces.³ The biologically active motif, by which FN mediates its adhesion to bacterium, has not been unambiguously identified. However, the preliminary, unpublished studies point towards a short terapeptide sequence, *Gly-Arg-Ile-Ser* (GRIS), which is highly conserved within FN. We proposed to elucidate the role of the native GRIS motif by synthesising a small, nonpeptidic molecule, which could mimic its biological properties and activities.



The first generation GRIS peptidomimetic

Table of Contents

Abstract	2
Table of Contents	4
Acknowledgements	6
Author's Declaration	7
List of Abbreviations	8

THE IGD PROJECT

1.0	Introduction	13
1.1	Fibronectin protein	14
1.1.1	Forms of fibronectin and fibrillogenesis	15
1.1.2	Structure of fibronectin molecule	18
1.1.3	Fibronectin and integrins	22
1.1.4	Alternative splicing of the fibronectin gene	25
1.2	Migration Stimulating Factor (MSF)	27
1.2.1	The IGD motif of MSF	31
1.2.2	First generation IGD peptidomimetics	34
1.2.3	First synthesis of the IGD peptidomimetic	37
2.0	Results and discussion	40
2.1	The aim of the project	40
2.1.1	Model synthesis of the IGD peptidomimetic	41
2.1.2	Enantiospecific synthesis of (<i>R</i>)-IGD peptidomimetic	51
2.1.3	Short synthesis of a photolabile group	55
2.1.4	Coupling of the IGD mimetic with the DANP group	64
2.2	Biological tests	66
2.3	Conclusions	70

THE GRIS PROJECT

3.0	Introduction	72
------------	--------------	----

3.1	Bacteria <i>Staphylococcus aureus</i>	73
3.2	Molecular basis of bacterial invasion	76
3.3	First generation GRIS peptidomimetics	82
4.0	Results and discussion	86
4.1	The aim of the project	86
4.1.1	The aza-Achmatowicz approach	87
4.1.2	The Diels-Alder approach	105
4.2	Conclusions	119
5.0	Experimental section	121
	References	176

Acknowledgements

I would like to take the opportunity to express my thanks to my supervisor, Dr. Rudi Marquez for all his help, advice and encouragement throughout my PhD. I would like to also thank my second supervisor, Dr. Richard Hartley for all constructive and creative comments on my work.

I would like to thank the staff who provided technical support at the University of Glasgow: especially Dr. David Adam, Jim Tweedie, and Ted Easdon. I am also very grateful to the X-ray crystallography team of the University of Glasgow for their contribution.

Thank you to the present and past members of Marquez and Clark groups, who made a PhD such an enjoyable time. Huge thanks goes to Neil, Phil, Seb and Marek!

I gratefully acknowledge Dr. Ian Sword and the University of Glasgow for financial support.

And finally I wish to say very special *thank you!* to my family: Mum, Dad, Daria, Basia, Dziadzio, for their fantastic support; and to my husband Neil, who made those years such a special and amazing time😊...thank you for being there for me😊.

Author's Declaration

This thesis represents the original work of Katarzyna Czosnyka unless explicitly stated otherwise in the text. The research on which this thesis is based was carried out at the University of Glasgow in the Henderson and Raphael laboratories, under the supervision of Dr. Rodolfo Marquez, during the period October 2006 to September 2009.

Katarzyna Czosnyka

September 2010

List of Abbreviations

Ac	acetyl
Al/Hg	aluminum amalgam
Ar	aromatic
ATP	adenosine 5'-triphosphate
Boc	<i>tert</i> -butyloxycarbonyl
BDP	benzodiazepine
br.	broad
CAN	cerium (IV) ammonium nitrate
cFN	cellular fibronectin
CI	chemical ionisation
COSY	correlation spectroscopy
Cy	cyclohexyl
d	doublet
DA	Diels-Alder
DANP	2-(dimethylamino)-5-nitrophenyl
de	diastereomeric excess
DCM	dichloromethane
DCC	dicyclohexylcarbodiimide
DFU	diabetic foot ulcer(s)
DGI	Asp-Gly-Ile
DIBAL-H	diisobutylaluminium hydride
DMAD	dimethyl acetylenedicarboxylate
DMAP	4-dimethylaminopyridine
DMF	<i>N,N</i> -dimethylformamide

DMSO	dimethyl sulfoxide
DNA	deoxyribonucleic acid
ECM	extracellular matrix
EDA	extra domain A
EDB	extra domain B
EDC	1-ethyl-3-(3-dimethylaminopropyl)carbodiimide
ee	enantiomeric excess
EI	electron ionisation
EtOAc	ethyl acetate
Eu(fod)₃	europium(III)-tris(1,1,1,2,2,3,3-heptafluoro-7,7-dimethyl-4,6-octanedionate)
FAB	fast atom bombardment
FCC	flash column chromatography
Fib-1/Hep-1	<i>N</i> -terminal fragment FNI ₁₋₅
Fib-2	second fibrin-binding site
FN	Fibronectin
FnBPA	Fibronectin-binding protein A
FnBPB	Fibronectin-binding protein B
FnBPs	Fibronectin-binding proteins
g	gram(s)
GBD	collagen/gelatine binding domain (of fibronectin)
GNGRG	Gly-Asn-Gly-Arg-Gly
GRIS	Gly-Arg-Ile-Ser
h	hour(s)
¹H NMR	proton nuclear magnetic resonance (spectroscopy)
HOMO	highest occupied molecular orbital
Hep-2	second heparin-binding domain

HMBC	heteronuclear multiple bond correlation
HPLC	high performance liquid chromatography
HRMS	high resolution mass spectrometry
HSQC	heteronuclear single quantum coherence
hν	energy of a photon (h= Planck constant, ν =frequency)
IE	infective endocarditis
IGD	Ile-Gly-Asp
IGDS	Ile-Gly-Asp-Ser
IGDQ	Ile-Gly-Asp-Gln
IR	infrared (spectroscopy)
IPN	isopropyl nitrate
kDa	kilodalton(s)
L-Selectride	lithium tri- <i>sec</i> -butylborohydride
LUMO	lowest unoccupied molecular orbital
LDV	Leu-Asp-Val
M	metal
mCPBA	3-chloroperoxybenzoic acid
MeCN	acetonitrile
MeOH	methanol
min	minute(s)
ml	millilitre(s)
mmol	millimole(s)
mRNA	messenger Ribonucleic Acid
MRSA	methicillin-resistant <i>Staphylococcus aureus</i>
MS	mass spectrometry
MSCRAMM	microbial surface components recognising adhesive matrix molecules

MSF	Migration Stimulating Factor
m/z	mass-to-charge ratio
NMR	nuclear magnetic resonance (spectroscopy)
NTR	<i>N</i> -terminal region
NOESY	nuclear Overhauser effect spectroscopy
NVOC	6-nitroveratroxyloxycarbonyl group
TMS	trimethylsilyl
Pd/C	palladium on carbon
Pd(OAc)₂	palladium (II) acetate
PEG 400	poly(ethylene glycol)
pFN	plasma fibronectin
Ph	phenyl
PHSRN	Pro-His-Ser-Arg-Asn
PG	protecting group
ppm	parts per million
PPTS	pyridinium <i>p</i> -toluenesulfonate
RaNi	Raney nickel
RCM	ring-closing metathesis
Red-Al®	sodium bis(2-methoxyethoxy)aluminum hydride
REDV	Arg-Glu-Asp-Val
R_f	retention factor (in chromatography)
RGD	Arg-Gly-Asp
RGE	Arg-Gly-Glu
<i>S. aureus</i>	<i>Staphylococcus aureus</i>
SDGI	Ser-Asp-Gly-Ile
SM	starting material
S_N2	bimolecular nucleophilic substitution

rt	room temperature
TBAHS	tetrabutylammonium hydrogen sulphate
TBSCI	<i>tert</i> -butyldimethylsilyl chloride
TFA	trifluoroacetic acid
TFAA	trifluoroacetic anhydride
(Tf)₂O	trifluoromethanesulfonic anhydride
TfOH	trifluoromethanesulfonic acid
THF	tetrahydrofuran
TLC	thin layer chromatography
Ts	tosyl (group)
TSA	<i>p</i> -toluenesulfonic acid
TSS	toxic shock syndrome
UV	ultraviolet (light)
V	variable region (of fibronectin)
WHO	World Health Organization
Yb(OTf)₃	ytterbium (III) triflate

THE IGD PROJECT

1.0 Introduction

The human extracellular matrix (ECM) is a complex network of proteins and macromolecules that fills the intercellular spaces. This three-dimensional matrix creates a living environment for cells and transmits external signals. Dynamic interactions between cells and proteins in the surrounding ECM regulate and stimulate most cellular functions and processes. One of the most remarkable ECM's proteins is fibronectin (FN). Fibronectin is a biologically active macromolecule engaged in a variety of events that take place in the ECM. Some of the processes that depend on FN and one of its isoforms termed Migration Stimulating Factor (MSF) are: wound healing, cancer and bacterial metastasis.^{2,3,4}

In recent years, new ideas and theories have arisen around two “hot” topics: wound healing and cancer pathogenesis.⁵ However, despite decades of research, current treatment of both lesions is still very difficult and often unsuccessful. Difficulties arise from the fact that both processes are complex and engage a cascade of cellular events, signalling molecules and receptors. As a result, pharmacological drugs and approaches tend to suffer from poor selectivity and efficiency.

Due to the histological similarities between tumour “microenvironment” and that of a healing wound, Harvard pathologist Harold Dvorak described cancer growth as “wound healing gone awry.” Both impaired tissues and tumours induce very similar biochemical and cellular responses. They both need rapid cell proliferation, cell migration and angiogenesis. However, in wounds these processes are normally reparative and end after the wound heals; in cancer they become invasive, aggressive and uncontrollable.

FN has long been linked to malignant diseases and is considered as a target for tumour therapy.⁶ Special attention has been focused on FN isoforms which included

an extra domain B (EDB), a sequence of 91 amino acids. The EDB domain has been shown to be expressed in tissues undergoing remodelling during angiogenesis or tumour invasion.⁷ Recently, another FN isoform was proved to be associated with angiogenesis and cancer. This new protein, termed Migration Stimulating Factor, is a truncated version of FN that exhibits interesting biological activities. Experiments conducted so far showed that MSF induces angiogenesis, cell migration and hyaluronan synthesis.² All these bioactivities, but especially stimulation of cell movement, make the MSF molecule relevant and interesting target for research in both areas: wound healing and tumour progression.

1.1 Fibronectin protein

In the early 1970's, during research on cancer development, scientists discovered a new protein that was present on the surface of normal cells but rarely on tumour cells. The protein was the first clear molecular difference observed between normal and cancer cells. Although further investigations proved that this molecule was not a central, single factor that could explain cancer progression, research on this new structural protein, termed fibronectin, started and has been continuing since.

Throughout 40 years of research, FN has been shown to stimulate many key cellular processes; i.e. cell adhesion, migration and differentiation, thrombosis and wound healing. Much information about FN has been gained, regarding its structure, distribution, receptors, and other potential functions. FN was also proved to be, after all, involved in cancer pathogenesis and angiogenesis. As interest in FN protein has prevailed, the new theories around FN and its role in biological processes have emerged: "I think that we all feel that fibronectin has been an incredible conceptual gold mine" (Kenneth Yamada, M.D., Ph.D).⁸

Until now, human fibronectin remains imperfectly understood. Fibronectin is not only structurally complex molecule with many independent binding sites, but also, during genetic processes, as many as 20 variants of FN are produced in humans.

Each variant has a different structure and activity. To further complicate the situation, fibronectin fragments (resulting from proteolysis) also have unique biological properties. Since all these molecules are coded by a single gene, fibronectin is also a term that describes a family of structurally and immunologically related glycoproteins. FNs are of crucial importance while researching complex and concerted molecular processes.⁹

1.1.1 Forms of fibronectin and fibrillogenesis

Fibronectin is a large, adhesive glycoprotein, with high molecular weight ca. 500 kDa, characteristically present only among vertebrates.¹⁰ Like many other ECM glycoproteins, FN is a multifunctional molecule that not only attaches cells to the ECM, but also mediates a range of biological processes throughout its active sequences. FN has been shown to be critically important in normal vertebrate development, what was demonstrated by the early embryonic lethality of mice with targeted inactivation of the FN gene.¹¹ In the human body FN exists in two distinctive forms: as plasma FN (pFN), present in body fluids, and cellular FN (cFN), crucial component of the ECM.

The plasma form of fibronectin is produced predominantly by hepatocytes and secreted into blood, to circulate as a soluble dimer in relatively high (micromolar) concentrations. In contrast to pFN, cellular FN is synthesised locally by various types of cells (e.g. fibroblasts, chondrocytes, macrophages and intestinal epithelial cells) and released as a compact globular molecule that has high affinity to quickly self-polymerise into insoluble fibrils.^{12,13} Cellular FN, along with collagen, is the main constituent of ECM that forms a highly dynamic network of fibres. This fibrillar matrix creates the necessary environment for cells' embryogenesis, growth, survival, differentiation and many other primary processes.¹⁴

Our understanding of how globular, soluble cFN molecules self-assemble into this functional fibrillar meshwork is limited. The mechanism of fibrillogenesis is complex and has been shown to be stepwise, proceeding from initiation, through

elongation to stabilization phase.¹⁵ There is nothing spontaneous about fibrillogenesis; each step is highly regulated by cells and their transmembrane receptors, integrins. Integrins initiate the fibrillogenesis process by binding soluble FN molecules and attaching them to cell surfaces. In order to do this, receptors have to be present in high affinity (active) conformation. The continuous binding of FN molecules eventually leads to relatively high local concentration of integrin-FN clusters, and finally become high enough to promote self-association of FN molecules (Figure 1).

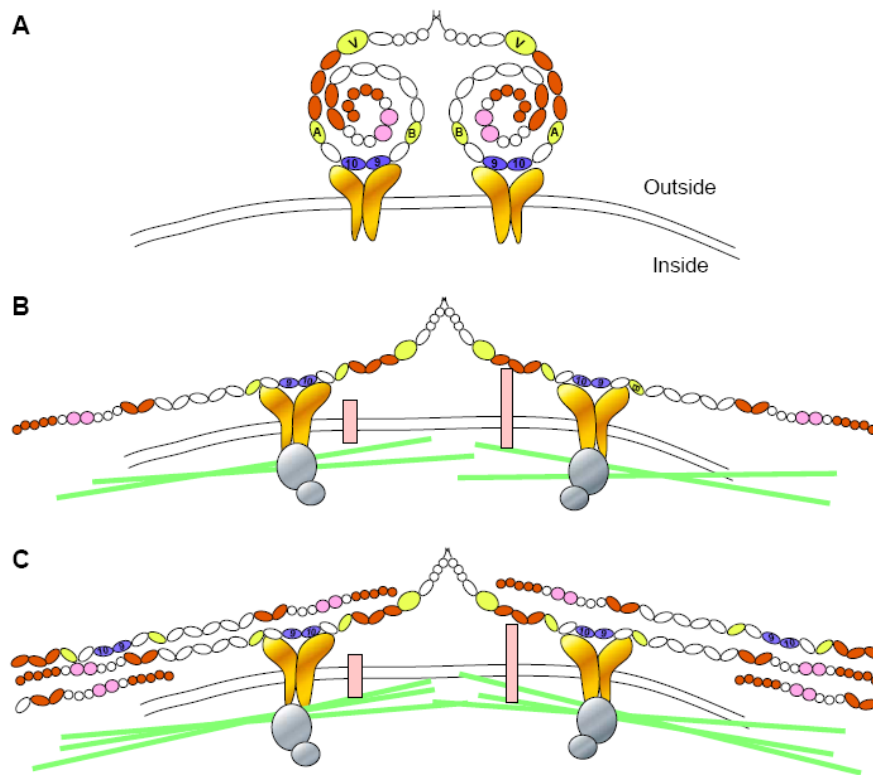


Figure 1. Assembly of fibronectin: (A) soluble FN binds to integrins (gold), (B) FN binding to integrins and other receptors (pink bars) induces stretching of FN molecules, (C) Fibrils form through FN-FN interactions.

Reprinted from *Matrix Biology*, 24, Y. Mao, J. E. Schwarzbauer, *Fibronectin fibrillogenesis, a cell-mediated matrix assembly process*, p. 389-399, Copyright 2005, with permission from Elsevier

Interestingly, initiation of fibrillogenesis requires not only molecular interactions, but also the application of mechanical forces generated by cells.^{16,17} It is speculated, that in the early stage of fibrillogenesis, cell-generated tension stretches the bound FN

protein and induces conformational changes within it. These force-induced changes in the FN three-dimensional structure are believed to uncover multiple binding sites that were cryptic within the molecule.¹⁸ These buried motifs are termed ‘self-association’ sites that allow binding between cell-associated FN molecules. The chain reaction of FN’s self-assembly eventually results in dense network of matured, elastic and highly stretched fibrils that form a stable matrix (Figure 2).^{17,19}

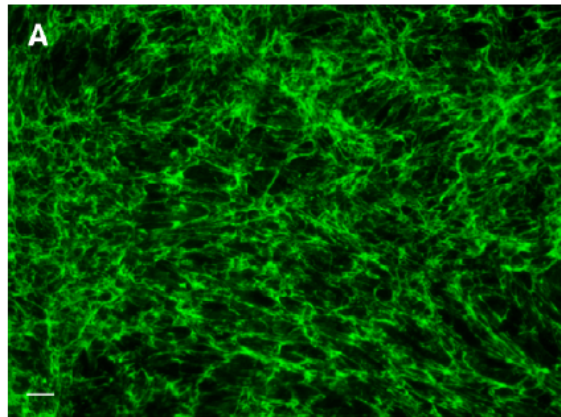


Figure 2. Fibrillar FN matrix.

Reprinted from *Matrix Biology*, 24, Y. Mao, J. E. Schwarzbauer, *Fibronectin fibrillogenesis, a cell-mediated matrix assembly process*, p. 389-399, Copyright 2005, with permission from Elsevier

The fibrillogenesis in tissues is an active and dynamic everyday process. On the contrary, normal fibrillogenesis in blood is required only under certain physiological conditions, when formation of thrombus is necessary. However, both processes, fibrillogenesis of cFN in tissues and pFN in blood are controlled by the same mechanism. The difference in demand for cellular and plasma fibrillogenesis is regulated by integrins present on cell surfaces. In tissues, cells normally express activated integrins that subsequently bind FN molecules. In the blood, integrins on hematopoietic cells remain in a low affinity conformation, what prevents FN’s adhesion.²⁰ However, during vascular injuries, platelets are activated and integrins on their surfaces shift into high affinity conformation what initiate FNs assemble and fibrils formation. Recent studies have shown that pFN matrix assembly contributes to the stability and proper growth of thrombus.²¹ It is postulated that FN supports

platelets aggregation by crosslinking other adhesive proteins present in blood (fibrinogen, thrombospondin) to platelets.²²

Control over the fibrillogenesis process is also necessary for proper deposition of the fibronectin matrix. Formation of biologically active FN fibrils is crucial for normal cell function, but incorrect accumulation of insoluble FN contributes to development of several pathological states. Experimental evidence has associated an increased deposition of FN and collagen with asthma and inflammatory diseases,²³ whereas reduced FN matrix deposition is correlated with impaired wound healing.²⁴

1.1.2 Structure of fibronectin molecule

The plasma and cellular FN forms play different roles in the human body but share structural similarities. Regardless the cell type, secreted and soluble FN molecules are dimers, composed of two similar or identical polypeptide chains of 220-250 kDa, held together by two disulphide bonds located near the carboxyl terminus of the protein (Figure 3).¹³ Each chain is a polypeptide composed of three types of homologues modules, repeated in the molecule in a highly organised manner. Each chain consists of 12 copies of type I module (FNI), 2 of type II (FNII) and 15-17 of III (FNIII), which together accounts for 90% of the FN sequence. The number of type III modules in FN depends on inclusion/exclusion of two extra domains of type III: A and B (EDA and EDB). Additionally, individual chains might also contain one variable region (V) that is not homologues to any other part of the FN protein (Figure 3).⁹ The modular structure of FN's chain is often compared to "beads on a string", because of the way the globular modules are connected to each other by short, linear amino acid sequences.

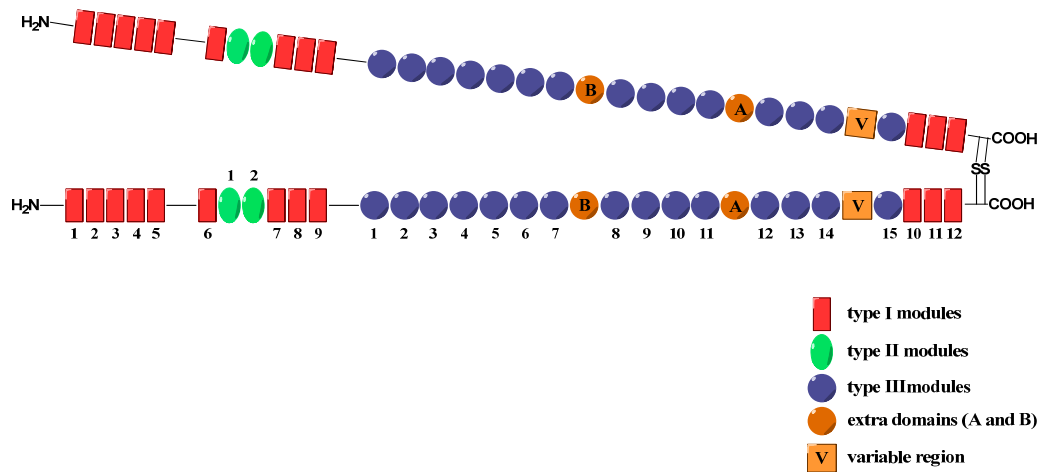


Figure 3. Schematic diagram of modular structure of FN dimer; individual modules are numbered according to their positions from *N*- to *C*-terminus along the FN molecule.

Structural studies on the isolated fibronectin modules clearly showed that all modules types are independently folded proteins, despite being part of the same polypeptide chain. They all have strictly organised, compact, three-dimensional structures that comprise of antiparallel β -sheets and turns (Figure 4). The tightly packed conformations of the fibronectin types I and II modules are stabilized, in addition to hydrophobic interactions between β -sheets, by two highly conserved disulphide bonds. The type I and II modules are rich in cysteine residues, which are involved in forming the disulphide bonds. Interestingly, the FNIII modules have no disulphide bonds, which evoke some flexibility within the proteins.¹⁶ This mechanical property of the FNIII modules has been linked to fibrillogenesis; individual FNIII modules have been proposed to undergo partial unfolding, providing for the elasticity of FN fibrils and also exposing the cryptic binding sites (i.e. buried binding sites that remain inactive until certain trigger expose them), needed for fibrils assembly.^{18,25}

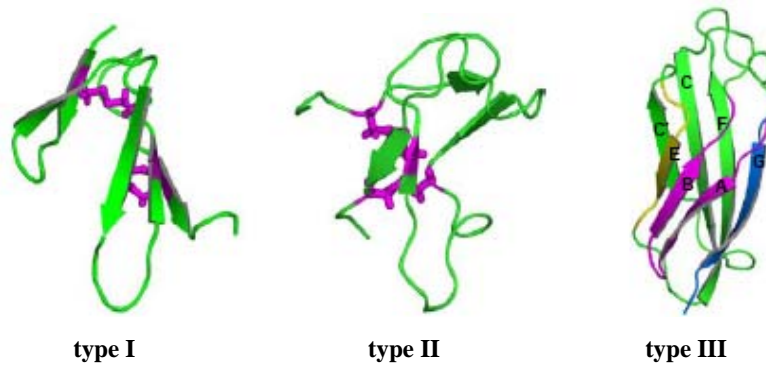


Figure 4. The ribbon structures of FN modules of types I, II and III. The cysteine residues and disulfide bonds are shown in purple (type I and II modules).

Reprinted from *Matrix Biology*, 24, Y. Mao, J. E. Schwarzbauer, *Fibronectin fibrillogenesis, a cell-mediated matrix assembly process*, p. 389-399, Copyright 2005, with permission from Elsevier

Structurally, the FNI and FNII modules are composed of approximately 45 and 60 amino acid residues respectively. The detailed primary sequence is known for several examples of both types of module. Modules of the same type share low sequence homology, which may be linked to their diverse biological functions.²⁶

In order to understand the structure-function relationships in FN, another interesting and important feature, which rises from the FN modular nature has to be considered. The individually folded modules of types I, II and III rarely exhibit biological functions independently. Instead, there are organized in larger fragments that act as functional domains capable of interacting with other macromolecules and cells. These functional domains, which are comprised of sets of modules and loops between them, have distinct conformational properties compared to separately considered modules and hold within their structures a range of active and cryptic sequences. These characteristics are diverse and unique to every individual domain, and are the reason for the broad biological activity of fibronectin protein.⁹

Several distinct functional domains of fibronectin have been identified by proteolytic fragmentation or recombinant DNA analyses.^{27,28} Starting from the *N*-terminus, mild proteolysis revealed several independent domains that retained their biological activity after being “cut off” from the FN polypeptide (Figure 5). The most important are:

- *N*-Terminal fragment FNI₁₋₅ (modules 1 to 5), abbreviated Fib-1/Hep-1, binds to fibrin, heparin and bacteria.
- Collagen/gelatine binding domain (GBD) includes modules FNII₆₋₉ and FNIII₁₋₂. This binds more effectively to denaturated collagen (gelatin) than to native collagen, suggesting a role in “cleaning” denaturated collagen materials from tissues and blood.
- Cell-binding domain, which includes modules FNIII₉₋₁₀, binds to integrins present on cell surfaces.
- Second heparin-binding domain (Hep-2), located in the *C*-terminal part of FN chain, and Fib-2 (second fibrin-binding site).²⁹

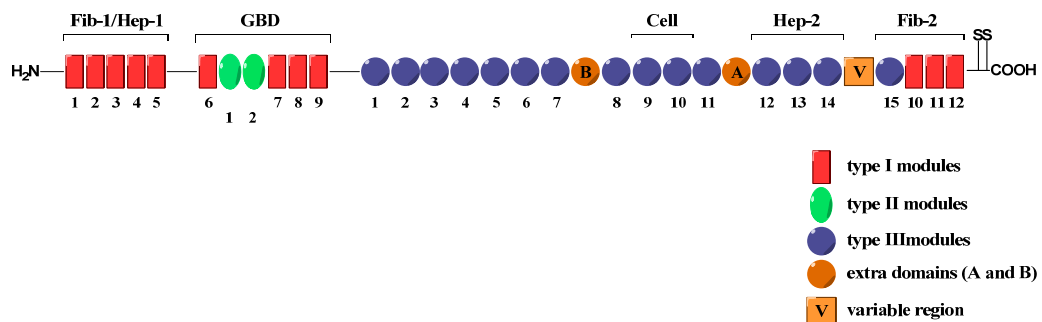


Figure 5. Schematic representation of functional domains of FN.

Since the FN modules of type III are the most ubiquitous of all modules, they have attracted the most attention and have been extensively studied.³⁰ The type III modules have been identified in many different proteins in species ranging from bacteria to humans.³¹ FNIII modules are present in the ECM protein tenascin, in cell surface adhesion molecules or cytokine receptors like growth hormone receptor. They are also present in the largest, central part of FN polypeptide chains.

Each FNIII module is composed of approximately 90 amino acid residues, organized in seven antiparallel β strands, arranged in two sheets E-B-A and G-F-C-D (Figure 6).¹⁰ The three-dimensional structure of FNIII units is highly conserved, unlike their primary sequences, as individual FNIII modules share only 20-40% of amino acid sequence homology within the FN protein. Interestingly, the primary sequence

homology for the same FNIII modules across different species is significantly higher, 80-90%, suggesting that sequence variability among the modules in each FN molecule is functionally important.¹⁶

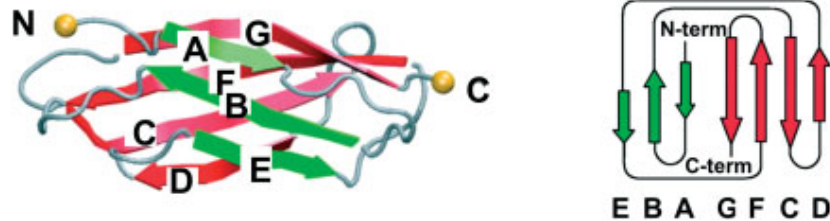


Figure 6. Schematic structure of FN module type III.¹⁰

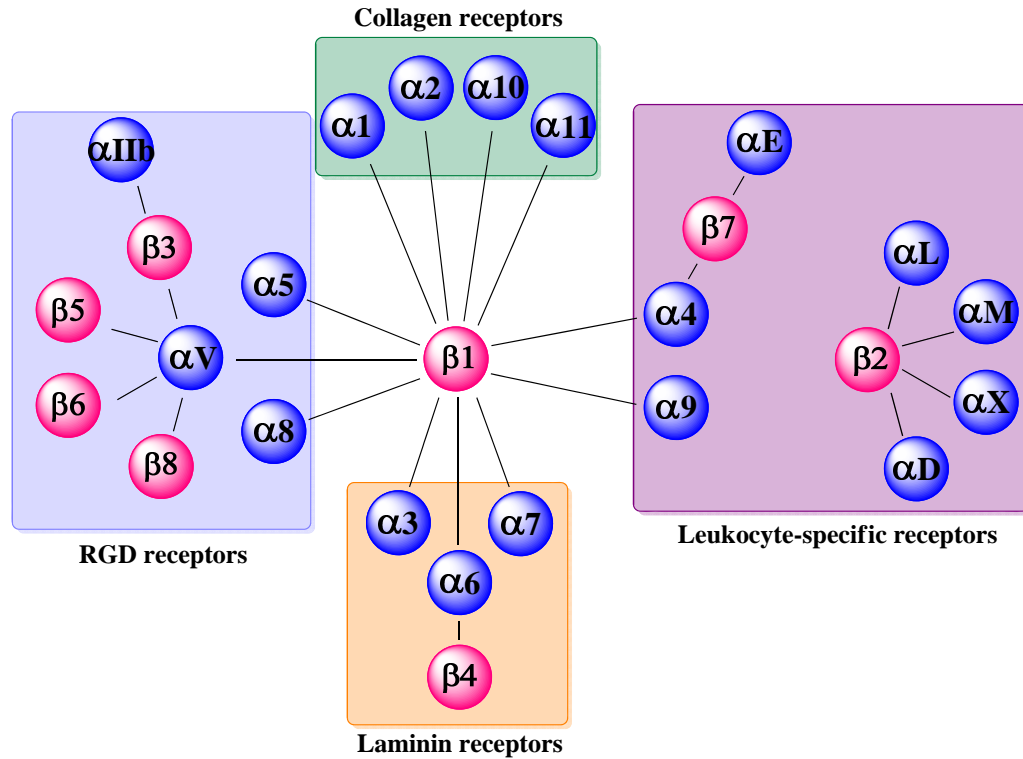
Reprinted from *Journal of Pathology*, 216, E. S. White, F. E. Baralle, A. F. Muro, *New insights into form and function of fibronectin splice variants*, p. 1-14, Copyright 2008, with permission from John Wiley & Sons

1.1.3 Fibronectin and integrins

Fibronectin, as one of most important signalling proteins that exists in the ECM, interacts actively with other ECM macromolecules and also cells. Biological information, in the form of mechanical and biochemical signals, are transmitted between cells and FN through a number of receptors located on cell surfaces. Distinct FN domains bind, *via* active sequences, to different receptors such as integrins and syndecans.¹⁵

The primary and most studied receptors that recognise FN protein are integrins. Integrins are a family of large transmembrane receptors, present on cell surfaces, which connect cells with ECM and transmit signals inside and outside the cells. Integrins are heterodimers, composed of 18 types of α and 8 types of β subunits that are variably paired. To date, 24 $\alpha\beta$ heterodimers have been identified in mammals.³² Each $\alpha\beta$ combination has its own binding specificity and signalling properties (Scheme 1).³³ The integrins mediate adhesion to many matrix protein (e.g. collagen, laminin), as well as between neighbouring cells through surface counterreceptors. Equally important as their adhesive function is their previously mentioned signalling

ability: integrins transduce information that control fundamental cell processes such as growth, proliferation and survival.³⁴



Scheme 1. The integrin family; solid lines indicate $\alpha\beta$ pairings that have been identified to date on mammalian cells.

The adhesive ability of integrins plays a key role in cells' organization into tissues and organs. This process requires not only association between cells themselves but also connections between cells and ECM. One of the processes that contribute to the establishment of tissues composition, architecture and functions is fibrillogenesis. The initiation of fibrillogenesis requires binding of FN molecules to cell surfaces, what is mediated by $\alpha_5\beta_1$ integrins. The FN's motif, necessary for integrin recognition, is a tripeptide Arg-Gly-Asp (RGD), located on the loop in FNIII₁₀ module (Figure 7).¹⁶ The recognition of this short sequence is complex and depends on flanking residues, its three-dimensional presentation and individual features of the integrin-binding pockets. For example, during the binding event, integrins recognise also another active motif, Pro-His-Ser-Arg-Asn (PHSRN), called synergy sequence,

located in the adjacent FNIII₉ module.³⁵ The synergy site promotes $\alpha_5\beta_1$ integrin binding to FN *via* interactions with the α_5 subunit (Figure 7). The importance of the PHSRN motif in integrin-mediated cell adhesion was recently evaluated. It was shown that mutations in the synergy site, as well as mechanical stretching of FNIII₉₋₁₀ fragment, could reduce FN binding to integrins $\alpha_5\beta_1$ by up to 90%.^{16,35}

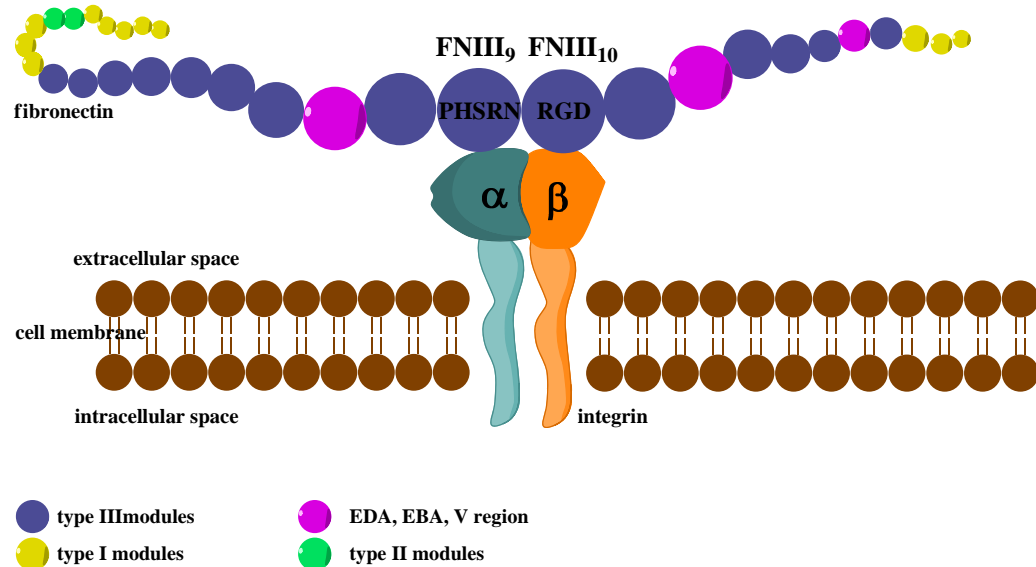


Figure 7. Model representation of fibronectin bound to integrin *via* RGD motif.

Interestingly, the RGD sequence is not specific to FN; this active motif has been found in other ECM proteins, such as tenascin, fibrinogen, trombospondin and vitronectin.³⁰ Moreover, recent research has questioned the importance of RGD motif in fibril formation. According to new findings, replacement of active RGD motif with the inactive RGE (Arg-Gly-Glu) didn't compromise assembly of FN molecules into normal, fibrillar matrix.³⁶

Nevertheless, the $\alpha_5\beta_1$ receptor remains the most important integrin that promotes cell binding to FN molecules. However, other integrins are also capable of RGD sequence recognition. These are: all members of α_v subfamily, $\alpha_5\beta_1$, $\alpha_8\beta_1$ and the platelet-specific $\alpha_{IIb}\beta_3$ integrins (see Scheme 1).³⁷ Moreover, integrin-mediated cell binding of FN molecules was shown to be promoted by additional active sites

recently discovered in the FN sequence, such as Gly-Asn-Gly-Arg-Gly (GNGRG) loop in FNI₅ module.³⁶

The signalling functions of integrins are a broad and not fully understood subject. Through linking ECM proteins, such as FN, with cells' cytoskeleton, integrins assemble large signalling complexes and activate multiple signalling pathways.³⁸ The ability of integrins to form aggregates of active molecules on both sites of cellular membrane is critical in initiating a variety of biochemical processes. Integrin-mediated cell-ECM interactions regulate cell migration, proliferation, spreading and survival.³⁸

1.1.4 Alternative splicing of the fibronectin gene

Fibronectin is one of many proteins that undergo the genetic process called alternative splicing. Alternative splicing in higher eukaryotes is a common method to generate diversity of proteins from a single gene. The complexity of human organism cannot be a result of the number of genes, since the human genome is surprisingly small, having 20,000 to 25,000 protein-coding genes, which is less than the smallest genome in the plant world.³⁹ Hence, additional processes have to take place in order to generate the 500,000 proteins present in the human body. One of these processes is alternative splicing of pre-mRNA. During alternative splicing, a pre-mRNA molecule can be spliced at different junctions to produce a variety of mature mRNA molecules, each containing different combinations of exons. As a result, various mRNAs can direct the synthesis of structurally and functionally different proteins, despite being coded by a single gene.⁴⁰

The FN gene was one of the first to be reported to undergo alternative splicing.^{41,42} In humans, alternative splicing of FN depends on cell type, developmental stage and age, and can result in as many as 20 different FN proteins (isoforms) with molecular masses in the region of full-length FN. Some of these FN isoforms are preferentially expressed by tumour cells and are believed to contribute to cancer pathogenesis.⁴³ In human fibronectin, there are three major sites of alternative splicing; two within

the type III modules and one in a V region. The post-translational variations in V region are the most complex. In the human body, the V region can be spliced in several places, producing 5 different V structural variants. In most species this region can be either partially or completely included or excluded; for example, in plasma fibronectin the V region is fully incorporated into one chain but entirely absent from the other.¹⁰ Importantly, since the V region has two integrin binding sites (Leu-Asp-Val (LDV) and Arg-Glu-Asp-Val (REDV) that are recognised by $\alpha_4\beta_1$ and $\alpha_4\beta_7$ integrins, its presence or absence has unquestionable affect on adhesion of some types of cells (e.g. endothelial cells,⁴⁴ lymphocytes⁴⁵).

The alternative splicing that occurs within the central type III modules (FN III₇ to FN III₁₅) defines the unique amino acid sequences of pFN and cFN. Two extra domains of type III, termed A (EDA) and B (EDB), could be included or excluded from the FN mRNA. As a consequence, matured cellular FN protein contains EDA and EDB in various combinations and variable proportions,⁹ whereas these both domains are totally absent from pFN molecule.⁴⁶

The biological functions of EDA and EDB are currently under investigation; so far increased inclusion of both exons in FN mRNA has been shown during embryonic development. However, once development is complete, the EDA and EDB gradually “disappear” from FNs in wide range of tissues, and are almost absent from adult tissues.⁴⁷ Those findings indicate that EDA and EDB are necessary for proper development. However, experiments have also shown that mice that constitutively include or exclude EDA developed normally, despite the fact that some biological functions were impaired.⁴⁶ In contrast, simultaneous ablation of both EDA and EDB exons in the FN gene leads to embryonic lethality of mice, caused by multiple cardiovascular defects.⁴⁸ Moreover, *in vivo* studies on transgenic mice with targeted mutation in the FN gene have confirmed that the presence of at least one of the extra domain EDA/EDB is critical for normal heart and blood vessel development.¹⁰

The exact roles of the EDA and EDB domains in development are not yet fully understood. However, knowledge of the EDA and EDB functions in pathological processes is better established. It is known that splicing patterns that again includes the EDA and/or EDB domain into the FN sequence is temporally re-established in

adult tissues under certain circumstances, such as tissue repair, tissue fibrosis and angiogenesis. Studies conducted have shown that in mature tissues EDA is locally expressed as a response to pathologies such as rheumatoid arthritis,⁴⁹ wound healing (along with EDB),⁵⁰ and pulmonary fibrosis.⁵¹

In recent years, attention has been directed to FN isoforms containing the EDB domain. The EDB-FN is expressed in tissues undergoing angiogenesis and remodelling, and is also totally absent from normal vessels and organs in adults (with exception of the female reproductive system where angiogenesis is a physiological process).⁷ Due to this selective expression, the EDB domain is an excellent marker of angiogenesis. Rapid angiogenesis is a characteristic feature of aggressive tumours, which requires new blood vessels for growth beyond certain size and spread. The tumour-associated markers known to date are often lacking the important feature: to be selectively expressed in cancerous cells. For instance, markers like integrins $\alpha_5\beta_3$ and $\alpha_5\beta_5$ are also widely expressed in normal tissues.⁵² As a result, drugs and therapies cannot selectively target abnormal cells. The discussed EDB domain that is expressed selectively in tissues undergoing remodelling is therefore a very promising angiogenesis marker and possible target for therapy of malignant diseases.⁵³

1.2 Migration Stimulating Factor (MSF)

The family of FN proteins remains of great importance for studying and understanding cellular processes. Recently, novel information about structures and functions of alternatively spliced isoforms of FN has been documented.⁵⁴ Furthermore, studies conducted by Prof. Schor and Dr Schor allowed identification of a new protein that turned out to be also a member of FN family.⁵⁵ The novel protein was termed Migration Stimulating Factor (MSF) because of the first biological activity ascribed to it: stimulation of cells movement.

Since its discovery, the MSF protein has been intensively studied. The molecule was shown to differ in structure and biological activities from FN itself and all other

known FN isoforms. The unique MSF's bioactivities include stimulation of cell migration, promotion of angiogenesis and hyaluronan synthesis, that is, processes that are primary in cancer and wound healing. It is believed that further studies on MSF will give significant insight into our understanding of these lesions.²

Migration Stimulating Factor is a product of the FN's gene, generated by alternative splicing of mRNA. Unlike FN, MSF is not a part of extracellular matrix, but a soluble protein, excreted by cells. Elucidation of MSF's structure revealed that the protein is a truncated isoform of FN, with a molecular mass of only 70 kDa. Primary sequence analysis of MSF showed its high homology with FN: MSF is identical to the *N*-terminus of FN, composed mainly by type I modules with included Fib-1/Hep-1 and gelatin-binding (GBD) domains (Figure 8). Moreover, the MSF protein differs from all other FN isoforms not only in size, but also by unique 10 amino acid sequence on the carboxyl terminus.⁵⁶

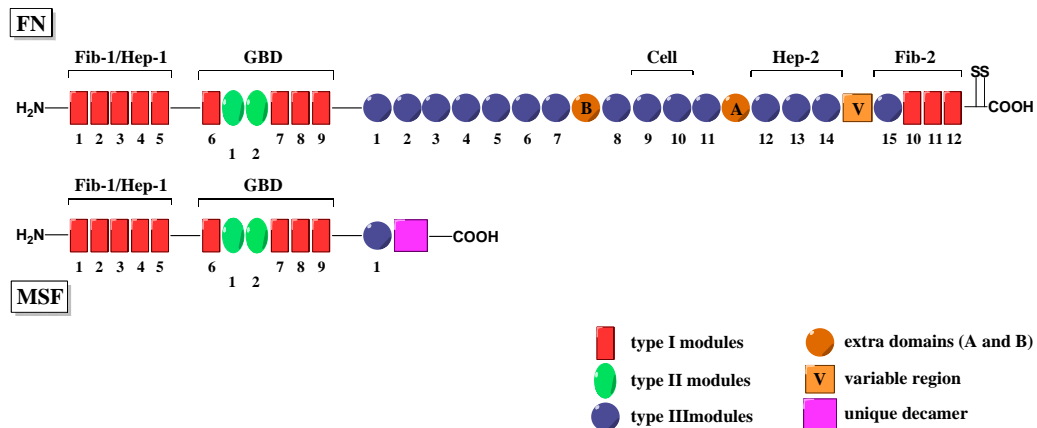


Figure 8. Comparison of the domain structure of fibronectin and MSF protein.

MSF was first identified as a soluble protein excreted by foetal fibroblasts.⁵⁷ Further work showed that MSF is almost not detectable in healthy adults skin fibroblasts, but is re-expressed in cells that undergo remodelling, for instance during malignant diseases. Schor and co-workers analysed the serum from breast cancer patients to reveal significant concentration of MSF in more than 90% of the group, in comparison to only 10% of healthy individuals.⁵⁸ Further immunohistochemical

studies extended the range of cells, which express MSF, from tumour-associated fibroblasts to carcinoma cells, and tumour-associated vascular endothelial cells.²

It has long been known, that cancerous “onkofetal” cells resemble foetal cells in terms of phenotype, and through the excretion of several biologically active molecules. The foetal and cancerous cells also have the ability to undergo directed and elevated migration.⁵⁵ Cell migration is a fundamental process that starts in the embryo, and contributes to tissues organization, organogenesis and homeostasis. It is also an essential component of tissue repair, angiogenesis and tumour invasion. The complexity of this process is reflected by the number of molecules that have been shown to affect motility and positioning of mammalian cells.⁵⁹ In a healthy human body, cell migration is induced periodically, as a response to situations such as tissue injury, and can be turned off and on by the highly specialised “machinery”, that engages actin cytoskeleton.⁶⁰ However, during malignant diseases, the control over cell motility is lost, and escalated cell migration causes spread of cancer to distant organs and body parts.

Initial work linked the expression of MSF protein with the enhanced motility of cells such as foetal and cancerous fibroblasts. This hypothesis was first tested *in vitro* using three-dimensional gels of native type I collagen. It was observed that foetal and oncofetal cells migrated into the matrix to much greater extent than normal adult cells.⁵⁵ Furthermore, experiments showed that when non-producing normal adult fibroblast were confluent with exogenous MSF, they also exhibited enhanced motility. Thus, although adult cells do not produce MSF, they clearly respond to it.⁶¹ The motogenic activity of MSF is however, also highly dependent on external factors and conditions, such as cell density, presence of other molecules and type of matrix. For example, the MSF displayed motogenic activity on fibroblasts that were attached to physiologically relevant matrix, in this case native type I collagen. Conversely, the protein did not show the expected bioactivity when tests were performed on denatured collagen.⁶²

All of the currently obtained information prompted the hypothesis about the direct involvement of MSF in cancer development. The vast majority of data collected strongly suggested that MSF plays an important role in both the initiation and

progression of cancer. This protein was shown to be expressed not only by cells of breast cancer patients but also in other common human cancers, such as lung, colorectal, oral and prostate.² Furthermore, MSF is believed to contribute to tumour pathogenesis by a number of mechanisms, which include stimulation of tumour cell motility, hyaluronan synthesis and angiogenesis. It is speculated, that peptidic or non-peptidic MSF antagonist could prevent tumour invasion and angiogenesis by inhibition of MSF activity.

The presented findings on the role of MSF in tumour pathology are equally important in the area of wound healing research. Histological analyses performed in mid-1980s, showed great similarities between a tumour microenvironment and that of a healing wound. These two processes induce very similar emergence response, that engage rapid cell proliferation, remodelling of tissues and the ECM, cell migration and blood vessels formation (angiogenesis).⁶³ Thus, cell migration and angiogenesis have been long a primary targets in understanding and fighting cancer, but also in the area of wound healing research.

As presented before, the MSF protein is persistently over-expressed in a number of common human cancers but it was also found to be transiently expressed during human acute wound healing. In both lesions MSF is targeting the same processes: cell motility and angiogenesis. However, while enhanced cell motility and rapid angiogenesis promote cancer by supporting tumour spread and growth, these processes are restorative during wound repair.⁵

Wound healing is a complex process of restoring cellular structure and tissue layers. It involves activation of keratinocytes, fibroblasts, endothelial cells, macrophages, platelets, as well as wide range of signalling molecules such as cytokines and chemokines.⁶⁴ The process, however, could be, under certain circumstances, interrupted and impaired, which might lead to the formation of a chronic wound that does not heal. There are several factors and diseases that contribute to the development of non-healing wounds; one of the major ones is diabetes. People with diabetes are in a constant danger of developing chronic wound that could result in amputation. Research and analysis have allowed the identification of pathogenic markers and phenotypic changes on the tissue level that correlate with delayed

wound healing. For instance, keratinocytes from the non-healing edge of diabetic foot ulcers (DFU) had shown an absence of migration and incomplete differentiation, whereas fibroblasts demonstrated decreased migration and proliferation.⁶⁴ Insufficient cell motility is therefore one of the most important factors that contribute to development of chronic non-healing wounds.

Initial work on MSF showed its involvement in the normal wound repair process. MSF was demonstrated to be produced during human acute wound healing by keratinocytes.⁶⁵ These findings combined with the ability of exogenous MSF to stimulate adult cell migration rendered it a candidate for therapeutic applications. It is believed, that topical application of MSF's agonists could speed-up cell movement and tissue repair in difficult, diabetic wounds.

Moreover, it is hypothesised, that pro-angiogenic properties of MSF could also contribute to wound healing by stimulating the growth of new capillary vessels. Successful wound closure depends on angiogenesis, because proliferating capillaries bring oxygen and micronutrients to growing tissues and remove catabolic waste products. Thus, MSF agonists could act in the wound site as both potent motogenic and angiogenic factor.⁶⁶

1.2.1 The IGD motif of MSF

MSF mediates a unique range of bioactivities that are not expressed by any other member of FN family (i.e. stimulation of cell migration, hyaluronan synthesis and angiogenesis). However, some of MSF-like activities were ascribed previously to gelatine-binding domain (GBD) of FN. The free GBD fragment was shown to stimulate fibroblasts migration into three-dimensional matrixes of native collagen type I.⁶⁷ Under the same conditions, the full-length FN and other FN's proteolytic fragments were devoid of this activity.

The motogenic activity of GBD was believed to be mediated by a novel, active sequence, since the GBD fragment does not contain any already known functional

motifs of FN, such as RGD, LDV or REDV (Figure 9). Thus, through a series of experiments the new amino acid sequence, isoleucine-glycine-aspartate (IGD), located within GDB was identified as a potential active motif responsible for GDB bioactivity.⁶⁸ The IGD tripeptide is highly conserved and repeated within type I modules of FN and GDB. Subsequent work showed that synthetic tri- and tetrapeptides containing IGD motif stimulated migration of human dermal fibroblasts.⁶⁸ Based on these experiments the motogenic activity of GDB fragment was assigned to its IGD sequence.

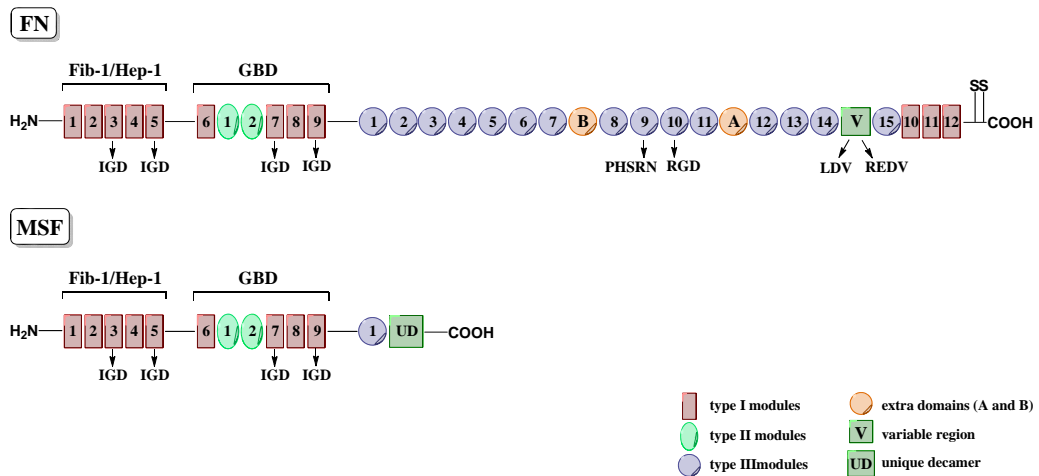


Figure 9. The modular structure of FN and MSF; known binding sequences (PHSRN, RGD, LDV, REDV) and novel IGD active motif are highlighted.

The motogenic activity of MSF has also been attributed to the IGD tri-amino acid motif. The MSF protein is essentially constructed of two FN's proteolytic fragments: Fib-1/Hep-1 and GBD (Figure 9). Each of these functional domains contains two IGD motifs located, respectively, in the third and fifth (Fib-1/Hep-1), seventh and ninth (GBD) type I modules of FN (Figure 9). However, only IGD sequences present within GBD of MSF appear to be active and available for relevant cell receptors. This was observed when a mutation of IGD to DGI in repeats seventh and ninth completely abolished MSF's bioactivity.² Consistently, proteolytically derived FNI₁₋₅ fragment was inactive. Thus, motogenic activity of MSF has been assigned only to IGD sequences presented within these two type I modules of FN (FNI₇ and FNI₉) (Figures 9 and 10).

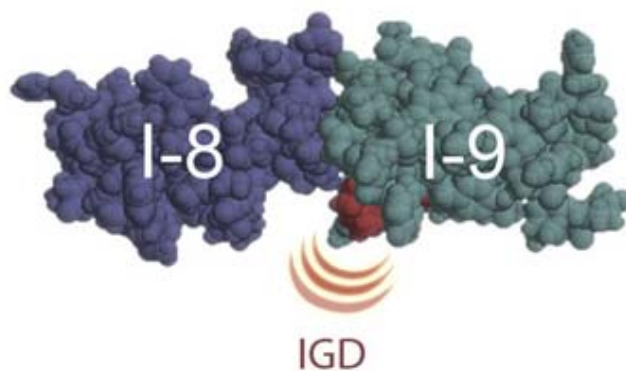


Figure 10. Schematic representation of IGD motif within the 9th type I module of FN, with neighbouring FNI₈.

Reprinted from *Current Opinion in Cell Biology*, 20, M. Leiss, K. Beckmanna, A. Girósa, M. Costella, R. Fässler, *The role of integrin binding sites in fibronectin matrix assembly in vivo*, p. 502-507, Copyright 2008, with permission from Elsevier

All three discussed proteins, MSF, GBD and full-length FN, contain number of IGD sequences. However, full-length FN is devoid of activity attributed to IGD. Preliminary results allow the speculation that the tertiary structures of these molecules play here a major role.⁶⁸ For instance, IGD-mediated bioactivity might be cryptic in native FN because of steric hindrance around the IGD amino acid sequences. However, the proteolytic digestion produces shorter GBD peptide with a different three-dimensional structure and possibly different conformational stability. As a result, IGD sequences of GBD are exposed through conformational change, hence no longer cryptic and fully available for interaction with cellular receptors. Similar reasoning applies to MSF. Potent motogenic activity mediated by MSF suggests that some IGD motifs had been exposed within this protein as a result of its native conformation.⁶⁹

Recently, Campbell and co-workers studied two active IGD motifs of MSF, present in the seventh and ninth FNI (FNI₇, FNI₉).⁶⁹ For the purpose of the experiments they cloned a series of human FN fragments, each containing at least one IGD motif: FNI₇-FNI₈, FNI₈-FNI₉, and FNI₇-FNI₈-FNI₉. A series of mutations within the active sequence, together with NMR studies and migration test assays, lead to several conclusions. Firstly, isoleucine is critical for the observed bioactivity of IGD motif, and secondly, any constrained protein with an IGD motif was more potent than short,

linear amino acid sequences carrying the IGD unit.⁶⁹ Thus, it seems that conformational constraints imposed on the IGD geometry may affect its interactions with its receptor.

1.2.2 First generation IGD peptidomimetics

The motogenic activity of MSF has rendered the protein a promising new drug candidate, and prompted work towards development of a synthetic, non-peptidic compound that could mimic its bioactivity. The early experiments showed that tri- and tetrapeptides that contain MSF active motif, the IGD sequence, exhibit significant motogenic activity.⁶⁸ Two of the tested synthetic peptides, Ile-Gly-Asp-Ser (IGDS) and Ile-Gly-Asp-Gln (IGDQ), were found to stimulate cell migration into a three-dimensional collagen gel at a concentration of 0.1 μ M.

However, the use of peptides as drugs tends to be associated with few problems. Synthetic peptides are usually poorly absorbed in the gastrointestinal tract and rapidly broken down by enzymes what results in their low bioavailability.⁷⁰ Therefore, efforts have been made to create non-peptidic molecular fragments that could “replace” active parts of native peptides and proteins in their biological functions. These compounds, termed “peptidomimetics”, have the advantage of being small, stable against human enzymes and able to cross biological membranes. However, they also carry higher risks of toxicity and potential of accumulation in the body. Despite these disadvantages, it is believed that peptidomimetic can display more favourable pharmacological properties than their prototypic peptides/proteins, such as improved receptor selectivity and potency.⁷⁰

The first generation of IGD peptidomimetics was design with respect to steric and electronic properties of the native IGD motif, identified as a minimal sequence required for biological activity of MSF.⁷¹ Firstly, the spatial arrangement of IGD tripeptide within FNI modules was analysed. The solution structures of several FNI modules of FN, including FNI₅ and FNI₇, have been previously calculated by high-resolution NMR.^{72,73} These studies revealed that IGD tripeptide is present within the

modules as a tightly constrained loop (Figure 11). The fact that the IGD motif is highly structured and has limited conformational mobility, strengthens the hypothesis that this motif is responsible for the binding and activation of the natural, and yet unidentified, MSF receptor.

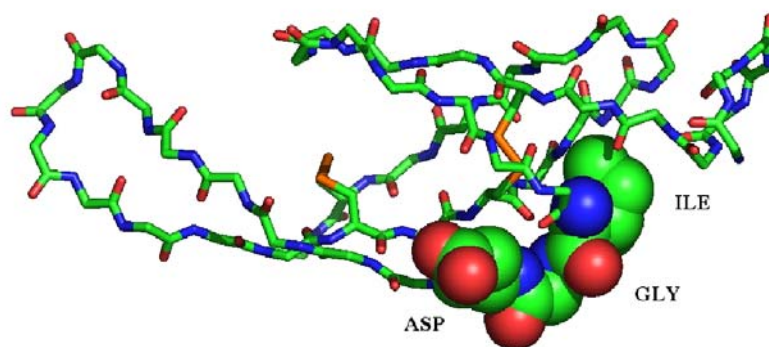


Figure 11. Three-dimensional structure of the FNI₇ module with highlighted IGD tripeptide motif.

Molecular BioSystems, 1, N. Shpiro, I. R. Ellis, T. J. Dines, A. M. Schor, S. L. Schor, D. G. Normand, R. Marquez, *Synthesis of an IGD peptidomimetic with motogenic activity*, p. 318-320, Copyright 2005, Reproduced by permission of The Royal Society of Chemistry

Computational methods, such as modelling studies and GAUSSIAN calculations were then used to design the IGD peptidomimetics' conformation to closely resemble the spatial arrangement of IGD tripeptide motif in native peptides (FN and MSF). Thus, the backbone dihedral angles observed in the native IGD sequences in FNI₅ and FNI₇ were measured. Based on this information, a number of small molecular weight entities that could potentially mimic the geometrical features of the IGD motif were selected. These structures were then optimised and their energy minimised using GAUSSIAN *ab initio* level calculations (using the hybrid SCF (self-consistent field) - DFT (density functional theory) method).⁷¹

Ultimately, it was determined that a benzodiazepine (BDP) unit (Figure 12, (B)) could exhibit structural similarity to the backbone conformation of native IGD tripeptide (Figure 12, (A)), while limiting the conformational mobility of the new molecule.⁷¹

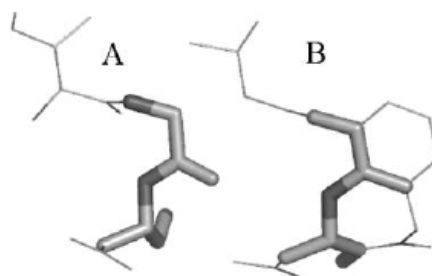
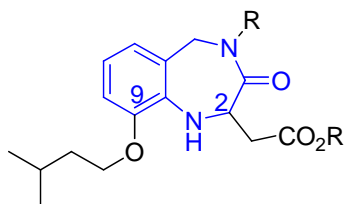


Figure 12. (A) Highlighted backbone bonds of the IGD tripeptide of MSF; (B) Highlighted bonds of the IGD peptidomimetic, which can mimic the IGD tripeptide conformation.

Molecular BioSystems, 1, N. Shpiro, I. R. Ellis, T. J. Dines, A. M. Schor, S. L. Schor, D. G. Normand, R. Marquez, *Synthesis of an IGD peptidomimetic with motogenic activity*, p. 318-320, Copyright 2005, Reproduced by permission of The Royal Society of Chemistry

Secondly, the electronic properties of the natural IGD tripeptide were considered. The amino acid sidechain functionalities are very important in terms of structure and biological activity of native IGD. Hydrophobic and steric effects might govern the protein folding and contribute to spatial arrangement of IGD sequence. Moreover, ionic interactions between amino acid residues and relevant receptor are likely to be responsible for the bioactivity of IGD motif. Thus, it was proposed that substitution at the C-2 and C-9 positions of the BDP skeleton should mimic, respectively, the aspartic acid and isoleucine residue of the native IGD tripeptide. Ultimately, combined model studies allowed designing the structure of first generation IGD peptidomimetics **1** as shown in Figure 13.⁷¹



1

Figure 13. The IGD peptidomimetic with highlighted 1,4-benzodiazepine core (blue), substituted in positions C-2 and C-9.

1.2.3 First synthesis of the IGD peptidomimetic

The first, model and racemic synthesis of IGD peptidomimetic ester **2**, bearing a methyl group at the nitrogen atom, was reported in 2005 (Figure 14).⁷¹

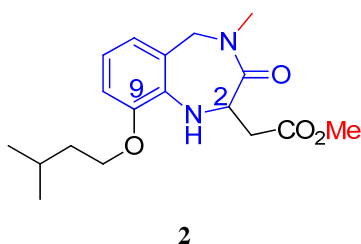
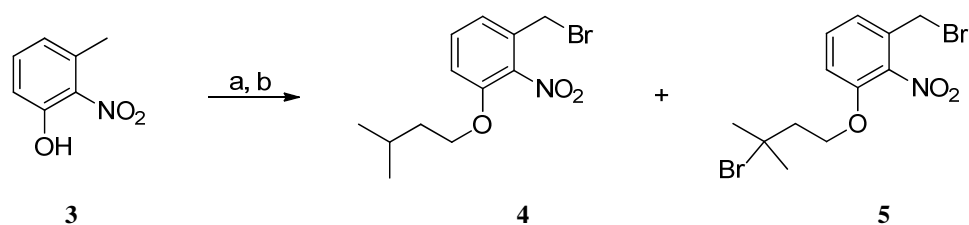


Figure 14. The targeted IGD peptidomimetic ester **2**.

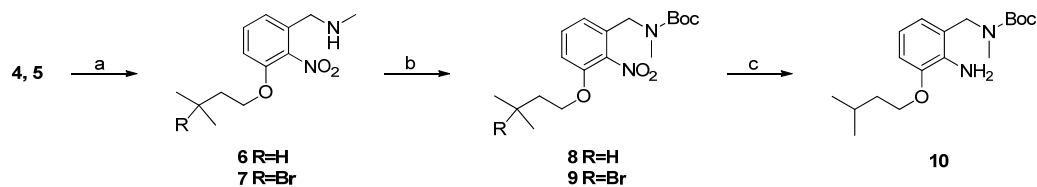
The synthesis of IGD mimetic **2** began with commercially available nitro-cresol **3**, which was alkylated and then brominated under radical conditions to generate compound **4**. Unfortunately, during the desired bromination of the benzylic methyl, the bromination of the alkyl side chain also took place, and led to significant amount of undesired compound **5**. Moreover, the separation of **4** and **5** was not possible (Scheme 2). Despite extensive investigation, the best yield obtained for the bromination step was 43%.



Scheme 2. *Reagents and conditions:* a) isobutyl bromide, K_2CO_3 , DMF, rt, 25 h, b) *N*-bromosuccinimide, azobisisobutyronitrile, CCl_4 , reflux, 12 h, 43% over 2 steps.

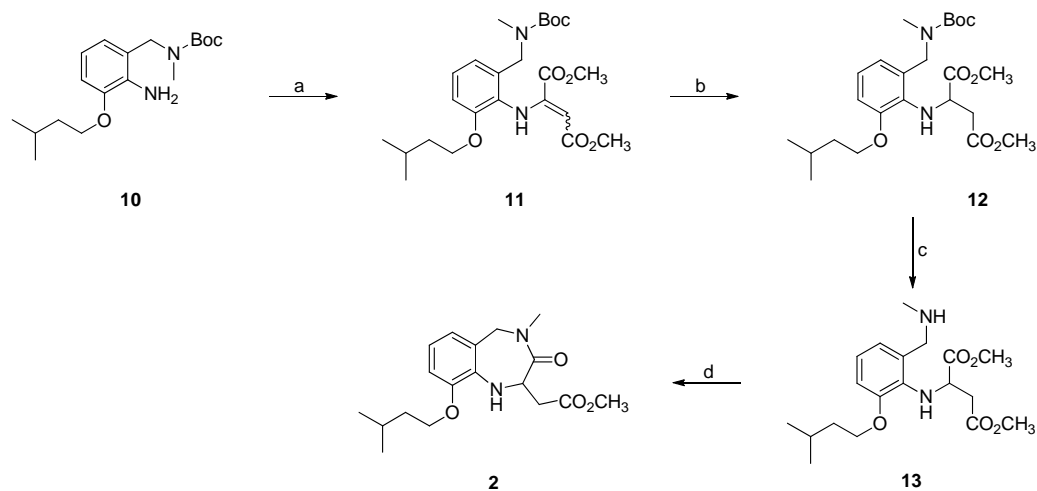
The synthesis was continued using the mixture of compounds **4** and **5**. Nucleophilic substitution of the benzylic bromides **4** and **5** with methylamine produced **6** and **7** respectively. Following protection of benzylic amines **6** and **7** with the *tert*-butyloxycarbonyl (Boc) group provided **8** and **9**. At this stage, Pd/C catalysed

hydrogenation reduced both the nitro functionality of **8** and **9** along with the tertiary bromide of **9** to produce cleanly the free amine unit **10** as a single compound (Scheme 3).



Scheme 3. Reagents and conditions: a) CH_3NH_2 (40% in water), THF, 12 h, rt, b) $(\text{Boc})_2\text{O}$, Et_3N , DMAP, CH_2Cl_2 , 0 °C to rt, 84% over 2 steps, c) Pd/C (10%), H_2 , CH_3OH , rt, 3 h, 75%.

As anticipated, condensation of aniline **10** with dimethyl acetylenedicarboxylate (DMAD) furnished compound **11**. The Pd-catalysed reduction of the double bond of **11** produced intermediate **12**. The next step, removal of Boc group, was accomplished by treatment of **12** with trifluoroacetic acid (TFA). The resulting free amine **13** was then exposed to basic conditions to furnish final compound - IGD peptidomimetic **2** (Scheme 4).



Scheme 4. Reagents and conditions: a) DMAD, CH_3OH , reflux, 1 h, 85%, b) Pd/C (10%), H_2 , CH_3OH , 30 min, 58%, c) TFA, DCM, 0 °C, 1 h, 96%, d) NaOCH_3 (25% in CH_3OH), 1 h, 45–77%.

The anticipated motogenic activity of racemic IGD mimetic **2** was tested using a cell migration assay.⁷¹ This method measured the movement of human fibroblast into a three-dimensional collagen matrix. The IGD mimetic **2** was found to stimulate cell migration in a dose-dependent fashion, as shown in Figure 15. Importantly, the potency of mimetic **2** was comparable with that of previously synthesised tripeptide IGDS.⁶⁸ The control reverse peptide Ser-Asp-Gly-Ile (SDGI) was devoid of biological activity under conditions of the assay.

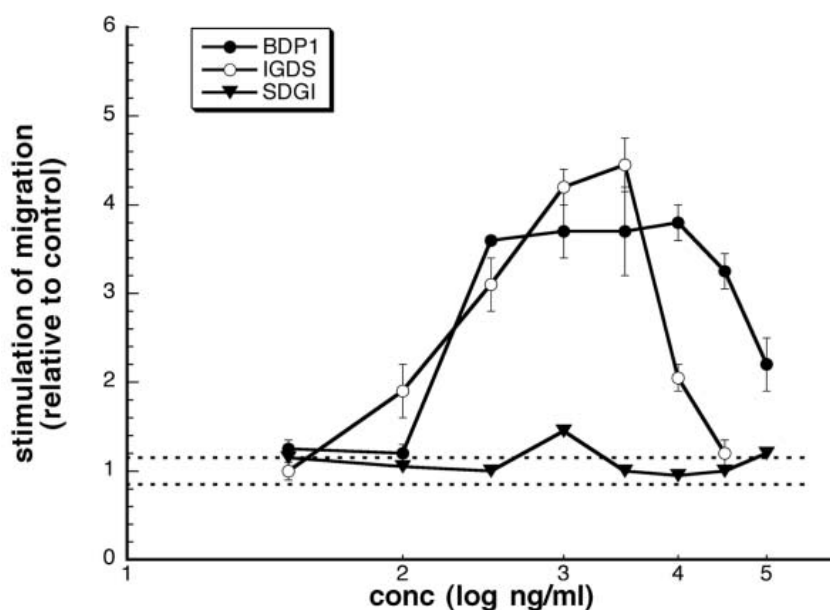


Figure 15. The motogenic activity of IGD mimetic **2** (here denoted as BDP1), synthetic peptide IGDS and control compound SDGI. Data are expressed as fold-stimulation of migration relative to control fibroblast in the absence of the test compound. The range of baseline migration is indicated by dotted lines.

Molecular BioSystems, 1, N. Shpiro, I. R. Ellis, T. J. Dines, A. M. Schor, S. L. Schor, D. G. Normand, R. Marquez, *Synthesis of an IGD peptidomimetic with motogenic activity*, p. 318-320, Copyright 2005, Reproduced by permission of The Royal Society of Chemistry

2.0 Results and discussion

2.1 The aim of the project

The ultimate objective of the *IGD project* was to synthesise the IGD peptidomimetic **2** (Figure 16) and its derivatives that could mimic the biological activity of the MSF in terms of stimulation of cell migration. The MSF protein is known to modulate diverse biological processes, and hence provides opportunity to research several different human disorders. However, our project is primarily focusing on studying the motogenic activity of MSF. Through our research we are hoping to gain better knowledge about cell migration in wound healing processes. We are expecting that synthetic IGD mimetics could be a first step towards a new treatment of wounds with impaired healing. We are planning to evaluate the anticipated agonistic activity of IGD peptidomimetics in series of biological tests.

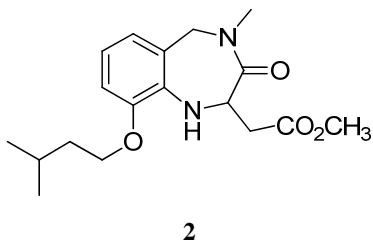


Figure 16. The structure of the IGD peptidomimetic **2**.

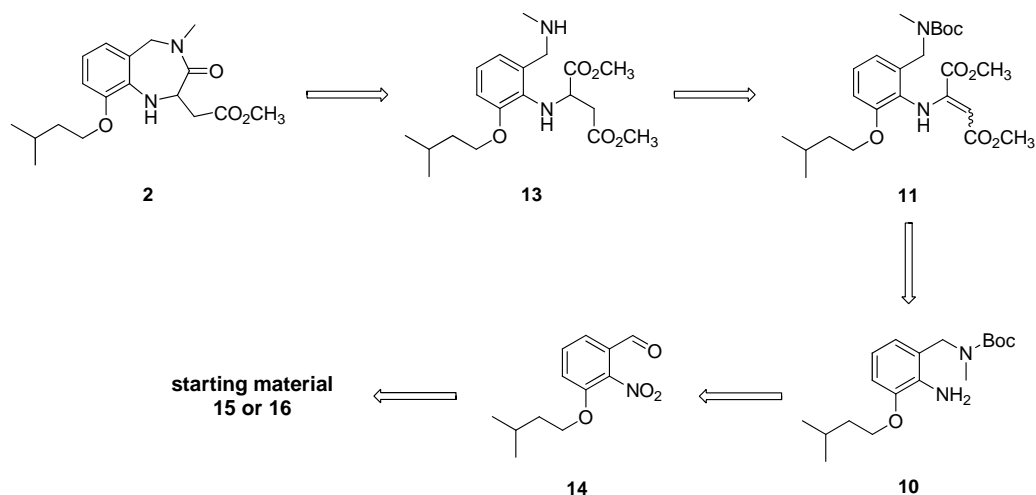
The IGD mimetic ester **2** (Figure 16) was previously synthesised in the Marquez group.⁷¹ However, this prototypic synthesis suffered from several problematic and low-yielding steps. Therefore, the first objective of the project was to revise and optimise the existing synthetic route to mimetic **2**. The new synthesis should be high-yielding, and relatively simple because of the view for possible industrial application. After optimising the reaction conditions *via* a model, racemic synthesis, we planned to develop a stereospecific synthesis for both enantiomers of IGD peptidomimetic **2**.

We are also planning to assess the biological activity of synthesised IGD mimetics. Preliminary results showed that IGD mimetic **2** can efficiently stimulate cell migration.⁶⁸ Hence, it is speculated that enantiomers of **2** and its structural derivatives can show increased potency or altered biological action.

For the purpose of evaluating the biological profile of the IGD peptidomimetics, and also considering further applications, we proposed to synthesise a photolabile trigger, which can be coupled to derivatives of the IGD peptidomimetic **2**. The photolabile group was chosen carefully, taking into consideration its chemical and biochemical properties. The photolabile protecting group should mask the bioactivity of the IGD mimetic, thus making it inert, until it reaches the target site. It should allow us to carry out kinetic and biological investigations that might lead to identification of the receptor for MSF.

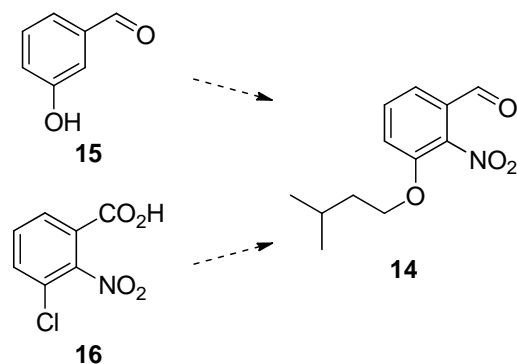
2.1.1 Model synthesis of the IGD peptidomimetic

A revised strategy to the IGD peptidomimetic **2** is outlined in Scheme 5. Our new approach required several changes in the previously established synthesis. Thus, we anticipated that benzodiazepine **2** could be obtained from enamine **13** *via* a ring-closing reaction. Requisite enamine **13** would in turn be prepared by condensation of aniline **10** and DMAD, followed by double-bond reduction and Boc-deprotection, accordingly to the previously established procedure.⁷¹ Finally, we envisioned that aniline **10** could be accessed from a new key intermediate, nitrobenzaldehyde **14**. We anticipated to prepare the crucial aldehyde **14** in a few simple, high yielding steps from commercially available materials.



Scheme 5. Retrosynthetic analysis of IGD peptidomimetic **2**.

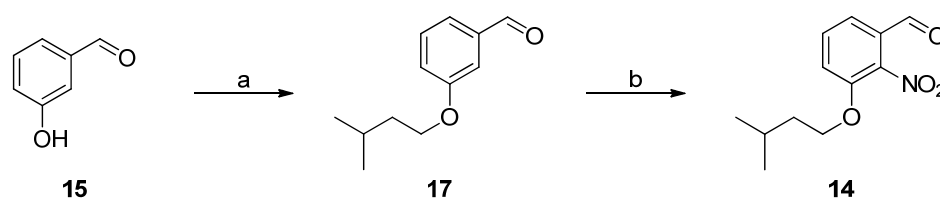
Our initial efforts focused on the synthesis of nitrobenzaldehyde **14**. We investigated two distinct approaches to the aldehyde **14**, utilizing either 3-hydroxybenzaldehyde **15** or 3-chloro-2-nitrobenzoic acid **16** (Scheme 6).



Scheme 6. Two different starting materials for the preparation of intermediate **14**.

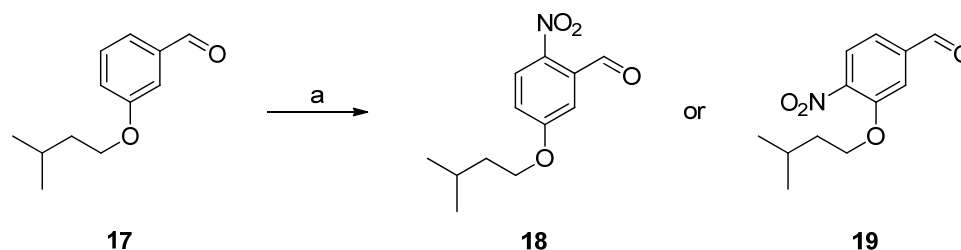
The first synthetic approach anticipated that nitrobenzaldehyde **14** could be quickly obtained from commercially available 3-hydroxybenzaldehyde **15**. This two-step synthesis required alkylation of hydroxyl functionality and nitration of the aromatic ring (Scheme 7). Thus, we began the synthesis of compound **14** by alkylation of **15** that lead successfully to aldehyde **17**. Nitration of aromatic aldehyde **17** with

nitronium tetrafluoroborate generated the desired *o*-substituted aromatic aldehyde **14**, together with nitration side products in good yield. After careful separation, however, the desired nitroaldehyde **14** was isolated in an acceptable 23% yield. Investigation of the reaction conditions allowed us to identify that the most suitable reaction temperature is $-28\text{ }^{\circ}\text{C}$. Maintaining this temperature while extending reaction time to 22 hours provided the desired isomer **14** in 53% yield. Unfortunately, despite our effort, we weren't able to reproduce this yield on a larger scale (4 g), mainly due to troublesome separation (Scheme 7).



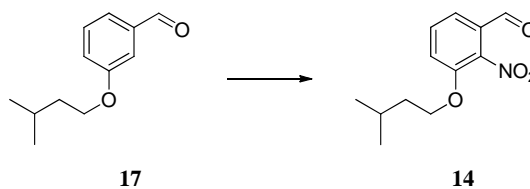
Scheme 7. Reagents and Conditions: a) K_2CO_3 , 1-bromo-3-methylbutane, DMF, 96%, b) NO_2BF_4 , DCM, $-28\text{ }^{\circ}\text{C}$, 22 h, 53%.

While nitration with nitronium tetrafluoroborate gave moderate yields, application of other mild reagents failed to generate *o*-nitrobenzaldehyde **14**. Treatment of compound **16** with reagent system $\text{Ph}_3\text{P}/\text{Br}_2/\text{AgNO}_3$ afforded cleanly and almost exclusively one of the mono-nitrated regioisomers, but not the desired one.⁷⁴ A splitting pattern that appeared on ^1H NMR spectrum in the aromatic region, combined with two-dimensional NMR data (COSY, HSQC, HMBC), clearly suggested that we synthesised one of two nitro regio-isomers, **18** and **19** (Scheme 8). This result indicated a clear preference for an electrophilic substitution under applied conditions to proceed at the one of the less sterically hindered position on the aromatic ring.



Scheme 8. Reagents and Conditions: a) $\text{Ph}_3\text{P}/\text{Br}_2/\text{AgNO}_3$, MeCN, rt, 98%.

Suprisingly, nitration of **17** with ceric ammonium nitrate (CAN) generated only traces of nitrated compound, leaving the starting material almost untouched.⁷⁵ (Table 1).



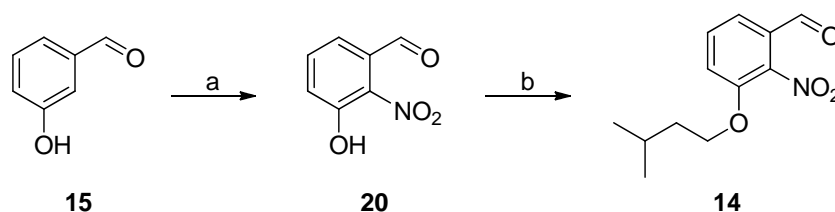
Entry	Reaction conditions	Yield of 14 (%)
1	BH_4NO_2 , MeCN, $-23\text{ }^\circ\text{C}$, o/n	23
2	BH_4NO_2 , MeCN, $-28\text{ }^\circ\text{C}$, 22 h	53 *
3	Ph_3P , Br_2 , AgNO_3 , MeCN, rt	0
4	CAN, MeCN, rt	untouched SM

* yield not reproducible during scale-up

Table 1. Aromatic nitration of compound **17**.

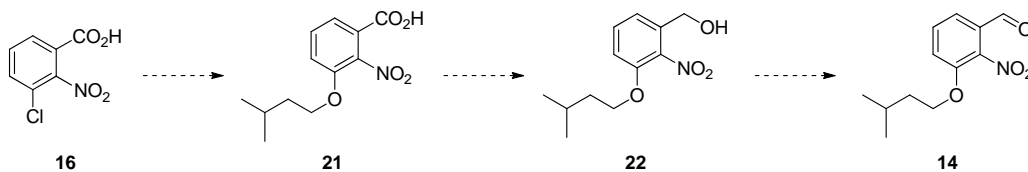
Finally, we applied alternative conditions for the regioselective, *ortho*-directed nitration of aromatic phenols.⁷⁶ Thus, we began the synthesis by treatment of free phenol **15** with a reagent system, comprising of tetrabutylammonium hydrogen sulphate (TBAHS), isopropyl nitrate (IPN) and sulphuric acid. While conducted in room temperature, the reaction delivered *o*-nitrobenzaldehyde **20** in 40% yield. Lowering the reaction temperature to $-15\text{ }^\circ\text{C}$ improved the yield to 56%. The advantage of this nitration method was easy purification of desired nitroaldehyde **20**, which precipitated from diethyl ether, and could be isolated by filtration. Moreover, in contrast to the results obtained previously (with nitronium tetrafluoroborate as

nitrating agent), this procedure produced comparable yields during scale-up (10 g). The next step, alkylation of compound **20**, was accomplished routinely with 1-bromo-3-methylbutane in the presence of a mild base to give ether **14** in very good 78% yield (Scheme 9).



Scheme 9. Reagents and Conditions: a) TBAHS, IPN, H₂SO₄, DCM, -15 °C, 56%, b) (CH₃)₂CHCH₂CH₂Br, K₂CO₃, DMF, 78%.

In parallel, we investigated the synthesis of **14** starting from commercially available 3-chloro-2-nitrobenzoic acid **16**. The plan assumed nucleophilic aromatic substitution of chlorine by alkoxide, which can be achieved with mixture of 3-methylbutanol/NaH. The acid **21** could then be treated with borane-tetrahydrofuran complex to furnish alcohol **22**, which in turn can be oxidised to the desired aldehyde **14** under Swern conditions (Scheme 10). This sequence, if successful, would allow us to prepare compound **14** without the need for nitration of the aromatic ring.



Scheme 10. Alternative route to intermediate **14**.

However, rather surprisingly, this synthetic approach resulted in the formation of an unexpected product, which was isolated and characterised. The ¹H NMR analysis revealed that the new compound was an aromatic aldehyde substituted in the ring by 3-methylbutoxy group. It was also deduced that aromatic ring carried a third

substituent; however, since the splitting pattern in the aromatic region of the spectrum differed from the one of previously synthesised aldehyde **14**, the presence of nitro group in the molecule was in doubt. In order to rule out any influence of the sample concentration on the NMR spectrum, aldehyde **14** and unexpected product were combined in one sample which was then analysed by ^1H NMR. The obtained spectrum revealed the presence of two different aldehyde signals. The presence of two separate species was further confirmed by TLC analysis and a series of 1-D and 2-D NMR experiments. Mass spectrum of the new product also failed to provide the required molecular ion peak (expected at $m/z = 237.2$), previously detected for the aldehyde **14**.

Interestingly, the mass spectrum of the 'new' aldehyde showed a characteristic fragmentation pattern, notably a chlorine isotopic signature. The molecular ion peak at 226 was accompanied by an additional molecular peak at 228, which strongly indicated the presence of a single chlorine atom in the molecule. The natural abundance of ^{35}Cl (75%) and ^{37}Cl (25%) was reflected in the observed 3:1 ratio of relative peak intensities. Further, analysis of other fragment ions revealed additional sets of peaks separated by two m/z units, confirming the presence of chlorine isotopes.

Further structural evidence was obtained from IR analysis. The IR spectrum of the previously synthesised aldehyde **14** showed two strong absorption bands at 1535 cm^{-1} and 1284 cm^{-1} ; a result of N-O asymmetric and N-O symmetric stretching respectively. Moreover, NO_2 scissor vibrations gave rise to band of medium strength at 837 cm^{-1} . On the contrary, spectrum of new aldehyde was lacking all infrared bands characteristic for the aromatic nitro group.⁷⁷

Based on all the collected experimental evidence we concluded that the newly obtained aldehyde was one of two possible structures, **23** and **24** (Figure 17). For example, mass spectra analysis with an electron impact ionisation (EI) detected the molecular ion $[\text{M}]^+$ at 226, which supports both structures **23** and **24**. The accurate mass of the product was then further confirmed by HRMS (observed m/z 226.0762).

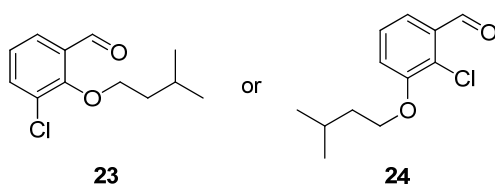
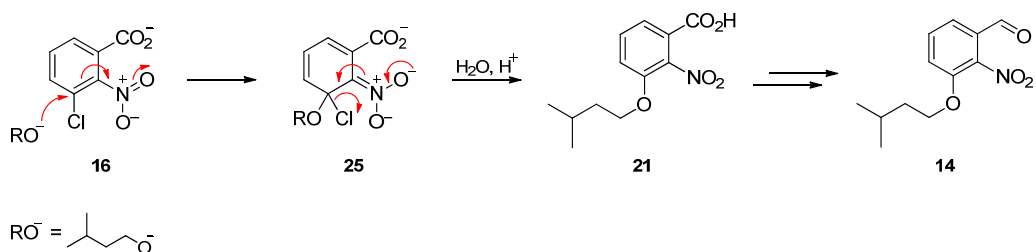


Figure 17. Two possible structures of new aldehyde.

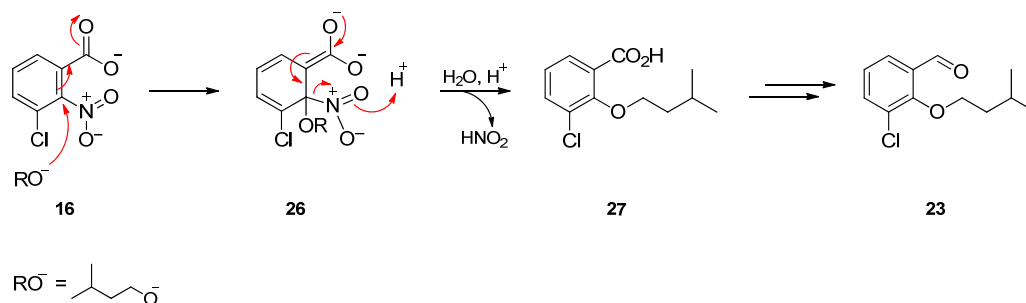
Based on the obtained analytical results, differentiation between regioisomeric aldehydes **23** and **24**, and unambiguous identification of the product structure was not possible. However, we proposed a reaction mechanism that can rationalise the formation of aldehyde **23**. We postulate that the nitro group was lost during nucleophilic aromatic substitution on acid **16**, which was the first step of the alternative synthetic approach (see Scheme 10). We had hoped for this reaction to proceed according to the expected addition-elimination mechanism, whereby an alkoxide anion would attack the chlorine position *ortho* to the nitro group of the acid **16** (Scheme 11). Electrons from the ring would then be delocalised on the strongly electron-withdrawing nitro group in the intermediate **25** (Scheme 11). Rearomatisation of the ring and expulsion of the chloride ion would generate desired aromatic nitro benzoic acid **21**, which could be converted to the aldehyde **14** according to the proposed alternative route.



Scheme 11. Expected addition-elimination mechanism.

However, as established, the product of the alternative synthetic approach was lacking the nitro group. Thus, in order to account for the loss of nitro functionality, we propose an alternative mechanism. We speculate that alkoxide anion could attack the nitro group position *ortho* to the carboxylic acid functionality of compound **16** (Scheme 12). Delocalization of electrons from the ring onto electron-withdrawing

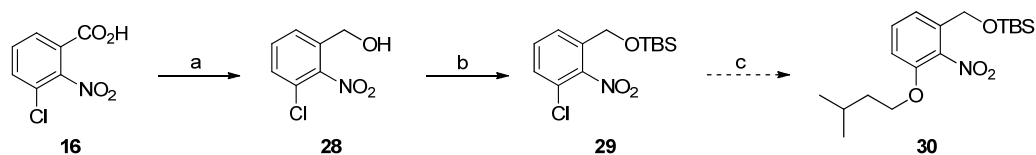
carboxylic acid group would form intermediate **26**. Rearomatisation of the ring and elimination of nitrous acid would produce benzoic acid **27**. Reduction of the acid function as proposed in the alternative approach could ultimately generate the aldehyde **23**.



Scheme 12. Speculative mechanism to explain formation of acid **27** and aldehyde **23**.

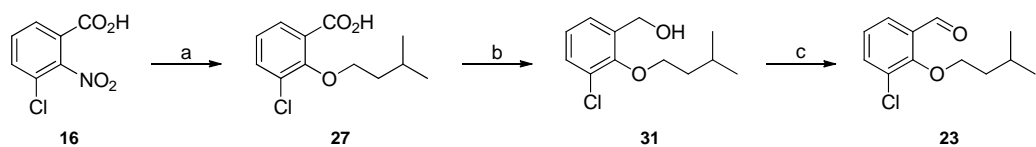
In the postulated mechanism the nitro group acts as a leaving group. This characteristic of nitro function has been reported previously; it was shown that nitro group in nucleophilic aromatic substitution may rival the leaving group capacity of e.g. chloride⁷⁸ or fluoride⁷⁹. Thus, it is not unusual for nitro group to undergo nucleophilic displacement.

We also speculate that the presence of the carboxylic acid functionality *ortho* to the nitro group is the reason for the observed loss of nitro group during the nucleophilic aromatic substitution reaction. It was thought that by masking the electron-withdrawing capacity of carboxylic acid group of **16** it would be possible to displace chlorine ion with alkoxide, retaining the nitro group. Hence, in order to investigate this theory, we were carried out additional experiments, in which the carboxylic acid **16** was reduced to alcohol **28** and subsequently protected as the silyl ether **29** (Scheme 13). Compound **29** was then exposed to mixture of 3-methylbutanol/NaH, but the reaction failed to generate even traces of desired nitrobenzaldehyde **30**.



Scheme 13. *Reagents and Conditions:* a) $\text{BH}_3 \cdot \text{THF}$, THF, 0 °C to rt, b) imidazole, TBSCl, DMF, rt, 84% over 2 steps, c) NaH, $(\text{CH}_3)_2\text{CHCH}_2\text{CH}_2\text{OH}$, DMF.

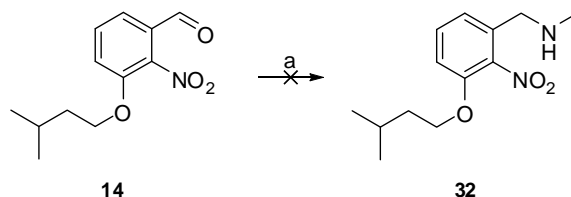
Finally, supported by mechanistic consideration, we postulate that structure of alternative aldehyde is more likely to be represented by compound **23** than **24**. There is no known mechanism that could account for the formation of regioisomeric aldehyde **24**. Hence, we believe that the alternative synthetic route which utilise acid **16** as starting material, ultimately produced the benzaldehyde **23** as presented in Scheme 14.



Scheme 14. *Reagents and Conditions:* a) NaH, $(\text{CH}_3)_2\text{CHCH}_2\text{CH}_2\text{OH}$, DMF, b) $\text{BH}_3 \cdot \text{THF}$, THF, 0 °C to rt, 93% over 2 steps, c) oxalyl chloride, DMSO, Et_3N , 84%.

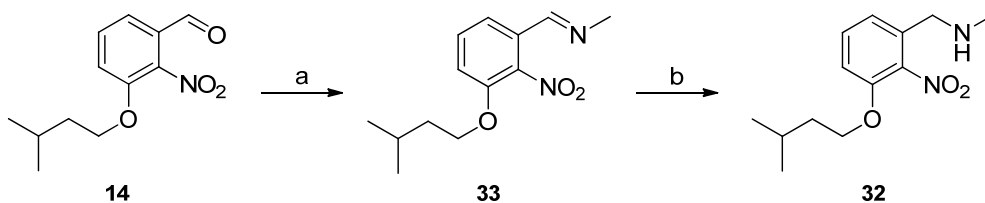
At this stage of our investigations, the nitration of aromatic phenol **15** followed by alkoxy group introduction, proved to be the most successful, efficient and suitable sequence for the synthesis of nitrobenzaldehyde **14** (see Scheme 9). Thus, having established the method for preparation of intermediate **14**, we turned our attention towards the next transformation, the reductive amination of the aldehyde group. We followed the work of Sato who reported a one-pot reductive amination with α -picoline borane (pic-BH_3).⁸⁰ α -Picoline borane and other amine-borane complexes are classical reducing agents for a variety of functional groups, including aldehydes, ketones, esters and nitriles. More importantly, they are capable of reducing a nitro group only in the presence of metal complexes *via* transition metal catalysed hydrogenation. Thus, under applied conditions, we expected the nitro functionality

of **14** to be unaffected. However, in our hands application of α -picoline borane as a reducing agent failed to generate amine **32** (Scheme 15).



Scheme 15. Reagents and Conditions: a) CH_3NH_2 , pic-BH₃, MeOH, rt.

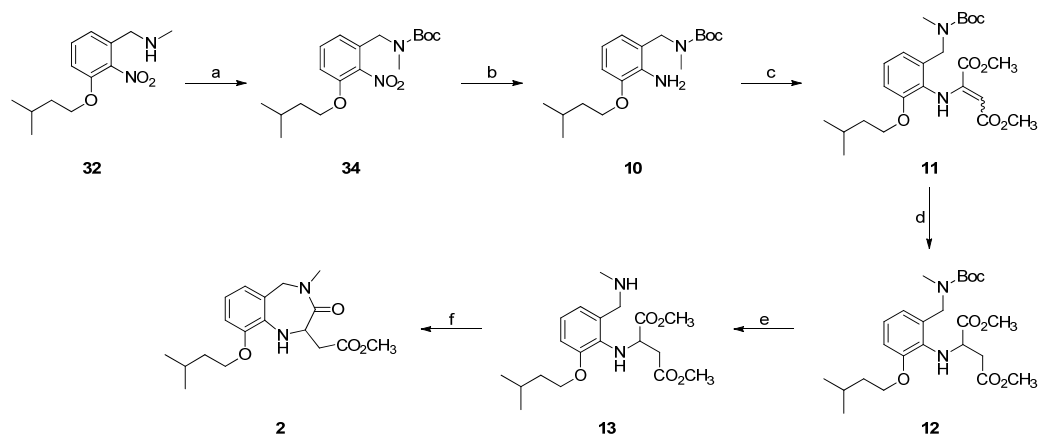
Since the one-pot transformation proved unsuccessful, a two-step reductive amination procedure was employed. Benzaldehyde **14** was reacted with aqueous methylamine in heptane to form an imine intermediate **33**, which was then extracted from the biphasic mixture and immediately reduced to amine **32** with sodium borohydride.⁸¹ It has been reported previously, that sodium borohydride could be successfully used for the preparation of nitro-containing amines.⁸² Indeed, under these conditions, imine **33** was selectively reduced in the presence of the nitro group. The reaction was clean, rapid and produced an amine **32** in excellent yield (94% from aldehyde **14**) (Scheme 16). Both compounds, **33** and **32**, could be isolated and stored for several weeks at low temperature ($-20\text{ }^\circ\text{C}$).



Scheme 16. Reagents and Conditions: a) CH_3NH_2 , heptane, rt, b) NaBH_4 , MeOH, rt, 94% from **14**.

To complete the synthesis of the racemic IGD peptidomimetic, we followed the procedure previously developed in the Marquez group. Thus, to reduce the nitro functionality efficiently, we protected amine **32** with a Boc group. Subsequent palladium catalysed hydrogenation of the nitro group of **34** gave expected aniline **10** in excellent yield (100%). Condensation of **10** with dimethyl acetylenedicarboxylate

(DMAD) generated enamine **11** as a single compound, which was then successfully converted to **12** by catalytic hydrogenation. Treatment of the racemic compound **12** with trifluoroacetic acid afforded the free amine **13** in good yield. After careful work-up, amine **13** was submitted to final ring closure reaction under basic conditions (Scheme 17). This transformation successfully accomplished the model synthesis of racemic IGD peptidomimetic **2**.



Scheme 17. Reagents and Conditions: a) $(\text{Boc})_2\text{O}$, Et_3N , THF, 93%, b) Pd/C, H_2 , MeOH, quantitative, c) DMAD, MeOH, reflux, 80%, d) $\text{Pd}(\text{OH})_2$, H_2 , MeOH, 90%, e) TFA, DCM, 82%, f) NaOMe, MeOH, reflux, 62%.

2.1.2 Enantiospecific synthesis of (*R*)-IGD peptidomimetic

Having developed an efficient, model synthesis of racemic IGD peptidomimetic **2**, we focused our efforts on establishing an analogues route to enantiomerically pure (*R*)-IGD ester **2a**. The IGD molecule has one asymmetric carbon atom in position two of benzodiazepine skeleton, enabling it to exist in two enantiomeric configurations (Figure 18). Previously performed modelling studies and GAUSSIAN calculations suggested that the (*R*) stereoisomer of IGD molecule would more closely resemble the geometrical features and spatial orientation of IGD tripeptide motif of MSF. Therefore we speculated that the (*R*)-IGD mimetic **2a** might have higher binding affinity to natural receptor of MSF than the (*S*)-IGD **2b**. Hence, the (*R*)-IGD mimetic would be potentially a more potent agonist of MSF than racemic IGD molecule or its (*S*) enantiomer. Moreover, the chirality of the IGD mimetic could

also have an effect on its toxicity as well as overall pharmacokinetic and pharmacodynamic profile.

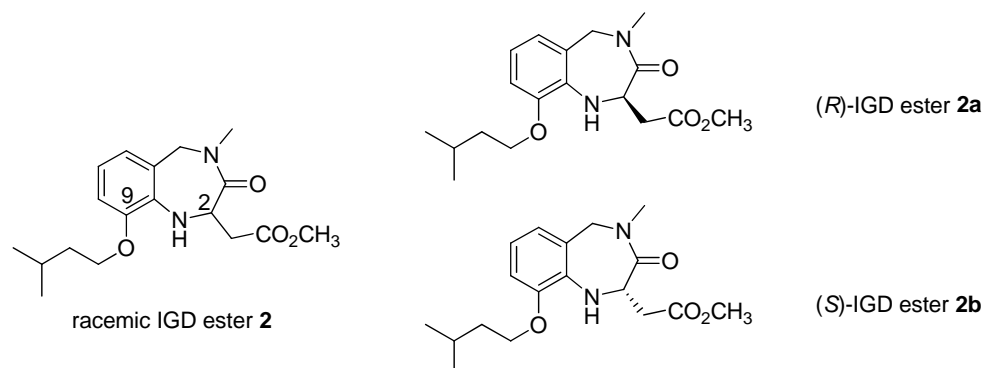
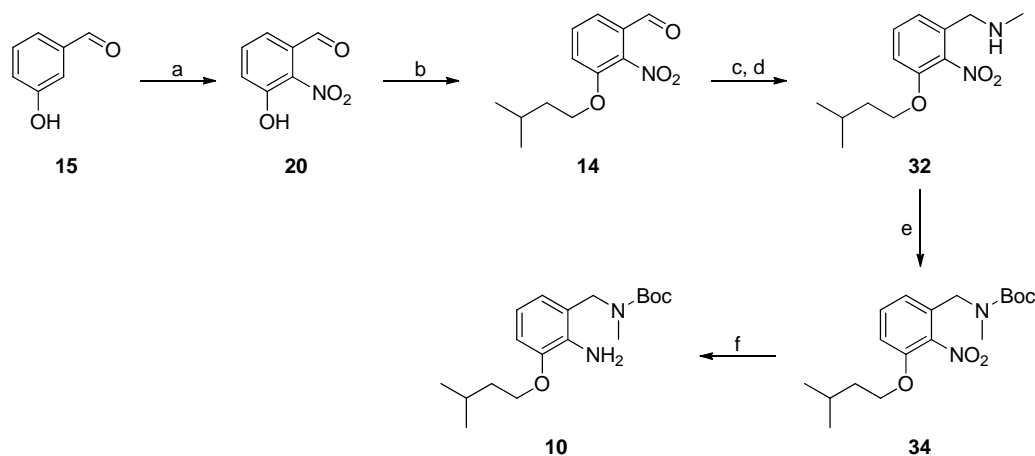


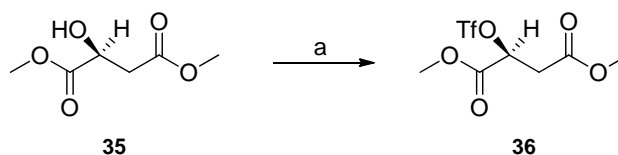
Figure 18. Racemic IGD peptidomimetic ester **2** and its enantiomers.

The previously established approach to the synthesis of racemic IGD mimetic **2** was now adapted towards the synthesis of (*R*)-IGD ester **2a**. Therefore, we started the synthesis of ester **2a** by preparation of common intermediate, aniline **10**, utilising our optimised synthetic procedures. Nitration of 3-hydroxybenzaldehyde **15**, followed by alkylation of intermediate **20**, afforded aldehyde **14**, which was transformed to amine **32** *via* two-steps reductive amination (Scheme 18). After Boc-protection, the resulting compound **34** was submitted to catalytic hydrogenation to furnish aniline **10**.



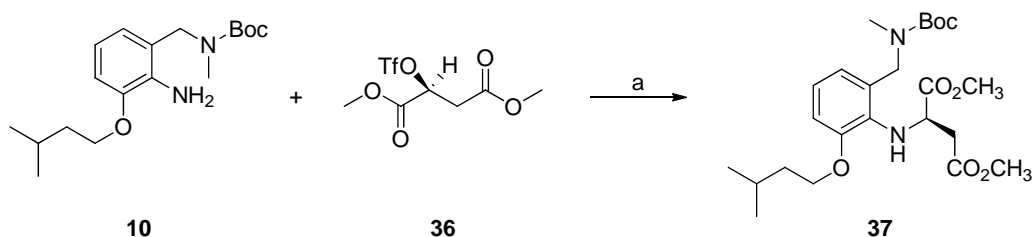
Scheme 18. Reagents and Conditions: a) TBAHS, IPN, H₂SO₄, DCM, -15 °C, 56%, b) (CH₃)₂CHCH₂CH₂Br, K₂CO₃, DMF, rt, 77%, c) CH₃NH₂, heptane, rt, d) NaBH₄, MeOH, rt, 94% from **14**, e) (Boc)₂O, Et₃N, THF, rt, 93%, f) Pd/C, H₂, MeOH, rt, quantitative.

At this point of the synthesis, we turned our attention towards introducing the desired chirality into the molecule. Although a number of approaches and methods were considered, we had found that S_N2 displacement of enantiopure triflate **36** (Scheme 19) with aniline **10** could provide us with both the required functional unit and the requisite stereochemistry.⁸³ Thus, optically pure triflate **36** was prepared in one step from commercially available dimethyl (*S*)-(-) malate **35** in excellent yield (100%) (Scheme 19).



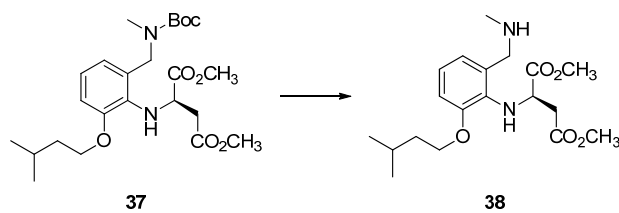
Scheme 19. Reagents and Conditions: a) (Tf)₂O, 2,6-lutidine, DCM, -78 °C, 100%.

As expected, the employed S_N2 reaction of chiral agent **36** with aniline **10** proceeded with inversion of configuration and furnished compound **37** as single (*R*) enantiomer (Scheme 20).



Scheme 20. Reagents and Conditions: a) 2,6-lutidine, DCM, reflux, quantitative

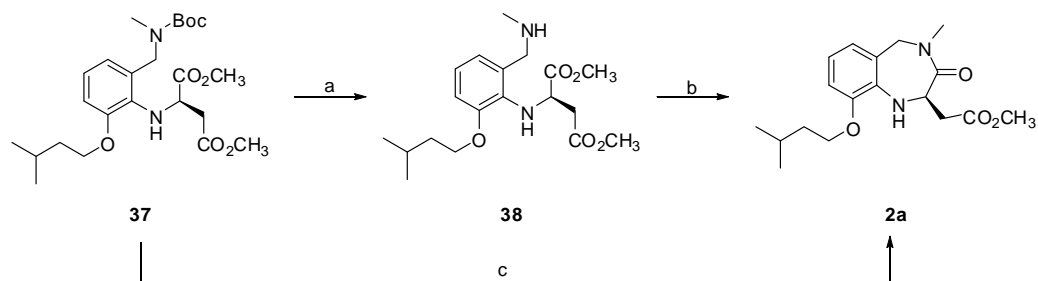
Having successfully introduced the desired stereocentre, we focused our effort on the final stages of the synthesis. Subsequent treatment of compound **37** with trifluoroacetic acid failed to remove the Boc protecting group as expected. This was surprising, since the same transformation under these conditions had been readily achieved during the synthesis of the racemic IGD ester **2**. Thus, after investigation of other reagents for Boc-deprotection, the removal of Boc group was finally accomplished using 5% HCl in ethyl acetate to furnish amine **38** (Table 2).⁸⁴



Entry	Reaction conditions	Yield (%)
1	TFA (1 eq), DCM	0
2	TFA (2 eq), DCM	0
3	5% HCl in MeOH	40
4	5% HCl in EtOAc	100

Table 2. Boc-deprotection of compound **37**.

During the course of investigation of reaction conditions for removal of Boc group, we had found that this transformation could produce directly an ester **2a**. It was observed that Boc-deprotection of compound **37** with HCl/EtOAc, followed by purification of crude reaction mixture by FCC with MeOH/DCM as a solvent system, resulted in a formation of final ester **2a**. Experimental evidence indicated that Boc-deprotection reaction did not itself produce the ester **2a**, but expected amine **38**, as confirmed by TLC and NMR of the crude reaction mixture. Therefore, it is believed that basic elution conditions on a column catalysed the cyclization of amine **38** to benzodiazepine **2a**. Consequently, in a next experiment, an amine **38** was isolated only upon aqueous work-up, analysed and judged clean by NMR and MS analysis. Next, crude amine **38** was treated with sodium methoxide, what furnished cleanly and in a very good yield (85%) the final (*R*)-IGD ester **2a** (Scheme 21).



Scheme 21. Reagents and Conditions: a) 5% HCl in EtOAc, rt, quantitative, b) NaOMe, MeOH, reflux, 85%, c) 5% HCl in EtOAc, then FCC 5% MeOH/DCM, 43%.

To verify the optical purity of the synthesised (*R*)-IGD mimetic ester **2a**, analytical chiral HPLC analyses were performed. The racemic IGD ester **2** and (*R*)-IGD ester **2a** were fractionated on OD-H chiral column that had a stationary phase consisting of cellulose tris(3,5-dimethylphenylcarbamate). Firstly, the racemic mixture was successfully resolved and shown to contain equal amounts of (*R*) and (*S*) enantiomers (49.3% and 50.7%). Then, the enantiomeric purity of the (*R*)-IGD **2a** was assessed, and was found to have satisfactory enantiomeric excess of 94.9% (Figure 19).

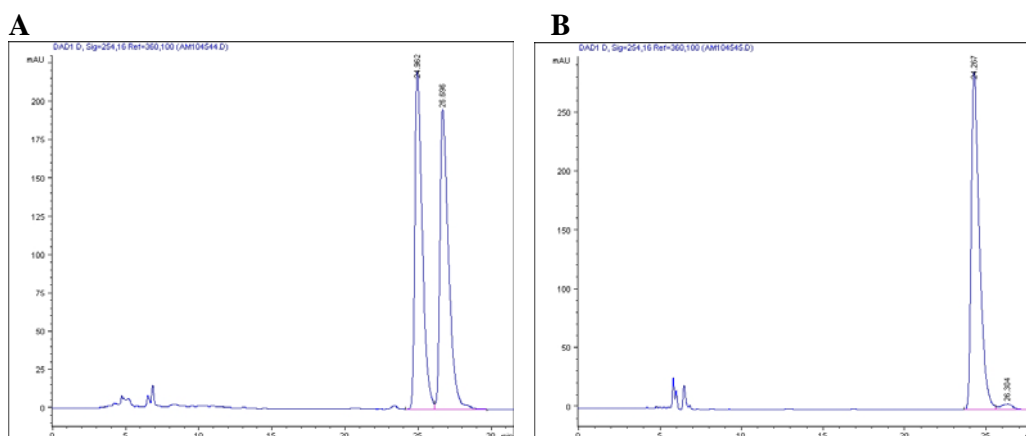


Figure 19. Chiral HPLC analysis; **A)** Racemic IGD ester, **B)** (*R*)-IGD ester.

In conclusion, the (*R*)-IGD peptidomimetic ester **2a** was synthesised in 9 steps and 32.4% overall yield. In addition to the satisfactory yield, the established methodology allows scaling up the synthesis without losing the excellent yields for each conversion step. Moreover, purification by FCC is required only for 1 intermediate and a final product. Thus, our synthetic protocol has great potential for possible industrial applications.

2.1.3 Short synthesis of a photolabile group

Photolabile protecting groups, also termed “caging” groups, have been known since the early 1960s.⁸⁵ Such compounds differ from traditional protecting groups in being

removable by the use of light at various wavelengths, instead of chemical reagents. Many different classes of caging groups, like benzoin, cinnamoyl, coumaryl, 2-nitrobenzyl or phenacyl, have found applications in synthetic chemistry⁸⁶, biology and biotechnology⁸⁷. Besides their application in organic synthesis as orthogonal protecting groups, they have been extensively used in biology for caging various biologically active molecules, such as antibodies,⁸⁸ Ca²⁺ ions,⁸⁹ nucleotides,⁹⁰ peptides,⁹¹ and mRNA.⁹²

Currently, photolabile protecting groups are one of the most powerful tools for studying physiological processes as well as the properties of bioactive molecules. Many different classes of small molecules, such as amino acids, steroids, ATP and neurotransmitters have been caged in order to gain a better understanding of their actions on a cellular level.⁹³ Broadly, “caging” involves the coupling of a bioactive molecule with a photolabile protecting group, what creates an inert precursor, devoid of biological activity. Exposure to light then rapidly releases the active compound by cleaving off the caging group. Light-mediated activation of caged compound provides a high level of control over *when* and *where* a bioactive molecule is released. In addition, by controlling light exposure time, intensity, or the number of laser pulses, it is possible to regulate an amount of active compound that is generated per time unit.⁹⁴

Application of caged compounds to study processes in living tissues is therefore very favourable, because it avoids using additional chemical reagents, and gives greater spatial and temporal control. However, to be useful in biological experiments, photolabile protecting groups must satisfy certain criteria. Firstly, the phototrigger and the resulting precursor must be biologically inert, soluble and stable in water and at physiological pH. Secondly, photochemical release of the active molecule should proceed at wavelengths in the near UV region (350-360 nm) or, ideally, in visible region, to minimize cell damage. It is also important that photolysis is fast and resulting by-products are both non toxic and inactive.

Among the photolabile protecting groups that have been commonly and successfully applied to the investigation of biological systems are *ortho*-substituted nitroaromatic compounds.⁹⁵ The photochemical properties of these compounds **39** can be modified

by varying the nature of the substituents at the benzyl carbon (R^1) and around aromatic ring (R^2 and R^3) (Figure 20, (A)). For example, one of the most popular photolabile groups, 6-nitroveratroyloxycarbonyl group (NVOC) **40**, incorporates two methoxy functionalities (Figure 20, (B)), and shows a maximal absorbance and reactivity at wavelengths longer than 320 nm. This characteristic of NVOC allowed its application as a caging group for light-sensitive amino acids such as tryptophan or tyrosine.⁹⁶ More recently, the photochemistry of nitroindolines, which represent another class of nitroaromatic compounds, have attracted considerable attention.⁹⁷ For example, 1-acyl-7-nitroindoline **41** (Figure 20, (C)) was found to be promising phototrigger for rapid release of carboxylic acids in aqueous solutions.

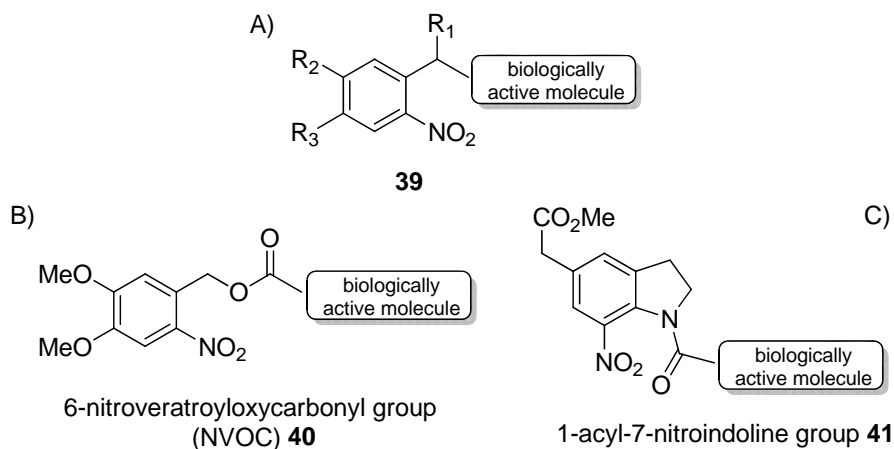


Figure 20. Examples of caging groups bearing nitro functionality.

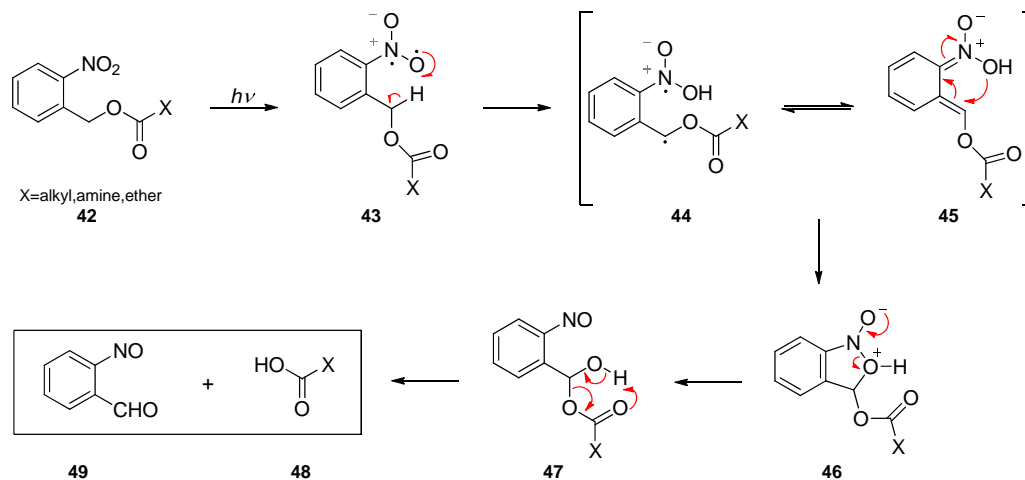
The unique photochemical properties of the compounds discussed result from the presence of the nitro functionality, which serves as an intrinsic chromophore. As a result, nitro aromatic photolabile groups absorb light directly and generate, during photolysis, products that are readily detectable by optical methods.⁹⁸ Moreover, nitroaromatic compounds are chemically stable and compatible with many functional groups (e.g., phosphate, carboxylates, hydroxyl and amines), which have made them the most widely used photoremovable protecting groups for application in organic synthesis, biochemistry and biology.

However, the extensive application of nitro compounds as caging groups has also brought attention to their weaknesses, such as toxicity and reactivity of by-products generated upon photolysis. Indeed, investigations of biological systems with nitro aromatic cages require tools and methods that allow to prevent or control these negative effects. For example, synthetic modifications can optimize reactivity and the light absorbing properties of photolabile groups and their by-products. Moreover, manipulations of the experimental solution, such as buffering or adding hydrophilic thiols, suppress reactivity of by-products towards proteins present on cell surfaces.

The growing interest in application of photolabile groups in biology and biotechnology has prompted detail studies of the mechanism underlying their photolability. Many photoreactions, which lead to the release of active molecule from “caged” precursor, were shown to be complex processes that proceed *via* a cascade of reactive intermediates. Moreover, the efficiency of the release of the active substrate from inert precursor may depends on solvent type, pH and, in some cases, on buffer concentration.⁹⁹

The mechanism of photolysis was studied for many different photoremovable groups and chromophores.¹⁰⁰ Generally, the process of *uncaging* is an intramolecular reaction, initiated by the absorption of a photon by the caged precursor that leads to the cleavage of the chemical bond. The model example is a photoreaction of *o*-nitrobenzyl derivatives **42**, which proceeds according to the mechanism showed in Scheme 22. The release of biologically active compounds, such as alcohols, carboxylic acids or phosphates, from *o*-nitrobenzyl cages, starts with the excitation of the nitro group that generates a highly reactive diradical species **43**. The species **43** could undergo further transformations *via* many possible reaction pathways. However, theoretical and experimental studies showed that species **43** undergoes the Norrish type II reaction, which is an intramolecular abstraction of a γ -hydrogen by an excited nitro group.⁹⁵ This transformation, driven by the greater strength of the O-H bond compared to C-H bond, is fast and produces a 1,4-diradical species **44**. A series of computational and experimental studies performed in recent years suggested that the more correct representation for the product of H-atom transfer to be an *aci*-nitro form **45**.⁹⁸ The formation of this ground state, active *aci*-nitro intermediate **45** was monitored by its strong absorption around 400 nm. The subsequent reactions leading

to the release of active molecule from caged precursor are not yet fully understood.^{101,102} However, it is accepted that next step involves the energetically favorable cyclization of the protonated form **45**, which produces intermediate **46**. The intermediate **46** rearranges to acetal **47**, which spontaneously collapses to release biologically active carbonyl compound **48** and nitrosoaldehyde **49**.



Scheme 22. Mechanism of photolysis of *o*-nitrobenzyl compound **42**.

In 2003, Hess reported the synthesis and characterisation of a new caging group that included the nitro functionality, the 2-(dimethylamino)-5-nitrophenyl group **50** (DANP) (Figure 21).¹⁰³ The DANP group **50** was design originally as a caging group for the carboxyl functionality, and was shown to have a major absorption band in the visible wavelength region with the maximum near 400 nm.

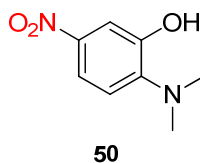
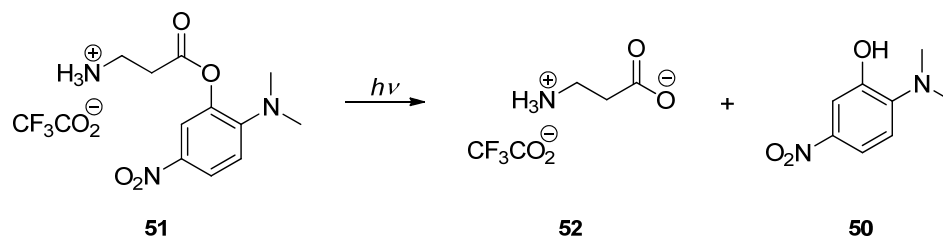


Figure 21. The photolabile DANP group **50**.

In the experiments performed by Hess,¹⁰³ the DANP group was used for caging the biologically active β -alanine, which activates the inhibitory glycine receptor in the mammalian central nervous system. Laser-pulse photolysis of caged precursor **51** showed that β -alanine **52** is released within 5 μ s, with a quantum yield around 0.03 at 308 and 350 nm (Scheme 23). The efficiency of uncaging was, however, lower in visible region (0.002 at 400 nm and above). Nevertheless, experiments demonstrated the desired biological inertness of DANP-caged β -alanine and the DANP group **50** towards the glycine receptors on cell surfaces. Furthermore, caged precursor **51** was water soluble and stable under physiological conditions (pH=7.4). These results of both the biological and photochemical investigations compared favourably with those obtained for other photolabile groups used for caging the biologically active carboxylic acids. Phenacyl caging groups,¹⁰⁴ nitroveratrole,¹⁰⁵ and substituted coumarins¹⁰⁶ were shown to suffer from poor solubility in aqueous medium and often a slow rate of release (minutes) of the bioactive compounds in the visible region.

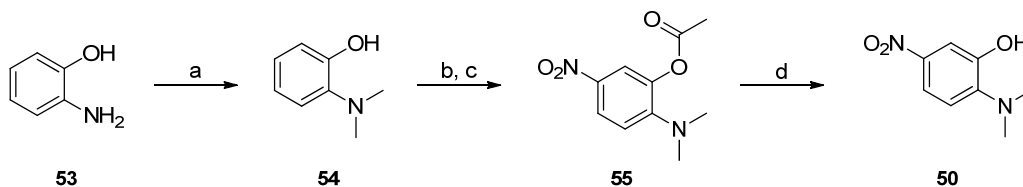


Scheme 23. Photolysis of the DANP-caged β -alanine **51**.

These promising biological and photochemical properties for the DANP group **50** prompted us to choose this compound as a photolabile protecting group that would be coupled to the derivatives of the IGD peptidomimetic **2a**. We hoped that the caging of the IGD mimetics with DANP group would allow us to carry out biological and kinetic investigations of the IGD molecules and could potentially help identify the natural receptor of MSF protein. In the long term, we also considered the possible application of caged IGD mimetics in treatment of wounds with impaired healing. Thus, DANP-caged IGD compounds might be applied topically to a wound in the temporally inactive form. The molecules could be then excited with visible wavelengths, releasing biologically active IGD mimetics. In principle this method

should allow application of active IGD mimetic in spatially very restricted manner. It might also provide better control over concentration of active molecules at the site of action. Additionally, use of visible light for photocleavage of DANP group might assure minimal damage to the cells.

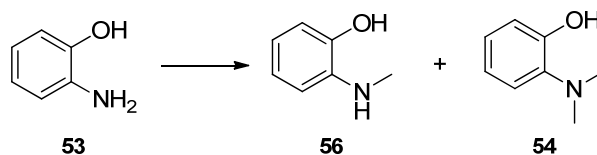
The synthetic route to the DANP group **50**, reported by Hess,¹⁰³ started from commercially available 2-aminophenol **53** (Scheme 24). Compound **53** was methylated with dimethyl sulfate to produce intermediate **54**. The acylation of phenolic hydroxyl group of **54** and nitration with nitric acid produced compound **55**. Resulting nitrobenzene **55** was then treated with sodium hydroxide to generate the DANP group **50** in overall yield of 23% (from **53**). The exact reaction conditions and yield for each step were not reported in the paper.¹⁰³



Scheme 24. Reagents: a) (CH₃)₂SO₄, b) Ac₂O, c) HNO₃, HOAc, d) NaOH, 23% from **53**.

Hence, in our synthesis of the DANP group **50**, we followed the general method reported by Hess; however we needed to determine suitable reaction conditions. The synthesis began with 2-aminophenol **53**, and required, as a first step, the dimethylation of amine functionality. We examined various conditions for this transformation. Initially, we attempted the alkylation of **53** with methyl iodide, in the presence of different bases. Under these conditions the monomethylated amine **56** was generated in good yields, however, only traces of desired dimethylated compound **54** were obtained (Table 3, entries 1-4). Treatment of aromatic amine **53** with formaldehyde, formic acid and LiAlH₄, seemed to be successful by TLC analysis, but only traces of compound **54** were isolated. We speculated that product **54** was bound by aluminium derivatives, and the resulting complexes were lost on celite during reaction work-up. Eventually, methylation of **53** with sodium

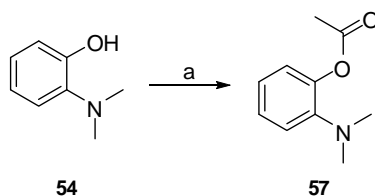
borohydride and formaldehyde produced cleanly and in excellent yield the requisite *N,N*-dimethylated aniline **54** (Table 3, entry 6).



Entry	Reaction conditions	Product 56	Product 54
1	CH ₃ I (1.2 eq), KHCO ₃ (1.1 eq), DMF	75%	0
2	CH ₃ I (2.2 eq), KHCO ₃ (3 eq), DMF	50%	<10%
3	CH ₃ I (1.2 eq), Cs ₂ CO ₃ (2 eq), DMF	90%	0
4	CH ₃ I (2.2 eq), Cs ₂ CO ₃ (4 eq), DMF	92%	0
5	i. Ac ₂ O, HCO ₂ H, LiAlH ₄ ii. Ac ₂ O, HCO ₂ H, LiAlH ₄	0	8.5%
6	i. NaBH ₄ (3 eq), HCHO (2.5 eq), MeOH ii. NaBH ₄ (1.8 eq), HCHO (1.5 eq), MeOH	30%	70%
			100%

Table 3. Dimethylation of 2-aminophenol **53**.

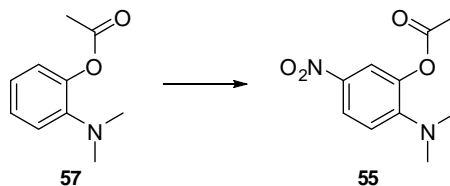
Having established the conditions for methylation, we continued the synthesis of DANP **50**. The ring-activating, phenolic hydroxyl group of **54** was protected as acetate **57**, which proved to be volatile (Scheme 25).



Scheme 25. Reagents and Conditions: a) Ac₂O, pyridine, DMAP, DCM, 75%.

Next, we explored a number of reagents and conditions for a selective nitration of the aromatic ring. Firstly, we treated compound **57** with nitronium tetrafluoroborate. This transformation afforded exclusively the dinitro-substituted isomer, which

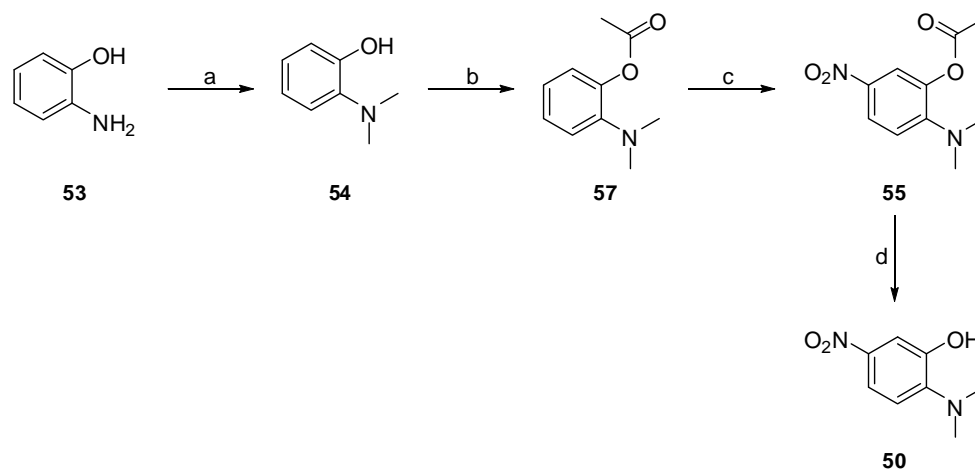
regiochemistry was not further investigated. Also another previously utilized nitrating reagent system, TBAHS/IPN, failed to deliver desired regioisomer **55** (Table 4).⁷⁶



Entry	Reaction conditions	Yield (% of 55)
1	BH ₄ NO ₂ , MeCN, rt	0
2	TBAHS, IPN, H ₂ SO ₄ , DCM, 0 °C-rt	0
3	CAN, MeCN, rt	30
4	Ph ₃ P, Br ₂ , AgNO ₃ , MeCN, rt	40

Table 4. Nitration of acetate **57**.

The nitration of **57** with cerium (IV) ammonium nitrate (CAN) in acetonitrile provided desired compound **55** in moderate 30% yield along with di-nitro isomers as major byproducts.⁷⁵ In an attempt to improve the yield of the nitration step, an alternative reagent system, Ph₃P/Br₂/AgNO₃, was employed. Under these conditions mono-nitrated amine **55** was generated in a slightly higher, 40% yield.⁷⁴ However, this method was found to be the most efficient for nitration step, as it requires only a very short reaction time (10 to 25 minutes) and allows relatively easy isolation of regioisomer **55** by flash column chromatography (FCC) (Scheme 26, Table 4). Purified nitroacetate **55** was then deprotected using sodium methoxide to furnish DANP group **45** in moderate yield (48%). However, the yield for deprotection step was greatly improved upon treatment of **55** with ammonium acetate (Scheme 26). These alternative, mild reaction conditions provided the final DANP molecule **50** in excellent 93% yield.¹⁰⁷

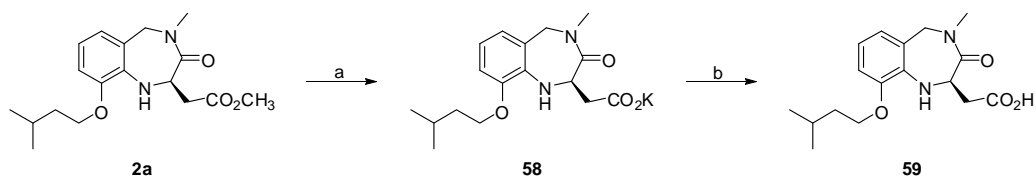


Scheme 26. Reagents and Conditions: a) NaBH₄, HCOH, MeOH, 77%, b) Ac₂O, pyridine, DMAP, DCM, 75%, c) Ph₃P/Br₂/AgNO₃, 40%, d) NH₄OAc, MeOH/H₂O, 93%.

2.1.4 Coupling of the IGD mimetic with the DANP group

Since the synthesised DANP group had been design as a caging group for carboxylic acid functionality, we needed to convert IGD ester **2a** to its respective acid.

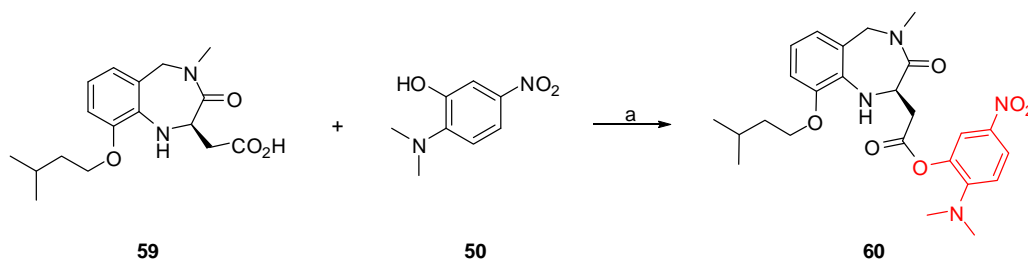
For this purpose of this transformation the (*R*)-IGD ester **2a** was added to suspension of potassium trimethylsilanolate in diethyl ether.¹⁰⁸ The reaction produced anhydrous acid salt **58**, which was then treated *in situ* with diluted hydrochloric acid to give free carboxylic acid **59** in excellent 97% yield (Scheme 27).



Scheme 27. Reagents and Conditions: a) KOSiMe₃, Et₂O, 0 °C, b) 1N HCl, 0 °C, 97% from **2a**

Having successfully synthesised both the (*R*)-IGD acid **59** and DANP caging group **50**, we turned our attention to the remaining coupling between these two molecules.

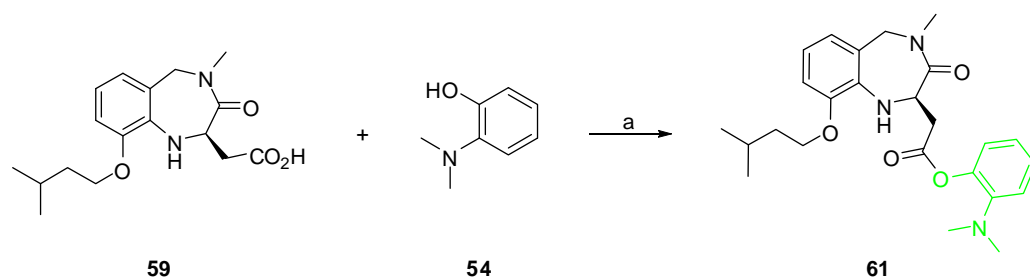
The coupling was based on simple esterification, thus we initially applied standard and mild Steglich conditions. This transformation, promoted by DCC (dicyclohexylcarbodiimide), was successful according to the ^1H NMR, however following purification of the crude reaction mixture by flash column chromatography failed to separate the DCC derivatives from product **60** (Scheme 28). Therefore, we decided to change the coupling reagent to EDC (1-ethyl-3-(3-dimethylaminopropyl) carbodiimide), which is a water soluble carbodiimide. These esterification conditions cleanly afforded ester **60** (Scheme 28).¹⁰⁹



Scheme 28. Reagents and Conditions: a) EDC, DMAP, DCM, 0 °C to rt, 80%

The synthesised ester **60** is a novel compound that requires series of tests to elucidate its photochemical, chemical and biological properties and potential application as a caged molecule. Among the strict requirements that compound **60** would have to meet to become a likely candidate for investigation of biological systems are: its solubility in aqueous media, inertness of precursor and efficiency of photorelease of (*R*)-IGD mimetic **59**. If successful, ester **60** could then be used in biological investigations on a cellular level.

For the purpose of studying the chemical and biological qualities of ester **60**, we also synthesised a control compound **61**. This molecule was created by coupling of (*R*)-IGD mimetic acid **59** with 2-dimethylamino-phenol **54**, which is an intermediate in the synthesis of DANP group **50** (Scheme 29). The phenol **54** is lacking a nitro group, which is responsible for photolabile properties of DANP molecule. For this reason, it is expected that photo-stimulation of ester **61** would not result in release of (*R*)-IGD molecule **59**.



Scheme 29. Reagents and Conditions: a) EDC, DMAP, DCM, 0 °C to rt, 31%

2.2 Biological tests

An important part of the *IGD project* was an evaluation of biological activity of synthesised (*R*)-IGD ester **2a** and (*R*)-IGD acid **59**. Those compounds were tested in a series of *in vitro* and *in vivo* experiments, together with (*S*)-IGD ester **2b** and (*S*)-IGD acid **59a**, which were synthesised by Dr. Philip McGivern (the Marquez group) (Figure 22). The aim of biological studies was to determine whether the synthesised compounds could mimic the biological activity of the MSF in terms of stimulation of cell migration. The work was carried out by Dr. Ian Ellis in collaboration with Dr. Ana Schor and Prof. Seth Schor from the University of Dundee.¹¹⁰ A brief synopsis of the results is herein presented.

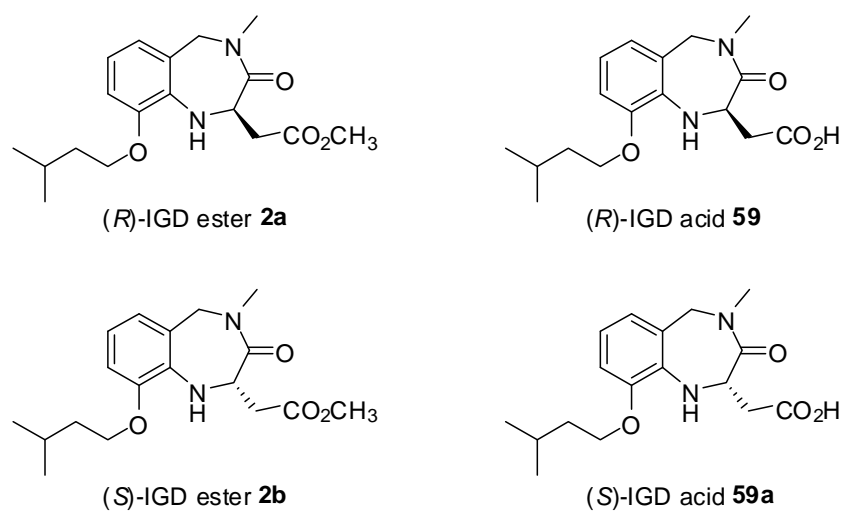


Figure 22. Structures of tested IGD peptidomimetics.

The ability of IGD peptidomimetics to stimulate cell migration was assessed in two *in vitro* assays, transmembrane assay and 3-D collagen gel, conventionally utilised to study cell chemotaxis. These experiments were performed with human skin fibroblast and endothelial cells, using different concentrations of DMSO solutions of peptidomimetics **2a**, **2b**, **59** and **59a**. As predicted by the initial modelling studies, the enantiomerically pure (*R*) methyl ester **2a** showed significant motogenic activity on both fibroblasts and endothelial cells (i.e. caused the cells to migrate and initiate angiogenesis), whereas the (*S*) methyl ester **2b** proved to be inactive under the assays conditions (results for peptidomimetics **2a** and **2b** are summarised in Table 5). The (*R*)-IGD acid **59** was significantly less potent than (*R*)-IGD ester **2a**, whereas (*S*)-IGD acid **59a** showed no motogenic activity on cells.

		Number of cells migrated (relative to control)					
		Fibroblasts		Fibroblasts		Endothelial	
		3D collagen assay		transmembrane assay		transmembrane assay	
IGD-ester concentration	<i>R</i>	<i>S</i>	<i>R</i>	<i>S</i>	<i>R</i>	<i>S</i>	
	0 (controls)	1.0 ± 0.10	1.0 ± 0.10	1.0 ± 0.08	1.0 ± 0.10	1.0 ± 0.03	1.0 ± 0.04
1ng/ml	1.53 ± 0.14	0.82 ± 0.06	1.07 ± 0.08	1.01 ± 0.08	1.03 ± 0.02	1.0 ± 0.06	
10ng/ml	2.17 ± 0.17	0.89 ± 0.10	1.39 ± 0.11	1.0 ± 0.08	2.14 ± 0.05	0.98 ± 0.02	
100ng/ml	3.32 ± 0.07	1.0 ± 0.0	2.03 ± 0.06	0.99 ± 0.11	2.17 ± 0.03	1.0 ± 0.05	
1µg/ml	3.37 ± 0.06	0.92 ± 0.07	2.53 ± 0.10	0.98 ± 0.12	2.27 ± 0.10	1.04 ± 0.05	
10µg/ml	3.46 ± 0.17	1.03 ± 0.07	2.53 ± 0.09	0.98 ± 0.10	2.04 ± 0.05	1.07 ± 0.06	

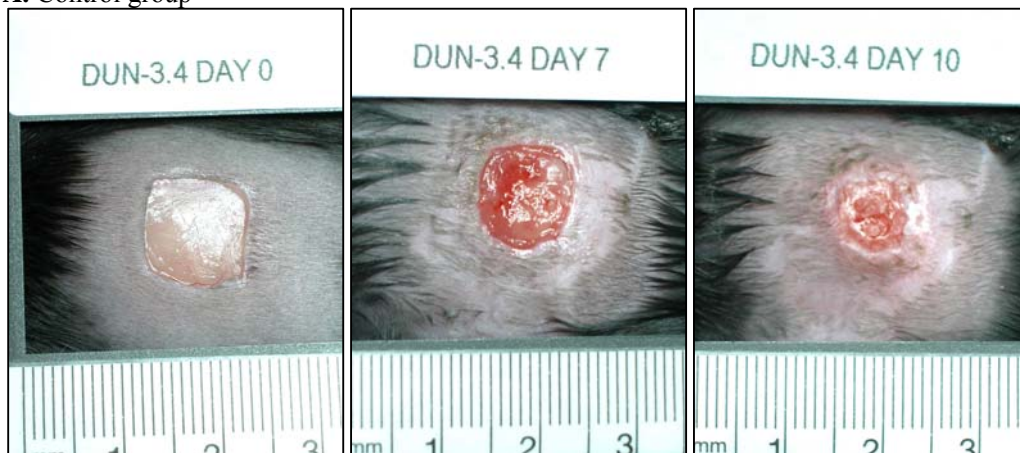
Table 5. Motogenic effect of (*R*)-IGD ester **2a** and (*S*)-IGD ester **2b** on fibroblasts and endothelial cells. Cells were tested on two migration assays: 3D collagen gels and transmembrane assay, as indicated. Figures show mean ± SD (n=3-6).

The methyl esters and the free acids were then evaluated for the ability to promote wound closure on genetically diabetic mice. Due to stringent Home Office regulations and the need for licenses to carry out animal testing, this work was outsourced to Cica Therapeutics. In the experiment, mice were anaesthetised on day 0 using isoflurane and air. Then their dorsal skin was clipped and cleansed according to protocol. A single standardised full thickness wound (10 mm x 10 mm) was created on the back of each experimental animal. Test variants or control

preparations were applied to each animal. Solutions of the IGD mimetics were applied directly to the wound base and were evenly distributed using the micropipette tip. A 1.5 cm² piece of ReleaseTM non-adherent film (i.e. ReleaseTM dressing [Johnson & Johnson Wound Management, UK] with the absorbent centre removed) was then placed over the wound and held in place with a circumferential band of the occlusive film dressing BioclusiveTM (Johnson & Johnson Wound Management, UK). All animals were re-anaesthetised and treatments were re-applied on days 2, 4, 7 and 10 post wounding.

The wound-healing effects of IGD peptidomimetics were then examined histologically. The results indicated that wounds treated with (*R*)-IGD ester **2a** and (*R*)-IGD acid **59** healed faster and showed significant difference in percent of wound size reduction as compared to control group (selected results presented in Figure 23). This may indicate that both mimetic variants can act to promote wound contraction in the diabetic mouse model. Interestingly, the (*S*)-IGD acid **59a** was, however, also found to promote a reduction in wound width, relative to the control groups, although not to the same extent as the higher doses of the two (*R*) mimetics **2a** and **59**.

A. Control group



B. (R)-IGD ester 1a

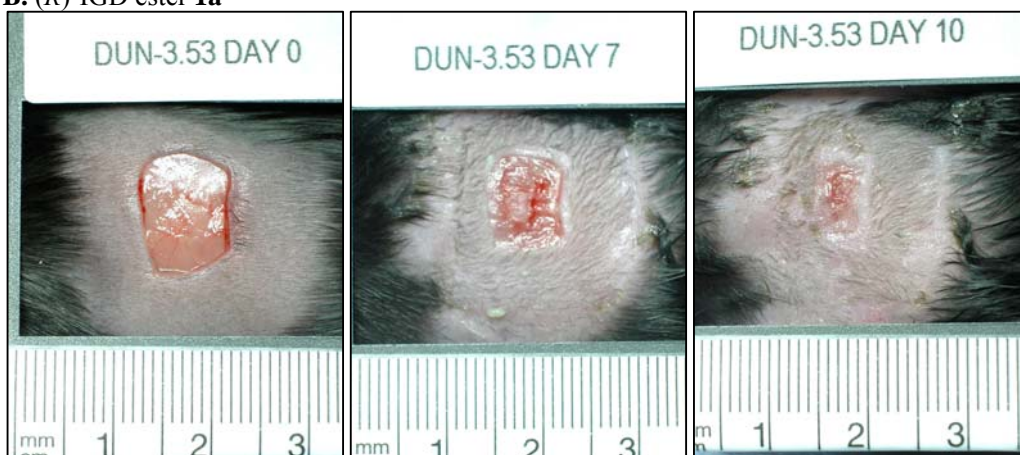


Figure 23. Effects of (R)-IGD ester **2a** on wound closure; (A) control group, (B) (R)-IGD ester **2a** treated group.

Taken together, the results of *in vivo* studies suggested that the (R)-IGD ester **2a** can promote wound healing in the diabetic mouse – an effect that was most apparent in terms of wound closure, wound contraction (wound tissue compaction), re-epithelialisation and cellular maturity. Similar, though somewhat less pronounced, effects were observed following application of the highest dose of (R)-IGD acid **59**. As expected, lower concentrations of both compounds tended to have reduced effects and higher concentrations may give rise to more substantial effects.

2.3 Conclusions

In summary, the syntheses of a “first generation” of IGD peptidomimetics was successfully accomplished according to the protocols reported in this thesis. The IGD peptidomimetic ester was synthesized in both racemic (**2**) and optically active (**2a**) forms. Optimization of the reaction conditions for the enantioselective route to (*R*)-IGD ester **2a** allowed us to produce this mimetic in 9 steps and 32.4% overall yield. Hence, the developed synthetic route proved to be efficient, high yielding, and produced **2a** in an enantiomeric excess of 94.9%. Our methodology utilizes simple transformations, easy to handle reagents and mild reaction conditions. As such, we speculate, that our synthetic protocol could be successfully adapted for use on an industrial scale.

We also synthesized the (*R*)-IGD mimetic acid **59** from (*R*)-IGD ester **2a**. Both compounds, **2a** and **59**, have been evaluated for their anticipated motogenic activity on cells, in a series of *in vitro* and *in vivo* experiments. The biological tests were performed by Dr. I. Ellis in collaboration with Prof. S. Schor and Dr. A. Schor. The initial results of these studies are promising. The (*R*)-IGD ester **2a** was shown to stimulate cell migration both *in vitro* and *in vivo*. Since (*R*)-IGD ester **2a** exhibits significant bioactivity, it is currently regarded as a likely lead-candidate for a drug in the topical treatment of wounds with impaired healing. Its clinical potential is currently being extensively investigated.

The DANP photolabile group **50** was synthesized and coupled to (*R*)-IGD acid **59**. The biological and chemical qualities of the obtained caged IGD mimetic **60** will be tested with a view to potential application in medicine as a drug delivery tool.

Future work will be also devoted to expanding the class of IGD mimetics. It is proposed to synthesize series of analogues of IGD peptidomimetic **2**, by modifying the substituents at nitrogen and carbon C-9 (Figure 24). It is hypothesized that these modifications might alter such important properties of compounds as receptor

affinity and bioactivity. Hence, it is hoped to develop analogues with high potency and specificity for MSF receptor.

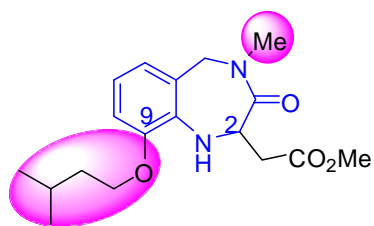


Figure 24. IGD peptidomimetic **2** with highlighted areas that will be modified.

THE GRIS PROJECT

3.0 Introduction

Although the vast majority of human diseases are caused by a combination of genetic, environmental and lifestyle factors, we cannot underestimate the risks of infections by pathogenic bacteria. Bacteria have been evolving for nearly 3.5 billion years and have acquired a high degree of flexibility and capacity for rapid growth and reproduction. Moreover, evolutionary success of bacteria relies on the constant mutation of genes resulting in their abilities to adapt and survive in a changing environment. These changes in genetic make-up are also responsible for the emerge of antibiotic-resistant bacterial strains that cause infections which are often difficult to treat.¹¹¹

A microorganism which has shown to be particularly adaptable to antibiotics is the bacterium *Staphylococcus aureus*, commonly present in the nose and on the skin of one third of people. Although *S. aureus* is usually harmless at these sites, when it breaks into the body causes infections, ranging from mild conditions like pimples or impetigo to serious diseases such as pneumonia, meningitis, toxic shock syndrome (TSS), or septicemia.¹¹² Historically, infections caused by *S. aureus* were treated with penicillin and since 1960 also with the derivative methicillin. However, the World Health Organization (WHO) recently reported that more than 95% of *S. aureus* worldwide is resistant to penicillin, and 60% to methicillin.¹¹³

Since the resistance of pathogenic bacteria, including *S. aureus*, to antibiotics has been steadily increasing and is predicted to become a major world health problem, there is an urgent need for new forms of therapeutic treatments for bacterial infections. The most plausible alternative approaches that have been of interest to scientists include; bacterial interference, bacteriophage therapy, and bacterial vaccines.¹¹⁴ Many of these approaches have been addressing the mechanism

underlying bacterial adhesion to eukaryotic cells, which is a crucial stage in colonization of tissues that leads to infection.

In recent years many research groups have presented new information regarding the mechanism for *S. aureus* adhesion to and invasion of human cells.^{115,116} This mechanism has been studied mostly in relation to cardiovascular diseases, and as such emphasis was placed on researching bacterial interactions with endothelial cells and platelets. As a result, it has been postulated that bacterium *S. aureus* can adhere to endothelial cells indirectly, utilising interactions between bacterial proteins adhesins, such as FnBPA, and the extracellular matrix protein fibronectin of the host.¹¹⁵ Since FN binds also to integrin receptors present on endothelial cell surfaces, it is believed to serve as a bridge between *S. aureus* and integrins and hence mediate bacterial adherence and presumable also internalization to endothelial cells. Furthermore, based on published NMR and X-ray structures of FnBPs of *S. aureus* in complex with ¹F1²F1 of FN, novel mechanism of interactions between these two proteins has been proposed.¹¹⁷

Despite the growing information regarding *S. aureus* adherence to and invasion of host endothelial cells, there is still a lot to be discovered. For example, there are no doubts about the role played by fibronectin in bacterial pathogenesis, however, it remains unanswered how interactions with bacterium affect the structure of FN, and if there exists a biologically active motif within FNI modules necessary to exhibit binding of bacterial adhesins.

3.1 Bacteria *Staphylococcus aureus*

The *Staphylococcus aureus* bacteria are gram-positive spherical *cocci* that can be observed microscopically as individual organisms, in pairs or in clusters resembling grapes (Figure 25). This bacterial species are a common inhabitant of nose, skin or gastrointestinal tract of almost a third of all humans, and their presence is normally harmless and asymptomatic.

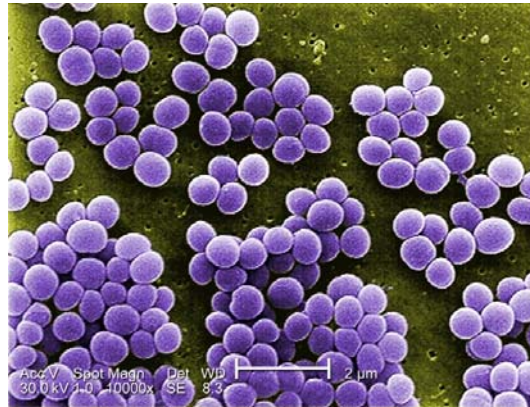
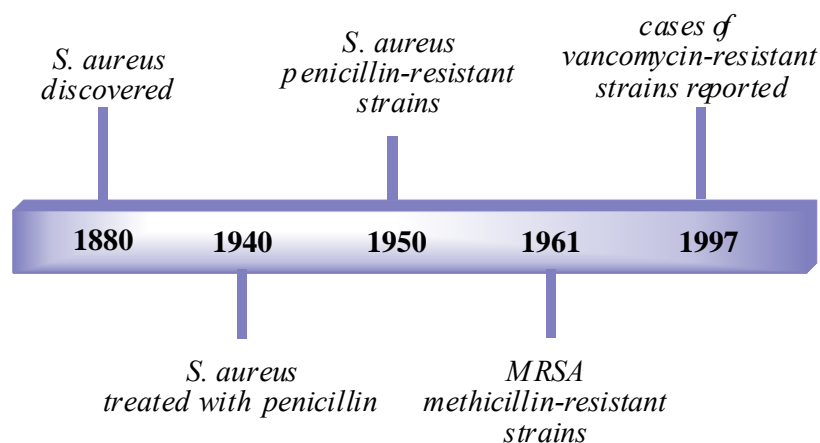


Figure 25. The scanning electron micrograph shows a strain of *Staphylococcus aureus* bacteria taken from a vancomycin intermediate resistant culture.

(by J. H. Carr, Public Health Image Library (PHIL))

However, the *S. aureus* is also the most virulent pathogen among the *Staphylococcus* species, and simple skin damage or other injury can be enough for the bacteria to enter the body, overcome the natural protective mechanisms and initiate infection. The most common infections caused by this pathogen are skin conditions, such as pimples and boils which are usually uncomplicated and easy to treat. However, if *S. aureus* enters the bloodstream and spreads to other organs it can produce wide range of serious and damaging illnesses like staphylococcal pneumonia,¹¹⁸ meningitis,¹¹⁹ endocarditis¹²⁰ or severe bone inflammation.¹²¹ Moreover, the bacterium is capable of excreting several toxins¹²² that induce toxic shock syndrome (TSS), food poisoning or pneumonia in children.

In recent years, infections caused by *S. aureus* have become more difficult to combat and widespread to such a scale that they have become a serious public health concern. The reason for that is the extraordinary ability of this pathogen to become resistant to antibiotics. The infections caused by *S. aureus* were originally treated with penicillin only for a short period of time; already in 1950 penicillin-resistant strains of bacterium were reported (Scheme 30). Currently, according to WHO, more than 95% of *S. aureus* worldwide is resistant to penicillin, 60% to methicillin (methicillin-resistant *Staphylococcus aureus* termed MRSA),¹²³ and since 1997 cases of vancomycin resistant *S. aureus* infections have been reported.¹²⁴



Scheme 30. Timeline of MRSA.

The resistance of *S. aureus* to antibiotics can be acquired through number of different mechanisms, such as spontaneous nucleotide base mutations, conjugations and from recombination with other bacterial DNA following transformation.¹²⁵ Although not all mutations of genes have to confer resistance to antibiotics, many of them actually do. Moreover, because of the rapid rate of division of bacterial cells, it is likely that bacterial population in an infected organism would ultimately consist mostly of mutants carrying resistance genes. To further complicate treatment, recent findings show that some mutants of *S. aureus* have certain phenotypes that suggest prevalence of multidrug resistant strains.^{126,127}

Thus, since antibiotics that once cured bacterial infections caused by *S. aureus* are no longer effective, and only few new classes of antibiotics are under development, there is an urgent need for the design and implementation of alternative treatments with novel modes of action. One way of combating the antibiotic resistant *S. aureus* pathogen is to directly inhibit the infection process by disrupting the first stage of bacterial invasion which is adhesion to the host cells.

The idea itself is not novel; however, only recent years have delivered enough information regarding the molecular basis of *S. aureus* adherence to host cells that could allow the development of new drugs capable of disrupting this process.

3.2 Molecular basis of bacterial invasion

The bacterial invasion of the human body is a complex process that often leads to the development of infectious diseases. Bacteria *S. aureus* is responsible for many topical and localised infections in humans, however the most dangerous and often fatal are systemic infections, such as *bacteraemia*, *staphylococcal sepsis* and *infective endocarditis* (IE), which start when the pathogen gains access to the bloodstream or other body fluids.¹²⁸ Once in the system, bacteria *S. aureus* begin exploitation of the host organism by adhesion to the cells, replication and growth of the colony that could potentially spread to distinct organs.

Until recently, there was little information available on the mechanism and consequences of cellular invasion in *S. aureus* pathology. However, in the last two decades this subject has been intensively studied by several research groups and as a result, new information has been gained regarding interactions between human cells and bacteria *S. aureus* on a molecular level. For instance, in contrast to the previous beliefs that *S. aureus* is an extracellular pathogen, it has been shown that it can invade and persist within a variety of non-professional phagocytes, such as human endothelial cells, bovine epithelial cells and murine fibroblasts. This internalization of pathogen by the host cells has obvious advantage for bacteria: it creates a protected environment where pathogens are shielded against host defenses and antibiotic treatment.¹²⁹ Furthermore, *S. aureus* has been found to actively replicate inside pulmonary epithelial cells and cause their apoptosis, what could be a strategy to facilitate pathogen survival in the host organism.¹²⁹

In addition to these discoveries, there has been significant progress in understanding the mechanism of invasion of cardiovascular system by *S. aureus*, and hence in understanding the interactions between bacterium and endothelial cells. The endothelium lining blood and lymphatic vessels is a key barrier separating body fluids from tissues, and an important component of the immune system, producing inflammatory cytokines and regulating leukocyte trafficking. Thus, the endothelium is a major target for many bacteria, including pathogenic strains of *S. aureus*, which

can adhere to and invade endothelial cells causing disruption of their protective functions. Moreover, rupture and breaching of the endothelial barrier might be a first step in bacterial dissemination into surrounding tissues and organs,¹³⁰ leading to various diseases (e.g. endocarditis, osteomyelitis).

Studies on the pathogenesis of *S. aureus* have shown that the initial adherence of bacterium to the host endothelial cells is mediated by certain adhesins expressed on its cell surfaces.¹³¹ Adhesins are wall-anchored proteins that belong to family of *microbial surface components recognising adhesive matrix molecules* (MSCRAMM), and are produced by many microorganisms. In line with the name, the MSCRAMM molecules specifically bind to a wide range of host extracellular matrix components. Moreover, some of the adhesins can also bind receptors on eukaryotic cells, thereby directly promoting bacterial internalisation into host cells.¹³² The biological importance and roles of MSCRAMMs proteins are only now beginning to be addressed; however, research performed so far suggests that MSCRAMMs are important virulence factors utilised by bacteria to engage host proteins and use them to exploit host cellular signalling.

Accordingly, adhesins expressed by many strains of *S. aureus* have been shown to promote bacterial pathogenesis by recognising components of ECM, such as fibrinogen, collagen and fibronectin. Since FN is strongly connected with cellular invasion, the interactions between bacterial adhesins and FN are currently the most widely investigated.^{133,134}

Among the many adhesins expressed by *S. aureus*, there are two major fibronectin-binding proteins (FnBPs): FnBPA and FnBPB. These FnBPs share a similar gene structure and domain organisation; both consist of four regions, termed A, D, C (also termed Du), and D, with multiple binding sites, that mediate bacterial association to fibrinogen, fibronectin and elastin.¹³⁵ Both FnBPA and FnBPB have been found to be expressed by a majority of clinical isolates of *S. aureus*, and have been shown to promote bacterial adherence to cultured human endothelial cells,¹³⁶ trigger active internalization into eukaryotic cells *in vitro* and *in vivo*, and cause platelet activation and aggregation.¹³⁷ FnBPA was recently implicated in the mediation of endothelial

cell invasion and development of experimental endocarditis by the synergistic binding of two host ECM proteins, fibronectin and fibrinogen.¹³⁸

The mechanism of association of the FnBPs of bacterium *S. aureus* with fibronectin molecule was recently investigated by U. Schwarz-Linek.¹¹⁷ Schwarz-Linek studied the solution structure of a streptococcal FnBP peptide in complex with the ¹FNI²FNI module pair of fibronectin. The NMR analysis of the complex structure, sequence analysis and isothermal titration calorimetry data allowed the team to not only propose a novel β -zipper mode of interactions, but also to identify an additional fibronectin-binding region in the bacterial FnBPs. The association of a bacterial peptide with fibronectin requires specific interactions between specialised regions of both proteins. It has been demonstrated that the bacterium-binding site is located in the *N*-terminal region of FN and consist of five sequential FN type I modules (¹-⁵FNI). The tertiary structure of type I modules of FN were previously resolved and found to be rather elongated, consisting of two antiparallel β -sheets linked together by disulphide bridge. The dominant, large β -sheet was shown to be triple-stranded (strands C, D, E), whereas the smaller one is build by two strands A and B (Figure 26).¹³⁹

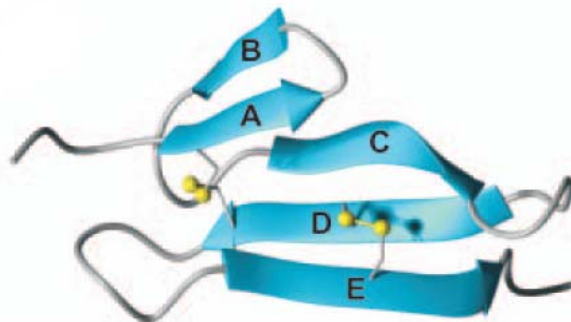


Figure 26. Ribbon diagram of the F1 module fold of ¹F1 with labelled β -strands (blue) and disulphide bonds indicated.

Reprinted from *Molecular Microbiology*, 52, U. Schwarz-Linek, M. Höök J. R. Potts, *The molecular basis of fibronectin-mediated bacterial adherence to host cells*, p. 631-641, Copyright 2004, with permission from John Wiley & Sons

The other binding partner, FnBPA of *S. aureus* was initially believed to mediate FN-association through C-terminal “D-region”. However, studies performed by Schwarz-Linek extended the binding region to the B and C (Du) domains (Figure 27). According to the novel model, FN-binding activity is mediated by 11 binding sites, composed of a series of short motifs arranged in the correct order to bind the sequential FNI-type modules of FN (Figure 27).^{140,141}

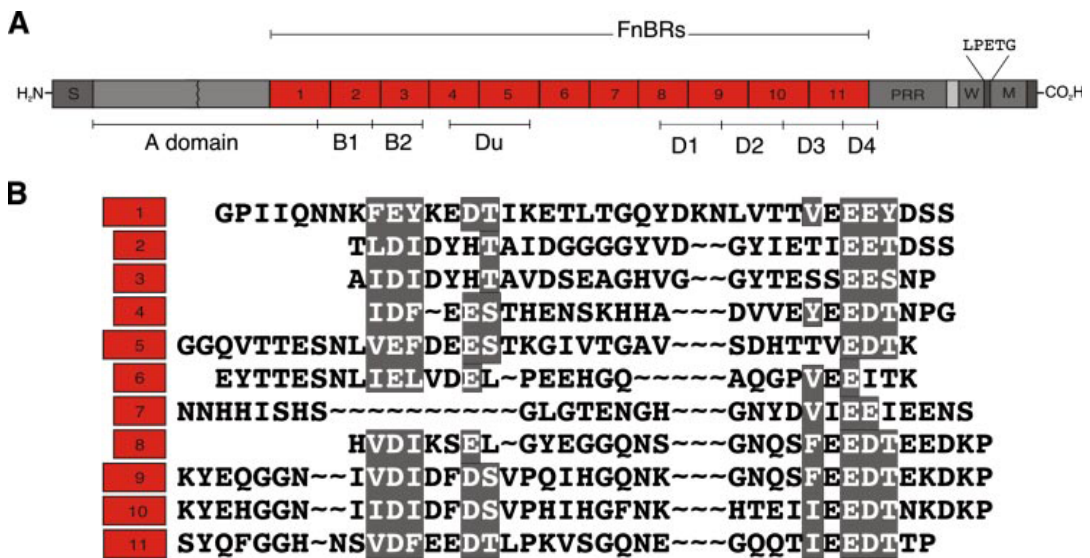


Figure 27. FnBPA from *S. aureus* contains 11 FN-binding sites predicted to bind FN with varying affinity. (A) Schematic representation of FnBPA from *S. aureus* showing the approximate position of the 11 predicted FN-binding regions (FnBRs marked in red) within the bacterial protein sequence. (B) The amino acid sequences of the 11 FnBRs with highlighted conserved residues (white text).

This research was originally published in *Journal of Biological Chemistry*, 282, N. A. G. Meenan, L. Visai, V. Valtulina, U. Schwarz-Linek, N. C. Norris, S. Gurusiddappa, M. Hook, P. Speziale, J. R. Potts, *The tandem β -Zipper model defines high affinity fibronectin-binding repeats within Staphylococcus aureus FnBPA*, p. 25893-25902, Copyright 2007, with permission from the American Society for Biochemistry and Molecular Biology

During the binding event, the bacterial peptide (denoted B3) was found to contribute to the fourth β -strand that aligns antiparallel to the existing triple-stranded β -sheets of FNI modules in a tandem β -zipper interaction (Figure 28). Further work on this protein-protein recognition mechanism suggested that actually each of 11 binding motifs of FnBPA binds to FNI using β -zipper model. Moreover, it was shown that

upon binding, the bacterial peptide undergoes a transition from a disordered state to an extended β -strand-like conformation, while the three-dimensional structure of F1 modules doesn't change significantly.¹⁴¹ It has been hypothesised that since FnBPA contains multiple FN-binding sites, it could associate several FN molecules at a time.¹⁴²

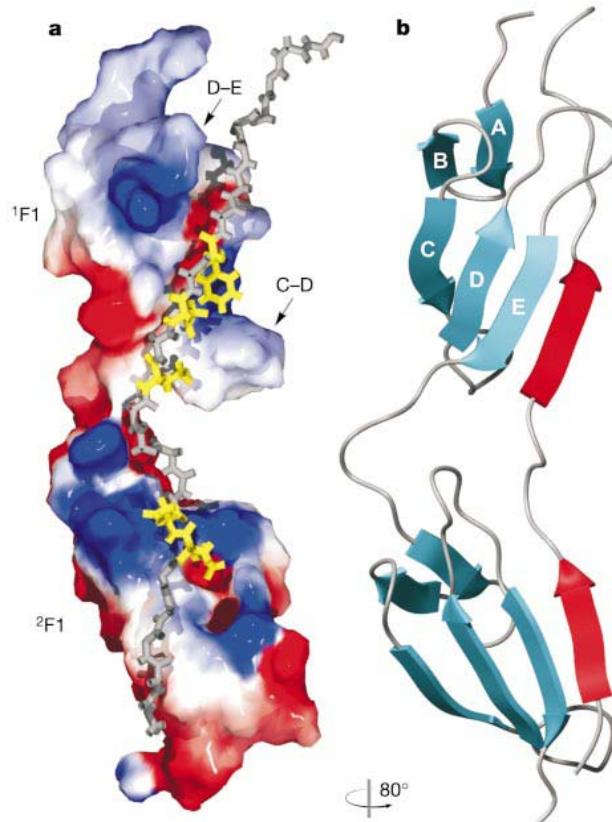


Figure 28. a) Molecular surface of $^1F1^2F1$ in a complex with bacterial peptide B3 (in grey). b) Ribbon diagram of the lowest-energy structure showing β -strands of the F1 module (cyan) and the fourth strand formed by B3 (red).

Reprinted by permission from Macmillan Publishers Ltd: *Nature* U. Schwarz-Linek, J. M. Werner, A. R. Pickford, S. Gurusiddappa, J. Hwa Kim, E. S. Pilka, J. A. G. Briggs, T. S. Gough, M. Hook, I. D. Campbell, J. R. Potts, 423, p. 177-181, copyright 2003

The tight association of FnBPA of *S. aureus* with FN present in the ECM of the host is only the first step in a cellular adhesion. Bacterium is simply using fibronectin as a molecular “bridge” to bind to specific integrin receptors of endothelial cells. It is well known that FN binds with high affinity to integrins $\alpha_5\beta_1$ through well-

characterised tripeptide motif, Arg-Gly-Asp (RGD), localised in FNIII module in the central part of molecule. Therefore, since association of bacterium with fibronectin is mediated by the *N*-terminal region of the latter, it leaves the crucial RGD motif free and ready to interact with integrins. In this way fibronectin with adhered bacterium can simultaneously bind to integrins of endothelial cells. These interactions not only tightly anchor *S. aureus* to host cells but also trigger a cascade of signals that eventually lead to pathogen internalisation and dissemination.^{130,143}

The recent findings rapidly advanced our knowledge of how *S. aureus* manipulate crucial intracellular pathways in its host in order to enter and invade endothelial cells. It was shown, that this bacterium, similarly to other pathogens, can attack, subvert and eventually control the host cell machinery to its advantage. Hence, it is speculated, that FN-mediated adherence of *S. aureus* to receptors $\alpha_5\beta_1$ initiates a cascade of signals that prompts integrin clustering and recruitment of focal adhesion proteins to the activated integrins. Recent work indicates the importance of tensin, an actin-binding protein, which is believed to transmit signals from integrin-bound bacterium to the actin cytoskeleton.¹⁴³ This message in turn triggers the reorganisation of actin cytoskeleton in a way that promotes bacterial movement on the surface of endothelial cells (Figure 29). This enhanced motility of *S. aureus* delays assembly of actin phagocytic cups and bacterial uptake into host cells. Such a phenomenon is thought to be an intended process that allows bacterium to persist at the cell surfaces. Supposedly, the pathogen is simply “buying some time” in order to synthesise certain cell-damaging toxins, which will allow it to survive within cells.^{130,143} This hypothesis is consistent with other findings, which showed that unless bacteria *S. aureus* exerted high molecular toxicity before uptake, most of the examined strains were efficiently eliminated in lysosomes of keratinocytes or endothelial cells.^{144,145} Thus, delay in the uptake process could be considered as an alternative strategy developed by *S. aureus*, a bacterium poorly adapted to transcytosis, by which it could efficiently cross the endothelial barrier and disseminate to surrounding tissues.

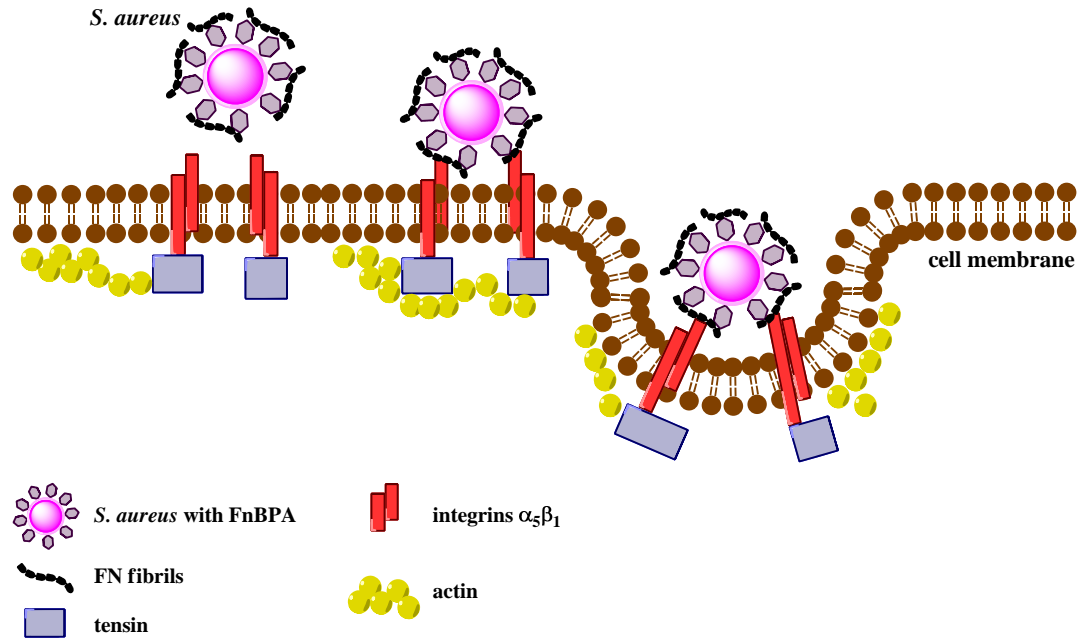


Figure 29. Simplified representation of *S. aureus* attachment to and invasion of endothelial cells.

3.3 First generation GRIS peptidomimetics

There has been a significant progress in our understanding of pathogenic strategies utilised by *S. aureus* in invasion of the host cells and organs. The combined results of many interdisciplinary studies gives a plausible explanation of *S. aureus* virulence on a molecular level, from the interaction mechanism between bacteria *S. aureus* and transmembrane receptors integrins to intracellular uptake scenario. Another important finding of these works was the identification of fibronectin protein as an active and crucial mediator of *S. aureus* adhesion to the endothelial cells. However, despite great progress, there is still a limited amount of information regarding whether and how the FN structure and functions are altered upon binding to bacterium *S. aureus*. Extensive investigations are also required in order to determine whether FN type-I modules carry a biologically active motif, specifically responsible for recognition of FnBPs of *S. aureus*.

The results reported to date indicate that FN protein is binding FnBPs of *S. aureus* through the *N*-terminal region (NTR), composed of a string of five type-I modules. The three-dimensional structure of type I modules has been provided based on NMR studies and showed to consist of two antiparallel β -sheets, the first one being a double-stranded one, and linked by a disulphide bond to the other, triple-stranded β -sheet. The second conserved disulphide bridge links the *C*-terminal adjacent strands of the domain.¹³⁹ Furthermore, important information regarding the conformation of the NTR has been obtained from NMR structures of the ⁴FNI-⁵FNI modules pair.¹⁴⁶ The NMR studies of the FnBP-derived peptide in complex with ¹F1²F1 from the NTR have also identified the protein-protein recognition mechanism as a tandem β -zipper.¹¹⁷

Thus, according to the accepted β -zipper model, the bacterium is primarily binding to ¹⁻⁵FNI region of FN by forming a β -strand along the triple-stranded β -sheet. The detailed analysis of structural results indicated the importance of electrostatic interactions, which might contribute to the binding event. Moreover, it was suggested that FNI proteins could carry highly conserved motifs specifically responsible for binding to FnBPs of *S. aureus*.¹¹⁷

The biologically active motif, by which FN mediates its adhesion to bacterium, has not yet been unambiguously identified. However, the preliminary results of unpublished studies¹⁴⁷ point towards short, tetrapeptide sequence Gly-Arg-Ile-Ser (GRIS) highly conserved within type-I modules of fibronectin (Figure 30). Presumably, the GRIS peptide could constitute a crucial motif mediating the binding of FnBPs to FN.

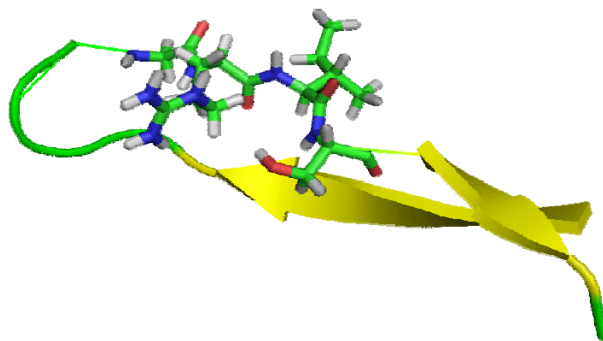
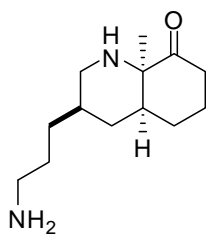


Figure 30. Cartoon structure of the part of ²FNI of FN; the GRIS motif is shown with sticks (R. Marquez).

Thus, in an effort to contribute to research on FN-mediated invasion of *S. aureus*, we proposed to elucidate the role of GRIS motif present in type-I FN modules. For this reason we propose to synthesise the small, nonpeptidic molecule, which could mimic the biological properties and activity of the native GRIS motif. We speculate that if the GRIS sequence is crucial for FN interactions with *S. aureus*, the “GRIS peptidomimetic”, when introduced to the system, could compete with FN in binding to bacterial adhesins. Therefore, a GRIS peptidomimetic would disrupt the interactions between FN and bacterium, necessary for bacterial adherence to host endothelial tissues. It is also possible, that if successful, this strategy and compound might be used in combating bacterial diseases. The idea behind our project isn't novel; in 1981, Beachey wrote that *an understanding of the mechanisms whereby bacteria attach to host cell surfaces would lead to new approaches to preventing serious bacterial infections by interrupting the interactions of bacterial adhesins with host receptors*.¹⁴⁸ This concept seems relatively straightforward; however implementation of this type of approach proved to be difficult, due to the complex nature of bacterial infections.¹⁴⁹

We now propose to synthesise and elucidate the biological properties of a GRIS peptidomimetic. The first generation GRIS mimetic was designed taking into account the steric and electronic properties of native GRIS tertapeptide motif, and it is shown on Figure 31.



62

Figure 31. The first generation GRIS peptidomimetic **62**.

4.0 Results and discussion

4.1 The aim of the project

The aim of *GRIS project* was to design, develop and execute an efficient synthetic route to the novel GRIS bicyclic peptidomimetic **62** (Figure 32).

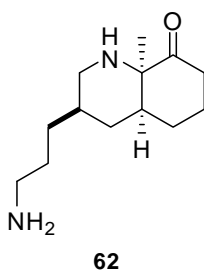


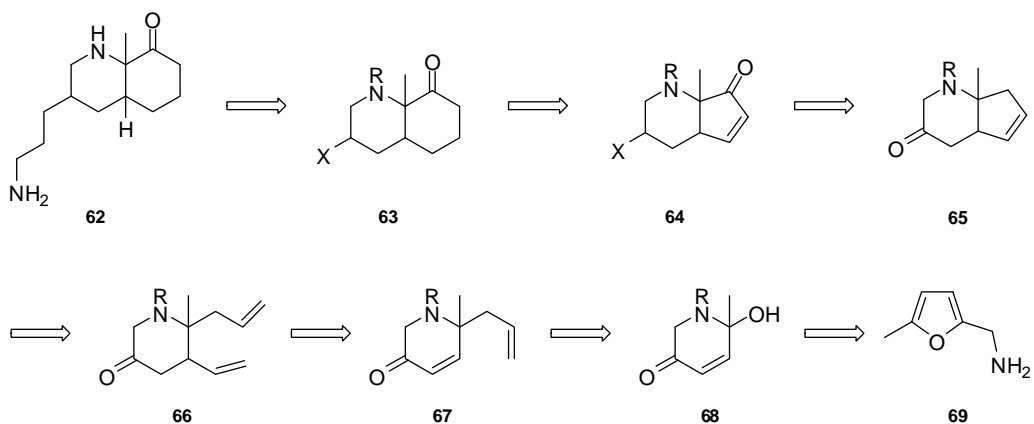
Figure 32. The structure of GRIS peptidomimetic **62**.

Despite possessing a deceptively simple structure, the GRIS molecule **62** presents several synthetic challenges. Firstly, little information is available in the literature on the synthesis of similar units, especially in respect to the 1,3 relation between the ketone and amine functionalities. Another potential difficulty rises from defined stereochemistry at both ring junctions, which needed to be addressed in the course of synthesis. Therefore, our efforts were focused on exploring different synthetic transformations that would allow the synthesis of GRIS mimetic in an efficient manner. In our first approach we referred to work carried out by Marko Ciufolini and Albert Padwa on the aza-Achmatowicz reaction. This oxidative rearrangement allows access to substituted piperidines and other nitrogen containing heterocycles in an elegant and simple manner.¹⁵⁰ The second approach that we attempted relies on Diels-Alder cycloaddition, and allows unique control over the stereochemistry of the product.¹⁵¹

4.1.1 The aza-Achmatowicz approach

Our initial work towards the synthesis of the GRIS peptidomimetics **62** were based on a synthetic strategy that employed the aza-Achmatowicz rearrangement in combination with ring closing metathesis (RCM) as the key transformations. It was decided to first focus our efforts on the development of model and racemic synthetic route to GRIS molecule **62** and to address stereochemical problems later.

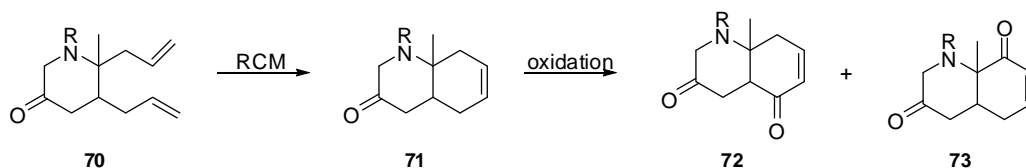
Our principal disconnections in the deconstruction of GRIS peptidomimetic **62** are outlined in Scheme 31. The final GRIS molecule **62** was envisioned to arise from attachment of the side chain on to the nitrogen-containing ring of compound **63**. That could be achieved by Wittig reaction and series of functional group transformations. The requisite 6,6-bicycle **63** could be accessed *via* ring expansion reaction from the 5,6-bicycle **64**. Enone **64** could be obtained by allylic oxidation of alkene **65**. We anticipated that the 5-membered ring of **65** might be constructed *via* RCM of diene **66**, which in turn could be accessed from pyridinone **68**. Finally, we expected to obtain the nitrogen-containing compound **68** *via* single oxidative rearrangement of furylamine **69**.



Scheme 31. Retrosynthetic analysis of GRIS peptidomimetic **62**.

We have chosen to pursue the synthesis of mimetic **62** *via* the 5,6-bicyclic system **65** in order to avoid regioselectivity problems during the oxidation step. We realised that it might be possible to prepare the 6,6-bicycle **71** directly *via* RCM reaction of **70**,

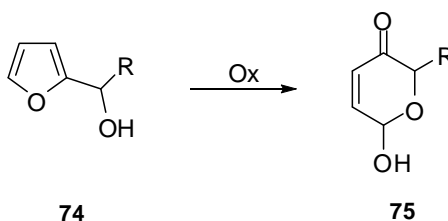
however, it became apparent that the alkene **71** might not be able to undergo a selective allylic oxidation, and it would likely give rise to two different enones **72** and **73** (Scheme 32). Therefore, in our synthetic approach we decided to overcome this problem by constructing firstly the 5,6-bicycle **65**, which would provide the starting point for the allylic oxidation step. Moreover, it was also assumed that the biological activity of compound **64** would be evaluated along with the final GRIS peptidomimetic **62** (see Scheme 31).



Scheme 32. Alternative RCM and allylic oxidation.

Execution of our synthetic plan required as a first step the aza-Achmatowicz rearrangement of furylamine **69**. The aza-Achmatowicz reaction deserves special mention as it is one of the key transformations in our synthetic route.

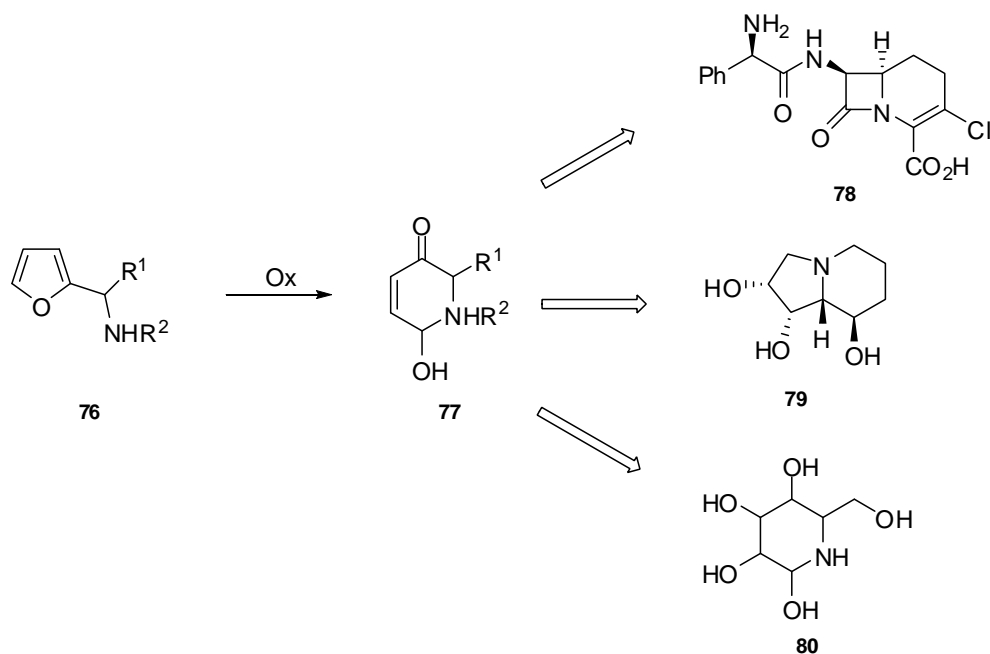
Since Achmatowicz reported in 1971 an oxidative rearrangement of furfuryl alcohols **74** into dihydropyranones **75** (Scheme 33) that could be further easily converted into sugars,¹⁵² similar oxidation of furylamines attracted considerable attention.¹⁵³



Scheme 33. Oxidative rearrangement of furfuryl alcohols **74** into dihydropyranones **75**.

It was quickly recognised that if successful, analogous rearrangement of furfuryl amine derivatives **76** could become a new synthetic strategy towards 6-membered nitrogen-containing heterocycles **77**. Furthermore, easy access to this type of nitrogenous substances would provide very useful building blocks for biologically

active carbacephems **78**,¹⁵⁴ unusual aminoacids,¹⁵⁵ piperidine and izidine alkaloids **79**,^{156,157} and azasaccharides **80**.¹⁵⁸ (Scheme 34).

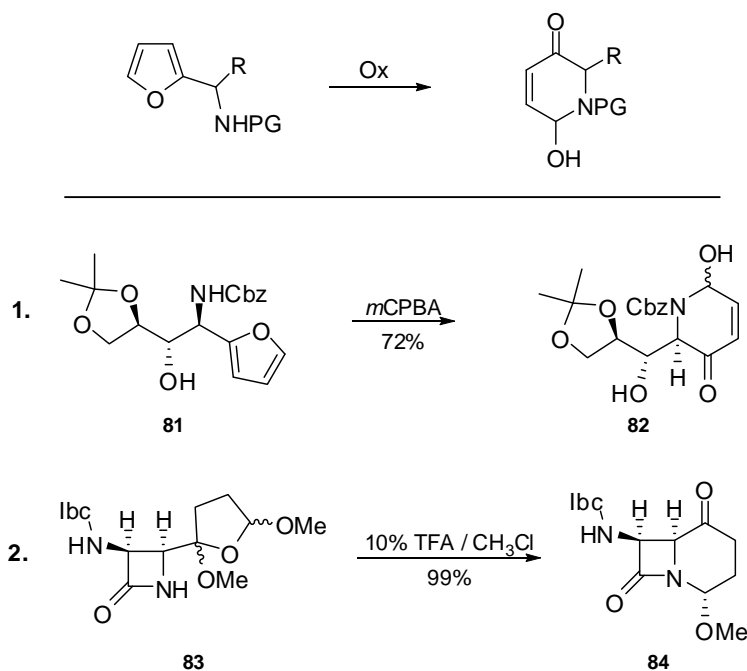


Scheme 34. Aza-Achmatowicz rearrangement and its possible applications in organic synthesis of loracarbef **78** (carbacephem antibiotic), swainsonine **79** (indolizidine alkaloid) and azasaccharide **80** (general structure). R¹ and R² maybe independent or joined into a ring.

The pioneering work on the *aza* variant of Achmatowicz reaction was performed by Ciufolini, who in 1986 reported the successful rearrangement of functionalised tetrahydrofurans into 6-membered nitrogenous rings.¹⁵³ Ten years later, Ciufolini applied this methodology for the preparation of structurally complex intermediate **84** in his synthesis of carbacephems antibiotics (Scheme 35, entry 2).¹⁵⁴ Recent studies have demonstrated the power of the aza-Achmatowicz reaction in preparing the highly functionalised molecule **82** with 4 stereocentres as a core building block during the total synthesis of swainsonine (Scheme 35, entry 1).¹⁵⁹

The presented examples illustrate an important feature of the aza-Achmatowicz rearrangement; the chirality at the furylic position as well as existing stereocentres, are conserved during rearrangement. For this reason, the aza-Achmatowicz products (e.g. **82** and **84**) derived from chiral starting materials are versatile intermediates in the asymmetric syntheses of biologically active and pharmaceutically important

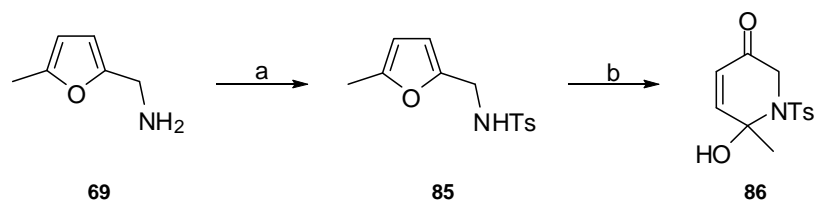
compounds such as antibiotic loracarbef **78**¹⁵⁴ or alkaloid swainsonine **79**,¹⁵⁹ a potential chemotherapy drug (Scheme 34 and 35).



Scheme 35. Synthetic applications of the aza-Achmatowicz reaction; **(1)** Rearrangement during the synthesis of 8a-*epi*-swainsonine,¹⁵⁹ **(2)** Preparation of key intermediate in the synthesis of loracarbef (carbacephem antibiotic).¹⁵⁴

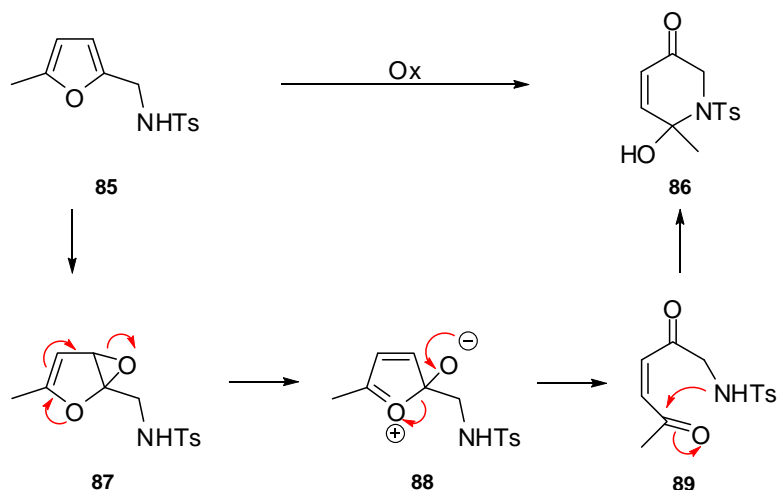
The aza-Achmatowicz rearrangements reported to date have been achieved with a variety of oxidative conditions, such as TFA/CH₃Cl, TfOH, *m*CPBA, as well as under the original conditions reported by Achmatowicz that employed Br₂ in MeOH, followed by mild acidic hydrolysis. In our synthesis we aimed to carry out aza-Achmatowicz rearrangement with *m*CPBA, influenced by the work of Padwa and co-workers.¹⁵⁷

Execution of our synthetic plan began with the protection of free amine functionality of 5-methylfurfurylamine **69** with tosyl chloride. The tosyl protecting group was chosen because of its compatibility with the relatively acidic conditions of the rearrangement, and the documented ease of purification of the resulting product.^{160,161} The obtained *N*-tosylaminofuran **85** was then treated with *m*CPBA to furnish aza-Achmatowicz product **86** (Scheme 36).



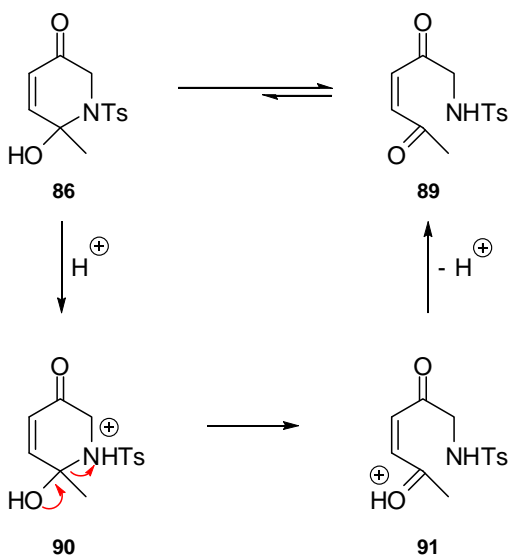
Scheme 36. *Reagents and Conditions:* a) TsCl, Et₃N, DCM, quant., b) *m*CPBA, DCM, 100% conversion by NMR.

A plausible mechanism for the aza-Achmatowicz rearrangement of furfurylamine **69** under oxidative conditions is presented (Scheme 37). This process begins with the nitrogen-directed epoxidation of the double bond of **85**, proximal to the amine group, to furnish epoxide **87**. Epoxide **87** then rearranges to generate zwitterion **88**, which opens to form diketone **89**. Finally, intramolecular attack of the nucleophilic nitrogen on the carbonyl group generates the aza-Achmatowicz product as hemiaminal **86**.



Scheme 37. The mechanism of aza-Achmatowicz rearrangement.

However, pyridinone **86** proved to be extremely unstable and none of attempts to modify it under Lewis acid catalysed conditions were successful. On the basis of NMR spectroscopy it was deduced that compound **86** which bears hemiaminal functionality favoured the open-chain form **89**. ¹³C NMR analysis showed two carbonyl signals, at 193.87 ppm and 197.98 ppm. It is suspected that the rate of ring opening of cyclic hemiaminal **86** was greatly increased by catalytic proton transfer (Scheme 38).



Scheme 38. The ring-opening mechanism of hemiaminal **86**.

Since our initial strategy failed due to the instability of cyclic hemiaminal **86**, a different starting material was considered for the aza-Achmatowicz reaction. To our knowledge, the synthetic work reported thus far in the literature have focused on the rearrangement of variety of furylamines **92** and furylamides **93** with unsubstituted furan rings (Figure 33).¹⁵⁰ Moreover, the reported rearrangement products were stable and successfully underwent a number of further modifications. Thus, it seems that the presence of methyl group in position 5 of the furyl framework in starting material **69**, although required in the final product **62**, was causing our synthetic approach to fail.

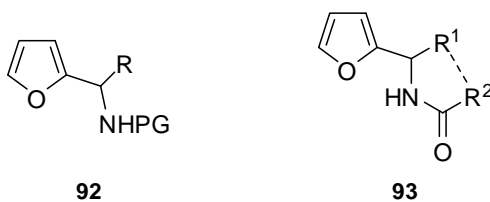
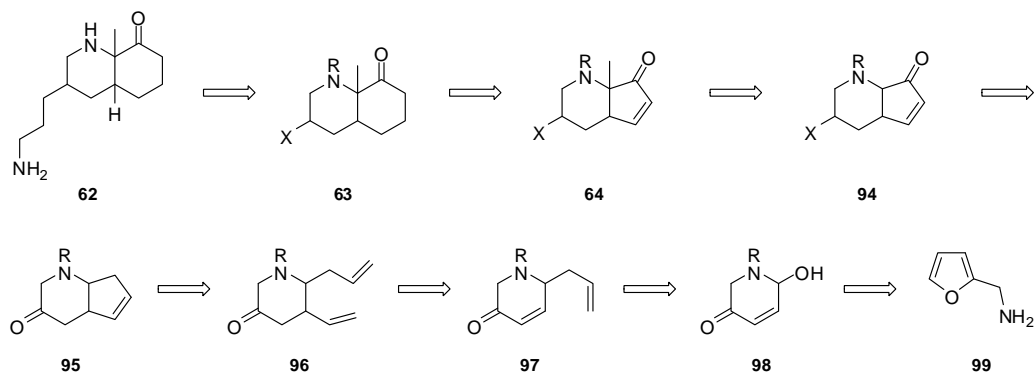


Figure 33. General structure of furylamines **92** and furylamides **93** utilised as starting materials for the aza-Achmatowicz rearrangement (PG=protecting group; R¹, R² might be independent or joint into a ring).¹⁵⁰

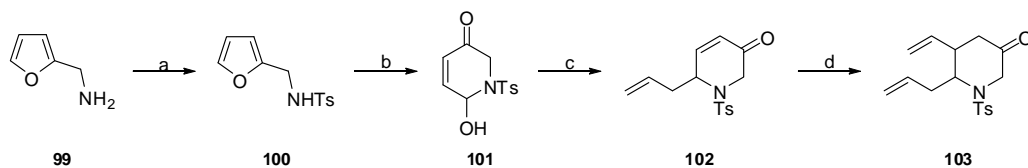
For this reason, it was decided to investigate the rearrangement of a furfurylamine **99** that could serve as a new starting material in the synthesis of GRIS molecule. At this

point of our investigation the successful rearrangement of compound **99** was critical to pursue the synthesis *via* an aza-Achmatowicz route. The revised synthetic plan followed in principle the first approach (see Scheme 31), but required assembling of the methyl group at the ring junction later in the synthesis as shown in Scheme 39.



Scheme 39. Revised retrosynthetic analysis of GRIS peptidomimetic **62**.

Execution of our modified approach began with the protection of furfurylamine **99** with tosyl chloride. The resulting tosyl amide **100** was then rearranged under oxidative conditions to furnish cleanly the aza-Achmatowicz product **101**. Pyridinone **101** was stable enough to undergo aqueous work-up, after which it was treated with allyltrimethylsilane in the presence of Lewis acid (i.e. boron trifluoride ethyl etherate). This reaction produced piperidone **102**. Due to its sensitive nature, enone **102** was not purified but reacted in crude form with the *in situ* generated vinyl cuprate reagent to furnish the 1,4 conjugate addition product **103**.¹⁵⁷ The stable diene **103** was produced as a single diastereoisomer in 67% yield over four steps (Scheme 40).



Scheme 40. *Reagents and Conditions:* a) TsCl, Et₃N, DCM, quant., b) *m*CPBA, DCM, rt, c) allyltrimethylsilane, BF₃·OEt₂, DCM, 0 °C, d) CuI, vinylMgBr, THF, -78 °C then -30 °C then -78 °C, 67% from **99**.

At this stage in our synthetic investigation we focused our attention on another crucial transformation: the ring closing metathesis (RCM) of diene **103**. According to our synthetic plan this reaction would generate the desired 5,6-bicycle.

The catalytic ring closing metathesis (RCM) is undoubtedly one of the most important and powerful methods for the generation of ring structures of various sizes and classes.¹⁶² The most developed and utilised method in synthetic organic chemistry is the alkene RCM, however, in recent years also the ring-closing alkyne¹⁶² and enyne¹⁶³ metatheses have found impressive applications (Figure 34). Nevertheless, for the purpose of our synthetic route, we were interested in the application of an olefin ring closing metathesis.

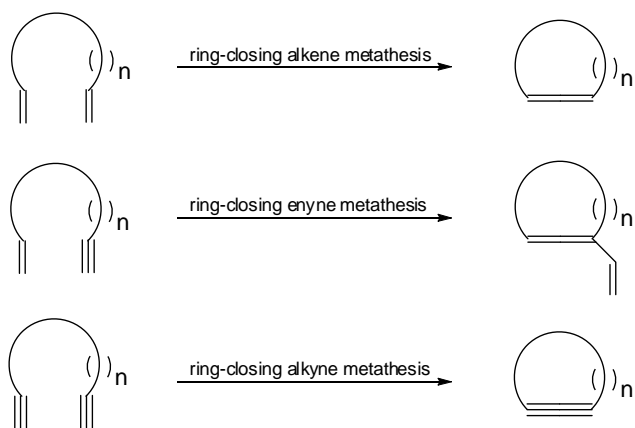


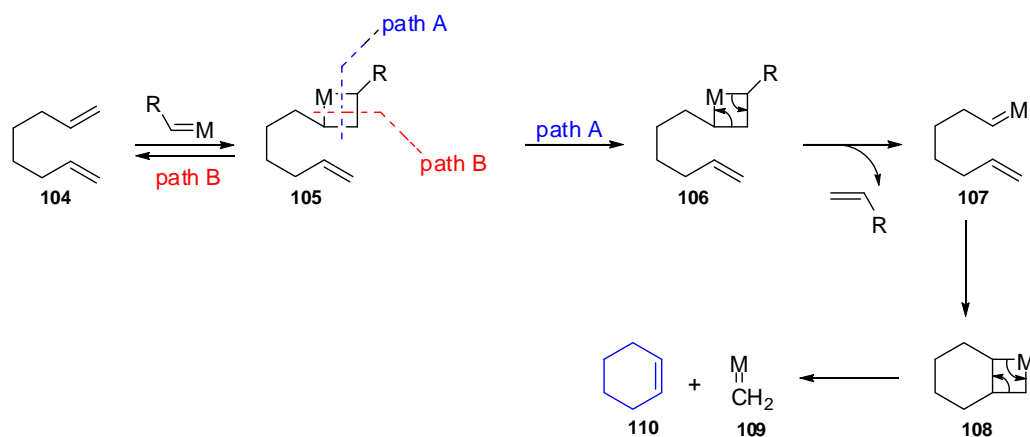
Figure 34. Different types of ring-closing metathesis.

In this process two terminal alkenes react with the catalyst to ultimately generate the cyclic olefin. A generalised pathway illustrating how this transformation proceeds is shown on Scheme 41.¹⁶⁴

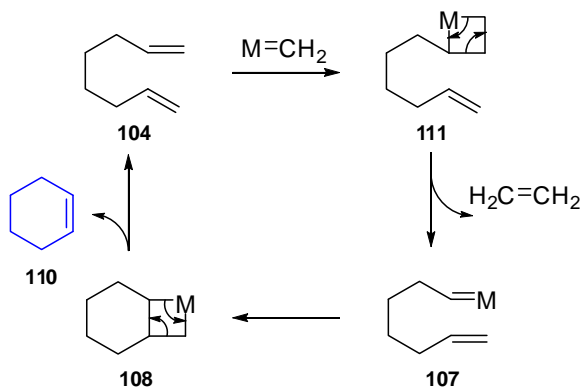
Mechanistically, the catalytic cycle consists of two phases: initiation and propagation. The initiation phase began with the association of the metal with one of the two olefins of the substrate **104** to generate metallacyclobutane **105** (Scheme 41, catalyst initiation). This active complex might revert to starting materials *via* path B because all olefin metathesis reactions are in principle reversible; but it could also

proceed *via* path A, in which the existing bonds break to furnish intermediate **107**. If this route is favoured, the metal (**M**) ends up within the substrate. Then formation of metallacyclobutane **108** followed by its break down produces desired cyclic molecule **110** and the metal-bearing compound **109** that serves as a catalyst during propagation phase (Scheme 41, catalyst propagation). In the propagation phase the active catalyst **109** promotes additional cycles. What typically drives the RCM reactions is that the cyclic product **110** does not easily react with the catalyst **109** to undergo ring-opening metathesis. The release of by-product, the volatile olefin (i.e. ethylene) easily removed by evaporation, also forces the equilibrium towards the production of the cyclic olefin.

Catalyst initiation



Catalyst propagation



Scheme 41. The general mechanism for ring-closing olefin metathesis (adapted from reference **164**).

Although complexes of several metals (such as tungsten, rhenium and osmium) were shown to promote metathesis reactions, the most reactive and stable, and therefore widely used are molybdenum (Mo) and ruthenium-based (Ru) catalysts. The routinely utilised Ru complexes have the advantage of being stable to air and moisture. Moreover, they tolerate wide range of substrates that carry hydroxyl, carboxylic acid, or aldehyde functionalities, but can be rendered inactive in the presence of structurally exposed amines and phosphines. On the contrary, the commercially available Mo catalyst, developed by Schrock, is more reactive, especially in the presence of amino groups, but needs to be handled under an inert atmosphere because of its sensitivity to moisture and oxygen (Figure 35).¹⁶⁴

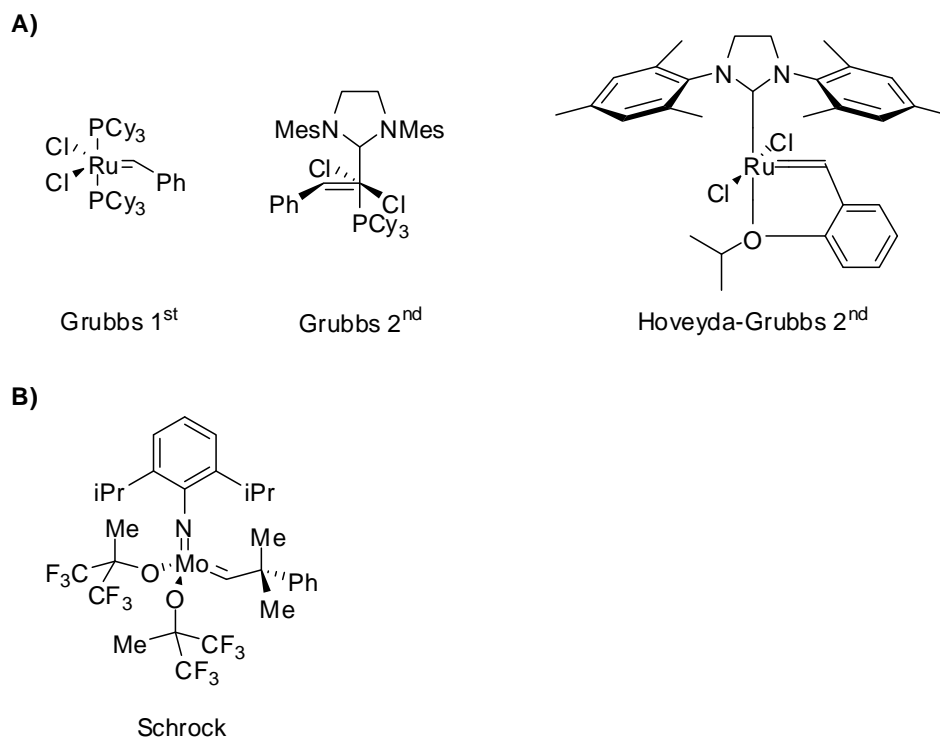
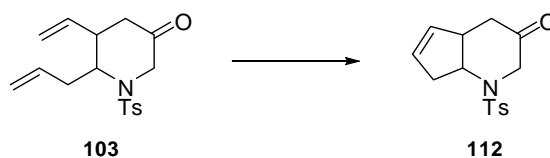


Figure 35. Common ruthenium (**A**) and molybdenum (**B**) complexes used in metathesis reaction (Ph = phenyl, Cy = cyclohexyl).

In our synthesis of the GRIS molecule, an alkene RCM was required for the construction of a 5-membered carbocycle, fused to the existing nitrogenous ring. We decided to start the synthesis of bicycle **112** by employing the first-generation Grubbs catalyst. This metal complex proved to be very successful in Padwa's syntheses of octahydroquinoline ring systems, that share some structural homology

with bicycle **112**.¹⁵⁷ Under these reaction conditions the desired 5-membered ring of **112** was formed, albeit in relatively low 37% yield (table 6, entry 1). Thus, we investigated other metal carbenes, which could catalyse the conversion of diene **103** to bicycle **112** more effectively. Therefore, we employed a more active, thermally stable and convenient to handle 2nd generation Grubbs catalyst. We also carried out the reaction with Hoveyda-Grubbs 2nd generation catalyst which is considered a good RCM initiator, tolerates wide range of substrates and is usually more reactive than Grubbs 2nd at lower temperature. The RCM reaction was conducted under varied temperatures, with different solvents and catalysts loading (Table 6, entry 2-4). However, the desired cyclic product **112** was not isolated under any of the conditions employed.



Entry	Catalyst	Catalyst loading	Lewis acid (20 % mol.)	Solvent	Conc.	Temp.	Yield
1	Grubbs 1 st gen.	10% mol	–	DCM	c=0.06	rt-37 °C	37%
2	Grubbs 2 nd gen.	7 + 7% mol	–	DCM	c=0.05	rt	<1%
3	Grubbs 2 nd gen.	7% mol	–	PhMe	c=0.05	rt	<1%
4	Hoveyda-Grubbs 2	5 + 5% mol	–	DCM	c=0.05	reflux	–
5	Hoveyda-Grubbs 2	5% mol	Ti(O ^{<i>i</i>} Pr) ₄	DCM	c=0.05	reflux	–
6	Grubbs 2nd gen.	10% mol	Ti(O^{<i>i</i>}Pr)₄	DCM	c=0.005	reflux	82%

Table 6. Optimisation of the catalyst and the reaction parameters of the RCM.

Finally, after careful analysis of the obtained results, the conditions reported by Yu for Lewis acid assisted RCM were employed.¹⁶⁵ To our gratification, in the presence of Grubbs 2nd generation catalyst and Ti(O^{*i*}Pr)₄ as a co-catalyst, the cyclization of diene **103** proceeded in excellent 82% yield (Table 6, entry 6).

On the basis of the experiments performed and NMR analysis we believe that the major problem in the cyclization of diene **103** originates from the nature of precursor **103**. Usually in the RCM reaction the major challenge comes from the competitive

cross-metathesis. However in this case there was no evidence that dimerisation or oligomerisation of compound **103** occurred. Thus, we focused our attention on the structure of diene **103** and its implication for the RCM reaction.

The diene **103** carries a Lewis-basic and potentially catalyst-deactivating nitrogen containing group. The Ru-based catalysts, utilised in our RCM reaction, are especially sensitive to the presence of nucleophilic nitrogen. Although the nitrogen atom is not a part of the newly formed 5-membered ring of compound **112**, its presence in the molecule seemed to affect the outcome of the reaction. According to the literature, a major issue associated with the use of amine-containing substrates for RCM concern their ability to coordinate to metal-alkylidene complexes.^{166,167} It is postulated that this interaction is responsible for the catalysts' inactivation, and hence unsuccessful RCM reactions.

Thus, several strategies have been developed and adopted to prevent catalyst deactivation by the Lewis-basic nitrogen atom. There are two principal approaches; the first relies on increasing the steric hindrance around an amine group, hence making it less accessible for the metal complex. The second relies on reducing the basic character of the amine unit. Consequently, widely used methods include conversion of amines to carbamates, sulphonamides, amides or ammonium salts.¹⁶⁶ Alternatively, RCM reaction of free amines can also be carried out in the presence of protonating agent, such as *p*-toluenesulfonic¹⁶⁸ or camphorsulfonic acid.¹⁶⁹ Also the tosyl protecting group, utilised in our synthetic strategy, should in principle have favoured the RCM by decreasing the electron density on the nitrogen atom. However, examples in the literature indicate that this effect is not always sufficient to achieve successful RCM.¹⁶⁶

The approach, eventually adopted in our synthesis, was developed by the group of Yu, during their work on the synthesis of amine-containing heterocyclic structures by RCM. Yu and co-workers reported a methodology for a mild, Lewis-acid assisted ring-closing olefin metathesis of diallylamine substrates.¹⁶⁵ Their model studies showed that introduction of a Lewis acid to the RCM of amine-containing compounds could significantly increase the yield or in some cases help the reaction to proceed. The Lewis acid is believed to compete with ruthenium species in

coordination to nitrogen atom, leaving Ru-catalyst available for olefinic part of the molecule.

Yu and co-workers studied different Lewis acids as co-catalysts for the RCM reaction of diallylamines. Of the Lewis acids tested, they found titanium isopropoxide to be the most promising for this transformation, with the second generation Grubbs as the preferred catalyst. Thus, as presented in Table 6, after employing Yu's conditions for the RCM of diene **103** we were able to successfully synthesise the bicyclic compound **112**. However, it should be noted that scaling-up of the RCM, while maintaining reaction parameters, proved to be troublesome and resulted in a significant drop in yield (40% on a 2g scale).

Since bicycle **112** was crystalline in nature, the relative stereochemistry was established using X-ray diffraction methods. The X-ray structure of **112** clearly showed an *anti*-relationship between the protons at the ring junction (Figure 36).

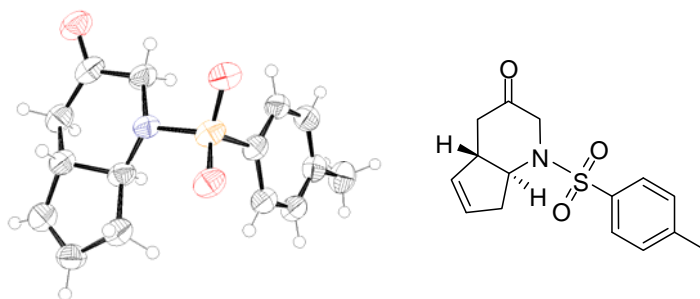
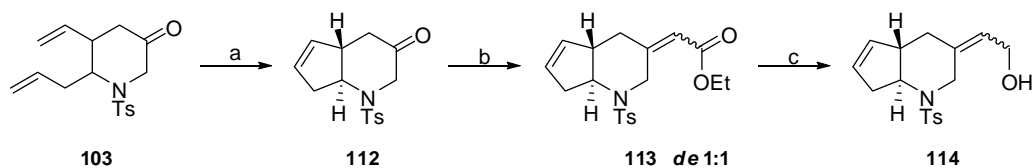


Figure 36. Crystal structure of bicycle **112**.

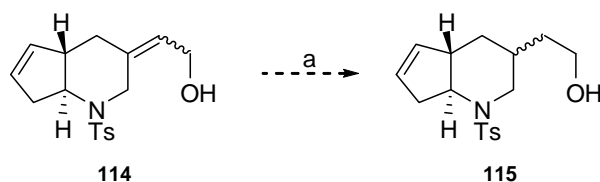
With the intermediate **112** in hand, the introduction of the amine-containing side chain was attempted. The assembly of the side chain began with the Wittig olefination of ketone **112** that worked in good yield (84%), and, as expected, produced compound **113** as a mixture of *E/Z* isomers (1:1 ratio based on NMR data). Subsequent reduction of ester functionality of **113** smoothly generated alcohol **114** as a mixture of diastereoisomers that weren't separable by flash column chromatography (Scheme 42).



Scheme 42. *Reagents and Conditions:* a) Grubbs 2nd gen., Ti(OⁱPr)₄, DCM, reflux, 82%, b) Ph₃PCHCO₂Et, DCM, reflux, 84%, c) DIBAL-H, Et₂O, 0 °C, quant.

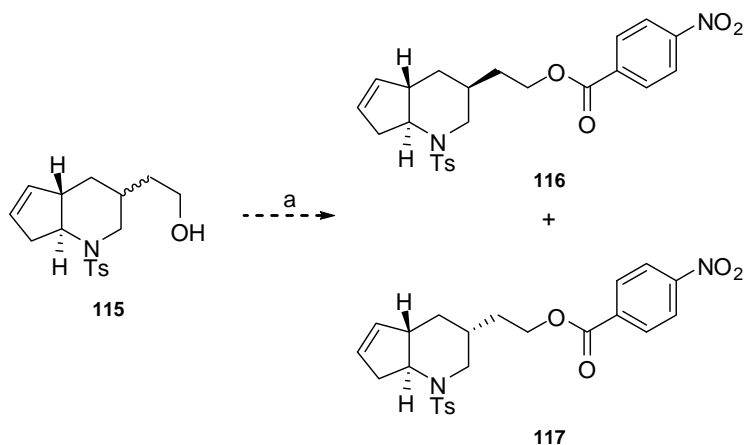
The next step in the synthesis involves the selective hydrogenation of hydroxy olefin **114**. For this purpose it was decided to employ the homogenous rhodium catalyst Rh(Cl)(PPh₃)₃ (Wilkinson's catalyst), which reduces alkenes under mild conditions. Previous studies from several laboratories have established that allylic and homoallylic alcohols can be selectively reduced in the presence of rhodium complexes.^{170,171} The hydroxyl group has been shown to direct the site of the hydrogenation, whilst accelerating the rate of hydrogenation.¹⁷²

Mechanistically, the hydroxyl group remains bound to the metal during the catalytic cycle and hence controls the stereochemical course of hydrogen delivery through chelation.¹⁷³ However, the level of diastereoselection during the hydrogenation of olefin **114** in our synthesis couldn't be determined as the starting material **114** was a mixture of *E/Z* isomers. Hence, it was expected, that the reduction of **114** will produce alcohol **115** as a mixture of stereoisomers (Scheme 43).¹⁷⁴ The NMR analysis suggested the presence of two diastereoisomers, which again, due to the similarities in their *R_s*, weren't separable by preparative chromatography. Additionally, the complexity of the NMR spectra made assignment of individual signals impossible.



Scheme 43. *Reagents and Conditions:* RhCl(PPh₃)₃, H₂, EtOH

Since based on NMR analysis it was not possible to confirm that we indeed synthesised the alcohol **115**, the recrystallization of one of the expected diastereoisomers from the complex mixture of **115** was attempted. For this purpose **115** was coupled with *para*-nitrobenzoic acid (Scheme 44). This transformation was expected to produce two compounds, **116** and **117**. The reaction generated yellow-orange solid, which was treated with various solvents and solvent mixtures. However, recrystallization failed to separate any pure compound from the mixture **115**.



Scheme 44. Reagents and Conditions: a) *p*-nitrobenzoic acid, DCC, DMAP, DCM

At this stage of the synthesis, we decided to focus our efforts on building the final bicyclic core, and postpone addressing the issue of the side chain assembly until later in the synthesis. In order to explore the remaining reactions, such as allylic oxidation, ring expansion and installation of methyl group at ring junction, the model compound **118** was envisioned and prepared (Figure 37). The simplified derivative **118** would allow us to carry out the synthetic investigations without the confusion caused by the presence of non-separable diastereoisomers.

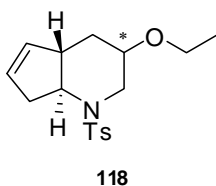
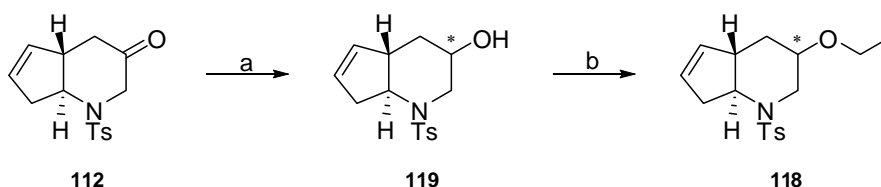


Figure 37. Model compound **118**.

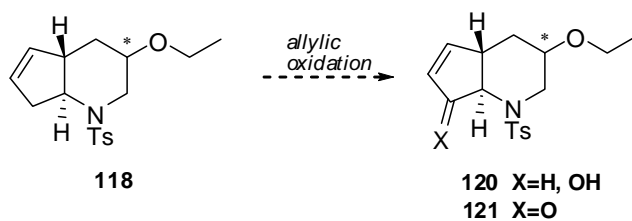
Synthesis of model system **118** was initiated by reduction of ketone **112** to the alcohol **119** under the influence of L-Selectride (Scheme 45). The application of the bulky reagent at low temperature was anticipated to give us a degree of stereocontrol for the reduction step. Alcohol **119** was obtained as a single diastereoisomer, as confirmed by NMR analysis. It was attempted to establish the relative stereochemistry of the crystalline **119** by X-ray analysis. However, that was not successful due to crystals quality.



Scheme 45. *Reagents and Conditions:* a) L-Selectride, THF, $-78\text{ }^{\circ}\text{C}$, 87%, b) NaH, $\text{CH}_3\text{CH}_2\text{I}$, DMF, $0\text{ }^{\circ}\text{C}$, 79%

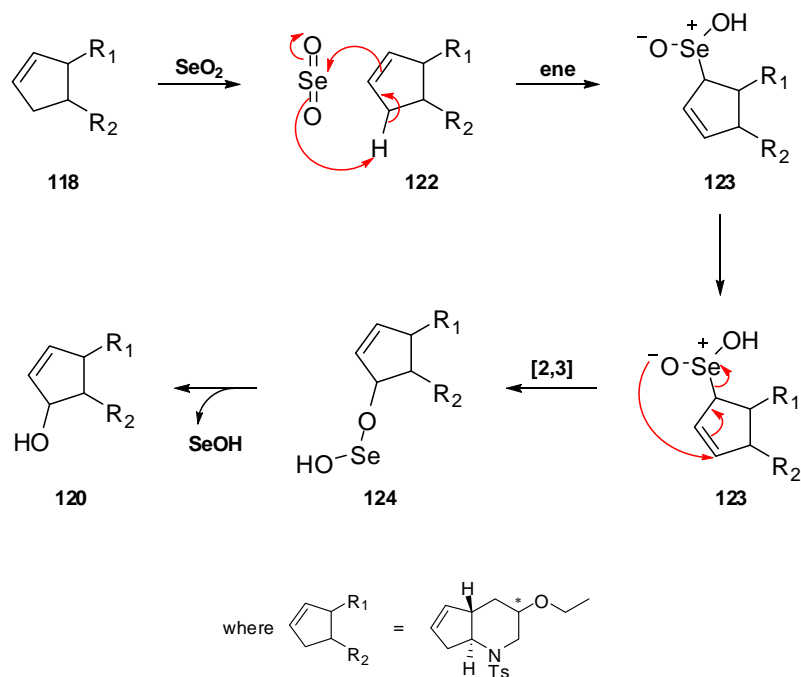
Based on NMR data it is reasonable to assume that we indeed synthesised **119** as a single diastereoisomer, as required for the purpose of our model studies. Alkylation of **119** protected the sensitive alcohol functionality (Scheme 45), and provided the requisite compound **118** that could then be used to define the conditions for allylic oxidation and to explore the subsequent steps in the synthesis.

Allylic oxidation is a well documented process that allows regioselective functionalization of an allylic C-H bond with oxygen. This transformation is known to be catalysed by a variety of transition metals, such as chromium (VI) manganese (III), bismuth (III), copper, cobalt and chromium. Usually, due to the cost of the catalysts and the toxicity of metallic by-products, the reaction is carried out with a substoichiometric amount of metal complex and a stoichiometric amount of a co-catalyst, such as peroxide, which reoxidises the metal. Depending on the catalysts and the nature of the substrate, an allylic oxidation can produce either an allylic alcohol such as **120** or the corresponding **121** (Scheme 46).



Scheme 46. Possible products (**120** and **121**) of allylic oxidation of alkene **118**.

Our initial studies on the allylic oxidation involved treatment of alkene **118** with selenium dioxide (SeO_2) and *tert*-butyl hydroperoxide.¹⁷⁵ Based upon the regioselectivity rules for the allylic oxidation with the SeO_2 , we expected that oxidation would take place at the α -methylene carbon of the double bond of **118**. A plausible pathway, illustrating how the oxidation of cyclopentene **118** by SeO_2 would proceed, is shown in Scheme 47.

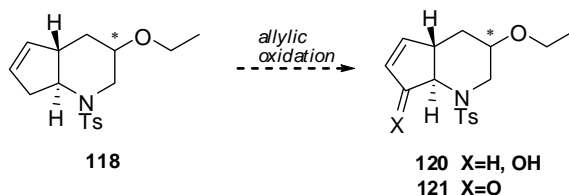


Scheme 47. The mechanism of allylic oxidation of alkene **118**

An allylic oxidation is initiated by the reaction of SeO_2 with alkene **118** in an ene cycloaddition that produces allylic seleninic acid **123**. This intermediate undergoes allylic rearrangement to give an unstable compound **124** that rapidly decomposes to

yield allylic alcohol **120**. In some cases, the oxidation can continue to produce an aldehyde or ketone, depending on the nature of the substrate.

However, the oxidation of alkene **118** with SeO_2 failed to yield allylic alcohol **120** (Table 7). We then employed various other catalysts that could affect the transformation of alkene **118** to alcohol **120** or ketone **121** (Table 7). Thus, olefin **118** was subjected to a bismuth (III) chloride catalysed oxidation but, again, the reaction failed to produce the desired enone **121**.¹⁷⁶ Alkene **118** was also treated with *tert*-butyl hydroperoxide in the presence of catalytic manganese (III) acetate under an oxygen atmosphere.¹⁷⁷ These conditions were reported as an alternative method for the mild and regioselective allylic oxidation of steroids and simple cyclic olefins, such as cyclopentene. However, despite prolonged reaction time (3 days), there was no evidence for the formation of enone **121**.



Entry	Reagents and conditions
1	SeO_2 , <i>t</i> BuOOH (70% in H_2O), salicylic acid, DCM
2	BiCl_3 , <i>t</i> BuOOH, MeCN, 70 °C
3	$\text{Mn}_3\text{O}(\text{OAc})_9$, <i>t</i> BuOOH, O_2 , EtOAc
4	$\text{Rh}_2(\text{cap})_4$, K_2CO_3 , <i>t</i> BuOOH, DCM, air

Table 7. Catalysts and reaction parameters of allylic oxidation of alkene **118**.

There are reports in the literature of other promising methods for the allylic oxidation of olefins. Catino and co-workers reported in 2004 a novel protocol for the allylic oxidation of alkenes, using rhodium complex **125** as a catalyst (Figure 38).¹⁷⁸

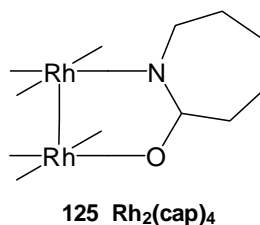


Figure 38. The structure of dirhodium (II) caprolactamate **125**.

These studies demonstrated that dirhodium (II) caprolactamate **125** ($\text{Rh}_2(\text{cap})_4$) is an exceptionally efficient catalyst for methylene oxidations to a corresponding ketone, with the reaction being completely selective, tolerant of air and moisture, and could be performed with as little as 0.1 mol % catalyst loading. Unfortunately, allylic oxidation of alkene **118** under these conditions also failed to generate desired product **121** (Table 7, entry 4).

Thus, no progress was made in the installation of the crucial ketone group on 5-membered ring of model compound **118**. Careful inspection of the data on the allylic oxidation under all conditions applied revealed that neither the allylic alcohol **120** nor enone **121** were formed. In addition to that principal drawback of our synthetic route, we also experienced a significant reduction in yield whilst scaling-up the RCM reaction and faced stereochemistry issues. For these reasons, a novel synthetic approach to the GRIS peptidomimetic **62** was designed.

4.1.2 The Diels-Alder approach

Since our studies on synthesis of GRIS molecule *via* aza-Achmatowicz route proved to be problematic, we turned our attention to other synthetic strategies that could allow us access to GRIS peptidomimetic **62** structure.

Upon searching the literature it was noticed that the target GRIS peptidomimetic **62** shares a number of structural similarities with an intermediate **126** (Figure 39)

synthesised by P. Stanetty and co-workers in their approach to the AB-ring system of certain 9-azasteroids.¹⁷⁹

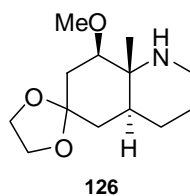
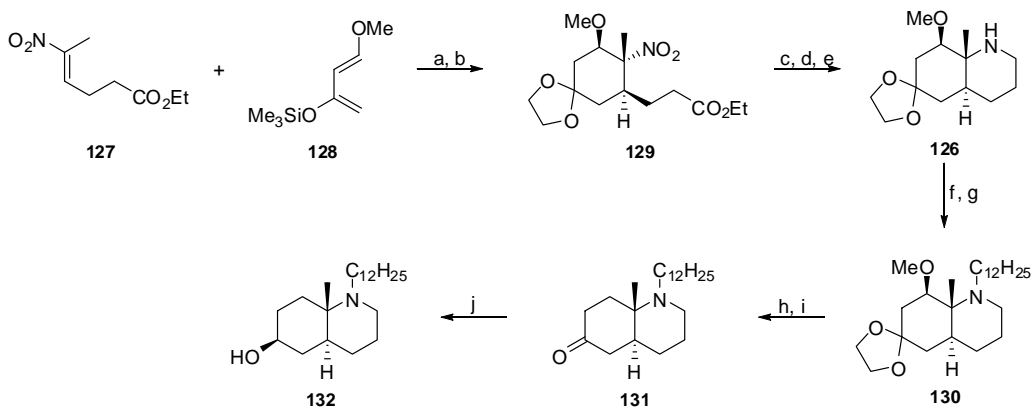


Figure 39. Intermediate **126** in the synthesis of 9-azasteroids

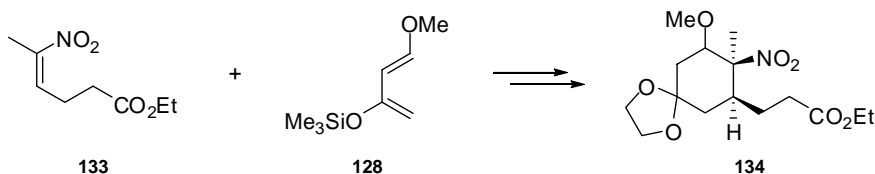
The synthetic route, developed and executed by this group, is outlined in Scheme 48. Attention focused specifically on intermediate **126** that possess structural features, such as heterocyclic core, methyl group at the rings junction, fixed stereochemistry at the ring junction and a methoxy group, which are very close to or could be related to those of GRIS molecule **62**.

The synthetic route developed by Stanetty relied on the highly stereoselective Diels-Alder (DA) cycloaddition of Danishefsky's diene **128** with *E*-nitroalkene **127**, which secured the stereochemistry required for the target product **132** (Scheme 48).



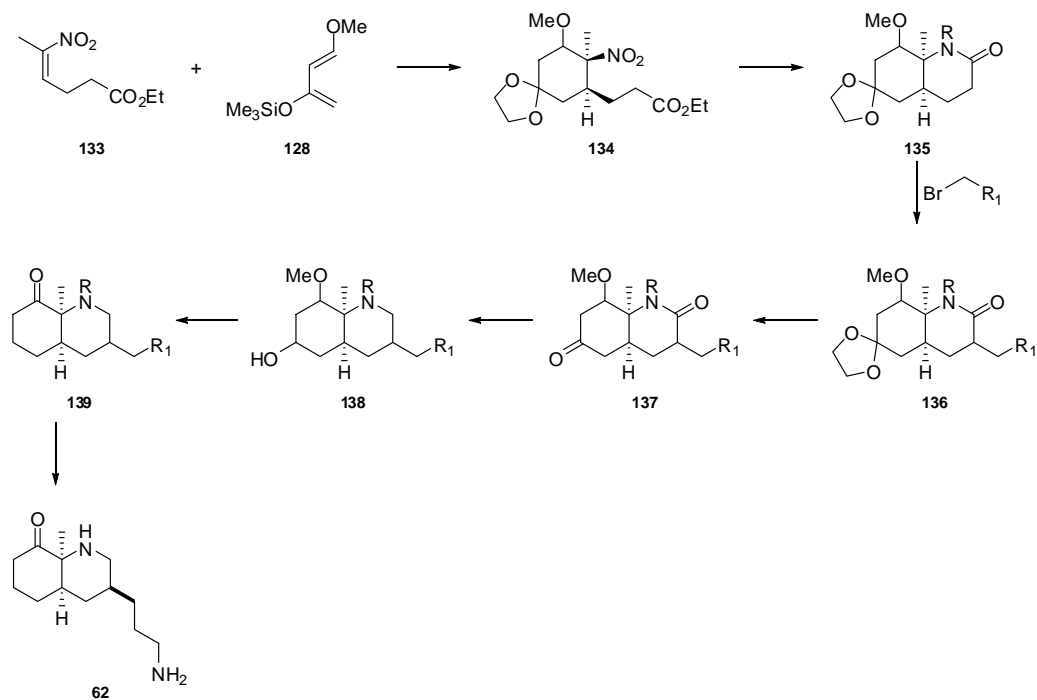
Scheme 48. *Reagents and Conditions:* a) benzene, reflux, 63%, b) (CH₂OH)₂, TSA, benzene, Dean–Stark separator, 98%, c) Al/Hg, THF/H₂O, 79%, d) TiCl₃, 75%, e) Red-Al®, 75%, f) C₁₁H₂₃COCl, NEt₃, DMAP, 75%, g) Red-Al®, 88%, h) 6N HCl, 76%, i) H₂, Pd/C, 97%, j) Red-Al®, 95%.

Thus, it was reasoned that an analogous DA transformation with the *Z*-nitroalkene **133**, and subsequent protection of the carbonyl group would generate a cyclohexene **134** with the opposite stereochemistry at the carbon bearing the nitro group (Scheme 49).



Scheme 49. Diels-Alder reaction and protection of carbonyl group to produce intermediate **134**.

As outlined in our new synthetic strategy for the construction of GRIS mimetic (Scheme 50), reduction of nitro group of adduct **134** and subsequent Lewis-acid mediated ring closure would then produce the bicycle **135** in diastereoisomerically pure form and with the desired *cis* stereochemistry at the ring junction.

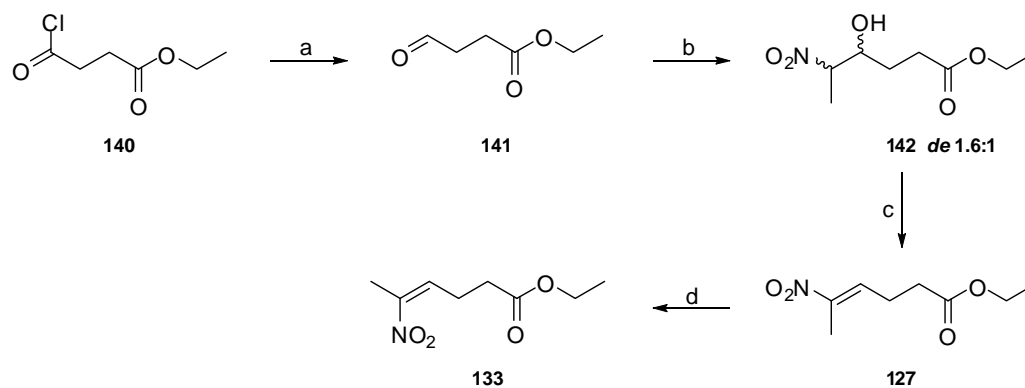


Scheme 50. Diels-Alder approach to GRIS peptidomimetic **62**.

The next step in the strategy would be to assemble the side chain using enolate chemistry. The resulting compound **136** could then undergo deprotection of the ketone functionality, followed by dual-reduction of both the ketone and amide functions to furnish alcohol **138**. Further reduction/cleavage of the alcohol group of compound **138** would provide bicycle **139** that after several functional group interconversions and deprotection of amine functionality should present us with the desired GRIS peptidomimetic **62** (Scheme 50).

Our studies towards the synthesis of the GRIS mimetic *via* a Diels-Alder strategy began with the preparation of both starting materials, the *Z*-nitroalkene **133** and Danishefsky's diene **128**. The *Z*-nitro olefin is not commercially available, it was therefore necessary to design a short synthesis that would allow us to access this compound. On the contrary, Danishefsky's diene could be purchased, however, due to its sensitive nature we aimed to prepare it ourselves and use in the DA cycloaddition before degradation.

Thus, the synthesis of *Z*-nitroalkene **133** began from acid chloride **140** which was reduced under Rosenmund conditions to cleanly furnished aldehyde **141** in excellent yield (94%) (Scheme 51).¹⁸⁰ The subsequent Henry reaction of **141** with nitroethane proceeded smoothly and yielded cleanly nitroaldol adduct **142**. However, as expected, β -nitro alcohol **142** was produced as a mixture of *syn*/*anti* diastereomers (*de* ratio 1.6:1) due to the reaction's reversibility and the easy epimerization at the nitro-substituted carbon.¹⁸¹



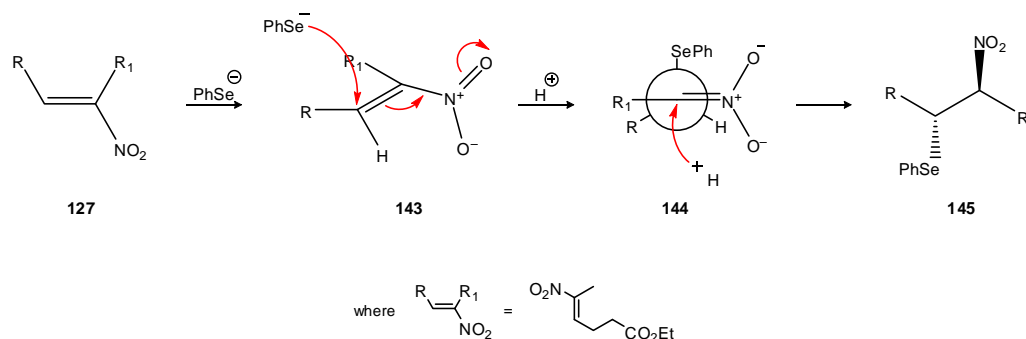
Scheme 51. *Reagents and Conditions:* a) 2,6-lutidine, H₂, Pd/C, THF, 94%, b) EtNO₂, *t*BuOK, THF/*t*BuOH, 98%, c) TFAA, Et₃N, DCM, 71%, d) i. (PhSe)₂, NaBH₄, EtOH, ii. solution of **127** in EtOH, then AcOH, -78 °C, iii. H₂O₂, DCM, 0 °C, 94% from **127**.

The next transformation, the dehydration of β -nitro alcohol **142**, was extensively studied. The Henry product **142** was first treated with acetic anhydride in the presence of a catalytic DMAP to afford the nitro acetate that subsequently underwent elimination reaction upon treatment with base.¹⁸¹ This two-step procedure furnished the desired nitroalkene **127** as the single *E* isomer, albeit in poor yield (Table 8, entry 1). The dehydration reaction was attempted under a variety of alternative conditions, with a view to improve the reaction yield (Table 8). Unfortunately, all attempts to affect the elimination of the alcohol **142** via the mesylate intermediate failed to deliver the desired product **127** (Table 8, entry 2-4).^{182,183} However, treatment of nitroalcohol **142** with trifluoroacetic anhydride (TFAA) and triethylamine under precise temperature control (-35 °C to -60 °C (3h) and -20 °C (2h)) over the course of reaction furnished 71% of the *E*-alkene **127** after purification (Table 8, entry 7).¹⁸⁴ The NMR data obtained for the *E*-nitroalkene **127** was consistent with data previously published in the literature.¹⁸⁵

Entry	Reagents and conditions	Yield of 127
1	i. Ac ₂ O, DMAP, Et ₂ O, 0 °C then rt ii. K ₂ CO ₃ , <i>t</i> BuOH, 35 °C	32%
2	MsCl, Et ₃ N, DCM, 0 °C then rt	compounds mixture
3	i. MsCl, Et ₃ N, DCM, 0 °C then 35 °C ii. DBU, 0 °C then rt	compounds mixture
4	i. MsCl, DMAP, Et ₃ N, DCM, 0 °C then rt ii. DBU, 0 °C then rt	compounds mixture
5	TFAA, Et ₃ N, DCM, -20 °C	60%
6	i. TFAA, Et ₃ N, DCM, -20 °C ii. DBU, -20 °C	32%
7	TFAA, Et ₃ N, DCM, -35 °C to -60 °C (3h) and -20 °C (2h)	71%

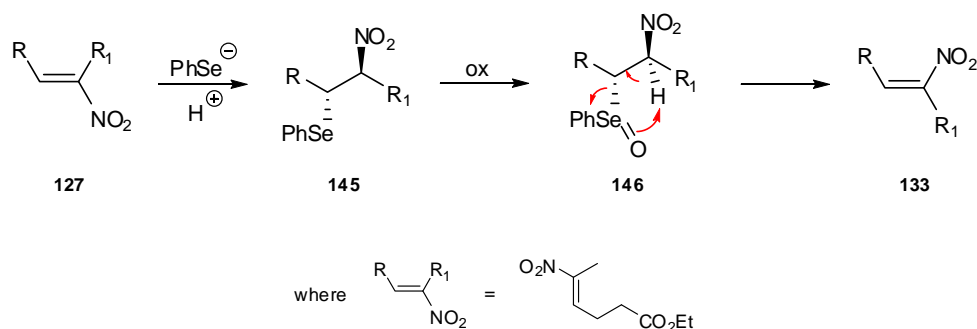
Table 8. Reaction conditions of dehydration step.

Having synthesised the desired *E*-olefin **127** as a single isomer, we focused on the transformation that would allow to access the *Z*-isomer **133**. Hence, we adopted methodology reported by N. Ono and co-workers for the conversion of *E*-nitroalkenes to *Z*-nitroalkenes *via erythro*- β -nitroselenides.^{186,187} Treatment of *E*-isomer **127** with the sodium benzeneselenoate (generated *in situ* from diphenyl diselenide and sodium borohydride), followed by the subsequent protonation with acetic acid gave intermediate **145** (Scheme 52). The stereoselectivity of the protonation step could be explained by assuming that under the reaction conditions (-78 °C), the protonation of intermediate **144** took place from the less hindered site to produce predominantly *erythro*-isomer **145**.



Scheme 52. Stereoselectivity in the formation of *erythro*-isomer **145**.

Further oxidation of selenide **145** with hydrogen peroxide resulted in the subsequent *syn*-elimination of benzeneselenic acid, and furnished the desired *Z*-isomer **133**. The mechanism of the elimination step, which is believed to proceed *via* 5-membered transition state, is shown on Scheme 53.¹⁸⁸ The overall isomerisation procedure occurred in excellent yield (94%) and produced **133** as an inseparable mixture of *Z/E* double bond isomers in a satisfying 9:1 ratio.



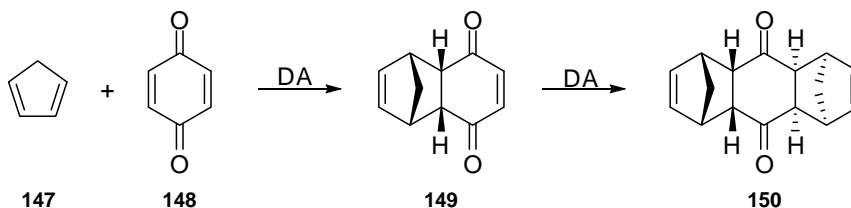
Scheme 53. Mechanism of the conversion of *E*-nitro alkene to *Z*-nitro alkene *via* *erythro*- β -nitroselenide.

After completing the synthesis of *Z*-nitroalkene **133**, we focused on the preparation of the Danishefsky's diene **128**. This highly reactive diene was synthesized according to standard procedures and it was immediately used in the Diels-Alder reaction, the crucial transformation in the synthetic route.¹⁸⁹

The Diels-Alder (DA) reaction is a one of the best known and fascinating [4+2] cycloadditions. This pericyclic transformation engages a conjugated diene (4 π -electron component) and dienophile (2 π -electron component) to produce an unsaturated 6-membered ring. The versatility and potential of the DA reaction is reflected in the predictable regio- and stereochemistry of the resulting cyclohexane rings, possessing up to four contiguous stereocenters. Furthermore, careful choice of substrates allows introduction of many functional groups to the DA adduct. Since its discovery in 1928, the DA cycloaddition has found impressive applications in total synthesis of various classes of biologically active compounds and natural products.¹²⁶ Important advances in the DA reaction, such as development of hetero-DA, intramolecular and transannular variants, have significantly broadened the scope and

utility of the methodology. It has long been recognized that the DA is a powerful tool for the construction of complex molecules and cyclic systems (up to three carbocyclic rings) in only one transformation.¹⁹⁰

The original DA reaction involved the cycloaddition of cyclopentadiene **147** with quinone **148** induced upon heating (Scheme 54).¹⁹¹

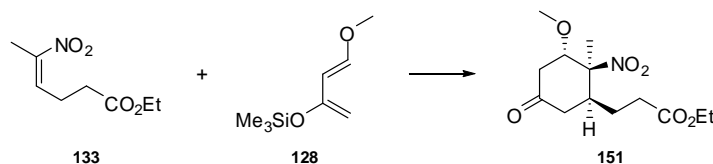


Scheme 54. The discovery of the Diels-Alder reaction.

However, recent studies in the area have focused on the use of Lewis acids as mild promoters of the cycloaddition. Various Lewis acids catalyse the DA reaction by decreasing the activation energy of the process. In a typical Lewis acid-mediated DA reaction, the metal complex coordinates reversibly to the dienophile and substantially lowers the LUMO energy, thereby enhancing the interaction with the diene HOMO.¹⁹² The application of catalysts to induce the cycloaddition has not only expanded the scope of the reaction to heat-sensitive dienes and dienophiles, but has also resulted in greater control over the reaction regioselectivity.

In our studies, the DA cycloaddition of Danishefsky's diene **128** with *Z*-nitro olefin **133** was attempted in both catalytic and thermal version (Table 9). Initially, DA reaction of **128** with **133** was attempted under standard thermal conditions. This method failed to deliver the desired product **151**. Also the use of the Lewis acid catalyst, TiCl_4 , failed to promote the reaction. The presence of strong Lewis acid catalyst or high temperature was possibly causing the decomposition of Danishefsky's diene. This diene has been previously demonstrated to be sensitive towards catalysts such as ZnCl_2 , AlCl_3 .¹⁹³ Upon searching the literature we found a successful example of a Lewis acid-mediated DA reaction with Danishefsky's diene.¹⁹⁴ Lanthanide salts have been shown to be efficient and mild catalysts for the DA cycloaddition of various dienophiles with Danishefsky's diene. We examined two

lanthanide compounds: ytterbium (III) triflate ($\text{Yb}(\text{OTf})_3$) and europium(III)-tris(1,1,1,2,2,3,3-heptafluoro-7,7-dimethyl-4,6-octanedionate) ($\text{Eu}(\text{fod})_3$). Under these conditions, the desired Diels-Alder adduct **151** was not formed (Table 9, entry 3 and 4). Furthermore, application of $\text{Eu}(\text{fod})_3$ as an catalyst resulted in the isomerization of the *Z*-nitroalkene **133** (Table 9, entry 4).



Entry	Reagents and conditions	Results
1	toluene, 75 °C	133 and 128 decomposition
2	TiCl_4 , DCM, -78 °C	133 and 128 decomposition
3	$\text{Yb}(\text{OTf})_3$, toluene, 0 °C	133 recovered
4	$\text{Eu}(\text{FOD})_3$, toluene, 0 °C to 40 °C	133 isomerisation (<i>Z/E</i> in 1:2)
5	i. benzene, 80 °C ii. 0.1N HCl, THF, c = 0.05	133 and 128 decomposition
6	i. benzene, 75 °C ii. 0.1N HCl, THF, c = 0.1	20% of 151
7	i. benzene, 60 °C ii. 0.1N HCl, THF, c = 0.05	25% of 151

Table 9. Conditions for the Diels-Alder reaction.

Since catalytic DA failed to generate compound **151**, the thermal version of DA reaction was re-examined. The thermally-induced cycloaddition of **133** with **128** in benzene, followed by subsequent desilylation, afforded 25% of desired methoxy ketone **151** (Table 9, entry 7).

The relative configuration of DA adduct **151** was determined by ^1H NMR spectroscopy. Analysis of the coupling constants clearly showed a large vicinal coupling (J_{ac} 9.3 Hz) and thus the diaxial orientation of protons H_a and H_c (Figure 40, (A)). This coupling constant, together with others, strongly suggested the equatorial orientation of ester chain and allowed us to conclude that the Diels-Alder product **151** is the *exo*-adduct (Figure 40, (A)).

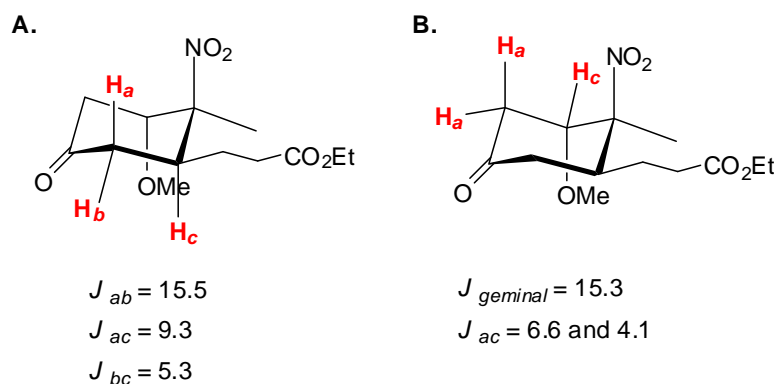


Figure 40. Experimental coupling constants for Diels-Alder adduct **151** in Hz.

The unusual *exo*-selectivity in DA reaction of nitro olefins with Danishefsky's diene has been investigated and reported previously by Node.¹⁹⁵ Node carried out a series of cycloadditions using Danishefsky's diene and various nitro olefins, both aliphatic and aromatic. All the reactions clearly exhibit *exo* selectivity, regardless of the kind of nitro alkenes or bulkiness of the substituent at β -carbon of nitro olefin. Furthermore, the DA cycloaddition of the same nitroalkenes with other popular dienes, such as 1-methoxybutadiene and cyclopentadiene, produced preferentially the *endo*-adduct. On the basis of these observations, Node concluded that the *exo*-selectivity in DA reactions of nitro olefins is a characteristic of Danishefsky's diene.

To rationalise the stereochemical outcome of the DA cycloadditions of nitroalkenes with Danishefsky's diene, Node considered the geometry and electronic features of possible *exo* and *endo* transition states. Mechanistically, the enhanced *endo*-selectivity of many DA reactions is governed by two factors: secondary orbital interactions and steric repulsions. However, as presented in Figure 41, in the reaction of nitro olefin **133** with Danishefsky's diene **128**, the *endo* transition state suffered from the electrostatic repulsions between the electron rich nitro group of the olefin, and the other electron rich group – OTMS of the diene. By applying Node's reasoning to our DA cycloaddition, we also speculated that electrostatic repulsions plays a major role in controlling the stereoselectivity of the transition state, and hence favoured the formation of *exo*-isomer. Furthermore, in case of our *Z*-alkene **133**, the *exo* transition state is free from steric repulsions as the ester chain is oriented away from the OTMS group (Figure 41).

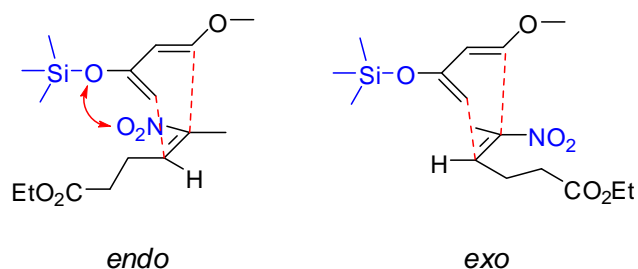
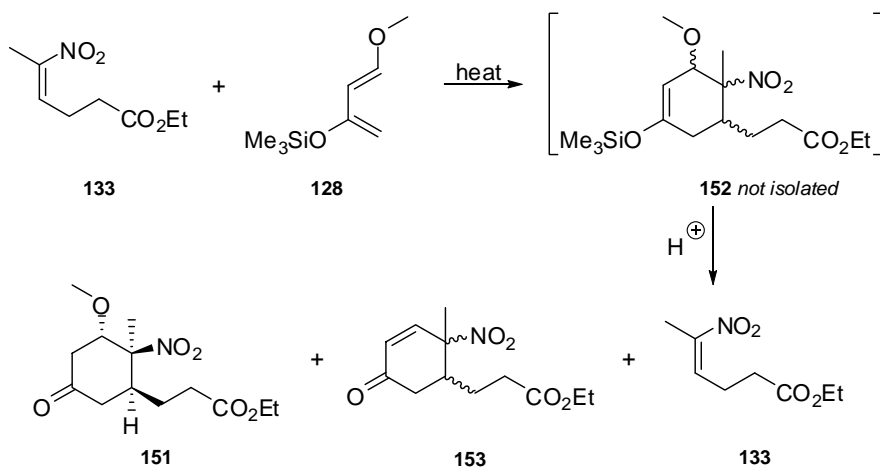


Figure 41. Proposed *endo* and *exo* transition states in the DA reaction of **133** and **128**.

NMR analyses of DA adduct **151** also allowed for assignment of the stereochemical configuration at the tertiary carbon bearing the methoxy group (Figure 40, (B)). The vicinal coupling between proton H_c and two magnetically distinct H_a protons gave values suggesting the axial-equatorial and equatorial-equatorial orientation of these protons. Therefore, it was deduced that the methoxy group occupies the axial position (Figure 40, (B)).

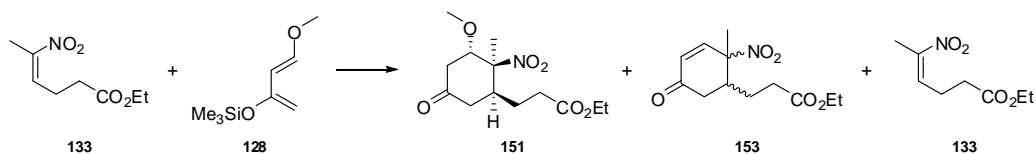
The structure of the major side-products furnished in the DA reaction of nitro olefin **133** and Danishefsky's diene **128** were identified as enones **153** and recovered starting material **133** (Scheme 55). The reaction suffered from poor conversion as well as acid-induced elimination of TMSOMe, concurrent with the desired hydrolysis of the silyl enol ether **152** to the ketone **151** (Scheme 55). Hence, by addressing the issue of elimination, it was hoped to improve the yield of DA cycloaddition.



Scheme 55. Diels-Alder cycloaddition of alkene **133** and diene **128**.

Literature survey showed that the problem of methoxy group elimination after acidic treatment of silyl enol ethers was discussed by Danishefsky as part of his work on the dienic component **128** for DA reaction.^{196,197} These studies showed that the geometry of the methoxy group of adducts such as **152**, could greatly affect the results of the acidic work-up. Upon treatment with diluted acid, the cleavage of the silyl protecting group is favourable for compounds bearing equatorially position methoxy unit. On the contrary, if molecule carries the axially oriented methoxy group, it is more likely that it will undergo the elimination of TMSOMe to yield enones, such as **153** (Scheme 55). Danishefsky's investigation postulated that utilization of stronger acidic conditions during the work-up of silyl enol ethers such as **152**, might favour the hydrolysis of the silyl group.

Therefore, on the basis of these results, the conditions of the DA cycloaddition were re-examined. The reaction was conducted in higher temperature, and with an alternative acidic work-up. When the cycloaddition was performed in 70 °C, and the subsequent work up carried out under stronger acidic conditions, the DA adduct **151** was obtained in acceptable 32% yield (Table 10, entry 2).

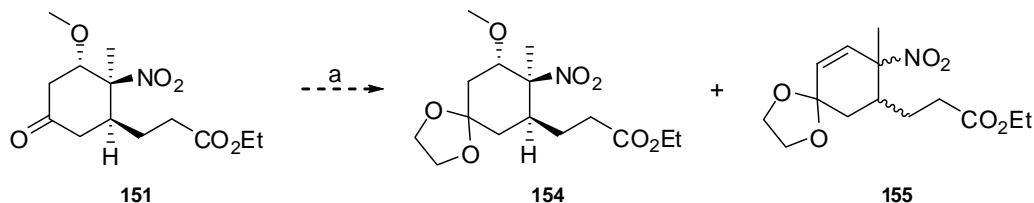


Entry	Reagents and conditions	Compound		
		151	153	133
1	i. benzene, 60 °C ii. 0.1N HCl, THF, c = 0.05	25%	26%	30%
2	i. benzene, 70 °C ii. 0.1N HCl, THF, c = 0.1	32%	traces	15%

Table 10. Improved conditions for the DA reaction.

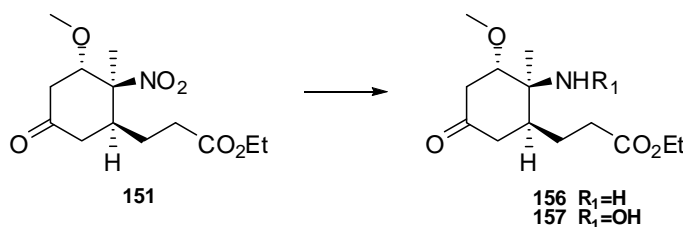
Having synthesized acceptable the DA adduct **151**, the next steps in the synthetic route towards GRIS molecule **62** were explored. Thus, protection of ketone

functionality of **151** as the corresponding ketal was carried out under standard conditions, using ethylene glycol.¹⁹⁸ NMR analysis of the purified fraction suggested the presence of two compounds **154** and **155** (Scheme 56).



Scheme 56. Reagents and Conditions: a) ethylene glycol, PPTS, 135 °C, Dean-Stark

However, it was not possible to separate the two compounds using FCC. Hence, it was decided to explore the following reaction, i.e. reduction of nitro group to corresponding amine **156** or hydroxylamine **157**, using unprotected ketone **151**.

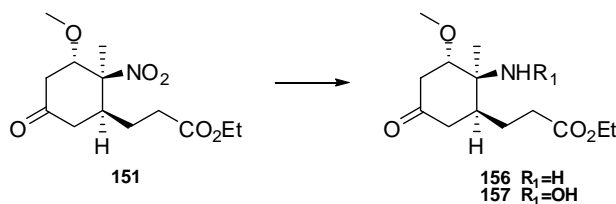


Scheme 57. Predicted products of nitro group reduction.

The investigation focused on the application of mild, catalytic hydrogenation procedures would allow for the selective reduction of the nitro group in the presence of ester function. The unprotected nitro compound **151** was subjected to hydrogenation over Pd/C (Table 11, entry 1). Transfer hydrogenation was also attempted using ammonium formate as the hydrogen source (Table 11, entry 2).¹⁹⁹ Unfortunately, both reactions failed to generate expected amine **156**.

Alternatively, the procedure developed by Maleczka *et al.* was adapted.²⁰⁰ Maleczka reported the use of silane as efficient reducing agents for the conversion of aliphatic nitro molecules to hydroxylamines. Thus, the nitro ketone **151** was treated with triethylsilane and catalytic amount of palladium (II) acetate (Table 11, entry 3).

Unfortunately, this procedure also failed; after the simple work-up the untouched starting material **151** was recovered.

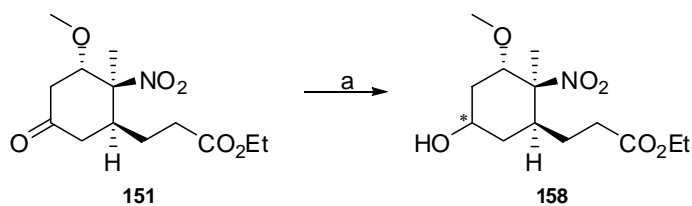


Entry	Reagents and conditions	Predicted product	Yield (%)
1	Pd/C, H ₂ , MeOH, rt	156	0
2	NH ₄ HCO ₂ , Pd/C, THF, rt	156	0
3	Et ₃ SiH, Pd(OAc) ₂ , THF/H ₂ O, rt	157	no reaction

Table 11. Conditions for nitro group reduction.

Finally, reduction of nitro ketone using Adam's catalyst in poly(ethylene glycol) (PEG 400) was attempted.²⁰¹ Adam's catalyst (platinum dioxide) is a very efficient catalysts for reduction of nitro group to amines and ketones to alcohols. Although under these conditions the unprotected ketone group was likely to undergo reduction, this would not be an issue, as the presence of ketone wasn't required in the final product.

However, the results of platinum catalysed reduction were disappointing; this reaction smoothly furnished corresponding alcohol **158** (Scheme 58), but left the targeted nitro group untouched.



Scheme 58. Reagents and Conditions: a) PtO₂, H₂, PEG 400, rt, 50%.

4.2 Conclusions

In summary, we have studied two distinct routes to GRIS peptidomimetic **62**. The first approach relied on an aza-Achmatowicz rearrangement and RCM as the key transformations, and the second approach utilised a Diels-Alder cycloaddition. Unfortunately, neither of these approaches proved fruitful.

During the work on the aza-Achmatowicz approach we successfully accomplished the construction of nitrogen-containing heterocycle **112**, which is anticipated to be a crucial intermediate in the synthesis of GRIS peptidomimetic **62** *via* the aza-Achmatowicz approach. Preparation of **112** was achieved *via inter alia* an aza-Achmatowicz rearrangement of furfurylamines, yielding functionalised pyridinones in a fast and efficient synthesis.

Preparation of pyridinone **86** *via* an aza-Achmatowicz rearrangement proved problematic. Regardless, we continued our synthetic approach to GRIS peptidomimetic **62** *via* the des-methyl pyridinone **101**, in order to prove the feasibility of our methodology and with a view to introducing the methyl group later on in the synthesis.

To this end, pyridinone **101** was converted to diene **103**. RCM metathesis of **103** produced nitrogen containing 5,6-bicycle **112**, in good to excellent yield. Disappointingly, any further attempts to functionalise heterocycle **112** were unsuccessful. Introduction of the ketone to **112** *via* an allylic oxidation proved unsuccessful utilising a variety of reaction conditions. The problematic nature of the allylic oxidation combined with a lack of viable alternative methods and issues with stereochemistry and separation of isomers prompted us to explore another synthetic approach.

In our alternative approach, the synthesis of GRIS mimetic **62** was attempted *via* a route that utilised a Diels-Alder (DA) reaction as a key transformation. We successfully executed a short and efficient synthesis of *Z*-nitro olefin **133**, which

underwent a DA cycloaddition with Danishefsky's diene to yield adduct **151** as a single diastereoisomer. The adduct **151** was shown to possess the correct stereochemical configuration, which would be essential if we were to complete the synthesis of GRIS mimetic **62** in a stereoselective fashion. In addition to this, another benefit of our synthetic route *via* a DA cycloaddition is that the required quaternary stereocentre is introduced early on in the synthesis.

Unfortunately, attempts at reduction of the nitro group of **151** to amine **156** or hydroxylamine **157** proved unsuccessful. One plausible explanation is that the nitro group is too sterically hindered to be susceptible to the attempted reaction conditions. However, only a few of the better known reduction conditions/reagents were investigated. It is possible that alternative conditions/reagents (such as aluminium amalgam) might yet prove successful.

5.0 Experimental section

General Information

All reactions were carried out under an atmosphere of argon in oven-dried glassware with magnetic stirring. Syringes, needles, cannulas and magnetic stirrer bars were also oven-dried. Tetrahydrofuran, diethyl ether and dichloromethane were purified through a Pure Solv 400-5MD solvent purification system (Innovative Technology, Inc). Unless otherwise noted, reagents were commercially available and used without further purification. Solvents were evaporated under reduced pressure at maximum temperature 48 °C, using a Buchi Rotavapor. Purification of reaction products were carried out by flash column chromatography using Apollo Scientific Silica Gel 60 (40-63 micron).

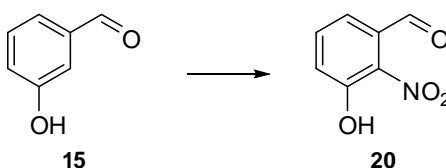
Analytical thin layer chromatography (TLC) was performed on aluminium sheets pre-coated with silica gel 60 (Merck). Visualization was accomplished with UV light and/or by staining with aqueous ceric ammonium molybdate solution, anisaldehyde, potassium permanganate and ethanolic ninhydrin solution, followed by heating. Melting points were measured with a Stuart Scientific Melting Point SMP1 apparatus, and are uncorrected. Optical rotations were determined using a JASCO DIP-370 digital polarimeter with a sodium lamp. $[\alpha]_D$ values were measured at the concentration and temperature reported.

Infrared spectra (IR) were recorded on a Shimadzu FTIR-8400 spectrophotometer with a Golden Gate ATR accessory, using CDCl_3 solutions of compounds. Some spectra were recorded as thin films on sodium chloride (NaCl) plates using a JASCO FTIR 410 spectrometer. High resolution mass spectra were recorded under EI, CI, and FAB conditions by the analytical services of the University of Glasgow.

^1H NMR spectra were recorded on a Bruker DPX 400 and Bruker AV 400 spectrometers at 400 MHz in room temperature and, in some cases, in 55 °C. Spectra were recorded in deuteriochloroform (CDCl_3), using residual chloroform as the internal standard ($\delta = 7.26$ ppm), and in deuterated benzene (C_6D_6), using residual

benzene as the internal standard ($\delta = 7.15$ ppm). J values are given in Hertz. Signals in NMR spectra are described as: br. = broad, app = apparent, s = singlet, d = doublet, t = triplet, q = quartet, s = sextet, m = multiplet, or combinations of these. Data are reported as follows: chemical shift in ppm, integration, multiplicity, coupling constant(s) and assignment. ^{13}C NMR spectra were recorded on a Bruker DPX 400 and Bruker AV 400 spectrometers at 100 MHz in room temperature unless stated otherwise. Spectra were recorded in deuteriochloroform (CDCl_3) and in deuterated benzene (C_6D_6), using solvent as the internal standard (CDCl_3 at 77.16 ppm and C_6D_6 at 128.06 ppm). Data are reported as follows: chemical shift in ppm and assignment. The proton and the carbon assignments were based on COSY, HSQC, HMBC and DEPT 135 experiments.

3-hydroxy-2-nitrobenzaldehyde **20**



To a stirred suspension of 3-hydroxybenzaldehyde **15** (3 g, 24.6 mmol, 1 eq) in dry DCM (250 cm^3) were added tetrabutylammonium hydrogen sulphate (0.42 g, 1.23 mmol, 5%mol eq) and isopropyl nitrate (6.2 ml, 6.46 g, 61.5 mmol, 2.5 eq) under an argon atmosphere. The resulting reaction mixture was cooled to $-15\text{ }^\circ\text{C}$ and pure sulphuric acid (14.4 ml, 26.54 g, 270.6 mmol, 11 eq) was added slowly to it via dropping funnel with pressure equalizing arm (highly exothermic reaction). After stirring at $-15\text{ }^\circ\text{C}$ for next 20 minutes, TLC analysis indicated complete consumption of the starting material. The cooling bath was removed and reaction mixture was quenched with water (200 cm^3) and diluted with diethyl ether (150 cm^3). Resulting biphasic mixture was stirred for next 20 minutes at room temperature. After this time the layers were separated and aqueous layer was extracted with fresh diethyl ether (2 x 200 cm^3). The organic phases were combined, washed with brine (400 cm^3), dried over sodium sulphate, filtered off, and solvents were removed *in vacuo*. The remaining residue was suspended in small amount of diethyl ether and resulting pale yellow precipitate was filtered off and dried to give the desired nitrobenzaldehyde **20**

(2.3 g, 13.7 mmol, 56% yield). Nitrobenzaldehyde **20** was used in synthesis without any further purification.

δ_{H} (400 MHz, CDCl_3): 7.31 (1H, dd, $J = 7.4$ and 1.4 Hz, one of C_6H_3), 7.37 (1H, dd, $J = 8.4$ and 1.4 Hz, one of C_6H_3), 7.67 (1H, ddd, $J = 8.4$, 7.4 and 0.7 Hz, one of C_6H_3), 10.31 (1H, appd, $J = 0.7$ Hz, CHO), 10.42 (1H, br. s, OH)

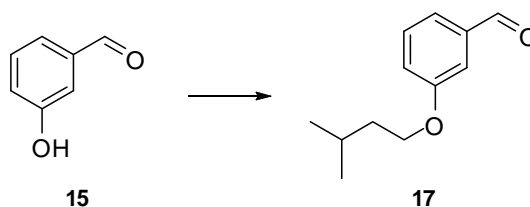
δ_{C} (100 MHz, CDCl_3): 121.6 (Ar-C), 124.4 (Ar-C), 135.1 (Ar-Cq), 136.8 (Ar-C), 155.1 (Ar-Cq), 188.1 (CHO), 1 x Cq unresolved

m/z [CI (+ve)], 168.13 ($[\text{M}+\text{H}]^+$, 100%), 138.15 ($[(\text{M}+\text{H})-\text{NO}]^+$, 60%); Found $[\text{M}+\text{H}]^+$, 168.0294, $\text{C}_7\text{H}_6\text{NO}_4$ requires 168.0297

ν_{max} (CDCl_3) / cm^{-1} : br. 3221, 3097, 2893, 2804, 1678, 1535, 1315

mp. 157-159 °C

3-(3-Methyl-butoxy)-benzaldehyde **17**



To a solution of 3-hydroxybenzaldehyde **15** (5 g, 41 mmol, 1 eq) in dry DMF (300 cm^3) was added potassium carbonate (11.3 g, 82 mmol, 2 eq) under an argon atmosphere and resulting reaction mixture was stirred for 20 minutes. Then reaction was treated with 1-bromo-3-methylbutane (15.4 ml, 18.6 g, 123 mmol, 3 eq) and stirring was continued overnight at room temperature. After this time the reaction was quenched with water (300 cm^3), and diluted with ethyl acetate (200 cm^3). After the biphasic mixture was stirred for 20 minutes, the phases were separated and the aqueous layer was extracted with fresh ethyl acetate (2 x 250 cm^3). All the organic layers were combined, washed with water (2 x 500 cm^3), brine (500 cm^3), dried over sodium sulphate, filtered off, and solvents were removed *in vacuo*. The resulting aldehyde **17** (yellow liquid, 7.61 g, 39.6 mmol, 96% yield) was judged clean based on NMR analysis and was reacted further without any purification.

δ_{H} (400 MHz, CDCl_3): 0.96 (6H, d, $J = 6.6$ Hz, $\text{CH}(\text{CH}_3)_2$), 1.69 (2H, appq, $J = 6.7$ Hz, OCH_2CH_2), 1.84 (1H, appsept., $J = 6.7$ Hz, $\text{CH}(\text{CH}_3)_2$), 4.03 (2H, t, $J = 6.6$ Hz, OCH_2), 7.15 (1H, m, one of C_6H_4), 7.37-7.38 (1H, m, one of C_6H_4), 7.42-7.43 (2H, m, two of C_6H_4), 9.96 (1H, s, CHO)

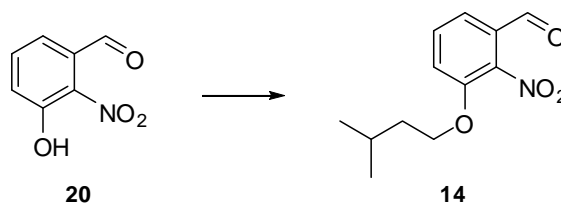
δ_{C} (100 MHz, CDCl_3): 22.6 ($\text{CH}(\text{CH}_3)_2$), 25.1 ($\text{CH}(\text{CH}_3)_2$), 37.9 (OCH_2CH_2), 66.7 (OCH_2), 112.7 (Ar-C), 122.1 (Ar-C), 123.4 (Ar-C), 130.1 (Ar-C), 137.8 (Ar-Cq), 159.8 (Ar-Cq), 192.4 (CHO)

m/z [EI (+ve)], 192.1 ($[\text{M}]^+$, 45%), 122.0 ($[\text{M}-\text{C}_5\text{H}_{10}]^+$, 56%), 70.1 ($[\text{C}_5\text{H}_{10}]^+$, 51%); Found $[\text{M}]^+$, 192.1151, $\text{C}_{12}\text{H}_{16}\text{O}_2$ requires 192.1150

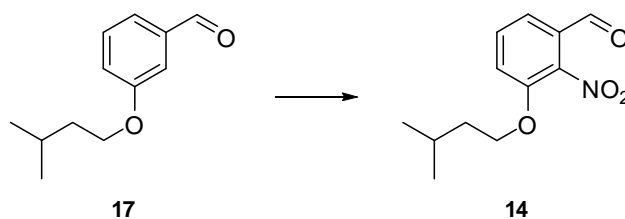
ν_{max} (CDCl_3) / cm^{-1} : 3070, 2957, 2871, 2724, 1697, 1597, 1451, 1263, 1025

3-(3-Methyl-butoxy)-2-nitro-benzaldehyde **14**

Procedure A



Procedure B



Procedure A

To a stirred solution of nitrobenzaldehyde **20** (4.8 g, 28.7 mmol, 1 eq) in dry DMF (300 cm³) was added potassium carbonate (7.9 g, 57.4 mmol, 2 eq) under an argon atmosphere. After being stirred for 30 minutes at room temperature, the reaction mixture was treated with 1-bromo-3-methylbutane (10.8 ml, 13 g, 86.1 mmol, 3 eq) and stirring was continued overnight. After this time the reaction was quenched with water (200 cm³) and biphasic mixture was stirred for 20 minutes. Phases were

separated and the aqueous layer was extracted with fresh ethyl acetate (2 x 250 cm³). All the organic layers were combined, washed with water (300 cm³), brine (300 cm³), dried over sodium sulphate and concentrated *in vacuo* to give nitrobenzaldehyde **14** as a viscous orange oil, which was judged pure by NMR spectroscopy and reacted further without purification (5.23 g, 22.0 mmol, 100% conversion by NMR, 77% yield).

Procedure B

To a stirred solution of aldehyde **17** (2.6 g, 13.5 mmol, 1 eq) in dry dichloromethane (80 cm³) at -28 °C was added nitronium tetrafluoroborate (2.7 g, 20.25 mmol, 1.5 eq) under an argon atmosphere. The reaction was stirred for 22 hours while temperature was maintained at -28 °C. After this time a cooling bath was removed, reaction was quenched by slow addition of water (60 cm³) and resulting biphasic mixture was stirred until reaching room temperature. The mixture was then diluted with ethyl acetate (60 cm³) and stirred for additional 20 minutes. Phases were separated, and aqueous layer was extracted with fresh ethyl acetate (2 x 60 cm³). Combined organic phases were washed with water (150 cm³), brine (150 cm³), dried over sodium sulphate and filtered off. The solvents were removed *in vacuo* to afford the residue that was purified by flash column chromatography (silica gel, gradient elution, eluting with 5% ethyl acetate in petroleum ether (40-60) to 25% ethyl acetate in petroleum ether (40-60)) to give nitrobenzaldehyde **14** as an viscous orange oil (1.71 g, 7.2 mmol, 53% yield).

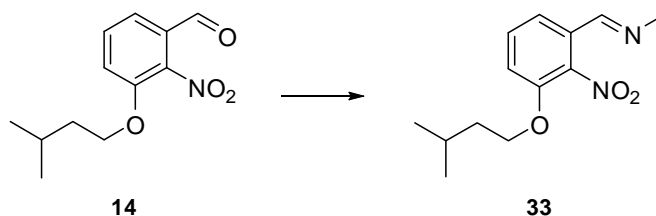
δ_{H} (400 MHz, CDCl₃): 0.93 (6H, d, $J = 6.6$ Hz, CH(CH₃)₂), 1.67 (2H, appq, $J = 6.5$ Hz, OCH₂CH₂), 1.78 (1H, appsept, $J = 6.6$ Hz, CH(CH₃)₂), 4.12 (2H, t, $J = 6.5$ Hz, OCH₂), 7.33 (1H, dd, $J = 8.3$ and 1.2 Hz, one of C₆H₃), 7.46 (1H, dd, $J = 7.7$ and 1.2 Hz, one of C₆H₃), 7.59 (1H, appt, $J = 8.0$ Hz, one of C₆H₃), 9.92 (1H, s, CHO)

δ_{C} (100 MHz, CDCl₃): 22.5 (CH(CH₃)₂), 24.9 (CH(CH₃)₂), 37.5 (OCH₂CH₂), 68.6 (OCH₂), 119.5 (Ar-C), 122.0 (Ar-C), 128.2 (Ar-Cq), 131.6 (Ar-C), 140.6 (Ar-Cq), 150.7 (Ar-Cq), 187.0 (CHO)

m/z [CI (+ve)], 238.28 ([M+H]⁺, 100%); Found [M+H]⁺, 238.1077, C₁₂H₁₆NO₄ requires 238.1079

ν_{max} (CDCl₃) / cm⁻¹: 2958, 2935, 2874, 1701, 1604, 1535, 1462, br. 1284

Methyl-[1-[3-(3-methyl-butoxy)-2-nitro-phenyl]-meth-(E)-ylidene]-amine **33**



A stirred solution of aldehyde **14** (1.71 g, 7.2 mmol, 1 eq) in heptane (40 cm³) was treated with methylamine (40 wt. % solution in water, 1.75 ml, 0.63 g, 20.16 mmol, 2.8 eq). The biphasic mixture was stirred vigorously at room temperature until completion of reaction as indicated by TLC analysis (2 hours). Heptane was then removed *in vacuo*, and remaining crude imine **33** was taken directly to the next reaction without purification.

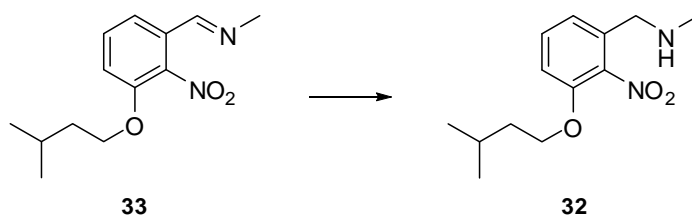
δ_{H} (400 MHz, CDCl₃): 0.93 (6H, d, $J = 6.6$ Hz, CH(CH₃)₂), 1.67 (2H, appq, $J = 6.6$ Hz, OCH₂CH₂), 1.79 (1H, appsept, $J = 6.6$ Hz, CH(CH₃)₂), 3.51 (3H, d, $J = 1.7$ Hz, NCH₃), 4.09 (2H, t, $J = 6.6$ Hz, OCH₂), 7.07 (1H, dd, $J = 8.2$ and 1.1 Hz, one of C₆H₃), 7.41 (1H, m, one of C₆H₃), 7.48 (1H, dd, $J = 7.9$ and 1.2 Hz, one of C₆H₃), 8.16 (1H, appq, $J = 1.6$ Hz, CHN)

δ_{C} (100 MHz, CDCl₃): 22.5 (CH(CH₃)₂), 25.0 (CH(CH₃)₂), 37.6 (OCH₂CH₂), 48.7 (NCH₃), 68.3 (OCH₂), 115.2 (Ar-C), 119.5 (Ar-C), 128.7 (Ar-Cq), 131.0 (Ar-C), 141.5 (Ar-Cq), 150.4 (Ar-Cq), 156.1 (CHN)

m/z [CI (+ve)], 251.3 ([M+H]⁺, 72%); Found [M+H]⁺, 251.1397, C₁₃H₁₉N₂O₃ requires 251.1396

ν_{max} (CDCl₃) / cm⁻¹: 2955, 2874, 1651, 1604, 1531, 1465, 1280

Methyl-[3-(3-methyl-butoxy)-2-nitro-benzyl]-amine **32**



A stirred solution of imine **33** (1.8 g, 7.2 mmol, 1 eq) in methanol (40 cm³) was cooled to 0 °C and sodium borohydride (0.4 g, 10.8 mmol, 1.5 eq) was added to it carefully in portions. The resulting reaction mixture was stirred at room temperature until complete consumption of starting material as indicated by TLC analysis (3 hours). The reaction mixture was then cooled to 0 °C and slowly quenched with water (40 cm³). After stirring for 20 minutes at 0 °C, a cooling bath was removed, the reaction was diluted with ethyl acetate (80 cm³) and resulting biphasic mixture was allowed to warm to room temperature. Phases were separated and the remaining aqueous layer was extracted with ethyl acetate (2 x 80 cm³). All the organic phases were combined, dried over anhydrous sodium sulphate and organics were removed *in vacuo* to give amine **32** in excellent yield (orange liquid, 1.72 g, 6.8 mmol, 94% from aldehyde **14**).

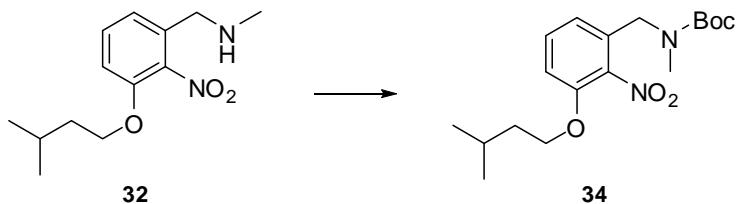
δ_{H} (400 MHz, CDCl₃): 0.92 (6H, d, $J = 6.6$ Hz, CH(CH₃)₂), 1.65 (2H, appq, $J = 6.6$ Hz, OCH₂CH₂), 1.78 (1H, appsept, $J = 6.7$ Hz, CH(CH₃)₂), 2.4 (3H, s, NCH₃), 3.7 (2H, s, CH₂N), 4.06 (2H, t, $J = 6.6$ Hz, OCH₂), 6.93 (1H, d, $J = 8.4$ Hz, one of C₆H₃), 7.03 (1H, d, $J = 7.8$ Hz, one of C₆H₃), 7.35 (1H, dd, $J = 8.2$ and 7.9 Hz, one of C₆H₃)

δ_{C} (100 MHz, CDCl₃): 22.5 (CH(CH₃)₂), 24.9 (CH(CH₃)₂), 36.1 (NCH₃), 37.6 (OCH₂CH₂), 51.3 (CH₂N), 68.0 (OCH₂), 112.3 (Ar-C), 121.3 (Ar-C), 130.9 (Ar-C), 133.3 (Ar-Cq), 141.7 (Ar-Cq), 150.4 (Ar-Cq)

m/z [CI (+ve)], 253.4 ([M+H]⁺, 100%); Found [M+H]⁺, 253.1551, C₁₃H₂₁N₂O₃ requires 253.1552

ν_{max} (CDCl₃) / cm⁻¹: 2958, 2874, 1535, 1284

Methyl-[3-(3-methyl-butoxy)-2-nitro-benzyl]-carbamic acid *tert*-butyl ester **34**



To a stirred solution of amine **32** (5.06 g, 20.05 mmol, 1 eq) in dry DMF (200 cm³) was added triethylamine (5.6 ml, 4.06 g, 40.1 mmol, 2 eq) under an argon atmosphere. After being stirred for 20 minutes, the reaction solution was treated with di-tert-butyl-dicarbonate (5.7 g, 26.06 mmol, 1.3 eq). Stirring was continued at room temperature until completion of reaction as indicated by TLC analysis (2.5 hours). After this time, the reaction was quenched with water (150 cm³) and diluted with ethyl acetate (150 cm³). Then phases were separated and the aqueous layer was extracted with fresh ethyl acetate (2 x 150 cm³). All the organic layers were combined, dried over anhydrous sodium sulphate, filtered off, and concentrated *in vacuo*. The remaining residue was purified by flash column chromatography (silica gel, eluting with 5% ethyl acetate in petroleum ether (40-60)) to give protected amine **34** as a pale yellow liquid (6.55 g, 18.6 mmol, 93%).

δ_{H} (400 MHz, CDCl₃, mixture of Boc rotamers, ratio: 1.3:1): 0.93 (6H, d, $J = 6.6$ Hz, CH(CH₃)₂), 1.42 (major) and 1.48 (minor) (9H, 2 x br. s, C(CH₃)₃), 1.65 (2H, appq, $J = 6.7$ Hz, OCH₂CH₂), 1.78 (1H, appsept, $J = 6.7$ Hz, CH(CH₃)₂), 2.78 (minor) and 2.83 (major) (3H, 2 x br. s, NCH₃), 4.07 (2H, t, $J = 6.5$ Hz, OCH₂), 4.4 (2H, br. s, CH₂N), 6.86 (1H, m, one of C₆H₃), 6.93 (1H, d, $J = 8.3$ Hz, one of C₆H₃), 7.36 (1H, t, $J = 8.1$ Hz, one of C₆H₃)

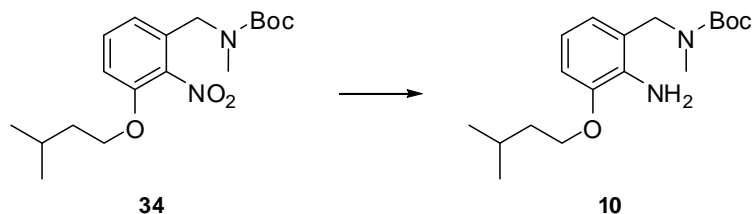
δ_{H} (400 MHz, CDCl₃, 55°C): 0.95 (6H, br. d, $J = 6.5$ Hz, CH(CH₃)₂), 1.46 (9H, br. s, C(CH₃)₃), 1.67 (2H, br. q, $J = 6.4$ Hz, OCH₂CH₂), 1.8 (1H, br. appsept, $J = 6.9$ Hz, CH(CH₃)₂), 2.82 (3H, br. s, NCH₃), 4.08 (2H, br. t, $J = 5.9$ Hz, OCH₂), 4.41 (2H, br. s, CH₂N), 6.89 (1H, br. d, $J = 7.0$ Hz, one of C₆H₃), 6.94 (1H, d, $J = 8.1$ Hz, one of C₆H₃), 7.35 (1H, br. dd, $J = 8.1$ and 7.8 Hz, one of C₆H₃)

δ_{C} (100 MHz, CDCl₃, 55°C): 22.5 (CH(CH₃)₂), 25.2 (CH(CH₃)₂), 28.5 (C(CH₃)₃), 34.4 (NCH₃), 37.8 (OCH₂CH₂), 48.0 (CH₂N), 68.5 (OCH₂), 80.3 (C(CH₃)₃), 112.7 (Ar-C), 119.8 (Ar-C), 131.0 (Ar-C), 131.9 (Ar-Cq), 150.7 (NCO₂), 2 x Cq unresolved

m/z [CI (+ve)], 353.4 ([M+H]⁺, 12%), 297.3 ([M+H]-tBu]⁺, 100%), 253.3 ([M+H]-Boc]⁺, 48%); Found [M+H]⁺, 353.2078, C₁₈H₂₉N₂O₅ requires 353.2076

ν_{max} (CDCl₃) / cm⁻¹: 2958, 2931, 2874, 1693, 1608, 1531, 1454, 1365

[2-Amino-3-(3-methyl-butoxy)-benzyl]-methyl-carbamic acid *tert*-butyl ester **10**



A vacuum dried amine **34** (6.4 g, 18.2 mmol, 1 eq) was dissolved in methanol (110 cm³) under an argon atmosphere. The resulting solution was then purged with argon for 20 minutes and a catalytic amount of 10% Pd/C was added to it. Reaction mixture was then immediately degassed under reduced pressure and refilled with hydrogen (three times), and stirring was continued overnight under hydrogen atmosphere. After this time the reaction mixture was diluted with ethyl acetate and filtered through a pad of celite and sand, which was washed with copious amount of ethyl acetate. The filtrate was collected and concentrated *in vacuo* to give aniline **10** as orange liquid (5.9 g, 18.2 mmol, 100% yield), which was judged pure by NMR spectroscopy, and reacted further without purification.

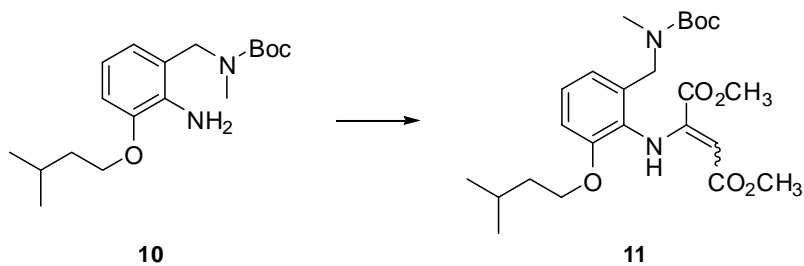
δ_{H} (400 MHz, CDCl₃): 0.96 (6H, d, $J = 6.6$ Hz, CH(CH₃)₂), 1.48 (9H, br. s, C(CH₃)₃), 1.7 (2H, appq, $J = 6.6$ Hz, OCH₂CH₂), 1.85 (1H, appsept, $J = 6.7$ Hz, CH(CH₃)₂), 2.74 (3H, s, NCH₃), 4.0 (2H, t, $J = 6.6$ Hz, OCH₂), 4.36 (2H, s, CH₂N), 6.57-6.61 (1H, m, one of C₆H₃), 6.66 (1H, dd, $J = 7.6$ and 1.5 Hz, one of C₆H₃), 6.74 (1H, dd, $J = 7.9$ and 1.5 Hz, one of C₆H₃)

δ_{C} (100 MHz, CDCl₃): 22.8 (CH(CH₃)₂), 25.2 (CH(CH₃)₂), 28.5 (C(CH₃)₃), 33.1 (NCH₃), 38.3 (OCH₂CH₂), 49.6 (CH₂N), 66.7 (OCH₂), 80.0 (C(CH₃)₃), 110.6 (Ar-C), 115.9 (Ar-C), 123.5 (Ar-C), 136.4 (Ar-Cq), 146.6 (Ar-Cq), 156.5 (NCO₂), 1 x Cq unresolved

m/z [EI (+ve)], 322.2 ([M]⁺, 80%), 266.2 ([M-^tBu]⁺, 53%), 222.2 ([M-Boc]⁺, 71%); Found [M]⁺, 322.2255, C₁₈H₃₀O₃N₂ requires 322.2256

ν_{max} (CDCl₃) / cm⁻¹: 3483, 3352, 2958, 2931, br. 1674, br. 1477, 1238

Dimethyl 2-(2-((tert-butoxycarbonyl(methyl)amino)methyl)-6-(isopentyloxy)phenylamino)maleate **11**



A flask equipped with reflux condenser was charged with solution of amine **10** (0.1 g, 0.31 mmol, 1 eq) in methanol (3 cm³) under an argon atmosphere. Then DMAD (0.06 ml, 0.07 g, 0.5 mmol, 1.6 eq) was added and resulting reaction mixture was refluxed until TLC analysis indicated complete consumption of starting material (4 hours). Heating bath was removed, reaction was allowed to cool to room temperature and solvent was removed *in vacuo*. The remaining residue was purified by flash column chromatography (silica gel, gradient elution, eluting with 100% petroleum ether (40-60) to 5% ethyl acetate in petroleum ether (40-60)) to give amine **11** as yellow oil (0.116 g, 0.25 mmol, 80% yield).

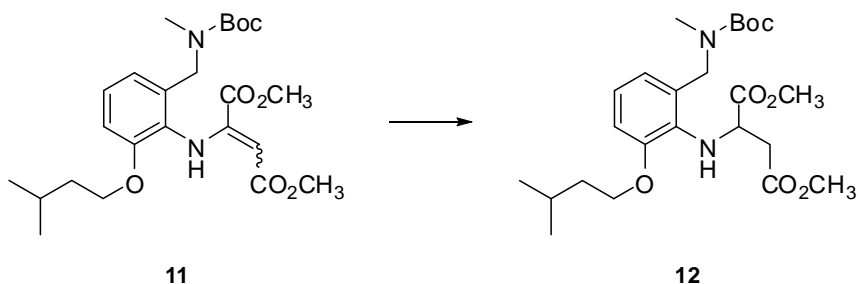
δ_{H} (400 MHz, CDCl₃): 0.9 (6H, d, $J = 6.6$ Hz, CH(CH₃)₂), 1.45 (9H, br. s, C(CH₃)₃), 1.57 (2H, appq, $J = 6.7$ Hz, OCH₂CH₂), 1.73 (1H, appsept, $J = 6.7$ Hz, CH(CH₃)₂), 2.81 (3H, br. s, NCH₃), 3.6 (3H, s, CO₂CH₃), 3.73 (3H, s, CO₂CH₃), 3.86 (2H, t, $J = 6.7$ Hz, OCH₂), 4.52 (2H, br. s, CH₂N), 5.45 (1H, s, HNC=CH), 6.75 (1H, dd, $J = 8.2$ and 1.0 Hz, one of C₆H₃), 6.79-6.81 (1H, m, one of C₆H₃), 7.08 (1H, t, $J = 7.9$ Hz, one of C₆H₃), 9.2 (1H, s, NHC=CH)

δ_{C} (100 MHz, CDCl₃): 22.6 (CH(CH₃)₂), 25.1 (CH(CH₃)₂), 28.5 (C(CH₃)₃), 34.0 (NCH₃), 37.7 (OCH₂CH₂), 48.6 (CH₂N), 51.1 (CO₂CH₃), 52.2 (CO₂CH₃), 67.6 (OCH₂), 79.7 (C(CH₃)₃), 90.3 (HNC=CH), 111.3 (Ar-C), 119.8 (Ar-C), 126.1 (Ar-C), 128.2 (Ar-Cq), 133.6 (Ar-Cq), 153.2 (Ar-Cq), 163.7 (CO₂CH₃), 170.6 (CO₂CH₃), 2 x Cq unresolved

m/z [CI (+ve)], 465.5 ([M+H]⁺, 100%), 323.4 ([M+H-(CO₂Me)CCH(CO₂Me)]⁺, 51%); Found [M+H]⁺, 465.2603, C₂₄H₃₇N₂O₇ requires 465.2601

ν_{max} (CDCl₃) / cm⁻¹: 2955, 2931, 2872, 1741, 1697, 1674, 1612, 1271, 1215, 1139

(±)-Dimethyl 2-(2-((tert-butoxycarbonyl(methyl)amino)methyl)-6-(isopentyloxy)phenylamino)succinate **12**



A vacuum-dried amine **11** (0.097 g, 0.21 mmol, 1 eq) was dissolved in methanol (5 cm³) under an argon atmosphere. Resulting solution was purged with argon for 20 minutes, and a catalytic amount of Pd(OH)₂ (20 wt. %) was added to it. Reaction mixture was then immediately degassed under reduced pressure and refilled with hydrogen (three times), and stirring was continued overnight under hydrogen atmosphere. After this time the reaction mixture was diluted with diethyl ether (15 cm³), and filtered through a pad of celite and sand, which was washed with copious amount of diethyl ether. The filtrate was collected and concentrated *in vacuo*. Crude amine **12**, obtained as very viscous yellow oil, was subsequently used in synthesis without purification (0.09 g, 0.19 mmol, 90% yield).

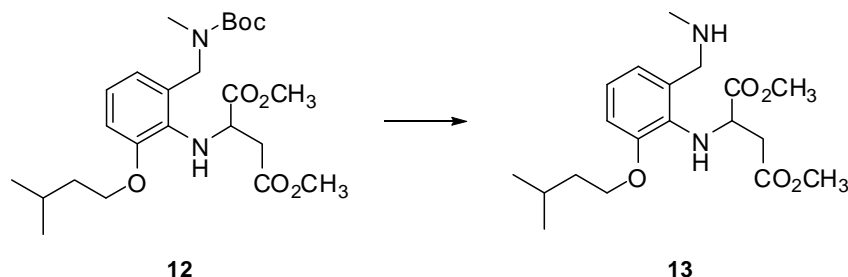
δ_H (400 MHz, CDCl₃, 55°C): 0.98 (6H, d, *J* = 6.6 Hz, CH(CH₃)₂), 1.48 (9H, s, C(CH₃)₃), 1.72 (2H, appq, *J* = 6.7 Hz, OCH₂CH₂), 1.83 (1H, appsept, *J* = 6.7 Hz, CH(CH₃)₂), 2.75 (3H, s, NCH₃), 2.81 (2H, br. s, NHCHCH₂), 3.65 (3H, br. s, CO₂CH₃), 3.66 (3H, br. s, CO₂CH₃), 3.99 (2H, t, *J* = 6.7 Hz, OCH₂), 4.36 (1H, br. d, *J* = 15.2 Hz, one of CH₂N), 4.6 (1H, br. s, NHCH), 4.63 (1H, d, *J* = 15.2, one of CH₂N), 6.7 (1H, appd, *J* = 7.5 Hz, one of C₆H₃), 6.77 (1H, appd, *J* = 7.9, one of C₆H₃), 6.85 (1H, appt, *J* = 7.8 Hz, one of C₆H₃)

δ_C (100 MHz, CDCl₃, 55°C): 22.7 (CH(CH₃)(CH₃)), 22.8 (CH(CH₃)(CH₃)), 25.4 (CH(CH₃)₂), 28.6 (C(CH₃)₃), 33.6 (NCH₃), 38.2 and 38.4 (OCH₂CH₂ and NHCHCH₂), 49.0 (CH₂N), 51.7 (CO₂CH₃), 52.0 (CO₂CH₃), 56.6 (NHCH), 67.3 (OCH₂), 79.9 (C(CH₃)₃), 111.7 (Ar-C), 121.6 (Ar-C), 121.7 (Ar-C), 151.3 (Cq), 156.3 (Cq), 171.2 (CO₂CH₃), 173.4 (CO₂CH₃), 2 x Cq unresolved

m/z [CI (+ve)], 467.2 ($[M+H]^+$, 70%); Found $[M+H]^+$, 467.2761, $C_{24}H_{39}N_2O_7$ requires 467.2757

ν_{\max} (CDCl₃) / cm⁻¹: 3329, 2955, 2933, 2872, 1739, 1693, 1674, 1166, 1143

(±)-Dimethyl 2-(2-(isopentyloxy)-6-((methylamino)methyl)phenylamino)succinate **13**



A vacuum dried amine **12** (0.09 g, 0.19 mmol, 1 eq) was dissolved in dry DCM (2 cm³) under an argon atmosphere, and subsequently treated with trifluoroacetic acid (0.015 ml, 0.022 g, 0.19 mmol, 1 eq). Resulting reaction mixture was stirred at room temperature until completion as indicated by TLC analysis (20 hours). After this time solvent was removed *in vacuo*, the remaining residue was taken up in fresh diethyl ether (5 cm³) and washed with water (5 cm³). Phases were separated and the organic layer was dried over anhydrous sodium sulphate, filtered off, and concentrated *in vacuo* to give amine **13** as yellow oil (0.055 g, 0.15 mmol, 82% yield). Amine **13** was used in the synthesis without purification.

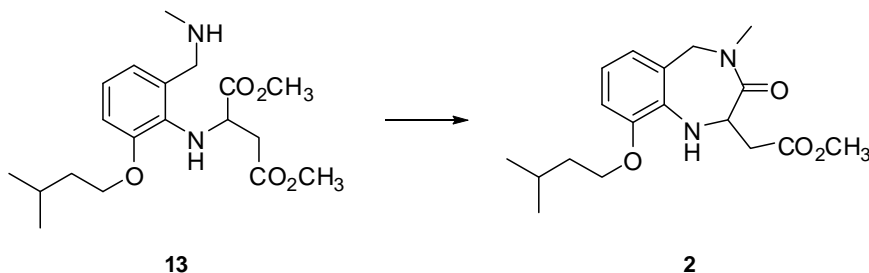
δ_H (400 MHz, CDCl₃): 0.94 (3H, d, $J = 6.6$ Hz, CH(CH₃)(CH₃)), 0.95 (3H, d, $J = 6.6$ Hz, CH(CH₃)(CH₃)), 1.65 (2H, appq, $J = 6.7$ Hz, OCH₂CH₂), 1.76 (1H, appsept, $J = 6.6$ Hz, CH(CH₃)₂), 2.61 (3H, s, NHCH₃), 2.88 (1H, dd, $J = 16.9$ and 5.3 Hz, one of NHCHCH₂), 2.96 (1H, dd, $J = 16.9$ and 5.3 Hz, one of NHCHCH₂), 3.69 (3H, s, CO₂CH₃), 3.72 (3H, s, CO₂CH₃), 3.88-4.0 (2H, m, OCH₂), 4.2-4.31 (3H, m, CH₂NH and NHCH), 6.86 (1H, dd, $J = 6.0$ and 3.6 Hz, one of C₆H₃), 6.99-7.01 (2H, m, two of C₆H₃)

δ_C (100 MHz, CDCl₃): 22.6 (CH(CH₃)₂), 25.1 (CH(CH₃)₂), 32.1 (NHCH₃), 37.0 (NHCH₂CH₂), 37.9 (OCH₂CH₂), 49.7 (CH₂NH), 52.2 (CO₂CH₃), 53.0 (CO₂CH₃), 57.1 (NHCH), 67.2 (OCH₂), 113.3 (Ar-C), 124.1 (Ar-C), 124.6 (Ar-C), 124.6 (Ar-Cq), 134.3 (Ar-Cq), 152.9 (Ar-Cq), 171.8 (CO₂CH₃), 174.0 (CO₂CH₃)

m/z [FAB (+ve)], 367.4 ([M+H]⁺, 100%), 221.6 ([M+H]-CH(CO₂CH₃)CH₂(CO₂CH₃)⁺, 77%); Found [M+H]⁺, 367.2236, C₁₉H₃₁N₂O₅ requires 367.2233

ν_{\max} (CDCl₃) / cm⁻¹: br. 3342, 2955, 2872, 1735, 1469, 1257, 1222

(±)-Methyl 2-(9-(isopentyloxy)-4-methyl-3-oxo-2,3,4,5-tetrahydro-1H-benzo[e][1,4]diazepin-2-yl)acetate **2**



Flask equipped with reflux condenser was charged with amine **13** (0.2 g, 0.55 mmol, 1 eq) and methanol (5 cm³). The solution was purged with argon for 20 minutes and then treated with sodium methoxide (25 wt. % in methanol, 0.26 ml, 0.06 g, 1.1 mmol, 2 eq) under an argon atmosphere. Resulting reaction mixture was refluxed until TLC analysis indicated complete consumption of starting material **13** (4 hour). The heating bath was removed, and the reaction was quenched with water (5 cm³), diluted with ethyl acetate (10 cm³) and stirred for 20 minutes at room temperature. The phases were separated, and the aqueous layer was extracted with fresh ethyl acetate (2 x 10 cm³). The combined organic fractions were washed with brine (30 cm³), dried over anhydrous sodium sulphate, filtered off, and concentrated *in vacuo*. The remaining residue was purified by flash column chromatography (silica gel, gradient elution, eluting with 100% petroleum ether (40-60) to 30% ethyl acetate in petroleum ether (40-60)) to give the benzodiazepine **2** as orange viscous oil (0.11 g, 0.34 mmol, 62%).

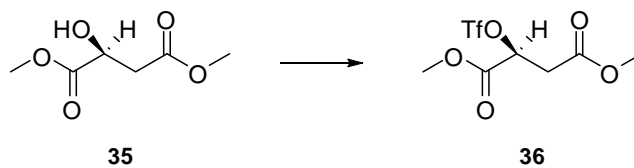
δ_{H} (400 MHz, CDCl_3): 0.95 (6H, d, $J = 6.6$ Hz, $\text{CH}(\text{CH}_3)_2$), 1.66 (2H, appq, $J = 6.6$ Hz, OCH_2CH_2), 1.8 (1H, appsept, $J = 6.6$ Hz, $\text{CH}(\text{CH}_3)_2$), 2.67 (1H, dd, $J = 15.9$ and 6.3 Hz, one of NHCHCH_2), 3.04 (1H, dd, $J = 15.9$ and 7.4 Hz, one of NHCHCH_2), 3.05 (3H, s, NCH_3), 3.7 (1H, d, $J = 16.3$ Hz, one of CH_2N), 3.72 (3H, s, CO_2CH_3), 3.93-3.99 (2H, m, OCH_2), 4.41 (1H, d, $J = 4.7$ Hz, NHCH), 5.04-5.09 (1H, m, NHCH), 5.46 (1H, d, $J = 16.3$ Hz, one of CH_2N), 6.54 (1H, dd, $J = 7.6$ and 2.2 Hz, one of C_6H_3), 6.56-6.59 (1H, m, one of C_6H_3), 6.7 (1H, dd, $J = 7.3$ and 2.2 Hz, one of C_6H_3)

δ_{C} (100 MHz, CDCl_3): 22.7 ($\text{CH}(\text{CH}_3)_2$), 25.2 ($\text{CH}(\text{CH}_3)_2$), 34.7 (NCH_3), 36.3 (NHCHCH_2), 38.0 (OCH_2CH_2), 51.5 (NHCH), 52.0 (CO_2CH_3), 53.1 (CH_2N), 66.9 (OCH_2), 110.6 (Ar-C), 116.8 (Ar-C), 119.3 (Ar-Cq), 121.3 (Ar-C), 135.0 (Ar-Cq), 146.6 (Ar-Cq), 169.6 (CO), 171.8 (CO)

m/z [EI (+ve)], 334.3 ($[\text{M}]^+$, 100%); Found $[\text{M}]^+$, 334.1891, $\text{C}_{18}\text{H}_{26}\text{O}_4\text{N}_2$ requires 334.1893

ν_{max} (CDCl_3) / cm^{-1} : 2955, 1739, 1666, 1489

(S)-2-Trifluoromethanesulfonyloxy-succinic acid dimethyl ester **36**



To a stirred solution of dimethyl (*S*)-(-)-malate **35** (4.2 ml, 5.2 g, 32 mmol, 1 eq) in dry dichloromethane (400 cm^3) at -78 °C was added 2,6-lutidine (7.1 ml, 6.5 g, 61 mmol, 1.9 eq) under an argon atmosphere. Resulting reaction solution was stirred for 15 minutes at -78 °C, and then treated with trifluoromethanesulfonic anhydride (11 ml, 18 g, 64 mmol, 2 eq). Stirring was continued at -78 °C until completion of reaction as indicated by TLC analysis (2 hours). After this time a cooling bath was removed, the reaction was quenched with water (250 cm^3), and biphasic mixture was stirred until reaching room temperature. The phases were separated and the organic phase was washed with saturated aqueous CuSO_4 (2 x 300 cm^3), dried over anhydrous sodium sulphate, filtered off, and concentrated *in vacuo* to give crude

triflate **36** as a pale brown oil (9.4 g, 32 mmol, 100% yield, 100% conversion by NMR), which was judged clean by NMR and used in synthesis without purification.

δ_{H} (400 MHz, CDCl_3): 3.06 (2H, d, $J = 5.8$ Hz, CH_2CH), 3.76 (3H, s, CH_3), 3.88 (3H, s, CH_3), 5.49 (1H, t, $J = 5.8$ Hz, CH_2CH)

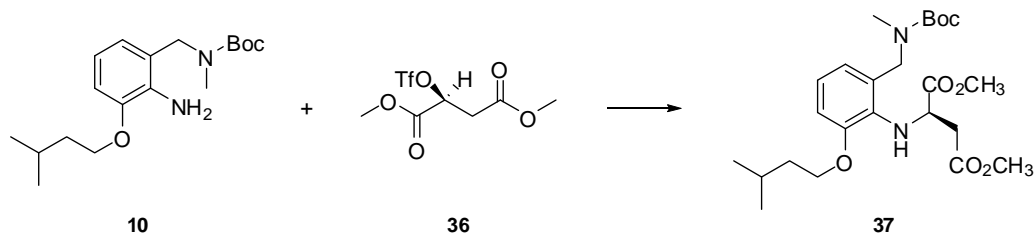
δ_{C} (100 MHz, CDCl_3): 36.7 (CH_2CH), 52.7 (CH_3), 53.8 (CH_3), 78.6 (CH_2CH), 166.6 (CO_2CH_3), 168.0 (CO_2CH_3)

m/z [CI (+ve)], 295.2 ($[\text{M}+\text{H}]^+$, 100%); Found $[\text{M}+\text{H}]^+$, 295.0098, $\text{C}_7\text{H}_{10}\text{O}_7\text{F}_3\text{S}$ requires 295.0099

$[\alpha]_{\text{D}}^{24} -45.2$ (c 1, CHCl_3)

ν_{max} (CDCl_3) / cm^{-1} : 2357, 2333, br. 1747, 1419, 1211, 1141

(R)-dimethyl 2-(2-((tert-butoxycarbonyl(methyl)amino)methyl)-6-(isopentyloxy)phenylamino)succinate **37**



A flask equipped with reflux condenser was charged with aniline **10** (6.0 g, 18.6 mmol, 1 eq) and dry dichloromethane (200 cm^3) under an argon atmosphere. While the solution was stirred, triflate **36** (9.4 g, 32 mmol, 1.7 eq) was added to it dropwise *via* cannula, followed by subsequent addition of 2,6-lutidine (4.1 ml, 3.8 g, 35.4 mmol, 1.9 eq). The resulting brown reaction solution was heated at 50 °C until TLC analysis indicated complete consumption of starting material **10** (5 hours). After this time the oil bath was removed, the reaction was quenched with water (200 cm^3) and stirred for 20 minutes at room temperature. The phases were separated and the aqueous layer was extracted with fresh dichloromethane (200 cm^3). All the organic layers were combined, washed with saturated aqueous CuSO_4 (2 x 350 cm^3), dried over anhydrous sodium sulphate, filtered off and the solvent was removed *in vacuo* to give aniline **37** as brown viscous oil (8.7 g, 18.6 mmol, 100% yield), which was reacted further without need of purification.

δ_{H} (400 MHz, CDCl_3 , 55°C): 0.98 (6H, d, $J = 6.6$ Hz, $\text{CH}(\text{CH}_3)_2$), 1.48 (9H, s, $\text{C}(\text{CH}_3)_3$), 1.72 (2H, appq, $J = 6.7$ Hz, OCH_2CH_2), 1.83 (1H, appsept, $J = 6.7$ Hz, $\text{CH}(\text{CH}_3)_2$), 2.75 (3H, s, NCH_3), 2.81 (2H, br. s, NHCHCH_2), 3.65 (3H, br. s, CO_2CH_3), 3.66 (3H, br. s, CO_2CH_3), 3.99 (2H, t, $J = 6.7$ Hz, OCH_2), 4.36 (1H, br. d, $J = 15.2$ Hz, one of CH_2N), 4.6 (1H, br. s, NHCH), 4.63 (1H, d, $J = 15.2$, one of CH_2N), 6.7 (1H, appd, $J = 7.5$ Hz, one of C_6H_3), 6.77 (1H, appd, $J = 7.9$, one of C_6H_3), 6.85 (1H, appt, $J = 7.8$ Hz, one of C_6H_3)

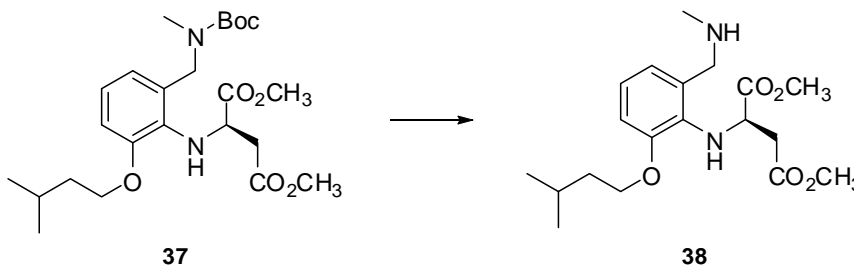
δ_{C} (100 MHz, CDCl_3 , 55°C): 22.7 ($\text{CH}(\text{CH}_3)(\text{CH}_3)$), 22.8 ($\text{CH}(\text{CH}_3)(\text{CH}_3)$), 25.4 ($\text{CH}(\text{CH}_3)_2$), 28.6 ($\text{C}(\text{CH}_3)_3$), 33.6 (NCH_3), 38.2 and 38.4 (OCH_2CH_2 and NHCHCH_2), 49.0 (CH_2N), 51.7 (CO_2CH_3), 52.0 (CO_2CH_3), 56.6 (NHCH), 67.3 (OCH_2), 79.9 ($\text{C}(\text{CH}_3)_3$), 111.7 (Ar-C), 121.6 (Ar-C), 121.7 (Ar-C), 151.3 (Cq), 156.3 (Cq), 171.2 (CO_2CH_3), 173.4 (CO_2CH_3), 2 x Cq unresolved

m/z [CI (+ve)], 467.2 ($[\text{M}+\text{H}]^+$, 70%); Found $[\text{M}+\text{H}]^+$, 467.2761, $\text{C}_{24}\text{H}_{39}\text{N}_2\text{O}_7$ requires 467.2757

$[\alpha]_{\text{D}}^{24} +27.7$ (c 1, CHCl_3)

ν_{max} (CDCl_3) / cm^{-1} : 3329, 2955, 2933, 2872, 1739, 1693, 1674, 1166, 1143

(R)-dimethyl 2-(2-(isopentyloxy)-6-((methylamino)methyl)phenylamino)succinate 38



A vacuum dried amine **37** (0.07 g, 0.15 mmol, 1 eq) was dissolved in a 5% solution of HCl in ethyl acetate (2 cm^3). After stirring for 1.5 hours, TLC analysis indicated complete consumption of the starting material **37**. Reaction was quenched with 5% aqueous NaHCO_3 (5 cm^3), diluted with ethyl acetate (5 cm^3), and stirred for next 10 minutes. After this time the phases were separated, the organic phase was collected, washed with water (5 cm^3), dried over anhydrous sodium sulphate, filtered off, and

concentrated *in vacuo* to give aniline **38** as yellow oil (0.05 g, 0.15 mmol, 100% yield), which was judged clean based on NMR analysis.

δ_{H} (400 MHz, CDCl_3): 0.94 (3H, d, $J = 6.6$ Hz, $\text{CH}(\text{CH}_3)(\text{CH}_3)$), 0.95 (3H, d, $J = 6.6$ Hz, $\text{CH}(\text{CH}_3)(\text{CH}_3)$), 1.65 (2H, appq, $J = 6.7$ Hz, OCH_2CH_2), 1.76 (1H, appsept, $J = 6.6$ Hz, $\text{CH}(\text{CH}_3)_2$), 2.61 (3H, s, NHCH_3), 2.88 (1H, dd, $J = 16.9$ and 5.3 Hz, one of NHCHCH_2), 2.96 (1H, dd, $J = 16.9$ and 5.3 Hz, one of NHCHCH_2), 3.69 (3H, s, CO_2CH_3), 3.72 (3H, s, CO_2CH_3), 3.88-4.0 (2H, m, OCH_2), 4.2-4.31 (3H, m, CH_2NH and NHCH), 6.86 (1H, dd, $J = 6.0$ and 3.6 Hz, one of C_6H_3), 6.99-7.01 (2H, m, two of C_6H_3)

δ_{C} (100 MHz, CDCl_3): 22.6 ($\text{CH}(\text{CH}_3)_2$), 25.1 ($\text{CH}(\text{CH}_3)_2$), 32.1 (NHCH_3), 37.0 (NHCHCH_2), 37.9 (OCH_2CH_2), 49.7 (CH_2NH), 52.2 (CO_2CH_3), 53.0 (CO_2CH_3), 57.1 (NHCH), 67.2 (OCH_2), 113.3 (Ar-C), 124.1 (Ar-C), 124.6 (Ar-C), 124.6 (Ar-Cq), 134.3 (Ar-Cq), 152.9 (Ar-Cq), 171.8 (CO_2CH_3), 174.0 (CO_2CH_3)

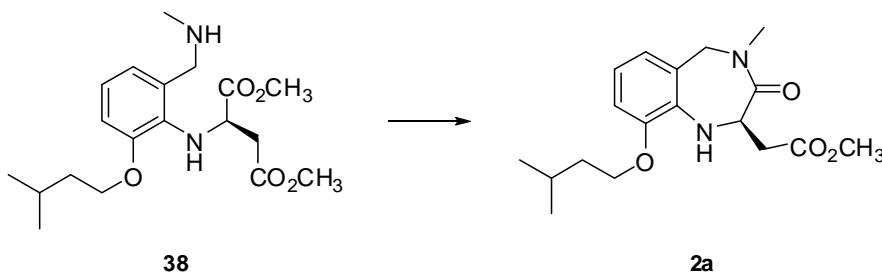
m/z [FAB (+ve)], 367.4 ($[\text{M}+\text{H}]^+$, 100%), 221.6 ($[\text{M}+\text{H}]-\text{CH}(\text{CO}_2\text{CH}_3)\text{CH}_2(\text{CO}_2\text{CH}_3)^+$, 77%); Found $[\text{M}+\text{H}]^+$, 367.2236, $\text{C}_{19}\text{H}_{31}\text{N}_2\text{O}_5$ requires 367.2233

$[\alpha]_{\text{D}}^{20} +16.1$ (c 1, CHCl_3)

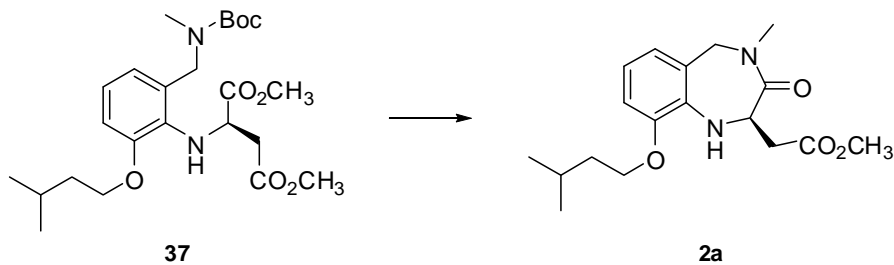
ν_{max} (CDCl_3) / cm^{-1} : br. 3342, 2955, 2872, 1735, 1469, 1257, 1222

(R)-methyl 2-(9-(isopentyloxy)-4-methyl-3-oxo-2,3,4,5-tetrahydro-1H-benzo[e][1,4]diazepin-2-yl)acetate 2a

Procedure A



Procedure B



Procedure A

Flask equipped with reflux condenser was charged with amine **38** (0.66 g, 1.8 mmol, 1 eq) and methanol (15 cm³). The solution was purged with argon for 20 minutes and then treated with sodium methoxide (25 wt. % in methanol, 0.63 ml, 0.15 g, 2.7 mmol, 1.5 eq) under an argon atmosphere. Resulting reaction mixture was refluxed until TLC analysis indicated complete consumption of starting material **38** (1 hour). The heating bath was removed, and the reaction was quenched with water (15 cm³), diluted with ethyl acetate (30 cm³) and stirred for 20 minutes at room temperature. The phases were separated, and the aqueous layer was extracted with fresh ethyl acetate (2 x 30 cm³). The combined organic fractions were washed with brine (60 cm³), dried over anhydrous sodium sulphate, filtered off, and concentrated *in vacuo* to give the benzodiazepine **2a** as orange viscous oil (0.51 g, 1.53 mmol, 85%). Prior to HPLC analysis, ester **2a** was purified by flash column chromatography (silica gel, gradient elution, eluting with 100% DCM to 3% MeOH in DCM).

Procedure B

A vacuum dried amine **37** (8.1 g, 17.4 mmol, 1 eq) was dissolved in a 5% solution of HCl in ethyl acetate (150 cm³). After stirring for 2 hours, TLC analysis indicated complete consumption of the starting material **37**. Reaction was quenched with saturated aqueous NaHCO₃ (200 cm³), diluted with ethyl acetate (100 cm³), and the biphasic mixture was stirred for additional 20 minutes. After this time the phases were separated, and the aqueous phase was extracted with fresh ethyl acetate (2 x 300 cm³). All the organic layers were combined, dried over anhydrous sodium sulphate, filtered off, and concentrated *in vacuo*. The remaining residue was purified by flash column chromatography (silica gel, gradient elution, eluting with 100%

DCM to 5% MeOH in DCM) to give the benzodiazepine **2a** as orange viscous oil (2.46 g, 7.36 mmol, 43%).

δ_{H} (400 MHz, CDCl_3): 0.95 (6H, d, $J = 6.6$ Hz, $\text{CH}(\text{CH}_3)_2$), 1.66 (2H, appq, $J = 6.6$ Hz, OCH_2CH_2), 1.8 (1H, appsept, $J = 6.6$ Hz, $\text{CH}(\text{CH}_3)_2$), 2.67 (1H, dd, $J = 15.9$ and 6.3 Hz, one of NHCHCH_2), 3.04 (1H, dd, $J = 15.9$ and 7.4 Hz, one of NHCHCH_2), 3.05 (3H, s, NCH_3), 3.7 (1H, d, $J = 16.3$ Hz, one of CH_2N), 3.72 (3H, s, CO_2CH_3), 3.93-3.99 (2H, m, OCH_2), 4.41 (1H, d, $J = 4.7$ Hz, NHCH), 5.04-5.09 (1H, m, NHCH), 5.46 (1H, d, $J = 16.3$ Hz, one of CH_2N), 6.54 (1H, dd, $J = 7.6$ and 2.2 Hz, one of C_6H_3), 6.56-6.59 (1H, m, one of C_6H_3), 6.7 (1H, dd, $J = 7.3$ and 2.2 Hz, one of C_6H_3)

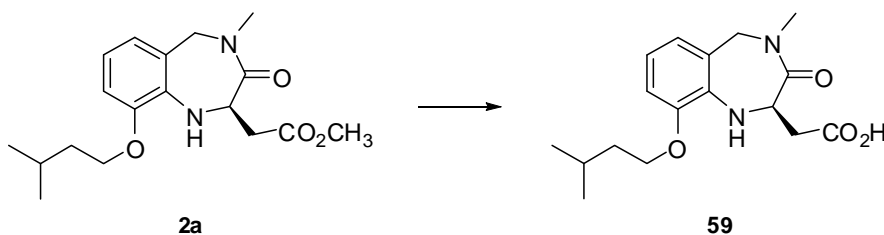
δ_{C} (100 MHz, CDCl_3): 22.7 ($\text{CH}(\text{CH}_3)_2$), 25.2 ($\text{CH}(\text{CH}_3)_2$), 34.7 (NCH_3), 36.3 (NHCHCH_2), 38.0 (OCH_2CH_2), 51.5 (NHCH), 52.0 (CO_2CH_3), 53.1 (CH_2N), 66.9 (OCH_2), 110.6 (Ar-C), 116.8 (Ar-C), 119.3 (Ar-Cq), 121.3 (Ar-C), 135.0 (Ar-Cq), 146.6 (Ar-Cq), 169.6 (CO), 171.8 (CO)

m/z [EI (+ve)], 334.3 ($[\text{M}]^+$, 100%); Found $[\text{M}]^+$, 334.1891, $\text{C}_{18}\text{H}_{26}\text{O}_4\text{N}_2$ requires 334.1893

$[\alpha]_{\text{D}}^{20} +58.8$ (c 1, CHCl_3)

ν_{max} (CDCl_3) / cm^{-1} : 2955, 1739, 1666, 1489

[(R)-4-Methyl-9-(3-methyl-butoxy)-3-oxo-2,3,4,5-tetrahydro-1H-benzo[e][1,4]diazepin-2-yl]-acetic acid 59



An ester **2a** (0.37 g, 1.11 mmol, 1 eq) was dissolved in dry diethyl ether (10 cm^3) under an argon atmosphere. Resulting solution was purged with argon for 20 minutes, cooled to 0 °C and potassium trimethylsilanolate (0.71 g, 5.55 mmol, 5 eq) was added to it. The resulting suspension was stirred at 0 °C for 10 minutes and then

at room temperature until TLC analysis indicated complete consumption of starting material **2a** (4.5 hours). The reaction mixture was cooled back to 0 °C and 1N HCl (1 ml) was added dropwise. Stirring was continued for 5 minutes at 0 °C. After this time the cooling bath was removed, and water (10 cm³) was added to the reaction. The phases were separated, the aqueous layer was acidified to pH 2 with 2N HCl, and extracted with fresh diethyl ether (2 x 10 cm³). The organic phases were combined, dried over anhydrous sodium sulphate, filtered off, and solvents were removed *in vacuo*. The remaining residue was purified by flash column chromatography (silica gel, gradient elution, eluting with 20% ethyl acetate in petroleum ether (40-60) to 70% ethyl acetate in petroleum ether (40-60)) to give acid **59** as yellow foam (0.344 g, 1.07 mmol, 97%).

δ_H (400 MHz, CDCl₃): 0.94 (6H, d, *J* = 6.7 Hz, CH(CH₃)₂), 1.66 (2H, appq, *J* = 6.6 Hz, OCH₂CH₂), 1.79 (1H, appsept, *J* = 6.7 Hz, CH(CH₃)₂), 2.75 (1H, dd, *J* = 15.9 and 5.8 Hz, one of CH₂CO₂H), 3.05 (1H, dd, *J* = 15.9 and 7.5 Hz, one of CH₂CO₂H), 3.08 (3H, s, NCH₃), 3.71 (1H, d, *J* = 16.4, one of CH₂N), 3.93-3.99 (2H, m, OCH₂), 5.07 (1H, dd, *J* = 7.2 and 5.9 Hz, NHCH), 5.46 (1H, d, *J* = 16.3 Hz, one of CH₂N), 6.54 (1H, dd, *J* = 7.7 and 1.6 Hz, one of C₆H₃), 6.59 (1H, appt, *J* = 7.7, one of C₆H₃), 6.71 (1H, dd, *J* = 7.7 and 1.6 Hz, one of C₆H₃)

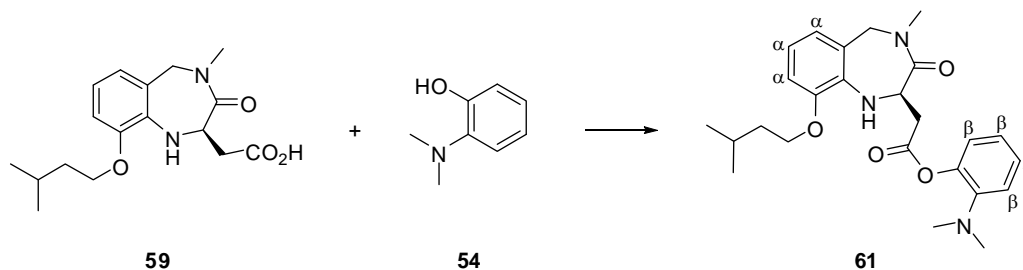
δ_C (100 MHz, CDCl₃): 22.67 (CH(CH₃)(CH₃)), 22.69 (CH(CH₃)(CH₃)), 25.2 (CH(CH₃)₂), 34.9 (NCH₃), 36.5 (CH₂CO₂H), 37.9 (OCH₂CH₂), 51.4 (NHCH), 53.3 (CH₂N), 66.9 (OCH₂), 110.7 (Ar-C), 117.0 (Ar-C), 119.0 (Ar-Cq), 121.3 (Ar-C), 134.8 (Ar-Cq), 146.7 (Ar-Cq), 170.1 (NCO), 175.1 (CO₂H)

m/z [CI (+ve)], 321.2 ([M+H]⁺, 100%); Found [M+H]⁺, 321.1810, C₁₇H₂₅N₂O₄ requires 321.1814

[α]_D¹⁹ +104.8 (*c* 1, CHCl₃)

v_{max} (CDCl₃) / cm⁻¹: 3400-2500, 3406, 2955, 2928, 1716, 1660, 1639, 1491, 1253

(R)-2-(dimethylamino)phenyl 2-(9-(isopentyloxy)-4-methyl-3-oxo-2,3,4,5-tetrahydro-1H-benzo[e][1,4]diazepin-2-yl)acetate **61**



A flask, protected from light with aluminium foil, was charged with phenol **54** (0.048 g, 0.35 mmol, 1 eq) and kept under vacuum for 1 hour. After the flask was refilled with argon, phenol **54** was dissolved in dry DCM (3 cm³). Resulting solution was purged with argon for 20 minutes, cooled to 0 °C and DMAP (0.04 g, 0.35 mmol, 1 eq), and EDC (0.1 g, 0.53 mmol, 1.5 eq) were successively added. Resulting reaction mixture was stirred at 0 °C for 5 minutes. In a separate flask vacuum dried acid **59** (0.17 g, 0.53 mmol, 1.5 eq) was dissolved in dry DCM (3 cm³) and then transferred via cannula to the reaction mixture over 5 minutes. Stirring was continued at 0 °C for additional 10 minutes, and then overnight at room temperature. After this time TLC analysis confirmed complete consumption of phenol **54**. The reaction was quenched with water (5 cm³) and resulting biphasic mixture was stirred for 20 minutes. The layers were separated, and aqueous layer was extracted with fresh DCM (2 x 5 cm³). Combined organic layers were dried over anhydrous sodium sulphate, filtered off, and the solvent was removed *in vacuo*. The remaining residue was purified by flash column chromatography (silica gel, gradient elution, eluting with 100% petroleum ether (40-60) to 30% ethyl acetate in petroleum ether (40-60)) to give ester **61** as pale yellow oil (0.05 g, 0.11 mmol, 31%).

δ_{H} (400 MHz, CDCl₃): 0.92 (3H, d, $J = 6.6$ Hz, CH(CH₃)(CH₃)), 0.93 (3H, d, $J = 6.6$ Hz, CH(CH₃)(CH₃)), 1.63-1.68 (2H, m, OCH₂CH₂), 1.78 (1H, appsept., $J = 6.7$ Hz, CH(CH₃)₂), 2.76 (6H, s, N(CH₃)₂), 2.96 (1H, dd, $J = 16.0$ and 6.7 Hz, one of NHCHCH₂), 3.09 (3H, s, CH₂NCH₃), 3.35 (1H, dd, $J = 16.0$ and 7.0 Hz, one of NHCHCH₂), 3.73 (1H, d, $J = 16.5$ Hz, one of CH₂N), 3.93-4.02 (2H, m, OCH₂), 4.51 (1H, br. d, $J = 4.7$ Hz, NHCH), 5.18-5.23 (1H, m, NHCHCH₂), 5.48 (1H, d, $J = 16.3$ Hz, one of CH₂N), 6.56-6.62 (2H, m, two of CH(C α)), 6.72 (1H, dd, $J = 7.5$ and 1.8

Hz, one of $CH(C\alpha)$), 6.92-6.96 (1H, m, one of $CH(C\beta)$), 7.0 (1H, dd, $J = 8.1$ and 1.5 Hz, one of $CH(C\beta)$), 7.06 (1H, dd, $J = 8.0$ and 1.5 Hz, one of $CH(C\beta)$), 7.13-7.18 (1H, m, one of $CH(C\beta)$)

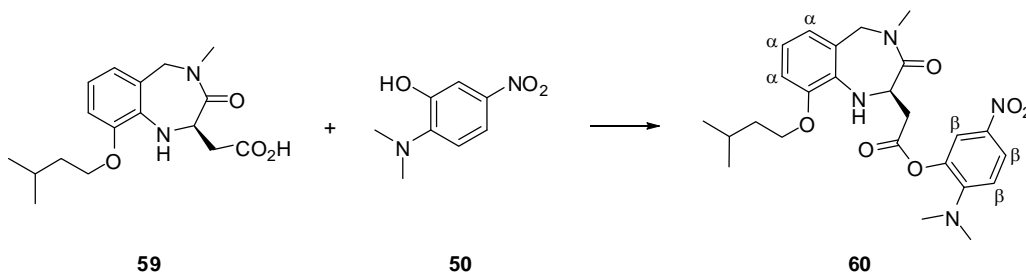
δ_C (100 MHz, $CDCl_3$): 22.7 ($CH(CH_3)(CH_3)$), 22.75 ($CH(CH_3)(CH_3)$), 25.3 ($CH(CH_3)_2$), 34.8 (CH_2NCH_3), 36.8 ($NHCHCH_2$), 38.0 (OCH_2CH_2), 43.4 ($N(CH_3)_2$), 51.8 ($NHCH$), 53.2 (CH_2N), 67.0 (OCH_2), 110.7 ($Ar-C(C\alpha)$), 117.0 ($Ar-C(C\alpha)$), 119.0 ($Ar-C(C\beta)$), 119.5 ($Ar-Cq$), 121.4 ($Ar-C(C\alpha)$), 121.8 ($Ar-C(C\beta)$), 123.6 ($Ar-C(C\beta)$), 126.7 ($Ar-C(C\beta)$), 135.1 ($Ar-Cq$), 143.4 ($Ar-Cq$), 145.4 ($Ar-Cq$), 146.8 ($Ar-Cq$), 169.5 (CO), 169.7 (CO)

m/z [$CI (+ve)$], 440.5 ($[M+H]^+$, 5%), 275.4 ($[M+H]-(CO_2)C_6H_4(N(CH_3)_2)^+$, 31%); Found $[M+H]^+$, 440.2545, $C_{25}H_{34}N_3O_4$ requires 440.2549

$[\alpha]_D^{25} +71.6$ (c 1, $CHCl_3$)

ν_{max} ($CDCl_3$) / cm^{-1} : 3414, 2955, 2924, 2870, 1759, 1662, 1496

(*R*)-2-(dimethylamino)-5-nitrophenyl 2-(9-(isopentyloxy)-4-methyl-3-oxo-2,3,4,5-tetrahydro-1H-benzo[e][1,4]diazepin-2-yl)acetate **60**



A flask, protected from light with aluminium foil, was charged with phenol **50** (0.01 g, 0.05 mmol, 1 eq) and kept under vacuum for 1 hour. After the flask was refilled with argon, phenol **50** was dissolved in dry dichloromethane (1 cm^3). Resulting solution was purged with argon, cooled to 0 °C, and DMAP (0.006 g, 0.05 mmol, 1 eq) and EDC (0.014 g, 0.075 mmol, 1.5 eq) were successively added to it. Resulting reaction mixture was stirred at 0 °C for 5 minutes. In a separate flask vacuum dried acid **59** (0.024 g, 0.075 mmol, 1.5 eq) was dissolved in dry dichloromethane (1 cm^3) and then transferred via cannula to the reaction mixture over 5 minutes. Stirring was continued at 0 °C for additional 10 minutes, and then overnight at room temperature. After this time TLC analysis confirmed complete consumption of phenol **50**. The

reaction was quenched with water (2 cm³), and resulting biphasic mixture was stirred for further 20 minutes. The phases were separated and aqueous layer was extracted with fresh dichloromethane (2 x 3 cm³). Combined organic layers were dried over anhydrous sodium sulphate, filtered off, and the solvent was removed *in vacuo*. The remaining residue was purified by flash column chromatography (silica gel, gradient elution, eluting with 100% petroleum ether (40-60) to 30% ethyl acetate in petroleum ether (40-60)) to give ester **60** as fluorescent yellow liquid (0.02 g, 0.04 mmol, 80% yield).

δ_{H} (400 MHz, CDCl₃): 0.92 (3H, d, $J = 6.6$ Hz, CH(CH₃)(CH₃)), 0.93 (3H, d, $J = 6.6$ Hz, CH(CH₃)(CH₃)), 1.63-1.69 (2H, m, OCH₂CH₂), 1.78 (1H, appsept, $J = 6.7$ Hz, CH(CH₃)₂), 2.97 (1H, dd, $J = 16.2$ and 5.9 Hz, one of NHCHCH₂), 3.05 (6H, s, N(CH₃)₂), 3.09 (3H, s, CH₂NCH₃), 3.35 (1H, dd, $J = 16.2$ and 7.8 Hz, one of NHCHCH₂), 3.74 (1H, d, $J = 16.5$ Hz, one of CH₂N), 3.94-4.05 (2H, m, OCH₂), 4.42 (1H, d, $J = 5.0$ Hz, NHCH), 5.15-5.2 (1H, m, NHCH), 5.48 (1H, d, $J = 16.3$ Hz, one of CH₂N), 6.58 (1H, dd, $J = 7.7$ and 1.5 Hz, one of CH(C α)), 6.62 (1H, t, $J = 7.7$ Hz, one of CH(C α)), 6.74 (1H, dd, $J = 7.8$ and 1.5 Hz, one of CH(C α)), 6.82 (1H, d, $J = 9.2$ Hz, one of CH(C β)), 7.9 (1H, d, $J = 2.6$ Hz, one of CH(C β)), 8.02 (1H, dd, $J = 9.2$ and 2.6 Hz, one of CH(C β))

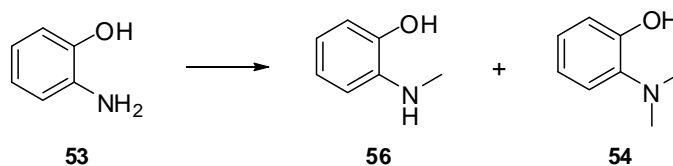
δ_{C} (100 MHz, CDCl₃): 22.7 (CH(CH₃)(CH₃)), 22.8 (CH(CH₃)(CH₃)), 25.3 (CH(CH₃)₂), 34.9 (CH₂NCH₃), 36.6 (NHCHCH₂), 38.0 (OCH₂CH₂), 42.5 (N(CH₃)₂), 51.6 (NHCH), 53.2 (CH₂N), 67.0 (OCH₂), 110.7 (Ar-C(C α)), 115.9 (Ar-C(C β)), 117.3 (Ar-C(C α)), 119.6 (Ar-Cq), 120.8 (Ar-C(C β)), 121.4 (Ar-C(C α)), 123.2 (Ar-C(C β)), 134.7 (Ar-Cq), 138.5 (Ar-Cq), 138.8 (Ar-Cq), 146.8 (Ar-Cq), 150.0 (Ar-Cq), 169.3 (2 x CO)

m/z [FAB (+ve)], 485.4 ([M+H]⁺, 27%), 303.3 ([M+H] - (HO)C₆H₃(NO₂)(N(CH₃)₂)]⁺, 100%); Found [M+H]⁺, 485.2399, C₂₅H₃₃N₄O₆ requires 485.2400

$[\alpha]_{\text{D}}^{20}$ +16.4 (*c* 1, CHCl₃)

ν_{max} (CDCl₃) / cm⁻¹: 2956, 2885, 2879, 1764, 1662, 1599, 1494, 1321

2-Methylamino-phenol **56** and 2-Dimethylamino-phenol **54**



Procedure A

To a solution of 2-aminophenol **53** (0.5 g, 4.58 mmol, 1 eq) in methanol (40 cm³), was added formaldehyde (37 wt. % in water, 0.9 ml, 0.34 g, 11.45 mmol, 2.5 eq). After stirring at room temperature for 0.5 hour, the reaction mixture was cooled to -15 °C and sodium borohydride (0.52 g, 13.74 mmol, 3 eq) was added to it in portions. The cooling bath was removed and stirring was continued overnight at room temperature. After this time, another portion of formaldehyde (0.9 ml, 0.34 g, 11.45 mmol, 2.5 eq) was added to the reaction and stirring was continued for 0.5 hour. Then reaction was cooled to -15 °C and second portion of sodium borohydride (0.52 g, 13.74 mmol, 3 eq) was added. The cooling bath was removed and the reaction was stirred at room temperature until completion as indicated by TLC analysis (6 hours). The reaction was quenched with water (40 cm³) and diluted with diethyl ether (80 cm³). The layers were separated, aqueous layer was acidified to pH=5 and extracted with fresh diethyl ether (2 x 80 cm³). The organic layers were combined, dried over anhydrous sodium sulphate, filtered off, and carefully concentrated *in vacuo* (product **54** proved to be volatile under reduced pressure). Aniline **54** was judged clean by NMR analysis and was used in synthesis without purification (0.63 g, 4.58 mmol, 100% yield).

Procedure B

To a stirred solution of 2-aminophenol **53** (0.2 g, 1.83 mmol, 1 eq) in dry DMF (10 cm³) were added potassium bicarbonate (0.55 g, 5.49 mmol, 3 eq) and methyl iodide (0.25 ml, 0.57 g, 4.03 mmol, 2.2 eq) under an argon atmosphere. The resulting reaction mixture was stirred overnight at room temperature. After this time, the reaction was quenched with water (15 cm³) and diluted with ethyl acetate (20 cm³). After biphasic mixture was stirred for 20 minutes, the layers were separated and the aqueous phase was extracted with fresh ethyl acetate (2 x 20 cm³). The organic

layers were combined, washed with brine (60 cm³), dried over anhydrous sodium sulphate, filtered off, and solvents were removed *in vacuo*. The residue was purified by flash column chromatography (silica gel, gradient elution, eluting with 100% petroleum ether (40-60) to 10% ethyl acetate in petroleum ether (40-60)) to give compound **56** as a white solid (0.11 g, 0.9 mmol, 50% yield) and **54** as colourless oil (0.02 g, 0.15 mmol, <10% yield).

Procedure C

To a stirred solution of 2-aminophenol **53** (0.2 g, 1.83 mmol, 1 eq) in dry DMF (10 cm³) were added cesium carbonate (2.38 g, 7.32 mmol, 4 eq) and methyl iodide (0.25 ml, 0.57 g, 4.03 mmol, 2.2 eq) under an argon atmosphere. The resulting reaction mixture was stirred overnight at room temperature. After this time, the reaction was quenched with water (15 cm³) and diluted with ethyl acetate (30 cm³). After biphasic mixture was stirred for 20 minutes, the layers were separated and the aqueous phase was extracted with fresh ethyl acetate (2 x 20 cm³). The organic layers were combined, washed with brine (60 cm³), dried over anhydrous sodium sulphate, filtered off, and solvents were removed *in vacuo*. NMR analysis of the crude material revealed the exclusive formation of undesired compound **56** (white solid, 0.22 g, 1.8 mmol, 100% yield) that wasn't purified.

Procedure D

To a stirred acetic anhydride (2.2 ml, 2.38 g, 23.27 mmol, 1.2 eq) was added formic acid (1.32 ml, 1.61g, 34.91 mmol, 1.8 eq) under an argon atmosphere. The resulting solution was heated at 60 °C for 2 hours, allowed to cool to room temperature, diluted with dry THF (15 cm³), and then cooled back to 0 °C. 2-aminophenol **53** (2.12 g, 19.39 mmol, 1 eq) in dry THF (15 cm³) was added, and stirring was continued at room temperature for 40 min. Volatile organic materials were removed *in vacuo*, the remaining residue was taken up in dry THF (50 cm³) and added to a vigorously stirred ice-cold suspension of lithium aluminium hydride (15 ml of 3.5 M solution in THF/toluene, 1.99 g, 52.32 mmol, 2.7 eq) in dry THF (20 cm³), all under an argon atmosphere. The solution was stirring overnight at room temperature. After this time, the resulting solution was cooled to 0 °C and quenched by dropwise addition of water (2 cm³), 15% aqueous NaOH (2 cm³), and another portion of water (6 cm³). The resulting suspension was allowed to warm to room temperature and

stirring was continued for 1 hour. The suspension was then diluted with diethyl ether, filtered through a pad of celite, and the filtrate was washed with copious amount of diethyl ether, followed by ethyl acetate, and 50% methanol in ethyl acetate. The solvent was removed *in vacuo*, and crude material was filtered through a pad of silica (gradient elution, eluting with 40% ethyl acetate in petroleum ether (40-60) to 100% ethyl acetate) to give compound **56**. Resulting compound **56** was taken directly to the next reaction.

To a stirred acetic anhydride (0.64 cm³, 0.7 g, 6.72 mmol, 1.2 eq) was added formic acid (0.38 cm³, 0.46g, 10.08 mmol, 1.8 eq) under an argon atmosphere. The resulting solution was heated at 60 °C for 2 hours, allowed to cool to room temperature, diluted with dry THF (5 cm³), then cooled back to 0 °C. 2-Methylamino-phenol **56** (0.69g, 5.6 mmol, 1 eq) in dry THF (15 cm³) was then added, and stirring was continued at room temperature for 1 hour. After the volatile organic materials were removed *in vacuo*, the remaining residue was taken up in dry THF (10 cm³) and added to a vigorously stirred ice-cold suspension of lithium aluminium hydride (3.84 ml of 3.5 M solution in THF/toluene, 0.51 g, 13.44 mmol, 2.4 eq) in dry THF (10 cm³) under an argon atmosphere. The resulting reaction was stirred overnight at room temperature. After this time, the reaction was cooled to 0 °C and quenched by dropwise addition of water (0.5 cm³), 15% aqueous NaOH (0.5 cm³), and another portion of water (1.5 cm³). The resulting suspension was allowed to warm to room temperature and stirring was continued for 2.5 hour. The suspension was then diluted with ethyl acetate (80 cm³) and added to water (80 cm³). The layers were separated and aqueous phase was extracted with fresh ethyl acetate (2 x 80 cm³). The organic layers were combined, washed with brine (200 cm³), dried over anhydrous sodium sulphate, filtered off, and solvents were removed *in vacuo*. The remaining residue was purified by flash column chromatography (silica gel, gradient elution, eluting with 100% petroleum ether (40-60) to 3% ethyl acetate in petroleum ether (40-60)) to give compound **54** as colourless oil (0.23 g, 1.66 mmol, 8.5% yield).

2-Methylamino-phenol **56**

δ_{H} (400 MHz, DMSO): 2.72 (3H, s, NHCH₃), 4.78 (1H, br. s, NHCH₃), 6.41-6.46 (2H, m, two of C₆H₄), 6.66-6.7 (2H, m, two of C₆H₄), 9.18 (1H, s, OH)

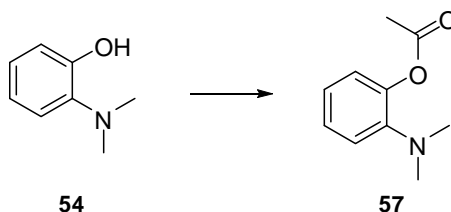
2-Dimethylamino-phenol **54**

δ_{H} (400 MHz, CDCl_3): 2.67 (6H, s, $\text{N}(\text{CH}_3)_2$), 6.86 (1H, ddd, $J = 7.6, 7.5$ and 1.5 Hz, one of C_6H_4), 6.94 (1H, dd, $J = 8.0$ and 1.5 Hz, one of C_6H_4), 7.04-7.08 (1H, m, one of C_6H_4), 7.17 (1H, dd, $J = 7.8$ and 1.5 Hz, one of C_6H_4)

δ_{C} (100 MHz, CDCl_3): 45.3 ($\text{N}(\text{CH}_3)_2$), 114.2 (Ar-C), 120.1 (Ar-C), 120.8 (Ar-C), 126.3 (Ar-C), 140.2 ($\text{Cq-N}(\text{CH}_3)_2$), 151.5 (Cq-OH)

m/z [EI (+ve)], 137.12 ($[\text{M}]^+$, 78%); Found $[\text{M}]^+$, 137.0837, $\text{C}_8\text{H}_{11}\text{NO}$ requires 137.0841

Acetic acid 2-dimethylamino-phenyl ester **57**



To a solution of phenol **54** (3.85 g, 28.1 mmol, 1 eq) in dry DCM (150 cm^3) cooled to 0°C were added pyridine (3.4 ml, 3.3 g, 42.15 mmol, 1.5 eq), catalytic amount of 4-dimethylaminopyridine and acetic anhydride (4.0 ml, 4.3 g, 42.15 mmol, 1.5 eq). The cooling bath was removed and the resulting reaction mixture was stirred overnight at room temperature under an argon atmosphere. After this time reaction was cooled back to 0°C and another portion of pyridine (2.3 ml, 2.2 g, 28.1 mmol, 1 eq), catalytic amount of 4-dimethylaminopyridine and acetic anhydride (2.6 ml, 2.8 g, 28.1 mmol, 1 eq) were added to it. Stirring was continued for 4 hours at room temperature. After this time organics were removed *in vacuo*, remaining residue was taken up in fresh DCM (150 cm^3) and washed with saturated aqueous CuSO_4 ($2 \times 100 \text{ cm}^3$). The phases were separated, the organic layer was collected, dried over anhydrous sodium sulphate, filtered off and the solvent was removed *in vacuo* to give acetate **57** (brown liquid, 3.79 g, 75%), which was judged clean based on NMR analysis and used in synthesis without purification.

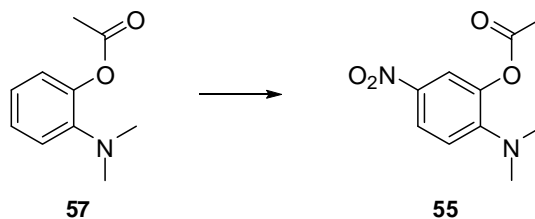
δ_{H} (400 MHz, CDCl_3): 2.32 (3H, s, C(O)CH_3), 2.76 (6H, s, $\text{N(CH}_3)_2$), 6.93-7.02 (3H, m, three of C_6H_4), 7.16 (1H, ddd, $J = 8.0, 6.8$ and 2.0 Hz, one of C_6H_4)

δ_{C} (100 MHz, CDCl_3): 21.2 (C(O)CH_3), 43.3 ($\text{N(CH}_3)_2$), 119.1 (Ar-C), 121.9 (Ar-C), 123.4 (Ar-C), 126.7 (Ar-C), 143.6 (Ar-Cq), 145.5 (Ar-Cq), 169.3 (CO)

m/z [EI (+ve)], 179.11 ($[\text{M}]^+$, 47%), 137.10 ($[\text{M}-\text{COCH}_3]^+$, 100%); Found $[\text{M}]^+$, 179.0943, $\text{C}_{10}\text{H}_{13}\text{NO}_2$ requires 179.0946

ν_{max} (CDCl_3) / cm^{-1} : 2947, 2835, 2785, 1759, 1496, 1192

Acetic acid 2-dimethylamino-5-nitro-phenyl ester **55**



Procedure A

To a stirred solution of triphenylphosphine (0.88 g, 3.36 mmol, 1.2 eq) in dry MeCN (30 cm^3) were added bromine (0.17 ml, 0.54 g, 3.36 mmol, 1.2 eq) and silver nitrate (0.57 g, 3.36 mmol, 1.2 eq) under argon atmosphere. While the resulting mixture was stirred, formation of white precipitate was observed. After stirring for 10 minutes, the reaction was treated with a solution of acetate **57** (0.5 g, 2.8 mmol, 1 eq) in dry MeCN under argon atmosphere and stirring was continued for 25 minutes. After this time the reaction was diluted with DCM and filtered through filter paper to remove white precipitate, which was washed with copious amount of DCM. The filtrate was collected and concentrated *in vacuo*. The remaining residue was taken up in fresh DCM (20 cm^3), washed with 5% aqueous NaHCO_3 (20 cm^3) and water (20 cm^3). The layers were separated, organic layer was collected, dried over anhydrous sodium sulphate, filtered off, and solvent was removed *in vacuo*. The residue was purified by flash column chromatography (silica gel, gradient elution, eluting with 100% petroleum ether (40-60) to 20% ethyl acetate in petroleum ether (40-60)) to give compound **55** as viscous, dense orange oil (0.26 g, 1.15 mmol, 40%).

Procedure B

A solution of acetate **57** (0.27 g, 1.51 mmol, 1 eq) in dry MeCN (7 cm³) was added dropwise *via* cannula to the stirred solution of cerium (IV) ammonium nitrate (0.83 g, 1.51 mmol, 1 eq) in dry MeCN (7 cm³) under an argon atmosphere. Resulting reaction mixture was stirred at room temperature until TLC analysis indicated complete consumption of starting material **57** (4 hours). The reaction was quenched with saturated aqueous K₂CO₃ (15 cm³) and stirred for further 20 minutes. After this time layers were separated and the aqueous layer was extracted with fresh EtOAc (2 x 15 cm³). All the organic phases were combined, dried over anhydrous sodium sulphate, filtered off, and concentrated *in vacuo*. The remaining residue was purified by flash column chromatography (silica gel, gradient elution, eluting with 100% petroleum ether (40-60) to 10% ethyl acetate in petroleum ether (40-60)) to give compound **55** as viscous orange oil (0.1 g, 0.45 mmol, 30% yield).

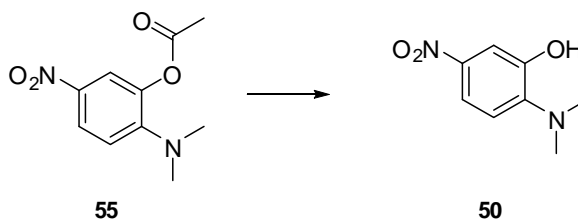
δ_{H} (400 MHz, CDCl₃): 2.33 (3H, s, C(O)CH₃), 2.99 (6H, s, N(CH₃)₂), 6.83 (1H, d, *J* = 9.2 Hz, one of C₆H₃), 7.83 (1H, d, *J* = 2.6 Hz, one of C₆H₃), 8.0 (1H, dd, *J* = 9.2 and 2.6 Hz, one of C₆H₃)

δ_{C} (100 MHz, CDCl₃): 21.0 (C(O)CH₃), 42.3 (N(CH₃)₂), 116.1 (Ar-C), 120.6 (Ar-C), 123.0 (Ar-C), 138.9 (Ar-Cq), 139.0 (Ar-Cq), 150.2 (Ar-Cq), 168.6 (CO)

m/z [CI (+ve)], 225.2 ([M+H]⁺, 100%); Found [M+H]⁺, 225.0872, C₁₀H₁₃N₂O₄ requires 225.0875

ν_{max} (CDCl₃) / cm⁻¹: 2955, 2924, 2854, 1770, 1597, 1319, 1188

2-Dimethylamino-5-nitro-phenol **50**



Procedure A

To a stirred solution of acetate **55** (0.26 g, 1.16 mmol, 1 eq) in methanol (15 cm³), was added sodium methoxide (25 wt. % in MeOH, 0.26 ml, 0.06 g, 1.16 mmol, 1 eq). The resulting reaction solution was stirred at room temperature until TLC analysis indicated complete consumption of starting material **55** (40 minutes). After this time the reaction was quenched with water (30 cm³), diluted with ethyl acetate (50 cm³) and stirred for 20 minutes. The layers were separated and aqueous layer was extracted with fresh EtOAc (2 x 50 cm³). All the organic layers were combined, dried over anhydrous sodium sulphate, filtered off, and concentrated *in vacuo*. The remaining residue was purified by flash column chromatography (silica gel, gradient elution, eluting with 100% petroleum ether (40-60) to 10% ethyl acetate in petroleum ether (40-60)) to give phenol **50** as a red solid (0.1 g, 0.55 mmol, 48%).

Procedure B

Acetate **55** (0.063 g, 0.28 mmol, 1 eq) was added to a mixture of MeOH (4 cm³) and water (1 cm³). The resulting mixture was heated to 30 °C until starting material **55** was fully dissolved. Then ammonium acetate (0.17 g, 2.24 mmol, 8 eq) was added to the reaction at room temperature and stirring was continued for 2 days. After this time the reaction was diluted with ethyl acetate (10 cm³), the layers were separated and the aqueous layer was extracted with fresh EtOAc (2 x 10 cm³). All the organic layers were combined, dried over anhydrous sodium sulphate, filtered off, and concentrated *in vacuo*. The remaining residue was purified by flash column chromatography (silica gel, gradient elution, eluting with 100% petroleum ether (40-60) to 7% ethyl acetate in petroleum ether (40-60)) to give phenol **50** as a red solid (0.048 g, 0.26 mmol, 93%).

δ_{H} (400 MHz, CDCl₃): 2.75 (6H, s, N(CH₃)₂), 7.15 (1H, d, *J* = 8.6 Hz, one of C₆H₃), 7.76-7.77 (1H, m, one of C₆H₃), 7.78 (1H, dd, *J* = 8.6 and 2.6 Hz, one of C₆H₃)

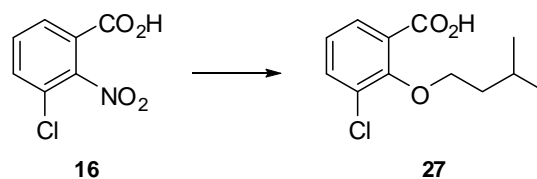
δ_{C} (100 MHz, CDCl₃): 44.2 (N(CH₃)₂), 110.2 (Ar-C), 116.4 (Ar-C), 119.8 (Ar-C), 147.2 (Ar-Cq), 150.7 (Ar-Cq), 1 x Cq unresolved

m/z [EI (+ve)], 182.1 ([M]⁺, 30%); Found [M]⁺, 182.0689, C₈H₁₀N₂O₃ requires 182.0691

ν_{max} (CDCl₃) / cm⁻¹: 3600-3200, 2956, 2922, 2850, 1591, 1521, 1498, 1323

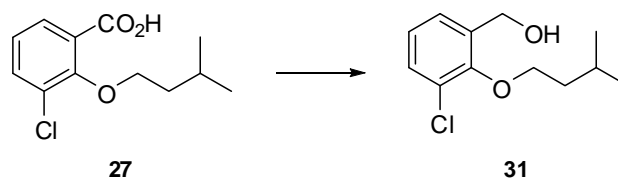
mp. 66-72 °C

3-Chloro-2-(isopentyloxy)benzoic acid **27**



A dispersion of NaH in oil (60% (w/w) in mineral oil, 0.5 g, 12.4 mmol, 5 eq) was washed three times with petroleum ether under an argon atmosphere, dried under vacuum and suspended in dry DMF (40 cm³). After the suspension was cooled to -15 °C, a solution of 3-methyl-1-butanol (0.8 ml, 0.66 g, 7.4 mmol, 3 eq) was added to it dropwise *via* syringe. Resulting reaction mixture was stirred for 10 minutes at -15 °C and further 1 hour at room temperature. After this time, the reaction was cooled to -10 °C, and a solution of acid **16** (0.5 g, 2.48 mmol, 1 eq) in dry DMF (10 cm³) was added dropwise *via* cannula. Resulting reaction mixture was stirred at -10 °C for 0.5 hour and then overnight at room temperature. After this time reaction was quenched with ice-cold water (50 cm³) and diluted with ethyl acetate (80 cm³). The fractions were separated, an aqueous fraction was acidified to pH 2, and extracted with fresh ethyl acetate (2 x 80 cm³). All the organic phases were combined, washed with brine (200 cm³), dried over anhydrous sodium sulphate, filtered off, and solvents were removed *in vacuo*. The remaining acid **27** (brown liquid) was reacted further without purification.

(3-chloro-2-(isopentyloxy)phenyl)methanol **31**



A vacuum-dried acid **27** (0.57 g, 2.48 mmol, 1 eq) was dissolved in dry THF (50 cm³) under an argon atmosphere. Resulting solution was cooled to 0 °C and treated with borane-tetrahydrofuran complex (1M in THF, 7.4 ml, 7.4 mmol, 3 eq). Cooling bath was removed and reaction mixture was stirred overnight at room temperature. After this time the reaction was cooled to 0 °C, carefully quenched with ice-cold water (50 cm³) and 2M HCl (20 ml), and diluted with ethyl acetate (100 cm³). Biphasic mixture was stirred for 20 minutes and then layers were separated. The aqueous phase was extracted with fresh ethyl acetate (2 x 100 cm³). All the organic layers were combined, dried over anhydrous sodium sulphate, filtered off, and solvents were removed *in vacuo*. The remaining residue was purified by flash column chromatography (silica gel, gradient elution, eluting with 100% petroleum ether (40-60) to 10% ethyl acetate in petroleum ether (40-60)) to give alcohol **31** as yellow oil (0.5 g, 2.3 mmol, 93% yield from **16**).

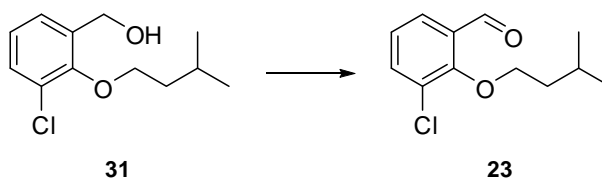
δ_{H} (400 MHz, CDCl₃): 0.98 (6H, d, $J = 6.6$ Hz, CH(CH₃)₂), 1.72 (2H, appq, $J = 6.7$ Hz, OCH₂CH₂), 1.87 (1H, appsept., $J = 6.7$ Hz, CH(CH₃)₂), 2.18 (1H, t, $J = 6.2$ Hz, OH), 4.03 (2H, t, $J = 6.8$ Hz, OCH₂), 4.71 (2H, br. d, $J = 6.2$ Hz, CH₂OH), 7.04 (1H, appt, $J = 7.8$ Hz, one of C₆H₃), 7.25-7.27 (1H, m, one of C₆H₃), 7.31 (1H, dd, $J = 7.9$ and 1.6 Hz, one of C₆H₃)

δ_{C} (100 MHz, CDCl₃): 22.7 (CH(CH₃)₂), 25.0 (CH(CH₃)₂), 39.1 (OCH₂CH₂), 61.5 (CH₂OH), 72.6 (OCH₂), 124.9 (Ar-C), 127.4 (Ar-C), 127.9 (Ar-Cq), 130.1 (Ar-C), 136.1 (Ar-Cq), 153.4 (Ar-Cq)

m/z [EI (+ve)], 230.1 ([M+2]⁺, 13%), 228.1 ([M]⁺, 40%), 140.0 ([M-(OCH₂CH₂CH(CH₃)₂)]⁺, 100%); Found [M]⁺, 228.0918, C₁₂H₁₇O₂Cl requires 228.0917

ν_{max} (CDCl₃) / cm⁻¹: 3600-3150, 2928, 2870, 1446, 775

3-chloro-2-(isopentyloxy)benzaldehyde **23**



An oxalyl chloride (0.36 ml, 0.53 g, 4.2 mmol, 2 eq) was dissolved in dry DCM (20 cm³) under an argon atmosphere. The resulting solution was cooled to -78 °C and solution of DMSO (0.6 ml, 0.66 g, 8.4 mmol, 4 eq) in dry DCM (5 cm³) was added to it. After stirring for 0.5 hour at -78 °C, solution of alcohol **31** (0.45 g, 2.1 mmol, 1 eq) in dry DCM (20 cm³) was added to the reaction *via* cannula, and stirring was continued for 2 hours at -78 °C. Then reaction was treated with triethylamine (2.3 ml, 1.7 g, 16.8 mmol, 8 eq), stirred for 10 minutes at -78 °C, and allowed to warm to room temperature. After being stirred at room temperature for 1 hour, the reaction was diluted with DCM (15 cm³) and quenched with water (30 cm³). The layers were separated, and organic phase was washed with 0.1N HCl (40 cm³), saturated aqueous NaHCO₃ (40 cm³), and brine (40 cm³). Organic fraction was collected, dried over anhydrous sodium sulphate, filtered off, and solvents were removed *in vacuo*. The remaining residue was purified by flash column chromatography (silica gel, gradient elution, eluting with 100% petroleum ether (40-60) to 1% ethyl acetate in petroleum ether (40-60)) to give aldehyde **23** as yellow liquid (0.4 g, 1.76 mmol, 84% yield).

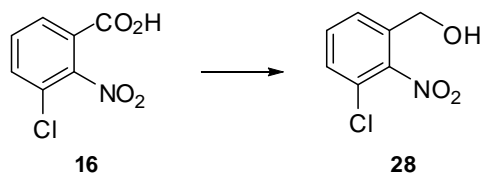
δ_H (400 MHz, CDCl₃): 0.98 (6H, d, *J* = 6.6 Hz, CH(CH₃)₂), 1.76 (2H, appq, *J* = 6.8 Hz, OCH₂CH₂), 1.88 (1H, appsept., *J* = 6.6 Hz, CH(CH₃)₂), 4.12 (2H, t, *J* = 6.8 Hz, OCH₂), 7.15 (1H, apptd, *J* = 7.8 and 0.8 Hz, one of C₆H₃), 7.62 (1H, dd, *J* = 7.9 and 1.7 Hz, one of C₆H₃), 7.74 (1H, dd, *J* = 7.8 and 1.7 Hz, one of C₆H₃), 10.37 (1H, br. d, *J* = 0.8 Hz, CHO)

δ_C (100 MHz, CDCl₃): 22.7 (CH(CH₃)₂), 25.0 (CH(CH₃)₂), 38.7 (OCH₂CH₂), 75.1 (OCH₂), 125.0 (Ar-C), 126.9 (Ar-C), 129.0 (Ar-Cq), 131.2 (Ar-Cq), 136.5 (Ar-C), 158.6 (Ar-Cq), 189.3 (CHO)

m/z [EI (+ve)], 228.1 ([M+2]⁺, 18%), 226.1 ([M]⁺, 39%), 156.0 ([M-((CH₂CH₂CH(CH₃)₂)]⁺, 100%); Found [M]⁺, 226.0762, C₁₂H₁₅O₂Cl requires 226.0761

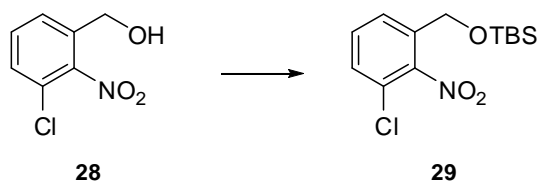
v_{max} (CDCl₃) / cm⁻¹: 2958, 2933, 2870, 1639, 1446 cm⁻¹

(3-chloro-2-nitrophenyl)methanol **28**



A flask equipped with a reflux condenser was charged with vacuum-dried 3-chloro-2-nitrobenzoic acid **16** (0.2 g, 1 mmol, 1 eq) and dry THF (10 cm³). Resulting solution was cooled to 0 °C and treated with borane-tetrahydrofuran complex (1M in THF, 2.4 ml, 2.4 mmol, 2.4 eq) under an argon atmosphere. After the cooling bath was removed, the reaction mixture was stirred at room temperature for 0.5 hour and overnight at 40 °C. After this time the reaction was cooled to 0 °C, quenched by slow addition of MeOH (10 cm³) and diluted with saturated aqueous NaHCO₃ (10 cm³) and ethyl acetate (20 cm³). Biphasic mixture was stirred for 0.5 hour and then layers were separated. The aqueous phase was extracted with fresh ethyl acetate (2 x 20 cm³). All the organic layers were combined, dried over anhydrous sodium sulphate, filtered off, and solvents were removed *in vacuo*. The remaining alcohol **28** was used in synthesis without purification (yellow viscous oil).

Tert-butyl(3-chloro-2-nitrobenzyloxy)dimethylsilane **29**



To a stirred solution of alcohol **28** (0.17 g, 0.9 mmol, 1 eq) in dry DMF (8 cm³) were added imidazole (0.13 g, 1.9 mmol, 2.1 eq) and *tert*-butyldimethylsilyl chloride (0.15 g, 1 mmol, 1.1 eq) under an argon atmosphere. The resulting reaction mixture was stirred at room temperature until TLC analysis indicated complete consumption of starting material **28** (3 hours). After this time, reaction was diluted with ethyl acetate (10 cm³) and water (10 cm³). Biphasic mixture was stirred for 20 minutes, then

layers were separated and aqueous phase was extracted with fresh ethyl acetate (2 x 20 cm³). Organic layers were combined, washed with water (40 cm³), brine (40 cm³), dried over anhydrous sodium sulphate, filtered off, and solvents were removed *in vacuo*. The remaining residue was purified on a short column of silica gel (gradient elution, eluting with 100% petroleum ether (40-60) to 20% ethyl acetate in petroleum ether (40-60)) to give product **29** as white, crystalline solid (0.23 g, 0.76 mmol, 84% yield from **16**).

δ_{H} (400 MHz, CDCl₃): 0.09 (6H, s, Si(CH₃)₂), 0.92 (9H, s, C(CH₃)₃), 4.72 (2H, d, *J* = 0.7 Hz, CH₂O), 7.41-7.42 (2H, m, two of C₆H₃), 7.5-7.52 (1H, m, one of C₆H₃)

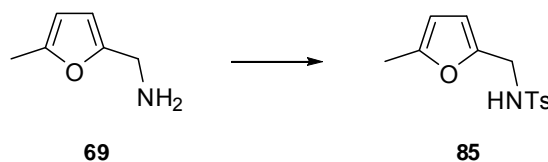
δ_{C} (100 MHz, CDCl₃): -5.4 (Si(CH₃)₂), 18.4 (C(CH₃)₃), 25.9 (C(CH₃)₃), 60.9 (CH₂O), 125.2 (Ar-Cq), 126.5 (Ar-C), 129.3 (Ar-C), 131.1 (Ar-C), 135.6 (Ar-Cq), 1 x Cq unresolved

m/z [FAB (+ve)], 302.1 ([M+H]⁺, 35%), 244.2 ([M-C(CH₃)₃]⁺, 100%);
Found [M+H]⁺, 302.0978, C₁₃H₂₁NO₃SiCl requires 302.0979

ν_{max} (CDCl₃) / cm⁻¹: 2929, 2858, 1523, 1462, 1367

mp. 84-86 °C

4-methyl-N-((5-methylfuran-2-yl)methyl)benzenesulfonamide **85**



To a solution of 5-methylfurfurylamine **69** (0.3 ml, 0.3 g, 2.7 mmol, 1 eq) in dry DCM (20 cm³) was added triethylamine (0.75 ml, 0.55 g, 5.4 mmol, 2 eq) under an argon atmosphere and resulting reaction solution was stirred for 10 minutes at room temperature. After this time the reaction was cooled to 0 °C and a solution of tosyl chloride (0.72 g, 3.78 mmol, 1.4 eq) in dry DCM (10 cm³) was slowly added to it. After stirring overnight at ambient temperature the reaction mixture was quenched with saturated aqueous NaHCO₃ (20 cm³), diluted with water (20 cm³) and the fractions were separated. An aqueous layer was extracted with fresh DCM (2 x 40 cm³). The combined organic layers were washed with brine (40 cm³), dried over sodium sulphate, filtered off, and concentrated *in vacuo*. The resulting product **85** was taken to the next step without need for purification (pale yellow solid, 0.72 g, 2.7 mmol, quantitative).

δ_H (400 MHz, CDCl₃): 2.12 (3H, s, furan-CH₃), 2.41 (3H, s, tosyl-CH₃), 4.1 (2H, d, *J* = 6.0 Hz, NHCH₂), 4.74 (1H, br. t, *J* = 5.9 Hz, NH), 5.76-5.77 (1H, m, furanyl-CH), 5.95 (1H, dd, *J* = 3.0 and 0.39 Hz, furanyl-CH), 7.25-7.28 (2H, m, two of C₆H₄), 7.69-7.72 (2H, m, two of C₆H₄)

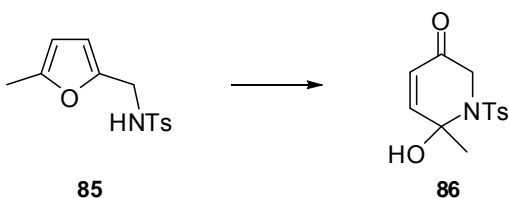
δ_C (100 MHz, CDCl₃): 13.4 (furan-CH₃), 21.6 (tosyl-CH₃), 40.4 (NHCH₂), 106.3 (furanyl-CH), 109.2 (furanyl-CH), 127.3 (Ar-C), 129.6 (Ar-C), 137.1 (Cq-SO₂), 143.4 (Cq-CH₃ (tosyl)), 147.6 (NHCH₂Cq), 152.3 (Cq-CH₃ (furan))

m/z [EI (+ve)], 109.0 ([M-Tosyl]⁺, 100%), 265.0 ([M]⁺, 8%); Found [M]⁺, 265.0771, C₁₃H₁₅NO₃S requires 265.0773

v_{max} (CDCl₃) / cm⁻¹: 3257, 2922, 1321, 1159

mp. 81-83 °C

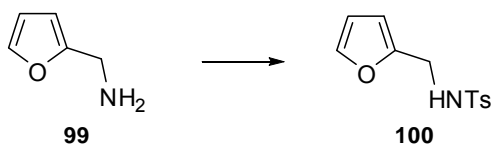
(±)-6-hydroxy-6-methyl-1-tosyl-1,2-dihydropyridin-3(6H)-one 86



To a solution of *m*-chloroperoxybenzoic acid (stabilised with *m*-chlorobenzoic acid; 0.18 g, 1.08 mmol, 1.3 eq) in dry DCM (5 cm³) at 0 °C was added dropwise a solution of amine **85** (0.22 g, 0.83 mmol, 1 eq) in dry DCM (5 cm³). The resulting reaction mixture was stirred for 20 minutes in 0 °C, and further 6 hours at room temperature under an argon atmosphere. After this time reaction was quenched by slow addition of saturated aqueous NaHCO₃ (10 cm³) and diluted with diethyl ether (10 cm³). The layers were separated and the aqueous layer was extracted with fresh diethyl ether (2 x 10 cm³). The organic phases were combined, washed with saturated aqueous NaHCO₃ (30 cm³), brine (30 cm³), dried over sodium sulphate, filtered off, and concentrated *in vacuo*. The obtained product **86** proved to be unstable; decomposition was observed within 1 hour upon storing at -4 °C (pale yellow solid, 100% conversion based on ¹H NMR).

δ_H (400 MHz, CDCl₃): 2.25 (3H, s, C(OH)CH₃), 2.41 (3H, s, tosyl-CH₃), 3.95 (2H, d, *J* = 5.1 Hz, NCH₂), 5.27-5.3 (1H, m, OH), 6.22 (1H, d, *J* = 11.8 Hz, CHCHC(O)), 6.41 (1H, d, *J* = 11.8 Hz, CHCHC(O)), 7.3 (2H, appd, *J* = 8.5 Hz, two of C₆H₄), 7.72-7.75 (2H, m, two of C₆H₄)

***N*-(furan-2-ylmethyl)-4-methylbenzenesulfonamide 100**



Stirred solution of furfurylamine **99** (1.82 ml, 2.0 g, 20.6 mmol, 1 eq) in dry DCM (150 cm³) was treated with triethylamine (5.74 ml, 4.17 g, 41.2 mmol, 2 eq) under an

argon atmosphere. Resulting reaction mixture was stirred for 30 minutes at room temperature, then cooled to 0 °C and a solution of tosyl chloride (4.71 g, 24.72 mmol, 1.2 eq) in dry DCM (30 cm³) was added to it via cannula. The cooling bath was removed and stirring was continued overnight at room temperature. After this time saturated aqueous NaHCO₃ (80 cm³) and water (80 cm³) were added slowly to the reaction. The resulting phases were separated and aqueous phase was extracted with fresh diethyl ether (2 x 150 cm³). The organic layers were combined, washed with brine (200 cm³), dried over sodium sulphate, filtered off, and solvents were removed *in vacuo*. The remaining product **100** was precipitated from diethyl ether and taken to the next step without further purification (white solid, 5.17 g, 20.6 mmol, quantitative).

δ_H (400 MHz, CDCl₃): 2.42 (3H, s, tosyl-CH₃), 4.17 (2H, d, *J* = 6.0 Hz, NHCH₂), 4.69 (1H, br. appt, *J* = 5.8 Hz, NH), 6.08 (1H, appdq, *J* = 3.2, 0.8 Hz, furanyl-CH), 6.21 (1H, dd, *J* = 3.2, 1.8 Hz, furanyl-CH), 7.24 (1H, dd, *J* = 1.8, 0.8 Hz, COCH), 7.26-7.29 (2H, m, two of C₆H₄), 7.7-7.73 (2H, m, two of C₆H₄)

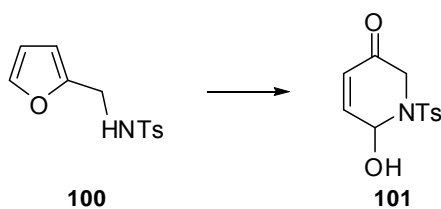
δ_C (100 MHz, CDCl₃): 21.6 (tosyl-CH₃), 40.3 (NHCH₂), 108.3 (furanyl-CH), 110.5 (furanyl-CH), 127.2 (Ar-C), 129.8 (Ar-C), 137.0 (Cq-SO₂), 142.6 (furanyl-CH), 143.6 (Cq-CH₃), 149.6 (NHCH₂Cq)

m/z [CI (+ve)], 252.4 ([M+H]⁺, 30%), 184.3 ([TsNHCH₂]⁺, 100%); Found [M+H]⁺, 252.0693, C₁₂H₁₄NO₃S requires 252.0694

v_{max} (CDCl₃) / cm⁻¹: 3253, 1598, 1435, 1320, 1158

mp. 118-120°C

(±)-6-hydroxy-1-tosyl-1,2-dihydropyridin-3(6H)-one 101

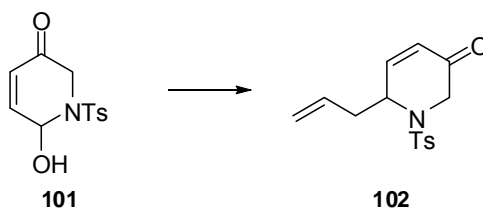


The reaction flask containing furfurylamine **100** (1.95 g, 7.76 mmol, 1 eq) was kept under vacuum for 1 hour, refilled with argon and charged with dry DCM (40 cm³).

Resulting solution was cooled to 0 °C and a solution of *m*-chloroperoxybenzoic acid (stabilised with *m*-chlorobenzoic acid; 1.82 g, 10.55 mmol, 1.36 eq) in dry DCM (40 cm³) was added *via* cannula. The reaction mixture was stirred for 20 minutes in 0 °C, and then in ambient temperature until completion indicated by TLC analysis (6 hours). After this time, saturated aqueous NaHCO₃ (80 cm³) and diethyl ether (40 cm³) were added to the reaction and resulting biphasic mixture was stirred for 20 minutes. The fractions were separated, and the aqueous layer was extracted with fresh diethyl ether (2 x 80 cm³). The organic layers were combined, washed with saturated aqueous NaHCO₃ (200 cm³), brine (200 cm³), dried over sodium sulphate, filtered off, and concentrated *in vacuo*. The remaining product **101** was taken subsequently to the next step without purification (pale yellow solid, decomposes within hours).

δ_{H} (400 MHz, CDCl₃): 2.43 (3H, s, tosyl-CH₃), 3.97 (1H, d, $J = 17.6$ Hz, one of NCH₂), 4.15 (1H, d, $J = 17.6$ Hz, one of NCH₂), 5.98 (1H, dd, $J = 4.9, 0.7$ Hz, CH(OH)), 6.07 (1H, d, $J = 10.2$ Hz, CHCHC(O)), 6.91 (1H, dd, $J = 10.2, 4.9$ Hz, CHCHC(O)), 7.30-7.33 (2H, m, two of C₆H₄), 7.7-7.72 (2H, m, two of C₆H₄)

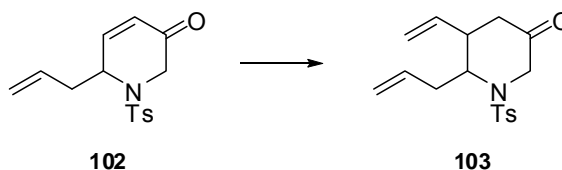
(±)-6-allyl-1-tosyl-1,2-dihydropyridin-3(6H)-one 102



A solution of pyridinone **101** (2.07 g, 7.76 mmol, 1 eq) in dry DCM (80 cm³) at 0 °C was treated with allyltrimethylsilane (3.7 ml, 2.66 g, 23.3 mmol, 3 eq) and boron trifluoride diethyl etherate (0.5 ml, 0.55 g, 3.88 mmol, 0.5 eq) under an argon atmosphere. The resulting reaction solution was stirred for 30 minutes in 0 °C before being quenched with saturated aqueous NH₄Cl (80 cm³). Resulting biphasic mixture was diluted with diethyl ether (50 cm³) and stirred for next 20 minutes. The layers were separated and aqueous layer was extracted with fresh diethyl ether (2 x 80 cm³). The organic layers were combined, washed with water (200 cm³), brine (200

cm³), dried over sodium sulphate, filtered off, and solvents were removed *in vacuo*. Crude compound **102**, obtained as dark orange viscous oil, was subsequently reacted further.

6-allyl-1-tosyl-5-vinylpiperidin-3-one **103**



A three-neck flask equipped with low temperature thermometer and protected from light with aluminium foil was charged with solution of copper iodide (2.05 g, 10.8 mmol, 1.4 eq) in dry THF (40 cm³) under an argon atmosphere. The solution was then cooled to -78 °C and treated with vinylmagnesium bromide (1M in THF, 23.0 ml, 23.1 mmol, 3 eq). Resulting reaction mixture was stirred for 5 minutes at -78 °C and then allowed to warm to -25 °C gradually over 20 minutes. After stirring for 5 minutes at -25 °C, the reaction mixture was cooled back to -78 °C and solution of piperidinone **102** (2.2 g, 7.7 mmol, 1 eq) in dry THF (40 cm³) was slowly added to it *via* cannula. Resulting reaction mixture was stirred at -78 °C until completion as indicated by TLC analysis (40 minutes). After this time the cooling bath was removed and the reaction was left stirring for 20 minutes before was quenched with saturated aqueous NH₄Cl (80 cm³) and diluted with diethyl ether (50 cm³). Biphasic mixture was stirred for another 20 minutes, then the phases were separated and an aqueous layer was extracted with fresh diethyl ether (2 x 80 cm³). Combined organic layers were washed with saturated aqueous Na₂S₂O₃ (200 cm³), dried over sodium sulphate, filtered off, and solvents were removed *in vacuo*. The remaining residue was purified by flash column chromatography (silica gel, gradient elution, eluting with 100% petroleum ether (40-60) to 7% ethyl acetate in petroleum ether (40-60)) to give compound **103** as pale yellow oil (1.65 g, 5.1 mmol, 66% yield from protected amine **100**).

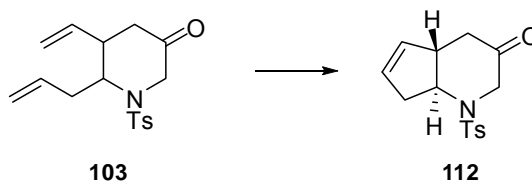
δ_{H} (400 MHz, CDCl_3): 1.68 (1H, dd, $J = 16.5$ and 11.8 Hz, one of $\text{C(O)CH}_2\text{CH}$), 2.16 (1H, dd, $J = 16.5$ and 3.8 Hz, one of $\text{C(O)CH}_2\text{CH}$), 2.31-2.38 (1H, m, one of $\text{NCH}(\text{CH}_2\text{CH}=\text{CH}_2)$), 2.42 (3H, s, tosyl- CH_3), 2.43-2.5 (1H, m, $\text{C(O)CH}_2\text{CH}$), 2.52-2.59 (1H, m, one of $\text{NCH}(\text{CH}_2\text{CH}=\text{CH}_2)$), 3.59 (1H, d, $J = 18.9$ Hz, one of NCH_2), 3.86-3.91 (1H, m, NCH), 4.15 (1H, d, $J = 18.9$ Hz, one of NCH_2), 5.0-5.14 (4H, m, $\text{NCH}(\text{CH}_2\text{CH}=\text{CH}_2)$ and $\text{CH}(\text{CH}=\text{CH}_2)$), 5.57 (1H, ddd, $J = 18.0$, 10.2 and 7.8 Hz, $\text{CH}(\text{CH}=\text{CH}_2)$), 5.77-5.88 (1H, m, $\text{NCH}(\text{CH}_2\text{CH}=\text{CH}_2)$), 7.29-7.31 (2H, m, two of C_6H_4), 7.65-7.68 (2H, m, two of C_6H_4)

δ_{C} (100 MHz, CDCl_3): 21.6 (tosyl- CH_3), 37.2 ($\text{NCH}(\text{CH}_2\text{CH}=\text{CH}_2)$), 40.5 ($\text{C(O)CH}_2\text{CH}$), 41.6 ($\text{C(O)CH}_2\text{CH}$), 51.6 (NCH_2), 57.3 (NCH), 117.5 and 119.2 ($\text{NCH}(\text{CH}_2\text{CH}=\text{CH}_2)$ and $\text{CH}(\text{CH}=\text{CH}_2)$), 127.3 (Ar-C), 130.1 (Ar-C), 133.2 ($\text{NCH}(\text{CH}_2\text{CH}=\text{CH}_2)$), 136.4 (Cq), 137.7 ($\text{CH}(\text{CH}=\text{CH}_2)$), 144.1 (Cq), 206.2 (CO)

m/z [CI (+ve)], 320.2 ($[\text{M}+\text{H}]^+$, 100%), 164.2 ($[(\text{M}+\text{H})-\text{Ts}]^+$, 83%); Found $[\text{M}+\text{H}]^+$, 320.1314, $\text{C}_{17}\text{H}_{22}\text{NO}_3\text{S}$ requires 320.1320

ν_{max} (CDCl_3) / cm^{-1} : 2978, 2924, 1732, 1346, 1157, 1091

(4a*S*,7a*S*)-1-tosyl-4,4a,7,7a-tetrahydro-1H-cyclopenta[b]pyridin-3(2H)-one 112



An oven-dried flask was charged with a pyridinone **103** (0.07 g, 0.22 mmol, 1 eq) and kept under vacuum for 0.5 h. After this time the flask was refilled with argon and starting material **103** was diluted with dry DCM (44 cm^3 , c $0.005 \text{ mol}\cdot\text{dm}^{-3}$). Resulting solution was degassed by bubbling argon through for 20 minutes and then treated with $\text{Ti}(\text{OPr-}i)_4$ (13 μl , 0.012 g, 0.044 mmol, 20 mol%). After the reaction was stirred at room temperature for 0.5 hour, the flask was protected from light with aluminium foil and Grubbs second generation catalyst $[\text{Cl}_2(\text{PCy}_3)(\text{IMes})\text{Ru}=\text{CHPh}]$ (0.02 g, 0.022 mmol, 10 mol%) was added to it in one portion under an argon atmosphere. The resulting reaction mixture was heated to reflux and stirred until completion indicated by TLC analysis (3 hours). After this time reaction mixture was

allowed to cool to room temperature, quenched with saturated aqueous NaHCO₃ (50 cm³) and stirred for another 20 minutes. Then the phases were separated and the aqueous layer was extracted with fresh DCM (2 x 50 cm³). All the organic layers were combined, washed with brine (100 cm³), dried over anhydrous sodium sulphate, filtered off, and the solvent was removed *in vacuo*. The remaining residue was purified by flash column chromatography (silica gel, gradient elution, eluting with 100% petroleum ether (40-60) to 10% ethyl acetate in petroleum ether (40-60)) to give compound **112** as a white crystals (0.053 g, 0.18 mmol, 82% yield).

δ_{H} (400 MHz, CDCl₃): 2.02 (1H, dd, $J = 16.5$ and 14.2 Hz, one of C(O)CH₂CH), 2.43 (3H, s, tosyl-CH₃), 2.69-2.78 (2H, m, NCH and one of C(O)CH₂CH), 2.82-2.85 (2H, m, NCHCH₂), 2.92-2.99 (1H, m, C(O)CH₂CH), 3.32 (1H, d, $J = 16.7$ Hz, one of NCH₂), 4.16 (1H, dd, $J = 16.7$ and 1.0 Hz, one of NCH₂), 5.66 (1H, appdq, $J = 6.1$ and 1.7 Hz, CH=CHCH₂), 5.86-5.9 (1H, m, CH=CHCH₂), 7.34-7.36 (2H, m, two of C₆H₄), 7.65-7.67 (2H, m, two of C₆H₄)

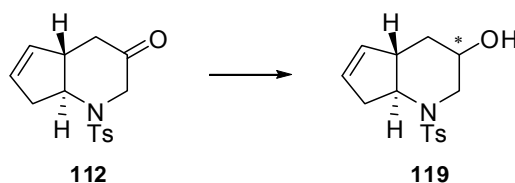
δ_{C} (100 MHz, CDCl₃): 21.7 (tosyl-CH₃), 37.1 (NCHCH₂), 43.5 (C(O)CH₂CH), 46.7 (C(O)CH₂CH), 57.8 (NCH₂), 65.0 (NCH), 128.1 (Ar-C), 130.1 (Ar-C), 130.2 (CH=CHCH₂), 131.7 (CH=CHCH₂), 132.1 (Cq), 144.4 (Cq), 202.8 (CO)

m/z [CI (+ve)], 292.0 ([M+H]⁺, 100%), 136.1 ([M+H-Ts]⁺, 79%); Found [M+H]⁺, 292.0997, C₁₅H₁₈NO₃S requires 292.1007

ν_{max} (CDCl₃) / cm⁻¹: 2955, 2924, 2854, 1728, 1350, 1165, 1091

mp. 152-154 °C (decomposition)

(4a*S*,7a*S*)-1-tosyl-2,3,4,4a,7,7a-hexahydro-1H-cyclopenta[*b*]pyridin-3-ol 119



To a stirred solution of pyridinone **112** (0.22 g, 0.75 mmol, 1 eq) in dry THF (7 cm³) at -78 °C, L-Selectride (1M solution in THF, 1.1 ml, 1.1 mmol, 1.45 eq) was added

dropwise *via* syringe. The resulting reaction mixture was stirred at $-78\text{ }^{\circ}\text{C}$ until completion indicated by TLC analysis (2 hours). After this time the cooling bath was removed, and reaction mixture was stirred for next 20 minutes before being quenched by addition of saturated aqueous NH_4Cl (1.1 cm^3) and water (6.6 cm^3). The biphasic mixture was diluted with diethyl ether, and stirring was continued for 20 minutes at room temperature. The phases were separated and the aqueous layer was extracted with fresh diethyl ether ($2 \times 10\text{ cm}^3$). All the organic layers were combined, dried over anhydrous sodium sulphate, filtered off, and concentrated *in vacuo*. The remaining residue was purified by flash column chromatography (silica gel, gradient elution, eluting with 100% petroleum ether (40-60) to 25% ethyl acetate in petroleum ether (40-60)) to give compound **119** as a white crystalline solid (0.19 g, 0.65 mmol, 87% yield).

δ_{H} (400 MHz, CDCl_3): 1.22 (1H, td, $J = 13.3$ and 2.8 Hz, one of $\text{C(OH)CH}_2\text{CH}$), 2.09-2.19 (2H, m, one of $\text{C(OH)CH}_2\text{CH}$ and NCH), 2.4 (1H, dd, $J = 12.3$ and 1.9 Hz, one of NCH_2), 2.42 (3H, s, tosyl- CH_3), 2.48 (1H, br. d, $J = 6.6$ Hz, OH), 2.65 (1H, ddd, $J = 15.0$, 6.4 and 3.0 Hz, one of NCHCH_2), 2.78-2.92 (2H, m, one of NCHCH_2 and $\text{C(OH)CH}_2\text{CH}$), 3.93 (1H, ddd, $J = 12.3$, 2.9 and 1.8 Hz, one of NCH_2), 4.12 (1H, br. apps, CH(OH)), 5.65-5.67 (1H, m, alkenyl- CH), 5.75-5.79 (1H, m, alkenyl CH), 7.32 (2H, dd, $J = 8.5$ and less than 1 Hz, two of C_6H_4), 7.65 (2H, dd, $J = 6.6$ and 1.8 Hz, two of C_6H_4)

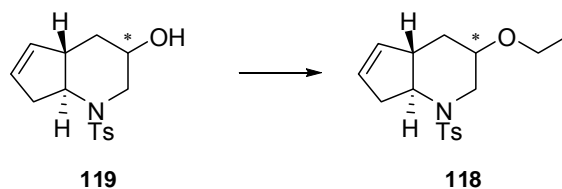
δ_{C} (100 MHz, CDCl_3): 21.6 (tosyl- CH_3), 34.7 ($\text{C(OH)CH}_2\text{CH}$), 36.8 (NCHCH_2), 43.7 ($\text{C(OH)CH}_2\text{CH}$), 55.6 (NCH_2), 65.5 (CH(OH)), 67.1 (NCH), 127.9 (Ar-C), 129.8 (Ar-C), 129.9 (alkenyl CH), 132.1 (alkenyl CH), 132.9 (Cq), 143.9 (Cq)

m/z [EI (+ve)], 293.2 ($[\text{M}]^+$, 48%), 138.1 ($[\text{M-Ts}]^+$, 100%); Found $[\text{M}]^+$, 293.1082, $\text{C}_{15}\text{H}_{19}\text{NO}_3\text{S}$ requires 293.1086

ν_{max} (CDCl_3) / cm^{-1} : 3510, 2920, 2854, 1599, 1338, 1159, 688

mp. 150-153 $^{\circ}\text{C}$

(4a*S*,7a*S*)-3-ethoxy-1-tosyl-2,3,4,4a,7,7a-hexahydro-1H-cyclopenta[b]pyridine
118



A dispersion of NaH in oil (60% (w/w) in mineral oil, 0.06 g, 1.44 mmol, 3 eq) was washed three times with petroleum ether under an argon atmosphere, dried under vacuum and suspended in dry DMF (3 cm³). After the suspension was cooled to 0 °C, a solution of alcohol **119** (0.14 g, 0.48 mmol, 1 eq) in dry DMF (3 cm³) was added to it dropwise via syringe. Resulting yellow reaction mixture was stirred for 10 minutes at 0 °C and further 45 minutes at room temperature. After the reaction was cooled back to 0 °C, ethyl iodide (0.1 ml, 0.19 g, 1.2 mmol, 2.5 eq) was added dropwise, what resulted in evolution of gas. The reaction mixture was stirred in 0 °C for 0.5 hour and then in room temperature until completion indicated by TLC analysis (2 hours). After this time saturated aqueous NH₄Cl (6 cm³) was added slowly to the reaction mixture (caused foaming), and stirring was continued for 20 minutes. Biphasic mixture was diluted with diethyl ether, the phases were separated and the aqueous layer was extracted with fresh diethyl ether (2 x 10 cm³). All the organic layers were combined, dried over anhydrous sodium sulphate, filtered off, and solvents were removed *in vacuo*. The remaining residue was purified by flash column chromatography (silica gel, gradient elution, eluting with 100% petroleum ether (40-60) to 7% ethyl acetate in petroleum ether (40-60)) to give compound **118** as white crystals (0.12 g, 0.38 mmol, 79% yield).

δ_{H} (400 MHz, CDCl₃): 1.15-1.19 (1H, m, one of CH(OEt)CH₂CH), 1.23 (3H, t, $J = 7.0$ Hz, OCH₂CH₃), 2.12-2.19 (1H, m, one of CH(OEt)CH₂CH), 2.22 (1H, dd, $J = 10.2$ and 3.7 Hz, NCH), 2.27 (1H, dd, $J = 12.6$ and 2.0 Hz, one of NCH₂), 2.42 (3H, s, tosyl-CH₃), 2.62-2.68 (1H, m, one of CH=CHCH₂), 2.72-2.79 (1H, m, one of CH=CHCH₂), 2.89-2.95 (1H, m, CH(OEt)CH₂CH), 3.42 (1H, dq, $J = 9.1$ and 7.0 Hz, one of OCH₂CH₃), 3.63-3.68 (2H, m, one of OCH₂CH₃ and CH(OEt)), 4.09 (1H, ddd, $J = 12.6$, 2.7 and 1.8 Hz, one of NCH₂), 5.63-5.65 (1H, m, alkenyl CH),

5.72-5.76 (1H, m, alkenyl CH), 7.3-7.32 (2H, m, two of C₆H₄), 7.66-7.68 (2H, m, two of C₆H₄)

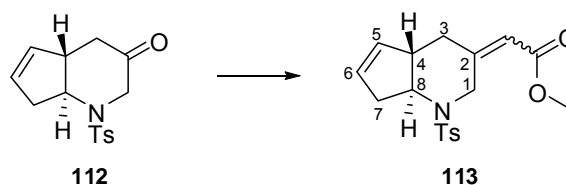
δ_C (100 MHz, CDCl₃): 15.5 (OCH₂CH₃), 21.6 (tosyl-CH₃), 33.2 (CH(OEt)CH₂CH), 36.9 (CH=CHCH₂), 44.0 (CH(OEt)CH₂CH), 51.2 (NCH₂), 63.8 (OCH₂CH₃), 66.8 (NCH), 72.3 (CH(OEt)), 128.0 (Ar-C), 129.6 (alkenyl-CH), 129.7 (Ar-C), 132.4 (alkenyl-CH), 133.6 (Cq), 143.5 (Cq)

m/z [EI (+ve)], 321.3 ([M]⁺, 5%), 166.2 ([M-Ts]⁺, 100%); Found [M]⁺, 321.1401, C₁₇H₂₃NO₃S requires 321.1399

ν_{\max} (CDCl₃) / cm⁻¹: 2974, 2922, 2868, 1600, 1338, 1160, 1095

mp. 101-103 °C

Ethyl 2-((4a*S*,7a*S*)-1-tosyl-4,4a-dihydro-1H-cyclopenta[b]pyridin-3(2H,7H,7aH)-ylidene)acetate **113**



A flask equipped with a reflux condenser was charged with solution of pyridinone **112** (0.29 g, 0.99 mmol, 1 eq) in dry DCM (10 cm³), and an (ethoxycarbonylmethylene) triphenylphosphorane (0.45 g, 1.29 mmol, 1.3 eq) was added to it under an argon atmosphere. Resulting reaction mixture was stirred at reflux for 48 hours. After this time the reaction was allowed to cool to room temperature and solvent was removed *in vacuo*. The remaining residue was purified by flash column chromatography (silica gel, gradient elution, eluting with 100% petroleum ether (40-60) to 10% ethyl acetate in petroleum ether (40-60)) to give ester **113** as a mixture of *E/Z* isomers (pale yellow viscous oil, 0.3 g, 0.83 mmol, 84% yield).

δ_H (400 MHz, CDCl₃, *de retio*: 1:1): 1.26 (3H, t, J = 7.1 Hz, OCH₂CH₃), 1.31 (3H, t, J = 7.2 Hz, OCH₂CH₃), 1.88-1.98 (2H, m, one of CH₂(C3) and one of CH₂(C7)), 2.42 (6H, s, 2 x tosyl-CH₃), 2.45-2.82 (9H, m, CH₂(C3), CH₂(C7), 2 x CH(C4), 2 x CH(C8) and one of CH₂(C7)), 3.05 (1H, d, J = 14.0 Hz, one of NCH₂),

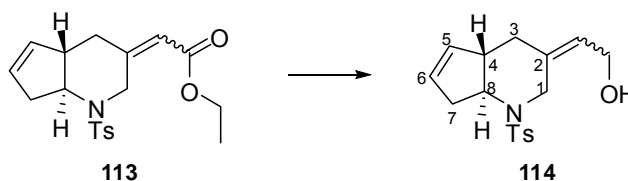
3.37 (1H, dd, $J = 13.9$ and 1.2 Hz, one of NCH_2), 3.7 (1H, dd, $J = 15.8$ and 4.0 Hz, one of $\text{CH}_2(\text{C}3)$), 4.13 (2H, q, $J = 7.1$ Hz, OCH_2CH_3), 4.2 (2H, q, $J = 7.1$ Hz, OCH_2CH_3), 4.21 (1H, d, $J = 13.9$ Hz, one of NCH_2), 5.67 (1H, d, $J = 14.1$ Hz, one of NCH_2), 5.66-5.84 (6H, m, 4 x alkenyl CH , 2 x $\text{C}=\text{CHCO}_2\text{Et}$), 7.31-7.34 (4H, m, two of C_6H_4 and two of C_6H_4), 7.64-7.71 (4H, m, two of C_6H_4 and two of C_6H_4)

δ_{C} (100 MHz, CDCl_3): 14.3 (2 x OCH_2CH_3), 21.7 (2 x tosyl- CH_3), 32.0, 37.2, 37.4, 38.5 (2 x $\text{CH}_2(\text{C}7)$ and 2 x $\text{CH}_2(\text{C}3)$), 47.5 ($\text{CH}(\text{C}4)$), 48.7 ($\text{CH}(\text{C}4)$), 48.9 (NCH_2), 55.2 (NCH_2), 60.2 (OCH_2CH_3), 60.5 (OCH_2CH_3), 65.8 ($\text{CH}(\text{C}8)$), 66.3 ($\text{CH}(\text{C}8)$), 118.5 ($\text{C}=\text{CHCO}_2\text{Et}$), 118.6 ($\text{C}=\text{CHCO}_2\text{Et}$), 128.0 (Ar-C), 128.1 (Ar-C), 129.8 (Ar-C), 129.9 (Ar-C), 130.8, 131.0, 131.1, 131.4 (4 x alkenyl CH), 132.8 (Cq), 132.9 (Cq), 143.8 (Cq), 144.1 (Cq), 150.8 (Cq), 152.1 (Cq), 165.6 (Cq), 165.9 (Cq)

m/z [EI (+ve)], 361.0 ($[\text{M}]^+$, 28%), 206.1 ($[\text{M}-\text{Ts}]^+$, 100%); Found $[\text{M}]^+$, 361.1344, $\text{C}_{19}\text{H}_{23}\text{NO}_4\text{S}$ requires 361.1348

ν_{max} (CDCl_3) / cm^{-1} : 2956, 2933, 2875, 2860, 1716, 1352, 1165, 1091

2-((4a*S*,7a*S*)-1-tosyl-4,4a-dihydro-1*H*-cyclopenta[*b*]pyridin-3(2*H*,7*H*,7a*H*)-ylidene)ethanol **114**



To a solution of ester **113** (0.057 g, 0.16 mmol, 1eq) in dry diethyl ether (2 cm^3) at 0 °C, DIBAL-H (1.0 M solution in hexanes, 0.45 ml, 0.45 mmol, 3eq) was added dropwise *via* syringe under an argon atmosphere. Resulting reaction mixture was stirred at 0 °C until completion indicated by TLC analysis (40 minutes). While maintaining temperature at 0 °C, reaction was diluted with fresh diethyl ether (2 cm^3) and quenched by careful addition of water (0.02 cm^3), followed by 15% aqueous NaOH (0.02 cm^3) and another portion of water (0.05 cm^3). The cooling bath was removed and resulting biphasic mixture was stirred for 20 minutes at room temperature. The fractions were separated, and the aqueous layer was extracted with fresh diethyl ether (2 x 5 cm^3). All the organic layers were combined and dried over anhydrous magnesium sulphate, filtered off, and the solvents were removed *in vacuo*

to yield alcohol **114** as a mixture *E/Z* isomers (pale yellow, gummy oil, 0.053 g, 0.16 mmol, 100% yield), which was reacted further without need of purification.

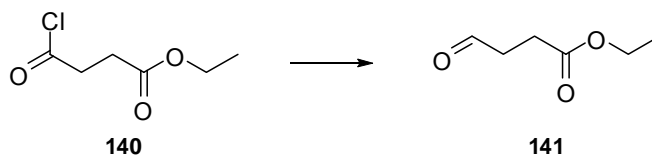
δ_{H} (400 MHz, CDCl_3 , *de retio*: 1:1): 1.57-1.63 (1H, m, one of $\text{CH}_2(\text{C}3)$), 1.79-1.86 (1H, m, one of $\text{CH}_2(\text{C}3)$), 2.33-2.43 (2H, m, 2 x $\text{CH}(\text{C}8)$, *cis* and *trans*), 2.41 (3H, s, tosyl- CH_3), 2.42 (3H, s, tosyl- CH_3), 2.45-2.54 (3H, m, 2 x $\text{CH}(\text{C}4)$ and one of $\text{CH}_2(\text{C}3)$), 2.67-2.71 (4H, m, 2 x $\text{CH}_2(\text{C}7)$), 2.75 (1H, d, $J = 13.0$ Hz, one of NCH_2), 2.77-2.83 (1H, m, one of $\text{CH}_2(\text{C}3)$), 3.12 (1H, d, $J = 13.0$ Hz, one of NCH_2), 4.04-4.29 (4H, m, 2 x $\text{C}=\text{CHCH}_2\text{OH}$), 4.15 (1H, d, $J = 13.0$ Hz, one of NCH_2), 4.59 (1H, d, $J = 12.9$ Hz, one of NCH_2), 5.56-5.61 (2H, m, 2 x $\text{C}=\text{CHCH}_2\text{OH}$), 5.65-5.67 (2H, m, 2 x alkenyl CH), 5.75-5.79 (2H, m, 2 x alkenyl CH), 7.3-7.33 (4H, m, two of C_6H_4 and two of C_6H_4), 7.65-7.68 (4H, m, two of C_6H_4 and two of C_6H_4)

δ_{C} (100 MHz, CDCl_3 , *de retio*: 1:1): 21.6 (tosyl- CH_3), 21.63 (tosyl- CH_3), 30.4 ($\text{CH}_2(\text{C}3)$), 36.9 ($\text{CH}_2(\text{C}7)$), 37.1 ($\text{CH}_2(\text{C}7)$), 38.0 ($\text{CH}_2(\text{C}3)$), 48.5 ($\text{CH}(\text{C}4)$), 49.0 (NCH_2), 49.7 ($\text{CH}(\text{C}4)$), 55.9 (NCH_2), 58.4 ($\text{C}=\text{CHCH}_2\text{OH}$), 58.47 ($\text{C}=\text{CHCH}_2\text{OH}$), 66.3 ($\text{CH}(\text{C}8)$), 66.7 ($\text{CH}(\text{C}8)$), 126.9 ($\text{C}=\text{CHCH}_2\text{OH}$), 127.4 ($\text{C}=\text{CHCH}_2\text{OH}$), 128.0 (Ar-C), 128.1 (Ar-C), 129.7 (Ar-C), 129.8 (Ar-C), 130.3 (alkenyl CH), 130.6 (alkenyl CH), 131.6 (alkenyl CH), 131.8 (alkenyl CH), 132.8 (Cq), 132.9 (Cq), 134.1 (Cq(C2)), 134.3 (Cq(C2)), 143.8 (Cq), 143.9 (Cq)

m/z [CI (+ve)], 320.5 ($[\text{M}+\text{H}]^+$, 94%), 302.5 ($[(\text{M}+\text{H})-\text{OH}_2]^+$, 100%); Found $[\text{M}+\text{H}]^+$, 320.1323, $\text{C}_{17}\text{H}_{22}\text{NO}_3\text{S}$ requires 320.1320

ν_{max} (CDCl_3) / cm^{-1} : 3547, 2967, 2847, 1346, 1165, 1091

Ethyl 4-oxobutanoate **141**



To a stirred solution of ethyl 4-chloro-4-oxobutanoate **140** (3.5 ml, 4.0 g, 24.3 mmol, 1 eq) in dry THF (200 cm^3) was added 2,6-lutidine (2.8 ml, 2.6 g, 24.3 mmol, 1 eq) under an argon atmosphere. Resulting colourless solution was purged with argon for

20 minutes, and a catalytic amount of 10% Pd/C was added to it. Reaction mixture was then immediately degassed under reduced pressure and refilled with hydrogen (three times), and stirring was continued under hydrogen atmosphere until completion as indicated by TLC analysis (5 hours). After this time the reaction mixture was diluted with diethyl ether and filtered through a pad of celite and sand, which was washed with copious amount of diethyl ether. The filtrate was collected and concentrated *in vacuo*. Resulting residue was taken up in fresh diethyl ether (80 cm³) and washed with saturated aqueous CuSO₄ (2 x 80 cm³). The layers were separated, and organic layer was dried over sodium sulphate, filtered off, and solvent was removed *in vacuo*. Crude aldehyde **141**, obtained as volatile, orange liquid, was used in synthesis without purification (100% conversion by NMR, 3.0 g, 23 mmol, 95% yield).

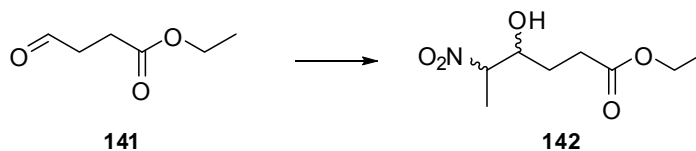
δ_{H} (400 MHz, CDCl₃): 1.23 (3H, t, $J = 7.2$ Hz, OCH₂CH₃), 2.59 (2H, t, $J = 6.7$ Hz, CH₂CH₂CO₂Et), 2.75-2.79 (2H, m, CH₂CH₂CO₂Et), 4.12 (2H, q, $J = 7.2$ Hz, OCH₂CH₃), 9.79 (1H, br. t, $J = 0.6$ Hz, CHO)

δ_{C} (100 MHz, CDCl₃): 14.2 (OCH₂CH₃), 26.7 and 38.6 (CH₂CH₂CO₂Et), 60.9 (OCH₂CH₃), 172.3 (CO₂Et), 200.2 (CHO)

m/z [CI (+ve)], 131.15 ([M+H]⁺, 72%); Found [M+H]⁺, 131.0705, C₆H₁₁O₃ requires 131.0708

ν_{max} (CDCl₃) / cm⁻¹: 2964, 2908, 1734, 1261, 1087, 1020

Ethyl 4-hydroxy-5-nitrohexanoate **142**



A round-bottom flask was charged with THF (60 cm³) and *t*BuOH (60 cm³) and the obtained solvent mixture was degassed by purging with argon for 20 minutes. Then nitroethane (4.9 ml, 5.2 g, 69 mmol, 3 eq) was added to it under an argon atmosphere. The resulting reaction solution was cooled to 0 °C, treated with *t*BuOK

(0.54 g, 4.8 mmol, 0.21 eq) and stirred for 10 minutes at 0 °C. Meanwhile, a solution of aldehyde **141** (3 g, 23 mmol, 1 eq) in dry THF (20 cm³) was prepared in a separate flask and added *via* cannula to the stirred reaction mixture at 0 °C. Resultant yellow suspension was stirred for additional 15 min at 0 °C and overnight at room temperature. After this time saturated aqueous NH₄Cl (150 cm³) was poured into the reaction and biphasic mixture was diluted with diethyl ether (50 cm³). The layers were separated and the aqueous layer was extracted with ethyl acetate (2 x 150 cm³). The organic phases were combined, dried over sodium sulphate, filtered off, and solvents were removed *in vacuo*. Crude nitroalcohol **142** (orange liquid, 4.62 g, 22.5 mmol, 98% yield) was obtained as mixture (1.6/1) of diastereoisomers, which was reacted further without purification.

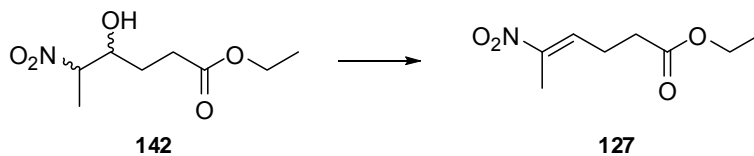
δ_H (400 MHz, CDCl₃, mixture of diastereoisomers, *de retio*: 1.6:1): 1.26 (3H, t, *J* = 7.1 Hz, OCH₂CH₃, major), 1.26 (3H, t, *J* = 7.1 Hz, OCH₂CH₃, minor), 1.57 (3H, d, *J* = 6.8 Hz, CH₃CH(NO₂), major), 1.58 (3H, d, *J* = 6.8 Hz, CH₃CH(NO₂), minor), 1.68-1.8 (3H, m, two of CH₂CH₂CO₂Et minor, one of CH₂CH₂CO₂Et major), 1.88-1.95 (1H, m, one of CH₂CH₂CO₂Et, major), 2.52-2.55 (2H, m, CH₂CH₂CO₂Et, major), 2.52-2.56 (2H, m, CH₂CH₂CO₂Et, minor), 2.73 (1H, d, *J* = 6.5 Hz, OH, major), 2.88 (1H, dd, *J* = 5.0 and 0.6 Hz, OH, minor), 3.96-4.02 (1H, m, CH(OH), major), 4.15 (2H, q, *J* = 7.1 Hz, OCH₂CH₃, major), 4.15 (2H, q, *J* = 7.1 Hz, OCH₂CH₃, minor), 4.17-4.22 (1H, m, CH(OH), minor), 4.49-4.57 (1H, m, CH₃CH(NO₂), major), 4.49-4.57 (1H, m, CH₃CH(NO₂), minor)

δ_C (100 MHz, CDCl₃, mixture of diastereoisomers): 13.1 (CH₃CH(NO₂), minor), 14.3 (OCH₂CH₃, major and minor), 16.2 (CH₃CH(NO₂), major), 27.8 (CH₂CH₂CO₂Et, major), 27.9 (CH₂CH₂CO₂Et, minor), 30.3 (CH₂CH₂CO₂Et, major and minor), 61.0 (OCH₂CH₃, major), 61.06 (OCH₂CH₃, minor), 71.6 (CH(OH), minor), 72.3 (CH(OH), major), 86.5 (CH₃CH(NO₂), minor), 87.8 (CH₃CH(NO₂), major), 173.7 (CO₂Et, major), 173.8 (CO₂Et, minor)

m/z [CI (+ve)], 206.3 ([M+H]⁺, 100%), 161.3 ([M+H-OEt]⁺, 35%); Found [M+H]⁺, 206.1029, C₈H₁₆NO₅ requires 206.1028

ν_{max} (CDCl₃) / cm⁻¹: 3464, 2982, 2931, 1728, 1550, 1180

(E)-ethyl 5-nitrohex-4-enoate 127



Nitroalcohol **142** (2.8 g, 13.64 mmol, 1 eq) was dissolved in dry DCM (100 cm³) under an argon atmosphere and the resultant orange solution was degassed by purging with argon for 20 minutes, cooled to -40 °C and trifluoroacetic anhydride (2.1 ml, 3.15 g, 15 mmol, 1.1 eq) was added to it dropwise. Stirring was continued for 0.5 hour at -40 °C. After this time the reaction was cooled to -50 °C and triethylamine (4.2 ml, 3.04 g, 30 mmol, 2.2 eq) was added to it via syringe over 10 minutes. Resulting reaction mixture was stirred for 3 hours at -60 °C and further 2 hours at -20 °C. After this time cooling bath was removed and the reaction was quenched with saturated aqueous NH₄Cl (100 cm³), diluted with diethyl ether (100 cm³) and stirred until reaching room temperature. The phases were separated and the aqueous layer was extracted with fresh diethyl ether (2 x 100 cm³). The organic layers were combined, dried over sodium sulphate, filtered off, and solvents were removed *in vacuo*. The residue was purified by flash column chromatography (silica gel, gradient elution, eluting with 100% petroleum ether (40-60) to 5% ethyl acetate in petroleum ether (40-60)) to give (E)-nitroalkene **127** as yellow liquid (1.8 g, 9.6 mmol, 71%).

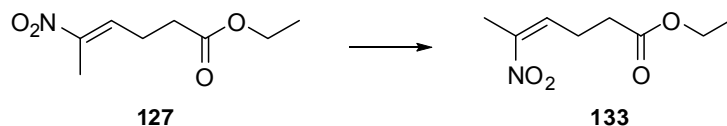
δ_H (400 MHz, CDCl₃): 1.26 (3H, t, *J* = 7.2 Hz, OCH₂CH₃), 2.2 (3H, d, *J* = 1.0 Hz, CH₃C(NO₂)), 2.48-2.58 (4H, m, CH₂CH₂CO₂Et), 4.15 (2H, q, *J* = 7.2 Hz, OCH₂CH₃), 7.05-7.09 (1H, m, C=CH)

δ_C (100 MHz, CDCl₃): 12.7 (CH₃C(NO₂)), 14.3 (OCH₂CH₃), 23.5 (CH₂), 32.6 (CH₂), 61.0 (OCH₂CH₃), 134.0 (C=CH), 148.7 (CH₃C(NO₂)), 171.9 (CO₂Et)

m/z [CI (+ve)], 188.21 ([M+H]⁺, 100%); Found [M+H]⁺, 188.0923, C₈H₁₄NO₄ requires 188.0923

ν_{max} (CDCl₃) / cm⁻¹: 2982, 2939, 1732, 1519, 1334, 1180

(Z)-ethyl 5-nitrohex-4-enoate 133



Diphenyl diselenide (0.15 g, 0.48 mmol, 0.6 eq) was dissolved in absolute ethanol (6 cm³) under an argon atmosphere. Resulting bright yellow solution was cooled to 0 °C and sodium borohydride (0.04 g, 0.96 mmol, 1.2 eq) was added to it carefully in portions. Stirring was continued at 0 °C until yellow reaction mixture turned colourless. Then the reaction was cooled to -78 °C and solution of (*E*)-nitroalkene **127** (0.15 g, 0.8 mmol, 1 eq) in absolute ethanol (4 cm³) was added dropwise *via* cannula. Resulting reaction mixture was stirred for 20 minutes at -78 °C and then gradually warmed up to -30 °C over 1 hour. After this time the reaction mixture was cooled back to -78 °C and glacial acetic acid (0.05 ml, 0.06 g, 0.96 mmol, 1.2 eq) was slowly added to it under an argon atmosphere. The resulting reaction mixture was stirred at -78 °C for 20 minutes, then the cooling bath was removed and reaction was allowed to slowly warm up to room temperature. The reaction was then quenched with water (10 cm³) and diluted with diethyl ether (10 cm³). The phases were separated and the aqueous phase was extracted with fresh diethyl ether (2 x 10 cm³). The organic phases were combined, dried over sodium sulphate, filtered off, and solvents were removed *in vacuo*.

The remaining residue (orange oil) was then transferred to the round-bottom flask, dried under reduced pressure and dissolved in fresh DCM (6 cm³). Resulting solution was cooled to 0 °C and hydrogen peroxide (30% solution in water, 0.73 ml, 0.82 g, 24 mmol, 30 eq,) was added to it dropwise over 20 minutes. Stirring was continued for 1 hour in 0 °C. After this time the reaction was quenched with saturated aqueous NaHCO₃ (10 cm³) diluted with diethyl ether (10 cm³) and biphasic mixture was stirred for 15 minutes at room temperature. The layers were separated and the organic layer was washed with saturated aqueous NaHCO₃ (2 x 10 cm³). The organic phase was collected, dried over sodium sulphate, filtered off, and concentrated *in vacuo*. Crude (*Z*)-nitroalkene **133** (yellow liquid, 0.13 g, 0.7 mmol, 87% yield) obtained as mixture of *Z/E* isomers (9:1), which weren't separable by flash column chromatography, was reacted further without purification.

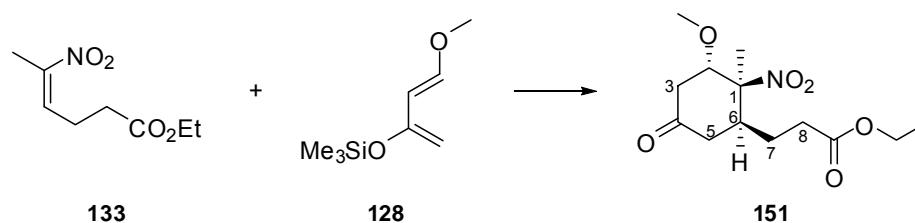
δ_{H} (400 MHz, CDCl_3): 1.26 (3H, t, $J = 7.2$ Hz, OCH_2CH_3), 2.19-2.2 (3H, m, $\text{CH}_3\text{C}(\text{NO}_2)$), 2.5 (2H, dd, $J = 7.2$ and 6.9 Hz, $\text{CH}_2\text{CH}_2\text{CO}_2\text{Et}$), 2.72-2.79 (2H, m, $\text{CH}_2\text{CH}_2\text{CO}_2\text{Et}$), 4.14 (2H, q, $J = 7.2$ Hz, OCH_2CH_3), 5.9 (1H, br. t, $J = 7.3$ Hz, $\text{C}=\text{CH}$)

δ_{C} (100 MHz, CDCl_3): 14.3 (OCH_2CH_3), 19.3 ($\text{CH}_3\text{C}(\text{NO}_2)$), 24.0 ($\text{CH}_2\text{CH}_2\text{CO}_2\text{Et}$), 33.2 ($\text{CH}_2\text{CH}_2\text{CO}_2\text{Et}$), 60.8 (OCH_2CH_3), 132.5 ($\text{C}=\text{CH}$), 147.4 ($\text{CH}_3\text{C}(\text{NO}_2)$), 172.4 (CO_2Et)

m/z [CI (+ve)], 188.2 ($[\text{M}+\text{H}]^+$, 100%); Found $[\text{M}+\text{H}]^+$, 188.0921, $\text{C}_8\text{H}_{14}\text{NO}_4$ requires 188.0923

ν_{max} (CDCl_3) / cm^{-1} : 2978, 2931, 2850, 1732, 1519, 1342, 1180

**Ethyl 3-((1S,2S,3S)-3-methoxy-2-methyl-2-nitro-5-oxocyclohexyl)propanoate
151**



An oven-dried round-bottom flask was charged with benzene (12 cm^3), which was then degassed by freeze-pump-thaw technique (three times). At the end of last cycle the flask was refilled with argon and (Z)-nitroalkene **133** (0.49 g, 2.6 mmol, 1 eq) and Danishefsky's diene **128** (1.26 ml, 1.1 g, 6.5 mmol, 2.5 eq) were added to it under an argon atmosphere. Resulting yellow reaction solution was stirred at 60°C for 24 hours. After this time another portion of diene **128** (0.5 ml, 0.4 g, 2.6 mmol, 1 eq) was added to the reaction solution and stirring was continued at 70°C for 2 days. After this time the reaction was allowed to cool to room temperature and solvent was removed *in vacuo*.

Remaining residue (orange liquid) was transferred to the round-bottom flask, dried under reduced pressure and dissolved in THF (13 cm^3). Resulting solution was cooled to -10°C and then solution of HCl (1N in water, 0.16 ml, 0.16 mmol, 0.06 eq) in THF (13 cm^3) was slowly added to it. Stirring was continued for 1 hour at -10°C . After this time cooling bath was removed, the reaction was quenched with

saturated aqueous NaHCO₃ (30 cm³), diluted with diethyl ether (15 cm³) and stirred for 20 minutes at room temperature. The layers were separated and the aqueous layer was extracted with fresh diethyl ether (2 x 30 cm³). All the organic layers were combined, dried over anhydrous sodium sulphate, filtered off, and concentrated *in vacuo*. The remaining residue was purified by flash column chromatography (silica gel, gradient elution, eluting with 100% petroleum ether (40-60) to 10% ethyl acetate in petroleum ether (40-60)) to give compound **151** as yellow liquid (0.24 g, 0.84 mmol, 32% yield).

δ_H (400 MHz, CDCl₃): 1.24 (3H, t, *J* = 7.1 Hz, OCH₂CH₃), 1.61-1.71 (1H, m, one of CH₂(C7)), 1.8 (3H, s, CH₃C(NO₂)), 1.93-2.01 (1H, m, one of CH₂(C7)), 2.18-2.26 (1H, m, one of CH₂(C8)), 2.29-2.34 (1H, m, CH(C6)), 2.4 (1H, ddd, *J* = 16.2, 8.0 and 5.6 Hz, one of CH₂(C8)), 2.51-2.53 (2H, m, CH₂(C5)), 2.58 (1H, dd, *J* = 15.5 and 5.9 Hz, one of CH₂(C3)), 2.66 (1H, dd, *J* = 15.4 and 3.9 Hz, one of CH₂(C3)), 3.4 (3H, s, CH(OCH₃)), 4.12 (2H, q, *J* = 7.1 Hz, OCH₂CH₃), 4.15 (1H, dd, *J* = 5.9 and 3.9 Hz, CH(OCH₃))

δ_C (100 MHz, CDCl₃): 14.3 (OCH₂CH₃), 21.2 (CH₃C(NO₂)), 24.8 (CH₂(C7)), 31.8 (CH₂(C8)), 40.4 (CH(C6)), 41.4 (CH₂(C5)), 41.7 (CH₂(C3)), 58.0 (CH(OCH₃)), 60.8 (OCH₂CH₃), 80.9 (CH(OCH₃)), 92.2 (Cq(C1)), 172.5 (CO₂Et), 205.8 (CO)

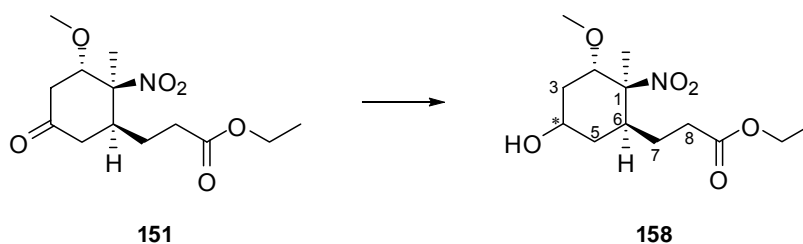
δ_H (400 MHz, C₆D₆): 0.9 (3H, t, *J* = 7.1 Hz, OCH₂CH₃), 1.33-1.43 (1H, m, one of CH₂(C7)), 1.38 (3H, s, CH₃C(NO₂)), 1.69-1.78 (2H, m, one of CH₂(C7) and one of CH₂(C8)), 1.86-1.91 (1H, m, one of CH₂(C8)), 1.93-1.97 (1H, m, one of CH(C6)), 2.01 (1H, ddd, *J* = 15.5, 6.8 and 1.4 Hz, one of CH₂(C3)), 2.05 (1H, ddd, *J* = 15.6, 5.2 and 1.4 Hz, one of CH₂(C5)), 2.14 (1H, ddd, *J* = 15.4, 9.3 and 1.0 Hz, one of CH₂(C5)), 2.24 (1H, ddd, *J* = 15.5, 4.1 and 1.0 Hz, one of CH₂(C3)), 2.75 (3H, s, CH(OCH₃)), 3.65 (1H, dd, *J* = 6.7 and 4.1 Hz, CH(OCH₃)), 3.85 (1H, dq, *J* = 14.3 and 7.1, one of OCH₂CH₃), 3.85 (1H, dq, *J* = 14.3 and 7.1, one of OCH₂CH₃)

δ_C (100 MHz, C₆D₆): 14.7 (OCH₂CH₃), 21.1 (CH₃C(NO₂)), 25.4 (CH₂(C7)), 32.0 (CH₂(C8)), 41.3 (CH₂(C6)), 41.6 (CH₂(C5)), 42.1 (CH₂(C3)), 57.7 (CH(OCH₃)), 60.9 (OCH₂CH₃), 80.8 (CH(OCH₃)), 92.7 (Cq(C1)), 172.4 (CO₂Et), 204.2 (CO)

m/z [CI (+ve)], 288.3 ($[M+H]^+$, 90%), 243.3 ($[M+H-NO_2]^+$, 87%), 211.2 ($[M+H-NO_2-OCH_3]^+$, 100%); Found $[M+H]^+$, 288.1451, $C_{13}H_{22}NO_6$ requires 288.1447

ν_{\max} (CDCl₃) / cm⁻¹: 2924, 2850, br. 1724, 1539

Ethyl 3-((1*S*,2*S*,3*S*)-5-hydroxy-3-methoxy-2-methyl-2-nitrocyclohexyl)propanoate **158**



To a flask charged with polyethylene glycol (400 MW) (1 cm³), ketone **151** (0.036 g, 0.12 mmol, 1 eq) was added under an argon atmosphere. Resulting mixture was purged with argon for 20 minutes, and a catalytic amount of PtO₂ was added to it. Reaction mixture was immediately degassed under reduced pressure, refilled with hydrogen (three times), and stirring was continued overnight under hydrogen atmosphere. After this time reaction mixture was diluted with diethyl ether (5 cm³) and filtered through a pad of celite and sand, which was washed with copious amount of diethyl ether. The filtrate was collected and concentrated *in vacuo*. Remaining residue was taken up in fresh diethyl ether (10 cm³), washed with water (10 cm³) and brine (10 cm³). The layers were separated, and organic layer was dried over sodium sulphate, filtered off, and solvent was removed *in vacuo*. The remaining residue was purified by flash column chromatography (silica gel, gradient elution, eluting with 100% petroleum ether (40-60) to 20% ethyl acetate in petroleum ether (40-60)) to give alcohol **158** as yellow, very viscous oil (0.018 g, 0.06 mmol, 50% yield).

δ_{H} (400 MHz, CDCl_3): 1.25 (3H, t, $J = 7.2$ Hz, OCH_2CH_3), 1.54-1.59 (1H, m, one of $\text{CH}_2(\text{C}5)$), 1.59 (1H, ddd, $J = 14.0, 7.8$ and 2.9 Hz, one of $\text{CH}_2(\text{C}3)$), 1.65 (3H, s, $\text{CH}_3\text{C}(\text{NO}_2)$), 1.87-1.98 (4H, m, $\text{CH}_2(\text{C}7)$, $\text{CH}(\text{C}6)$ and one of $\text{CH}_2(\text{C}5)$), 2.11 (1H, appdt, $J = 14.0$ and 5.4 Hz, one of $\text{CH}_2(\text{C}3)$), 2.24-2.32 (1H, m, one of $\text{CH}_2(\text{C}8)$), 2.39-2.46 (1H, m, one of $\text{CH}_2(\text{C}8)$), 3.41 (3H, s, $\text{CH}(\text{OCH}_3)$), 3.92-3.97 (1H, m, $\text{CH}(\text{OH})$), 3.99 (1H, dd, $J = 5.3$ and 2.9 Hz, $\text{CH}(\text{OCH}_3)$), 4.13 (2H, q, $J = 7.1$ Hz, OCH_2CH_3)

δ_{C} (100 MHz, CDCl_3): 14.3 (OCH_2CH_3), 22.0 ($\text{CH}_3\text{C}(\text{NO}_2)$), 25.0 ($\text{CH}_2(\text{C}7)$), 32.8 ($\text{CH}_2(\text{C}8)$), 34.1 ($\text{CH}_2(\text{C}3)$), 34.5 ($\text{CH}_2(\text{C}5)$), 40.0 ($\text{CH}(\text{C}6)$), 58.1 ($\text{CH}(\text{OCH}_3)$), 60.6 (OCH_2CH_3), 65.6 ($\text{CH}(\text{OH})$), 80.3 ($\text{CH}(\text{OCH}_3)$), 92.5 ($\text{Cq}(\text{C}1)$), 173.4 (CO_2Et)

m/z [$\text{CI} (+ve)$], 290.2 ($[\text{M}+\text{H}]^+$, 62%); Found $[\text{M}+\text{H}]^+$, 290.1603, $\text{C}_{13}\text{H}_{24}\text{NO}_6$ requires 290.1604

ν_{max} (CDCl_3) / cm^{-1} : br. 3448, 2937, br. 1732, 1537

References

1. R. O. Hynes, *Proc. Nat. Acad. Sci. USA* **1973**, *70*, 3170-3174
2. S. L. Schor, I. R. Ellis, S. J. Jones, R. Baillie, K. Seneviratne, J. Clausen, K. Motegi, B. Vojtesek, K. Kankova, E. Furrrie, M. J. Sales, A. M. Schor, R. A. Kay *Cancer Res* **2003**, *63*, 8827-8836
3. U. Schwarz-Linek, M. Höök, J. R. Potts *Molecular Microbiology* **2004**, *52*, 631-641
4. M. Kaspar, L. Zardi, D. Neri *Int. J. Cancer* **2006**, *118*, 1331-1339
5. R. Grose *Genome Biology* **2004**, *5*, 228
6. H. Matsuura, S. Hakomori *Proc. Natl. Acad. Sci. USA* **1985**, *82*, 6517-6521
7. M. Santimaria, G. Moscatelli, G. L. Viale, L. Giovannoni, G. Neri, F. Viti, A. Leprini, L. Borsi, P. Castellani, L. Zardi, D. Neri, P. Riva *Clin Cancer Res* **2003**, *9*, 571-5
8. R. Longtin *J. Natl. Cancer Inst.* **2004**, *96*, 6-8
9. R. Pankov, K. M. Yamada *J. Cell Sci.* **2002**, *115*, 3861-3863
10. E. S. White, F. E. Baralle, A. F. Muro *J Pathol* **2008**, *216*, 1-14
11. E. L. George, E. N. Georges-Labouesse, R. S. Patel-King, H. Rayburn, R. O. Hynes *Development* **1993**, *119*, 1079-1091
12. D. M. Pesciotta Peters, D. E. Mosher *J. Cell Biol.* **1987**, *104*, 121-130
13. M. Leiss, K. Beckmann, A. Giros, M. Costell, R. Faessler *Curr. Opin. Cell Biol.* **2008**, *20*, 502-507
14. T. Scott-Burden *News in Physiological Sciences*, **1994**, *9*, 110-115
15. J. E. Schwarzbauer, Y. Mao *Matrix Biology* **2005**, *24*, 389-399
16. M. Gao, M. Sotomayor, E. Villa, E. H. Lee, K. Schulten *Phys. Chem. Chem. Phys.* **2006**, *8*, 3692-3706
17. I. Vakonakis, D. Staunton, L. M. Rooney, I. D. Campbell *The EMBO Journal* **2007**, *26*, 2575-2583
18. G. Baneyx, L. Baugh, V. Vogel *Proc. Natl. Acad. Sci. USA* **2002**, *99*, 5139-5143
19. I. Wierzbicka-Patynowski, J. E. Schwarzbauer *J. Cell Sci.* **2003**, *116*, 3269-3276

20. B. H. Luo, C. V. Carman, T. A. Springer *Annu Rev Immunol* **2007**, *25*, 619-647
21. J. Cho, D. F. Mosher *J Thromb Haemost* **2006**, *4*, 1461-1469
22. H. Ni, P. S. T. Yuen, J. M. Papalia, J. E. Trevithick, T. Sakai, R. Faessler, R. O. Hynes, D. D. Wagner *Proc. Natl. Acad. Sci. USA* **2003**, *100*, 2415-2419
23. D. C. Hocking *Chest* **2002**, *122*, 275S-278S
24. D C. Roy, S. J. Wilke-Mounts, D. C. Hocking *Biomaterials*, **2011**, *32*, 2077-2087
25. M. Gao, D. Craig, O. Lequin, I. D. Campbell, V. Vogel, K. Schulten *Proc. Natl. Acad. Sci. USA* **2003**, *100*, 14784-14789
26. J. R. Potts, I. D. Campbell *Matrix Biology* **1996**, *15*, 313-320
27. K. M. Yamada, R. A. F. Clark *Provisional matrix* In: *The Molecular and Cellular Biology of Wound Repair* R. A. F. Clark, editor, Plenum Press, New York, **1996**, 51-93
28. D. F. Mosher, editor, *Fibronectin* Academic Press, San Diego, **1989**
29. L. Zardi, B. Carnemolla, E. Balza, L. Borsi, P. Castellani, M. Rocco, A. Siri *Eur J Biochem.* **1985**, *146*, 571-579
30. I. D Campbell, C. Spitzfaden *Structure* **1994**, *2*, 333-337
31. R. F. Doolittle, P. Bork *Scientific American Magazine* **1993**, *269*, 50-56
32. M. Barczyk, S. Carracedo, D. Gullberg *Cell Tissue Res* **2010**, *339*, 269-280
33. Y. Takada, X. Ye, S. Simon *Genome Biology* **2007**, *8*, Article 215
34. R. O. Hynes *Matrix Biology* **2004**, *23*, 333-340
35. A. Krammer, D. Craig, W. E. Thomas, K. Schulten, V. Vogel *Matrix Biology* **2002**, *21*, 139-147
36. S. Takahashi, M. Leiss, M. Moser, T. Ohashi, T. Kitao, D. Heckmann, A. Pfeifer, H. Kessler, J. Takagi, H. P. Erickson, R. Faessler *The Journal of Cell Biology* **2007**, *178*, 167-178
37. R. O. Hynes *Cell* **2002**, *110*, 673-687
38. F. G. Giancotti, E. Ruoslahti *Science* **1999**, *285*, 1028 – 1033
39. L. Pray *Nature Education* **2008**, *1*(1), (Article: Eukaryotic genome complexity)
40. A. R. Kornblihtt *Current Opinion in Cell Biology* **2005**, *17*, 262-268
41. A. R. Kornblihtt, K. Vibe-Pedersen, F. E. Baralle. *Nucleic Acids Res* **1984**, *12*, 5853-5868
42. J. E. Schwarzbauer, J. W. Tamkun, I. R. Lemischka, R. O. Hynes *Cell* **1983**, *35*, 421-431

43. P. Castellani, G. Viale, A. Dorcaratto, G. Nicolo, J. Kaczmarek, G. Querze, L. Zardi *Int. J. Cancer* **1994**, *59*, 612-618
44. R. O. Hynes *J Thromb Haemost* **2007**, *5* (Suppl. 1), 32-40
45. E. A. Wayner, A. Garcia-Pardo, M. J. Humphries, J. A. McDonald, W. G. Carter, *J Cell Biol* **1989**, *109*, 1321-1330
46. A. F. Muro, A. K. Chauhan, S. Gajovic, A. Iaconcig, F. Porro, G. Stanta, F. E. Baralle *The Journal of Cell Biology* **2003**, *162*, 149-160
47. V. L. Magnuson, M. Young, D. G. Schattenberg, M. A. Mancini, D. L. Chen, B. Steffensen, R. J. Klebe *J. Biol. Chem.* **1991**, *266*, 14654-14662
48. S. Astrof, D. Crowley, R. O. Hynes *Developmental Biology* **2007**, *311*, 11-24
49. K. Hino, S. Shiozawa, Y. Kuroki, H. Ishikawa, K. Shiozawa, K. Sekiguchi, H. Hirano, E. Sakashita, K. Miyashita, K. Chihara *Arthritis Rheum.* **1995**, *38*, 678-683
50. C. Ffrench-Constant, L. Van de Water, H. F. Dvorak, .R. O. Hynes *J. Cell Biol.* **1989**, *109*, 903-914
51. A. F. Muro, F. A. Moretti, B. B. Moore, M. Yan, R. G. Atrasz, C. A. Wilke, K. R. Flaherty, F. J. Martinez, J. L. Tsui, D. Sheppard, F. E. Baralle, G. B. Toews, E. S. White *Am J Respir Crit Care Med* **2008**, *177*, 638-645
52. P. Alessi, Ch. Ebbinghaus, D. Neri *Biochimica et Biophysica Acta* **2004**, *1654*, 39-49
53. D. Berndorff, S. Borkowski, S. Sieger, A. Rother, M. Friebe, F. Viti, Ch. S. Hilger, J. E. Cyr, L. M. Dinkelborg *Clin Cancer Res* **2005**, *11*, 7053s-7063s
54. K. Goossens, A. Van Soom, A. Van Zeveren, H. Favoreel, L. J Peelman *BMC Developmental Biology* **2009**, *9* (1)
55. S. L. Schor, A. M. Schor, A. M. Grey, G. Rushton *Journal of Cell Science* **1988**, *90*, 391-399
56. R. A. Kay, I. R. Ellis, S. J. Jones, S. Perrier, M. M. Florence, A. M. Schor, S. L. Schor *Cancer Res* **2005**, *65*, 10742-10749
57. A-M. Grey, A. M. Schor, G. Rushton, I. Ellis, S. L. Schor *Proc. Natl. Acad. Sci. USA* **1989**, *86*, 2438-2442
58. M. Picardo, S. L. Schor, A-M. Grey, A. Howell, I. Laidlaw, J. Redford, A. M. Schor *The Lancet* 1991, *337*,130-133
59. E. M. Rosen, I. D. Goldberg *In Vitro Cell Dev Biol.* **1989**, *25*, 1079-1087

60. M. Vicente-Manzanares, D. J. Webb, A. R. Horwitz *Journal of Cell Science* **2005**, *118*, 4917-4919
61. S.L. Schor, A.M. Schor, A.M. Grey, J. Chen, G. Rushton, M.E. Grant, I. Ellis *In Vitro Cell Dev Biol.* **1989**, *25*, 737-746
62. S. L. Schor, A. M. Schor *Breast Cancer Res* **2001**, *3*, 373-379
63. H. Y. Chang, J. B. Sneddon, A. A. Alizadeh, R. Sood, R. B. West, K. Montgomery, J-T. Chi, M. van de Rijn, D. Botstein, P. O. Brown *PLoS Biology* **2004**, *2*, 206-214
64. H. Brem, M. Tomic-Canic *The Journal of Clinical Investigation* **2007**, *117*, 1219-1222
65. S. J. Jones, M. M. Florence, I. R. Ellis, K. Kankova, S. L. Schor, A. M. Schor *Experimental Cell Research* **2007**, *313*, 4145-4157
66. S. L. Schor, A. M. Grey, I. Ellis, A. M. Schor, B. Coles, R. Murphy *Symp Soc Exp Biol.* **1993**, *47*, 235-251
67. S. L. Schor, I. Ellis, C. Dolman, J. Banyard, M. J. Humphries, D. F. Mosher, A. M. Grey, A. P. Mould, J. Sottile, A. M. Schor *Journal of Cell Science* **1996**, *109*, 2581-2590
68. S. L. Schor, I. Ellis, J. Banyard, A. M. Schor *Journal of Cell Science* **1999**, *112*, 3879-3888
69. Ch. J. Millard, I. R. Ellis, A. R. Pickford, A. M. Schor, S. L. Schor, I. D. Campbell *J. Biol. Chem.* **2007**, *282*, 35530-35535
70. A. Giannis, T. Kolter *Angew. Chem. Int. Ed. Engl.* **1993**, *32*, 1244-1267
71. N. Shpiro, I. R. Ellis, T. J. Dines, A. M. Schor, S. L. Schor, D. G. Normand, R. Marquez *Mol. BioSyst.* **2005**, *1*, 318-320
72. J. R. Potts, J. R. Bright, D. Bolton, A. R. Pickford, I. D. Campbell *Biochemistry* **1999**, *38*, 8304-8312
73. E. Rudiño-Piñera, R. B. G. Ravelli, G. M. Sheldrick, M. H. Nanao, V. V. Korostelev, J. M. Werner, U. Schwarz-Linek, J. R. Potts, E. F. Garman *Journal of Molecular Biology* **2007**, *368*, 833-844
74. N. Iranpoor, H. Firouzabadi, N. Nowrouzia, D. Firouzabadi *Tetrahedron Lett.* **2006**, *47*, 6879-6881
75. X. Yang, Ch. Xi, Y. Jiang *Tetrahedron Lett.* **2005**, *46*, 8781-8783
76. D. A. Learmonth, *UK Patent Application*, GB 2 377 934 A, **2003**

77. B. C. Smith *Infrared Spectral Interpretation: a systematic approach* Publisher: CRC Press, Boca Raton, **1998**
78. L. Forlani *J. Chem. Soc., Perkin Trans. 2*, **1991**, *11*, 1699-1702
79. J. R. Beck *Tetrahedron*, **1978**, *34*, 2057-2068
80. S. Sato, T. Sakamoto, E. Miyazawa, Y. Kikugawa *Tetrahedron* **2004**, *60*, 7899-7906
81. T. J. Connolly, A. Constantinescu, T. S. Lane, M. Matchett, P. McGarry, M. Paperna *Organic Process Research and Development* **2005**, *9*, 837-842
82. W. R. Meindl, E. von Angerer, H. Schoenenberger, G. Ruckdeschel *J. Med. Chem.* **1984**, *27*, 1111-1118
83. T. P. Kogan, T. E. Rawson *Tetrahedron Lett.* **1992**, *33*, 7089-7092
84. G. L. Stahl, R. Walter, C. W. Smith *J. Org. Chem.* **1978**, *43*, 2285-2286
85. J. A. Barltrop, P. Schofield *Tetrahedron Lett.* **1962**, *3*, 697-699
86. V. N. Rajasekharan Pillai *Synthesis* **1980**, *1*, 1-26
87. J. E.T. Corrie *Photoremovable Protecting Groups Used for the Caging of Biomolecules* In *Dynamic Studies in Biology* Edited by M. Goeldner, R. Givens, 2005, WILEY-VCH Verlag GmbH & Co. KGaA, Weinheim
88. C. H. Self, S. Thompson *Nature Medicine* **1996**, *2*, 817-820
89. J. H. Kaplan, G. C. Ellis-Davies *Proc. Natl. Acad. Sci. USA* **1988**, *85*, 6571-6575
90. J. W. Walker, G. P. Reid, J. A. McCray, D. R. Trentham *J. Am. Chem. Soc.* **1988**, *110*, 7170-7177
91. D. M. Rothman, E. J. Petersson, M. E. Vázquez, G. S. Brandt, D. A. Dougherty, B. Imperiali *J. Am. Chem. Soc.* **2005**, *127*, 846-847
92. H. Ando, T. Furuta, R. Y. Tsien, H. Okamoto *Nature Genetics* **2001**, *28*, 317-325
93. S. Giovannardi, L. Lando, A. Peres *News Physiol. Sci.* **1998**, *13*, 251-255
94. D. E. Falvey, Ch. Sundararajan *Photochem. Photobiol. Sci.* **2004**, *3*, 831-838
95. Ch. G. Bochet *J. Chem. Soc., Perkin Trans. 1*, **2002**, *2*, 125-142
96. A. Blanc, Ch. G. Bochet *J. Org. Chem.* **2002**, *67*, 5567-5577
97. J. Morrison, P. Wan, J. E. T. Corrie, G. Papageorgiou *Photochem. Photobiol. Sci.* **2002**, *1*, 960-969
98. Y. V. Il'ichev, M. Schwoerer, J. Wirz *J. Am. Chem. Soc.* **2004**, *126*, 4581-4595
99. A. P. Pelliccioli, J. Wirz *Photochem. Photobiol. Sci.* **2002**, *1*, 441-458

100. R. S. Givens, P. G. Conrad, A. L. Yousef, J.-I. Lee *Photoremovable Protecting Groups In: CRC Handbook of Organic Photochemistry and Photobiology, Second Edition* W. M. Horspool, F. Lenci, editors, CRC Press, **2003**
101. B. Hellrung, Y. Kamdzhilov, M. Schwęrcer, J. Wirz *J. Am. Chem. Soc.* **2005**, *127*, 8934-8935
102. Y. V. Il'ichev *J. Phys. Chem. A.* **2003**, *107*, 10159-10170
103. A. Banerjee, Ch. Grewer, L. Ramakrishnan, J. Jaeger, A. Gameiro, H-G. Breiting, K. R. Gee, B. K. Carpenter, G. P. Hess *J. Org. Chem.* **2003**, *68*, 8361-8367
104. A. Banerjee, K. Lee, Q. Yu, A. G. Fang, D. E. Falvey *Tetrahedron Lett.* **1998**, *39*, 4635-4638
105. Ch. G. Bochet *Angew. Chem. Int. Ed.* **2001**, *40*, 2071-2073
106. T. Furuta, S. S.-H. Wang, J. L. Dantzker, T. M. Dore, W. J. Bybee, E. M. Callaway, W. Denk, R. Y. Tsien *Proc Natl. Acad. Sci. USA* **1999**, *96*, 1193-1200
107. C. Ramesh, G. Mahender, N. Ravindranath, B. Das *Tetrahedron* **2003**, *59*, 1049-1054
108. E. D. Laganis, B. L. Chenard *Tetrahedron Lett.* **1984**, *25*, 5831-5834
109. K. C. Nicolaou, P. K. Sasmal, H. Xu, K. Namoto, A. Ritzen *Angew. Chem. Int. Ed.* **2003**, *42*, 4225-4229
110. R. Marquez, A. Schor, S. Schor, I. Ellis, *unpublished results*
111. H. H. McAdams, B. Srinivasan, A. P. Arkin *Nature Reviews Genetics* **2004**, *5*, 169-178
112. J. R. Fitzgerald, D. E. Sturdevant, S. M. Mackie, S. R. Gill, J. M. Musser *Proc Natl. Acad. Sci. USA* **2001**, *98*, 8821-8826
113. World Health Organization (WHO), *Overcoming Antimicrobial Resistance World Health Report on Infectious Diseases* **2000**
114. Y.-T. Tan, D. J. Tillett, I. A. McKay *Molecular Medicine Today* **2000**, *6*, 309-314
115. A. M. Edwards, J. R. Potts, E. Josefsson, R. C. Massey *PLoS Pathogens* **2010**, *6*, e1000964
116. F. Agerer, S. Lux, A. Michel, M. Rohde, K. Ohlsen, Ch. R. Hauck *Journal of Cell Science* **2005**, *118*, 2189-2200

117. U. Schwarz-Linek, J. M. Werner, A. R. Pickford, S. Gurusiddappa, J. Hwa Kim, E. S. Pilka, J. A. G. Briggs, T. S. Gough, M. Hook, I. D. Campbell, J. R. Potts *Nature* **2003**, *423*, 177-181
118. S. F. Bradley *Semin Respir Crit Care Med* **2005**, *26*, 643-649
119. J. Aguilar, V. Urday-Cornejo, S. Donabedian, M. Perri, R. Tibbetts, M. Zervos *Medicine* **2010**, *89*, 117-125
120. Y-A. Que, J-A. Haefliger, L. Piroth, P. François, E. Widmer, J. M. Entenza, B. Sinha, M. Herrmann, P. Francioli, P. Vaudaux, P. Moreillon *J. Exp. Med.* **2005**, *201*, 1627-1635
121. J. A. Wright, S. P. Nair *Int J Med Microbiol.* **2010**, *300*, 193-204
122. D. Thomas, S. Chou, O. Dauwalder, G. Lina *Diversity in Staphylococcus aureus Enterotoxins* In: *Superantigens and Superallergens* G. Marone, editor, S. Karger AG **2007**
123. E. J. Gorak, S. M. Yamada, J. D. Brown *Clin Infect Dis.* **1999**, *29*, 797-800
124. M. B. Edmond, R. P. Wenzel, A. W. Pasculle *Ann Intern Med* **1996**, *124*, 329-334
125. N. McCallum, B. Berger-Bächli, M. M. Senn *Int J Med Microbiol.* **2010**, *300*, 118-129
126. G. W. Kaatz, F. McAleese, S. M. Seo *Antimicrobial Agents and Chemotherapy* **2005**, *49*, 1857-1864
127. S. Raju, A. Kumar Oli, S. A. Patil, K. Chandrakanth *World J Microbiol Biotechnol* **2010**, *26*, 171-176
128. *Staphylococcus aureus infection and disease* A. Honeyman, H. Friedman, M. Bendinelli, editors, Springer **2001**
129. B. C. Kahl, M. Goulian, W. van Wamel, M. Herrmann, S. M. Simon, G. Kaplan, G. Peters, A. L. Cheung *Infect Immun.* **2000**, *68*, 5385-5392
130. E. Lemichez, M. Lecuit, X. Nassif, S. Bourdoulous *Nature Reviews Microbiology* **2010**, *8*, 93-104
131. T. Fowler, E. R. Wann, D. Joh, S. Johansson, T. J. Foster, M. Hook *Eur. J. Cell Biol.* **2000**, *79*, 672-679
132. A. P. Bhavsar, J. A. Guttman, B. B. Finlay *Nature* **2007**, *449*, 827-834
133. E. R. Wann, S. Gurusiddappa, M. Hook *The Journal of Biological Chemistry* **2000**, *275*, 13863-13871

134. R. C. Massey, M. N. Kantzanou, T. Fowler, N. P. J. Day, K. Schofield, E. R. Wann, A. R. Berendt, M. Hook, S. J. Peacock *Cellular Microbiology* **2001**, *3*, 839-851
135. K. Jonsson, C. Signas, H. P. Muller, M. Lindberg *Eur. J. Biochem.* **1991**, *202*, 1041-1048
136. R. Heying, J. van de Gevel, Y. A. Que, P. Moreillon, H. Beekhuizen *Thrombosis and Haemostasis* **2007**, *97*, 617-626
137. J. R. Fitzgerald, A. Loughman, F. Keane, M. Brennan, M. Knobel, J. Higgins, L. Visai, P. Speziale, D. Cox, T. J. Foster *Molecular Microbiology* **2006**, *59*, 212-230
138. L. Piroth, Y.-A. Que, E. Widmer, A. Panchaud, S. Piu, J. M. Entenza, P. Moreillon *Infection and Immunity* **2008**, *76*, 3824-3831
139. M. Baron, D. Norman, A. Willis, I. D. Campbell *Nature* **1990**, *345*, 642-646
140. N. A. G. Meenan, L. Visai, V. Valtulina, U. Schwarz-Linek, N. C. Norris, S. Gurusiddappa, M. Hook, P. Speziale, J. R. Potts *J. Biol. Chem.* **2007**, *282*, 25893-25902
141. E. S. Pilka, J. M. Werner, U. Schwarz-Linek, A. R. Pickford, N. A. G. Meenan, I. D. Campbell, J. R. Potts *FEBS Letters* **2006**, *580*, 273-277
142. U. Schwarz-Linek, E. S. Pilka, A. R. Pickford, J. Hwa Kim, M. Hook, I. D. Campbell, J. R. Potts *J. Biol. Chem.* **2004**, *279*, 39017-39025
143. A. Schroeder, B. Schroeder, B. Roppenser, S. Linder, B. Sinha, R. Faessler, M. Aepfelbacher *Molecular Biology of the Cell* **2006**, *17*, 5198-5210
144. O. Krut, O. Utermohlen, X. Schlossherr, M. Kronke *Infect. Immun.* **2003**, *71*, 2716-2723
145. A. Schroeder, R. Kland, A. Peschel, C. von Eiff, M. Aepfelbacher *Med. Microbiol. Immunol.* **2006**, *195*, 185-194
146. M. J. Williams, I. Phan, T. S. Harvey, A. Rostagno, L. I. Gold, I. D. Campbell *J. Mol. Biol.* **1994**, *235*, 1302-1311
147. J. R. Potts, D. G. Normand, R. Marquez, *unpublished results*
148. E. H. Beachey *J. Infect. Dis.* **1981**, *143*, 325-345
149. T. S. Zaidi, M. J. Preston, G. B. Pier *Infect. Immun.* **1997**, *65*, 1370-1376
150. Review: M. A. Ciufolini, C. Y. W. Hermann, Q. Dong, T. Shimizu, S. Swaminathan, N. Xi *Synlett* **1998**, *2*, 105-114

151. Review: K. C. Nicolaou, S. A. Snyder, T. Montagnon, G. Vassilikogiannakis *Angew. Chem. Int. Ed.* **2002**, *41*, 1668-1698
152. O. Achmatowicz Jr., P. Bukowski, B. Szechner, Z. Zwierzchowska, A. Zamojski *Tetrahedron* **1971**, *27*, 1973-1996
153. M. A. Ciufolini, C. Y. Wood *Tetrahedron Lett.* **1986**, *27*, 5085-5088
154. M. A. Ciufolini, Q. Dong *Chem. Commun.* **1996**, *7*, 881-882
155. M. A. Ciufolini, T. Shimizu, S. Swaminathan, N. Xi *Tetrahedron Lett.* **1997**, *38*, 4947-4950
156. J. M. Harris, A. Padwa *Org. Lett.* **2002**, *4*, 2029-2031
157. J. M. Harris, A. Padwa *J. Org. Chem.* **2003**, *68*, 4371-4381
158. M. H. Haukaas, G. A. O'Doherty *Org. Lett.* **2001**, *3*, 401-404
159. J. Bi, V. K. Aggarwal *Chem. Commun.* **2008**, *1*, 120-122
160. C.-F. Yang, Y.-M. Xu, L.-X. Liao, W.-S. Zhou *Tetrahedron Lett.* **1998**, *39*, 9227-9228
161. H.-J. Altenbach, R. Wischnat *Tetrahedron Lett.* **1995**, *36*, 4983-4984
162. K. C. Nicolaou, P. G. Bulger, D. Sarlah *Angew. Chem. Int. Ed.* **2005**, *44*, 4490-4527
163. H. Villar, M. Frings, C. Bolm *Chem. Soc. Rev.* **2007**, *36*, 55-66
164. A. H. Hoveyda, A. R. Zhugralin *Nature* **2007**, *450*, 243-251
165. Q. Yang, W.-J. Xiao, Z. Yu *Org. Lett.* **2005**, *7*, 871-874
166. P. Compain *Adv. Synth. Catal.* **2007**, *349*, 1829-1846
167. A. Deiters, S. F. Martin *Chem. Rev.* **2004**, *104*, 2199-2238
168. D. L. Wright, J. P. Schulte, M. A. Page *Org. Lett.* **2000**, *2*, 1847-1850
169. A. S. Edwards, R. A. J. Wybrow, C. Johnstone, H. Adams, J. P. A. Harrity *Chem. Commun.* **2002**, *14*, 1542-1543
170. D. A. Evans, M. M. Morrissey, R. L. Dow *Tetrahedron Lett.* **1985**, *26*, 6005-6008
171. D. A. Evans, M. M. Morrissey *J. Am. Chem. Soc.* **1984**, *106*, 3866-3868
172. J. P. Candlin, A. R. Oldham *Discuss. Faraday Soc.* **1968**, *46*, 60-71
173. J. M. Brown *Angew. Chem. Int. Ed. Engl.* **1987**, *26*, 190-203
174. A. Fuerstner, N. Takashi, *J. Am. Chem. Soc.* **2007**, *129*, 1906-1907
175. P. Bremond, G. Audrau, T. Juspín, H. Monti, *Eur. J. Org. Chem.* **2007**, *2007*, 2802-2807
176. J. A. R. Salvador, S. M. Silvestre *Tetrahedron Lett.* **2005**, *46*, 2581-2584

177. T. K. M. Shing, Y. Yeung, P. L. Su *Org. Lett.* **2006**, *8*, 3149-3151
178. A. J. Catino, R. E. Forslund, M. P. Doyle *J. Am. Chem. Soc.* **2004**, *126*, 13622-13623
179. P. Stanetty, M. Kremslehner, M. D. Mihovilovic *Tetrahedron Lett.* **2000**, *41*, 1717-1719
180. P. D. Rege, Y. Tian, E. J. Corey *Org. Lett.* **2006**, *8*, 3117-3120
181. S. E. Denmark, L. Gomez *J. Org. Chem.* **2003**, *68*, 8015-8024
182. H-X. Jin, Q. Zhang, H-S. Kim, Y. Wataya, H-H Liu, Y. Wu *Tetrahedron* **2006**, *62*, 7699-7711
183. A. Gangjee, J. Yanga, S. F. Queener *Bioorg. Med. Chem.* **2006**, *14*, 8341-8351
184. S. E. Denmark, L. R. Marcin *J. Org. Chem.* **1995**, *60*, 3221-3235
185. P. Stanetty, M. Kremslehner *Synth. Commun.* **1998**, *28*, 2491-2498
186. N. Ono, A. Kamimura, T. Kawai, A. Kaji *J. Chem. Soc., Chem. Commun.* **1987**, 1550-1551
187. E. Dumez, R. Faure, J-P. Dulcere *Eur. J. Org. Chem.* **2001**, *13*, 2577-2588
188. N. Kondo, H. Fueno, H. Fujimoto, M. Makino, H. Nakaoka, I. Aoki, S. Uemura *J. Org. Chem.* **1994**, *59*, 5254-5263
189. M. Sax, S. Berning, B. Wunsch, *Tetrahedron* **2005**, *61*, 205-211
190. D. A. Evans, J. S. Johnson *Diels-Alder Reactions* In: *Comprehensive Asymmetric Catalysis* E. N. Jacobsen, A. Pfaltz, H. Yamamoto, editors, Springer-Verlag, Heidelberg, Vol. III, **1999**, 1178-1235.
191. O. Diels, K. Alder *Liebigs Ann. Chem.* **1928**, *460*, 98-122
192. N. Celebi-Olcum, D. H. Ess, V. Aviyente, K. N. Houk *J. Org. Chem.* **2008**, *73*, 7472-7480
193. Y. Sudo, D. Shirasaki, S. Harada, A. Nishida *J. Am. Chem. Soc.* **2008**, *130*, 12588-12589
194. T. Inokuchi, M. Okano, T. Miyamoto *J. Org. Chem.* **2001**, *66*, 8059-8063
195. M. Node, K. Nishide, H. Imazato, R. Kurosaki, T. Inoue, T. Ikariyab *Chem. Commun.* **1996**, 2559-2560
196. S. Danishefsky, T. Kitahara, C. F. Yan, J. Morris *J. Am. Chem. Soc.* **1979**, *101*, 6996-7000
197. S. Danishefsky *Acc. Chem. Res.* **1981**, *14*, 400-406

198. W. Katona, N. P. Rath, S. Anant, W. F. Stenson, D. F. Covey *J. Org. Chem.* **2007**, *72*, 9298–9307
199. A. G. M. Barrett, Ch. D. Spilling *Tetrahedron Lett.* **1988**, *29*, 5733-5734
200. R. J. Rahaim Jr., R. E. Maleczka Jr. *Org. Lett.* **2005**, *7*, 5087-5090
201. S. Chandrasekhar, S. J. Prakash, Ch. L. Rao *J. Org. Chem.* **2006**, *71*, 2196-2199